Airborne Hyperspectral Remote Detection of Water Quality Parameters in the Inland and Coastal Waters of the Cowichan Watershed, British Columbia

by

Christiaan Piller
B.A.Sc., University of Waterloo, 1999

A Thesis Submitted in Partial Fulfillment of the Requirements for the Degree of

MASTER OF SCIENCE

in the Department of Geography

© Christiaan Piller, 2006
University of Victoria

All rights reserved. This thesis may not be reproduced in whole of in part, by photocopy or other means, without the permission of the author.

Airborne Hyperspectral Remote Detection of Water Quality Parameters in the Inland and Coastal Waters of the Cowichan Watershed, British Columbia

by

Christiaan Piller
B.A.Sc., University of Waterloo, 1999

Supervisory Committee

Dr. M. Costa (Department of Geography)
Supervisor

Dr. D. Smith (Department of Geography)
Departmental Member

Dr. K. Telmer (School of Earth and Ocean Sciences)
Outside Member

Dr. J. Gower (Institute of Ocean Sciences, Department of Fisheries and Oceans)
External Member

Supervisory Committee

Dr. M. Costa (Department of Geography)
Supervisor

Dr. D. Smith (Department of Geography)
Departmental Member

Dr. K. Telmer (School of Earth and Ocean Sciences)
Outside Member

Dr. J. Gower (Institute of Ocean Sciences, Department of Fisheries and Oceans)
External Member

Abstract

Optical remote detection of surface water quality for open ocean waters has been ongoing since the 1960's. This method of detection is much more challenging, and not yet standard practice, for the more optically complex inland and coastal waters. A series of empirically developed models were built relating remote sensing reflectance (R_{rs}) for Compact Airborne Spectrographic Imagery (CASI), acquired over both inland and coastal water bodies of the Cowichan River watershed in British Columbia, to concurrently sampled water parameter concentrations. The models predict concentrations of chlorophyll-*a* and its pheopigments (as a proxy signal of phytoplankton), coloured dissolved organic matter (CDOM) and total suspended solids (TSS), using techniques including simple regression, step-wise regression, band ratios, derivative analysis, and fluorescence line height (FLH). The most statistically significant models were ultimately applied. Each of the models was found to be statistically significant, although confidence in the lake models and the CDOM model for the bay are limited due to potential chance correlations. The Chl-*a* and TSS models for Cowichan Bay were found to be acceptable based upon an understanding of the phenomenon being investigated. These two parameters were correlated to short blue wavelengths, where Chl-*a* is primarily correlated with absorption at 451nm and TSS with scattering at 462nm. These findings provide support of the application of the standard configuration of MERIS bands as the common configuration for further coastal and inland water remote sensing studies.

Table of Contents

SUPERVISORY COMMITTEE ii
ABSTRACT iii
TABLE OF CONTENTS iv
LIST OF TABLES vii
LIST OF FIGURES viii
ACKNOWLEDGEMENTS x
DEDICATION xi

1.0 INTRODUCTION AND OBJECTIVES 1
1.1 RESEARCH RATIONALE 2
1.2 RESEARCH OBJECTIVES 3
1.3 ORGANIZATION OF THESIS 3

2.0 REMOTE SENSING OF WATER QUALITY 4
2.1 LIGHT AND WATER 4
2.1.1 Attenuation by the Atmosphere 5
2.1.1.1 Empirical Line Calibration 6
2.1.2 Attenuance by the Air-Water Interface 6
2.1.3 Attenuation by the Parameters of Interest 7
2.1.3.1 Phytoplankton 8
2.1.3.2 Colour Dissolved Organic Matter 10
2.1.3.3 Total Suspended Solids 10
2.1.3.4 Total Attenuance 11
2.2 REMOTE SENSING SYSTEMS 11
2.2.1 Airborne Remote Sensing 12
2.2.1.1 Compact Airborne Spectrographic Imager 12
2.3 REVIEW OF PREVIOUS STUDIES 13
2.3.1 History of Ocean Colour Detection Sensors 13
2.3.2 Developed Detection Techniques 15
2.3.2.1 Phytoplankton 15
2.3.2.2 Colour Dissolved Organic Matter 16
2.3.2.3 Total Dissolved Solids 17

3.0 STUDY SITE 18
3.1 COWICHAN WATERSHED 18

3.1.1 Climate 19
3.2 LAKE COWICHAN 20
3.2.1 Physiography 20
3.2.2 Hydrography 20
3.2.3 Biology 22
3.3 COWICHAN BAY 22
3.3.1 Physiography 22
3.3.2 Hydrography / Oceanography 23
3.3.3 Biology 24
4.0 DATA COLLECTION AND ANALYSIS 26
4.1 *IN SITU* SPECTRA COLLECTION 26
4.2 WATER SAMPLING 30
4.2.1 Collection Methods 30
4.2.2 Laboratory Analysis 31
4.2.2.1 Chlorophyll-*a* (*Phytoplankton Proxy*) 31
4.2.2.2 Colour Dissolved Organic Matter 32
4.2.2.3 Total Suspended Solids 33
4.3 AIRBORNE IMAGERY 34
4.3.1 Image Acquisition 34
4.3.2 Image Processing 34
4.3.2.1 Geometric Correction 36
4.3.2.2 Attenuation Correction 37
4.3.2.3 Line-to-line Correction 39
4.3.2.4 Mosaicking 40
4.3.2.5 Spectra Extraction 40
4.3.2.5.1 Lake Cowichan 42
4.3.2.5.2 Cowichan Bay 42
4.3.2.5.3 Finalized Spectra 43
5.0 RESULTS AND DISCUSSION 44
5.1 *IN SITU* SPECTRA 44
5.2 WATER QUALITY 45
5.2.1 Parameter Correlations 45
5.2.2 Spatial Distribution 48
5.3 CASI SPECTRA 49
5.4 PARAMETERS OF INTEREST MODELS 52
5.4.1 Model Development 52

5.4.1.1 Single Band Linear Regression 52
5.4.1.2 Stepwise Linear Regression 53
5.4.1.3 Band Ratios 55
5.4.1.4 Derivative Analysis 56
5.4.1.5 Fluorescence Line Height 58
5.4.1.6 Ocean Colour 4 Algorithm 60
5.4.2 Model Statistical Validations 61
5.4.2.1 Lake Cowichan Models 62
5.4.2.1.1 Chlorophyll-*a* 63
5.4.2.1.2 Colour Dissolved Organic Matter 63
5.4.2.1.3 Total Suspended Solids 64
5.4.2.2 Cowichan Bay Models 64
5.4.2.2.1 Chlorophyll-*a* 65
5.4.2.2.2 Colour Dissolved Organic Matter 65
5.4.2.2.3 Total Suspended Solids 65
5.4.3 Model Implementation 65
5.4.3.1 Lake Cowichan Model Outputs 71
5.4.3.2 Cowichan Bay Model Outputs 75
5.5 RECOMMENDATIONS 79
6.0 CONCLUSIONS 81
7.0 REFERENCES 83

List of Tables

TABLE 2.1: List of ocean colour scanners 14
TABLE 2.2: Previous Landsat vs. TSS Studies 17
TABLE 4.1: CASI acquisition band configuration 34
TABLE 4.2: Geometric correction error 37
TABLE 4.3: Line-to-line correction error 40
TABLE 5.1: Matrix of correlations for parameters of interest 45
TABLE 5.2: Lake Cowichan single band regression models 52
TABLE 5.3: Cowichan Bay single band regression models 53
TABLE 5.4: Lake Cowichan multiple band regression models 54
TABLE 5.5: Cowichan Bay multiple band regression models 54
TABLE 5.6: Lake Cowichan band ratio regression models 55
TABLE 5.7: Cowichan Bay band ratio regression models 56
TABLE 5.8: Lake Cowichan derivative analysis regression models 57
TABLE 5.9: Cowichan Bay derivative analysis regression models 58
TABLE 5.10: Ocean Colour 4 algorithm band configuration 61
TABLE 5.11: Lake Cowichan models for validation 63
TABLE 5.12: Cowichan Bay models for validation 64
TABLE 5.13: Standard Band Configuration of the MERIS sensor 80

List of Figures

FIGURE 2.1: Radiance attenuation 5
FIGURE 2.2: Empirical line calibration 6
FIGURE 2.3: Refraction of light at the air-water interface 7
FIGURE 2.4: Attenuance due to absorption 9
FIGURE 2.5: Attenuance due to scattering 9
FIGURE 3.1: Cowichan watershed 19
FIGURE 3.2: Normal precipitation and temperature distributions 19
FIGURE 3.3: Lake Cowichan study site 20
FIGURE 3.4: Lake Cowichan 2003 hydrograph 21
FIGURE 3.5: Cowichan Bay study site 23
FIGURE 3.6: Phytoplankton observations in Saanich Inlet for 1975 25
FIGURE 4.1: Historical study site cloud coverage 26
FIGURE 4.2: Satlantic HyperSAS sampling configuration 27
FIGURE 4.3: Lake Cowichan sample collection distribution 28
FIGURE 4.4: Cowichan Bay sample collection distribution 29
FIGURE 4.5: Vertical Profile Conditions 30
FIGURE 4.6: Lake Cowichan CASI flightlines 35
FIGURE 4.7: Cowichan Bay CASI flightlines 35
FIGURE 4.8: Lake Cowichan CASI mosaic 41
FIGURE 4.9: Cowichan Bay CASI mosaic 41
FIGURE 5.1: *In situ* Spectra versus CASI R_{rs} and L 44
FIGURE 5.2: Lake Cowichan sampling results 46
FIGURE 5.3: Cowichan Bay sampling results 47
FIGURE 5.4: Water quality correlations 48
FIGURE 5.5: CASI spectra extracted from samplig site locations 50
FIGURE 5.6: Fluorescence Line Height theoretical diagram 59
FIGURE 5.7: Chl-*a* versus FLH for combined data 60
FIGURE 5.8: Ocean Colour 4 algorithm outputs 61
FIGURE 5.9: Lake Cowichan model outputs 67

FIGURE 5.10: Cowichan Bay model outputs 68
FIGURE 5.11: Speckle and striping in CASI imagery..... 69
FIGURE 5.12: Across-track variations in CASI imagery..... 69
FIGURE 5.13: Progressive model output resoltuions..... 70
FIGURE 5.14: Along-track plume development in CASI imagery..... 71
FIGURE 5.15: Lake Cowichan final Chl-*a* mode output 72
FIGURE 5.16: Lake Cowichan final CDOM mode output..... 73
FIGURE 5.17: Lake Cowichan final TSS mode output..... 74
FIGURE 5.18: Cowichan Bay final Chl-*a* mode output..... 76
FIGURE 5.19: Cowichan Bay final CDOM mode output..... 77
FIGURE 5.20: Cowichan Bay final TSS mode output 78

Acknowledgements

First and foremost I would like to extend my deepest gratitude to my supervisor Maycira Costa. I would not have been able to complete this thesis without her input and constant assistance and encouragement. I would also like to thank the other members of my committee, Dan Smith, Kevin Telmer and Jim Gower, for all their input and for giving so generously of their time.

I am most grateful to my colleagues and close friends Laurie Gallagher and Eduardo Loos for their constant enthusiasm and encouragement! These two, along with Andrew Hamilton and Mike Sanborn, were wonderful to work alongside during the field campaign and without their capable assistance the necessary data simply could not have been collected in such a timely and professional manner.

Everyone in my life is owed a great debt of thanks for all their encouragement throughout the development of this thesis, however, listing everyone would create a second volume. I thank you all and would like to mention those key people on the front lines cheering me on on a daily basis: Tamara Donnelly, Craig Stait-Gardner, George Tsintzouras, Roger MacLeod, Angus and Kumiko Forsyth, John Barron, Trevor Haynes, and Lior Malka.

I would like to express my sincere gratitude to my family. Thank-you Erika and Erinn for your constant support and respect. Most importantly thank-you mum and dad (Clare and Heinar Piller) for all that you have done for me. Without your motivation and tireless belief in me from the start I would never have been able to surmount each progressive academic challenge I've faced in my life.

This work was financially supported by GEOIDE, the GEOmatics for Informed Decisions Network. I would like to thank GEOIDE for their interest and support in this project.

Dedication

This thesis is dedicated to my parents, Heinar and Clare Piller.

1.0 INTRODUCTION AND OBJECTIVES

Our knowledge of physical and chemical oceanography has increased significantly over the past half-century. This expansion of knowledge is primarily a result of advancements in the technology of remote sensing, which has been proven effective in the detection of chlorophyll concentrations in Case I waters of the mid-oceans since the 1970's. Exploratory attempts have been made to apply these techniques to coastal and inland Case II waters (Carpenter and Carpenter, 1983; Jerome and Bukata, 1994; Kloiber *et al.*, 2002) concluding that greater spatial and spectral resolution from the data-acquiring-sensors is required. Hyperspectral sensors such as the Compact Airborne Spectrographic Imager (CASI), Airborne Visible/Infrared Imaging Spectrometer (AVIRIS), and Hyperion, provide the necessary increases of spatial and spectral resolution, thereby creating an opportunity for their use to study the more optically complex Case II waters.

Case I and II waters differ in more ways than simply salinity concentrations and are considered distinct water types. Case I waters are waters whose concentration of phytoplankton is high compared to other particles (Morel and Prieur, 1977). Case II waters are considered more complex due to the additional presence of particulate inorganic and non-chlorophyll related dissolved materials known as yellow substance (Jacques *et al.*, 1998; Doxaran *et al.*, 2002b). Due to heavier input loadings, often from human activities such as liquid waste discharge, land reclamation, fish farming, and shoreline erosion, both coastal and inland waters are considered Case II waters (Smith, 1992; and Gin *et al.*, 2003).

Case II waters are typically described by their parameters of dissolved oxygen (DO), pH, biological oxygen demand (BOD), temperature, conductivity, total dissolved solids (TDS), turbidity, and fecal coliform bacteria (type and count). These parameters, which are measured *in situ*, dictate a water body's trophic status, or ability to support life, as either oligotrophic, mesotrophic, or eutrophic (Tchobanoglous and Schroeder, 1987). Water bodies generally begin oligotrophic and if they become over-enriched by nutrients, there is a responsive increase in phytoplankton growth and the water body is considered to be eutrophic in status. The process of moving from oligotrophic through mesotrophic to eutrophic conditions is called eutrophication. This process is a natural one, which can be accelerated by the influences of human activities (Smith, 1992) due to interconnections between individual water parameters. Together these parameters can also be used to describe water's quality.

Water quality is a means of describing water's physical, biological and chemical impurities (Tchobanoglous and Schroeder, 1987). The concentrations and characteristics of these impurities change with time and space due to seasonal changes in minerals picked up from surface runoff affecting water quality. Silt and debris presence results in turbid or murky waters. Plant and algae growth are typically found in areas of slow moving or stagnant water.

Anthropogenic inputs can further impact water quality. Monitoring of water quality is often necessary, especially where human usage is of concern.

Inland and coastal water quality monitoring is still performed through intensive fieldwork. Many of the drawbacks associated with fieldwork include the lack of an extensive spatial coverage, the manpower required, and the need for repeat sampling intervals. The impact of these drawbacks and seasonal influences on logistics can be resolved through the use of remote sensing (Dierberg and Carrlker, 1994). Remote sensors have the ability to cover vast areas in a single image frame. With a means of extracting water quality data from remotely acquired imagery, remote sensors have the ability to greatly decrease the economic costs associated with traditional fieldwork (Dekker and Bukata, 2002; Hakvoort *et al.*, 2002).

The majority of existing water targeting systems are satellite based sensors that have been designed spectrally and spatially to study oceanic waters where attenuation is caused primarily by photosynthetic pigments (Gordon *et al.*, 1983; Sathyendranath *et al.*, 2001). Proper delineation of the multiple optically active constituents found in coastal and inland waters requires finer spatial and spectral resolution than those considered acceptable for oceanic water studies. Coastal and inland water properties also change over short distances and small bodies of water are physically difficult to determine without sensors capable of finer spatial resolution. With the advent of spaceborne hyperspectral fine resolution sensors we now have the potential to monitor the key parameters for inland and coastal waters. Prior to employing these sensors, however, a better understanding of the interactions between radiant light and the parameters total suspended solids (TSS), colour dissolved organic matter (CDOM), and chlorophyll-*a* needs to be acquired. These parameters are targeted as they optically impact on the radiant light. An airborne hyperspectral sensor has been employed for this study in order to achieve this better interactions understanding, as well as for the minimization of the atmospheric interferences associated with the use of a higher altitude spaceborne sensor. The findings of this research will also aid in the isolation of the optimal wavelengths to be employed for any future spaceborne satellite sensors designed for Case II waters.

1.1 Research Rationale

Relative to the other countries of the world, Canada is considered to have the greatest amount of coastal and inland water (DeVilliers, 1999). These waters, which hold fisheries operations, provide recreational enjoyment and supply much of our population's fresh water supply, have played an important role in the history of Canada and will continue to contribute to the economic and social development of the country (Shrubsole, 1990). According to a State of the Environment report published by Environment Canada, Bird and Rapport (1986) suggested that although Canada has not experienced the levels of water degradation found in parts of the industrial world, nor the kind of competition for water found in densely populated Third World

countries, an overall assessment of the state of Canada's aquatic ecosystem did not suggest grounds for complacency. Davies and Mazumder (2003) state that there is a need to create a sustainable framework for human utilization of the environment and specifically for the protection of drinking water supplies so as to ensure human and environmental health. They suggest this be done through the protection of the watersheds themselves, rather than through the protection of individual bodies of water or the current practice of constant improvement of our water treatment supply facilities to compensate for degrading water sources.

Water management, protection and monitoring of coastal and inland water quality are shared by the federal and provincial government. The results of this research will propel them in their management and protection by providing a more efficient means of surface water quality monitoring.

1.2 Research Objectives

The goal of this research is to develop and validate algorithms for the estimating of water quality parameters, including TSS, CDOM, and chlorophyll-*a* (inclusive of its pheopigments), from coastal and inland waters, using airborne hyperspectral imaging. This objective will be reached by isolating the optimal spectral wavelengths necessary for the imaging of these parameters.

1.3 Organization of Thesis

This thesis is organized into seven chapters. The rationale for this research, the study objectives and organization of the thesis have been presented in Chapter 1. The theory and principles for remotely detecting water quality parameters are presented in Chapter 2. Chapter 3 describes the study site used in this research in terms of its physiography, hydrography, biology, and socio-economy. The data collected, as well as its methods of collection and laboratory analysis, are described in Chapter 4. The water quality results and collected spectra are then discussed in Chapter 5 and the prediction models are also developed and validated. Chapter 6 summarizes the conclusions drawn from this study.

2.0 REMOTE SENSING OF WATER QUALITY

2.1 Light and Water

The ability of a remote sensor to detect parameters from a target relies upon the ability of the sensor to measure the object's reflectivity of electromagnetic energy or electromagnetic radiation (EMR). Electromagnetic energy occurs in indivisible units referred to as photons which travel at the speed of light in a vacuum (Kirk, 1994). These photons travel in a harmonic, sinusoidal fashion and, consequently, have an associated wavelength (λ) and a frequency (v).

The visible light region of the electromagnetic spectrum is the signal source for passive optical remote sensors, such as Landsat, MODIS (Moderate Resolution Imaging Spectrometer), and AVIRIS, All of these sensors rely on a natural energy, typically the earth's sun, as their signal source. These sensors are responsive to traveling EMR that arrive at the sensor within a field-of-view (FOV) defined by the geometric configuration of the optical device (Bukata *et al.*, 1995). This travelling EMR is referred to as a *radiant flux* (Φ) (Kirk, 1994).

The two most important terms required for understanding the behaviour of a radiant flux are *radiance* (L) and *irradiance* (E) (Bukata *et al.*, 1995). Both terms refer to the amount of EMR measured during a specified time period per unit area. The former is for light from a given direction or solid angle and the latter for light from all directions. These terms are qualified by whether they are incident on the upper or lower face of a horizontal surface with the addition of a subscript identifier, where:

L_d, E_d – downwelling radiance, irradiance

L_u, E_u – upwelling radiance, irradiance

The ratio of upward to downward irradiance is referred to as *irradiance reflectance* (R), and the ratio of upward radiance to downward irradiance is referred to as the *remote sensing reflectance* (R_{rs}).

$$R = E_u / E_d \quad \text{and} \quad R_{rs} = L_u / E_d \qquad \textbf{(2.1 \& 2.2)}$$

Both R and R_{rs} are of great importance to optical water studies (Mobley, 1994; Bukata *et al.*, 1995). These two ratios respond spectrally to the constituents present in a water column independent of variations in irradiance. An increase of R or R_{rs} is the result of *spectral scattering*, while a decrease of R or R_{rs} is the result of *spectral absorption* (Dekker, 1993). Spectral scattering and absorption are the two potential losses on Φ while passing through a medium. Their combined effect is termed *attenuation*, where:

$$\textbf{Attenuation = Scattering + Absorption} \qquad \textbf{(2.3)}$$

Upwelling radiance or irradiance from an aquatic medium, collected by a remote sensor above the earth's atmosphere, has been subject to attenuation on its downward trip through the atmosphere, then into, through, and out of the water column. The return trip through the earth's

atmosphere further increases the attenuation (Figure 2.1). Areas of shallow water depth should be avoided so that bottom reflectance is not a problematic concern.

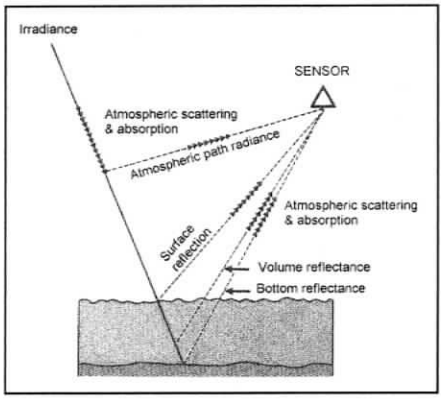


FIGURE 2.1: Radiance detected by a sensor over water is subject to attenuation processes on its downward and upward trips through the atmosphere, as well as into, through and out of the targeted water body (adapted from Mather, 2004).

2.1.1 Attenuation by the Atmosphere

Atmospheric attenuation is the result of EMR being scattered by air and dust particles, as well as it being absorbed by water vapour, oxygen, ozone, and carbon dioxide, which are present in the earth's atmosphere. Even when the sky is clear the intensity of a solar beam is significantly reduced by attenuation (Kirk, 1994). These atmospheric interactions not only reduce the amount of radiant flux but can also re-emit attenuated radiation at different wavelengths (Chandrasenkhar, 1960). The degree of atmospheric attenuation varies geographically on both the local and global levels. Much like the water masses that make up the world's oceans, the earth's atmosphere is comprised of dynamic air masses that vary in the amounts of particulate and moisture (Manahan, 1994). The radiance recorded by a remote sensor (L_s) is composed of the summation of these interfering path radiances (L_p) and that of the target under investigation (L_T).

$$L_s = L_T + L_p \qquad \textbf{(2.4)}$$

Correcting for these interferences allows for the isolation of radiance reflected from the intended target under investigation by the removal of L_p. Radiance values detected by the sensor are also generally converted to reflectance or remote sensing reflectance during atmospheric correction (Clark *et al.*, 2002). Three of the most common means of attenuation correction and unit conversion are (i) normalization to a spectrally flat target, (ii) radiative transfer modelling (RTM), and (iii) empirical line calibration (ELC). This last method is a relatively simple method, which forces the remote sensing imaging spectrometer data to match *in situ* reflectance spectra (Gladden, 2003). An ELC has been applied in this study.

2.1.1.1 Empirical Line Calibration

The ELC provides a logistically simple means of generating values of surface reflectance (Smith and Milton, 1999). This method forces remotely sensed imaging spectra to match *in situ* R_{rs} spectra collected by means of a spectroradiometer. The reference *in situ* spectra are collected from a few metres above targets found within the image bounds. These target spectra are collected as L_u, typically concurrent with image acquisition. However, if the targets are spectrally stable over time, the measurements need not be concurrent with data acquisition (Teillet *et al.*, 1990). Downwelling irradiance must also be collected during *in situ* target spectra collection in order to convert these reference L_u spectra to R_{rs}.

Using these collected *in situ* reference, force fitting is completed with the application using a best fit regression line that pairs either image digital numbers (DN) or image radiance with corresponding *in situ* R_{rs} values for each target being considered. Typically a minimum of two ground reference spectra of contrasting albedo are used for an ELC, where the force fitting is done for all bands individually, producing separate prediction lines for each waveband (Ben-Dor *et al.*, 1994) (Figure 2.2).

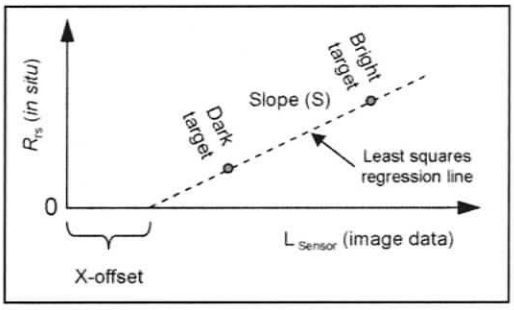


FIGURE 2.2: The ELC correction method fits a regression line of best fit to a bright and a dark target for each wavelength in an image and uses the equation of this line to predict the R_{rs} based on L_s (adapted from Smith and Milton, 1999).

The prediction line, shown in Figure 2.2, can be described mathematically as:

$$R_{rs} = (L_s - \text{"x-offset"}) \bullet S \qquad \textbf{(2.5)}$$

Where the prediction line intersects the x-axis it is indicative of zero R_{rs} being recorded *in situ*.

2.1.2 Attenuance by the Air-Water Interface

The EMR that manages to pass through the earth's atmosphere must then penetrate the water's surface crossing an air-water interface to become available in the aquatic environment. Of the EMR that interacts with the water surface, a portion is reflected and the remainder is transmitted into the water (Bukata *et al.*, 1995). There is no absorption caused by the air-water interface. However, as shown in Figure 2.3a, the photons that pass through this interface experience a change in direction towards the vertical due to differing velocities of light in air and

water where the change in directional angle is governed by *Snell's Law* (Kirk, 1994). Reflection by the water surface is a function of the incident photon's zenith (θ) angle and governed by the *Fresnel Equation*, where the zenith is the angle between any spot directly above the observation location and the line of sight to the sun.

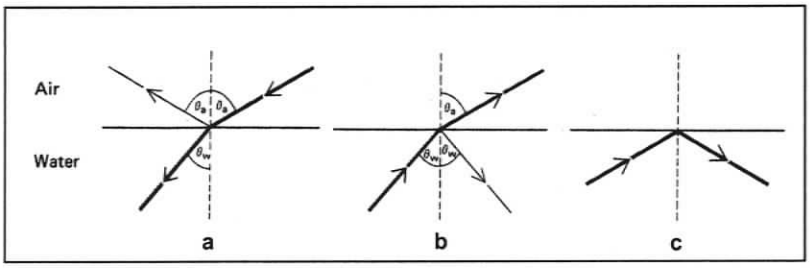


FIGURE 2.3: Refraction of light at the air-water interface. (a) Light incident from above is refracted downwards toward the vertical, while a portion is reflected upwards at the angle of incidence; (b) Light incident from below is refracted away from the vertical, while a portion is reflected downward again; (c) Light at $\theta_w \geq 49°$ experiences complete internal reflection, (adapted from Kirk, 1994).

Similarly, the emergent flux that is reflected back up from below the water surface is once again subject to Snell's law of refraction. Opposite in direction to the refraction of light entering the aquatic system, light emerging from it is diverged away from the vertical (Figure 2.3b). About half of the subsurface upwelling light is reflected downwards again. This reflected light is mainly that which is at $\theta_w \geq 49°$, which experiences complete internal reflection (Figure 2.3c). As most remote sensors measure upward radiance which, below the surface, is at angles between 0-40°, this does not represent a serious loss. Under calm conditions this represents only a 2-6% of light flux loss at the water-air interface (Kirk, 1994).

2.1.3 Attenuation by the Parameters of Interest

Photons entering an aquatic environment are then subject to being absorbed and scattered by water itself, as well as by each of the parameters of interest. Kirk (1994) summarizes the total absorption (a) and total backscattering coefficients (b_b) as the sum of the effects of each of these components:

$$a = a_w + a_{ph} + a_{cdom} + a_{tss} \quad \textbf{(2.6)}$$

$$b_b = b_{b(w)} + b_{b(ph)} + b_{b(tss)} \quad \textbf{(2.7)}$$

where,

w = pure water
ph = phytoplankton (chl-*a* as proxy)
cdom = colour dissolved organic matter
tss = total suspended solids

Figures 2.4 and 2.5 depict the individual effects of absorption and scattering that water and each of the parameters of interest have on photons in an aquatic environment. These spectra were collected from Chilko Lake in B.C. (Gallie and Murtha, 1992) and represent the widely accepted absorption and scattering trends associated with each of the parameters of interest.

Phytoplankton, CDOM, and TSS represent the parameters of interest to the remote sensing, not only because of their perceptible attenuation affects on light, but also because increased concentration in one or more of these components causes the degradation of water quality. This degradation then affects how humans can use the water, as well as how flora and fauna live and survive in the water.

2.1.3.1 Phytoplankton

Phytoplankton are microscopic plants that drift freely with water motion. Under normal conditions, they are beneficial and at the base of the food chain that marine life depends on. In elevated concentrations they can increase dissolved oxygen demand, which is necessary to aquatic life. Blooms of harmful species can also develop and interrupt the shellfish economy. Elevated concentrations of phytoplankton can result from human activities, such as agricultural runoff and sewage processing discharge that increase nutrient loadings to a water body.

Phytoplankton are the part of the plankton community that have the greatest impact on water colour. This is because of their relative abundance of photosynthetic pigments. These pigments act as collectors and suppliers of energy for the process of photosynthesis. The three types of photosynthesizing agents are: chlorophylls, carotenoids, and phycobilins, the first being present in all algal species (Bukata *et al.*, 1995). Of all the chlorophyllous pigments, chlorophyll-*a* has the most predominant impact on the collection and supply of energy (Mobley, 1994). Typically, the concentration of chlorophyll-*a* plus its degradation product phaeophytin-*a* are measured together as a proxy indicator of phytoplankton abundance and biomass in the water column (Hamilton *et al.*, 1993; Östlund *et al.*, 2001; Kunzig, 2002). It represents an important piece of information for understanding the health of a water body. From this point on, "Chl-*a*" is used in reference to the concentration of chlorophyll-*a* plus phaeophytin-*a*.

The absorption spectra for Chl-*a* (Figure 2.4) is characterized by strong absorption bands in the blue and in the red. There are two absorption peaks associated with Chl-*a*: (i) $\lambda \approx 430$nm and (ii) $\lambda \approx 665$nm, where the first peak is one to three times as high as the second due to the contribution of absorption by accessory pigments (Mobley, 1994).

Scattering by phytoplankton is dictated by their species, which vary in terms of shape, size, structure, and refractive index (Kirk, 1994). Although the organic suspended solids do not backscatter light as intensely as inorganic suspended solids, they share the same shape of backscattering cross-sectional spectra, exhibiting a slight increase in scattering towards the shorter wavelengths. The low refractive index (relative to water) of the living cells, compared with

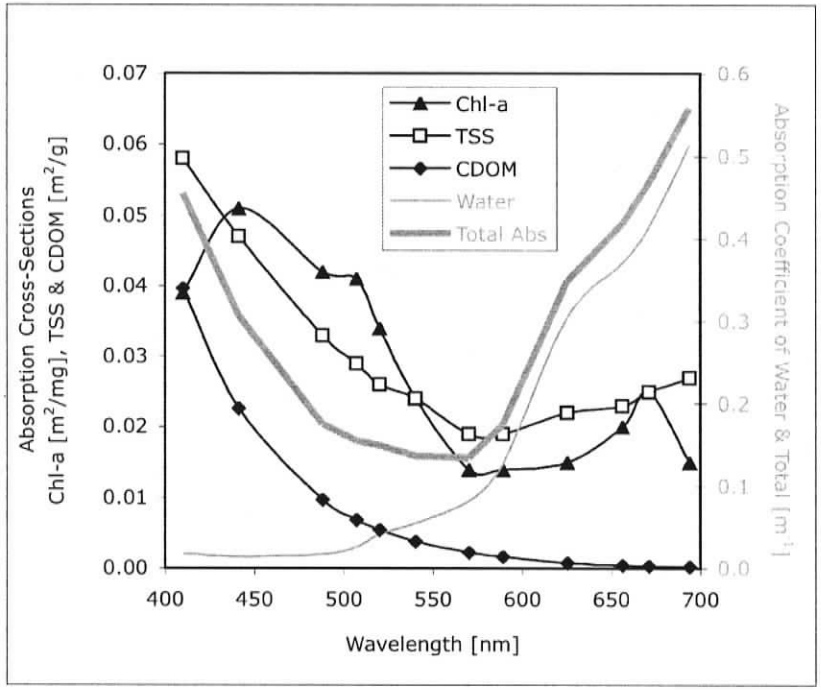


FIGURE 2.4: Attenuance cross-sectional spectra due to absorption (data source: Gallie and Murtha, 1992)

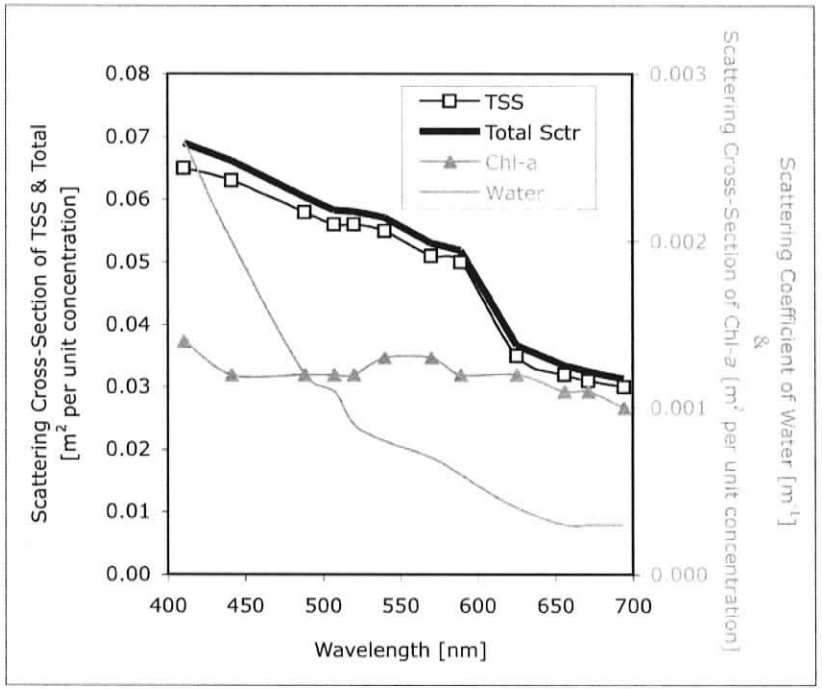


FIGURE 2.5: Attenuance cross-sectional spectra due to scattering (data source: Gallie and Murtha, 1992)

that of the inorganic particles, is the reason that backscattering due to phytoplankton is significantly less intense (Kirk, 1994).

2.1.3.2 Colour Dissolved Organic Matter

Decomposition of phytoplankton cells by bacterioplankton and other organic material results in the chemical transformation of organic material, through microbial action on time-scales of days to weeks, into carbon dioxide and inorganic nitrogen, sulfur, and phosphorous compounds. This decomposition process consumes DO and results in the creation of a variety of complex polymers, generally referred to as water humus or humic substances. When not dampened by suspended particulate, the presence of humic substances in natural waters is readily apparent in inland and coastal waters by varying degrees of yellow colouration, due to absorption of light in the ultraviolet (UV) and blue wavelengths (Jerlov, 1968). Consequently, these humic substances are referred to as yellow substance. They allow for the detection of CDOM through remote sensing, where CDOM refers to the dissolved organic matter (DOM) that passes through a filter with pore size 0.45μm (presently there is a new trend to use 0.22μm pore size; Schofield *et al.*, 2004). The greater the amount of organic material, the greater the depletion of DO from the water, which is necessary to both fish and zooplankton in order to breathe. Organic matter in water also causes problems for humans, as there are taste and odour problems associated with high organic matter concentrations.

CDOM is considered to have little to no light scattering impact and its attenuation to be solely due to its absorption properties (Bukata *et al.*, 1995). These light absorption properties are very low or absent in the red end of the spectrum and rise steadily with decreasing wavelength towards the blue (Figure 2.4), where absorption in the ultraviolet region is higher still (Jerlov, 1968). Absorption measurement at 440nm is referred to as the g_{440} measurement and provides a means of relative comparison between water bodies. CDOM not only varies between marine and inland water, but also amongst different inland waters.

2.1.3.3 Total Suspended Solids

TSS is the sum of the suspended organic and inorganic material in natural waters. It may include mineral particles, plankton, detritus, and volcanic ash. It is indicated by the commonly monitored turbidity. Similar to increases of CDOM, increases of TSS can have a negative impact on a water body's health and its aquatic inhabitants by blocking light and reducing photosynthesis and the rate of DO generation. If light is completely blocked from the bottom dwelling plants, these plants die and increase the demand of DO through decomposition by bacteria. High TSS can also increase the surface water temperature, as the suspended particles absorb heat from sunlight. This heat further depletes DO levels because warmer water holds less DO (USEPA, 1987). Other detrimental impacts associated with high TSS include the inability of fish to catch

food, clogging of their gills, reduced growth rates, decreases in resistance to disease, and the prevention of egg and larval development. Over longer time periods, this settling can reduce the size of water bodies and threaten their existence (Smith, 1992).

The absorption and scattering efficiency per unit weight of TSS in water is a function of particle size, shape, and refractive index (Kirk, 1994). As size, shape, and refractive index are variable with time and place, so too is the scattering efficiency. Figures 2.4 and 2.5 show the general response of light attenuation to the presence of TSS in a water body. Kirk (1994) indicates that light attenuation by TSS is predominately due to scatterance and not attenuation.

The general absorption trend shows a distinct minimum is evident around 590nm to 630nm and the maximum occurs at shorter wavelengths. In a review of several published scatterance cross-section spectra, Bukata *et al.* (1995) describe the general trend as relatively uneventful with increased scatterance towards the shorter wavelengths. As the scatterance cross-section spectra of Chilko Lake (Figure 2.5) was part of Bukata *et al.*'s 1995 review, it is in agreement with this physical description. However, Bukata *et al.* also confirm their observations by noting that they are similar to those observations made by Morel and Prieur (1977), who suggest that particulate scattering within the water column can be expressed as a power law distribution in wavelength, with an exponent ranging from 0 to -1.

2.1.3.4 Total Attenuance

Equations 2.6 and 2.7 dictate that the attenuation effects of each of these parameters must be summed along with those attenuation effects of pure water. Jerlov (1976) indicates that comparison of absorption and scattering shows that attenuance by water is dominated by its absorption effect (i.e. $a_w \gg b_{b(w)}$). Figures 2.4 and 2.5 show the absorption and scattering coefficients of pure water for the visible spectrum range. Within this range the water molecules act as a monochromator of blue light, by absorbing weakly within this range and increasing into the red and near-IR ranges, and conversely, scattering heavily in the blue range and decreasing into the red and near-IR ranges. This combined effect gives water its blue colour. The total absorption and total scatterance cross-sectional spectral for the Gallie and Murtha (1992) Chilko Lake data are also shown in Figures 2.4 and 2.5, and represent that which is detected by a remote sensing system.

2.2 Remote Sensing Systems

The collection of information without contact requires the application of remote sensing (Aronoff, 1995). Today, technology has advanced to such a degree that a variety of sensors are available to be mounted on manned and/or unmanned platforms to collect information and transmit it back over hundreds of metres, even kilometres or more. The major differentiating element of these various sensors is in their resolution, where recent increases in *spatial* and

spectral resolutions have improved the potential use of newer sensors to the detection of inland and coastal water quality.

Spatial resolution refers to the smallest spatially discernable target element, where the higher spatial resolution results in greater data volumes, as more information needs to be stored (Campbell, 2000). *Spectral* resolution refers to the smallest spectrally discernable target difference. To increase spectral resolution, a sensor's band widths and centre wavelengths can be adjusted to detect finer spectral differences, or the number of bands which a sensor is capable of detecting can be increased. The number of bands which a sensor is capable of detecting classifies it as a multispectral (~10) or a hyperspectral sensor (>200).

The majority of optical sensors are responsive to photons within a FOV defined by the geometric configuration of the optical device and are, therefore, generally recorded as radiance (Bukata *et al.*, 1995). The conversion of these radiance values through atmospheric correction allows for the comparison of results collected between multiple epochs or sites (Price *et al.*, 1995).

2.2.1 Airborne Remote Sensing

Remote sensors can be handheld or mounted onboard remote platforms such as airplanes and spaceborne satellites. As altitude of the sensor is increased, the scale of the imagery will become smaller and the amount of discernable detail is sacrificed for a better overall view.

Of the various platform levels available to researchers, the airborne level has shown to be very useful for testing experimental ideas at a pre-satellite stage, due to relatively easy accessibility as compared to spaceborne sensors (Harper, 1983). This easy accessibility allows for quick recovery of data, as well as instrument adaptation, calibration and maintenance. Unlike spaceborne sensors, airborne sensors can be flown for imaging in accordance with the optimum schedule of the phenomenon being researched. The use of an airborne sensor also allows for the avoidance of inclement weather and undesired cloud coverage (Harper, 1983). The Compact Airborne Spectrographic Imager (CASI) was employed for this study.

2.2.1.1 Compact Airborne Spectrographic Imager

The CASI system measures electromagnetic radiation between 405 and 950nm using a linear array charge couple device (CCD). It uses real-time attitude and GPS (differential or non-differential) measurements to provide geocoded imagery for information extraction. The sensor has two modes of operation, (i) *spectral*; and, (ii) *spatial* (Babey and Anger, 1989). It uses fixed bands when operated in its *spectral* mode and samples data in all 288 wavebands at 1.9nm increments across a 35° swath. However, in the sensor's second *spatial* operating mode, the system can be programmed to desired centre wavelengths and bandwidths to create up to 15 non-overlapping bands.

CASI's CCD dictates a fixed imaging array with dimensions 512x288 and is not restricted to airplane mounting, but can also be affixed to helicopters or crane booms. CASI is used for generating information for forestry, agriculture, water, military, and target identification applications (Wentzell-Brehme, 1999). Hu *et al.* (2000) used CASI in a forestry experiment to retrieve leaf area index and canopy closure over Thompson, Manitoba. Goel *et al.* (2003) employed a CASI in a precision agriculture experiment, to monitor nitrogen loadings in cornfields outside Montreal, Quebec. It has also been applied in several optical water studies such as: Jorgensen & Edelvang (2000), George & Malthus (2001), Östlund *et al.* (2001), and Shafique *et al.* (2001).

Where the CASI sensor is being used to image water quality, Bukata *et al.* (1995) suggest that image acquisition times be limited to within 2 to 3 hours of solar noon in order to avoid large amounts of surface reflection. Surface reflectance presence over water is related to both the solar zenith angle and water surface roughness and can overwhelm any water leaving radiance being targeted. Ideally, the water surface should be flat with no waves at all and imaging should only be acquired at solar zenith angles of ≤50°.

2.3 Review of Previous Studies

2.3.1 History of Ocean Colour Detection Sensors

The use of spaceborne remote sensing technology to provide spatial estimates of Chl-*a* concentration has been ongoing since the launch of the Coastal Zone Colour Scanner (CZCS) in 1978 (Matthews *et al.*, 2001a). The CZCS, aboard Nimbus-7 was the first satellite sensor to specifically target aquatic environments (Bukata *et al.*, 1995). Table 2.1 outlines the technical facts of the CZCS, as well as some of its successors. Reflectance measurements were collected at the blue and green wavelengths and related to Chl-*a* concentrations for open ocean waters using the widely accepted blue:green ratio method. Despite its name, the CZCS was not applied to coastal or other optically-complex waters due to its lack of sufficient spectral resolution (Bukata *et al.*, 1995).

After the CZCS ceased data collection in 1986, there was a long period without sensors designed specifically to target aquatic environments. In 1997, the Sea-viewing Wide Field-of-View Sensor (SeaWiFS) sensor was launched with a bandset similar to that of CZCS, but included the addition of a band at 412nm (to assist in the delineation of increase sensitivity for chlorophyll concentration estimations), as well as bands at 765nm and 865nm (near-IR bands to assist in the removal of atmospheric interventions) (Bukata *et al.*, 1995).

More recently, MODIS and MERIS (Medium Resolution Imaging Spectrometer) were launched in early 1999 and 2002. MODIS is a finer spectral resolution version of SeaWiFS with 36 contiguous 10nm bands in the 400-1040nm range, of which any 16 bands can be selected for transmission (NASA, 2005). Similarly, MERIS is capable of transmitting any programmable 15

TABLE 2.1: List of ocean colour sensors

SENSOR	DATES OF OPERATION	ORBIT	RESOLUTION			
			Spatial	Radiometric	Spectral	Temporal
SPACEBORNE SENSORS						
CZCS	Nov-78 to Jun-86	near-polar, sun-synchronous, 955km	825m	8 bit	Bnd 1: 430-450nm Bnd 2: 510-530nm Bnd 3: 540-560nm Bnd 4: 660-680nm Bnd 5: 700-800nm Bnd 6: 10.5-12.50um	daily
SeaWiFS	Sep-97 to present	near-polar, sun-synchronous, 705km	0.88km locally & 4km globally	16 bit	Bnd 1: 402-422nm Bnd 2: 433-453nm Bnd 3: 480-500nm Bnd 4: 500-522nm Bnd 5: 545-563nm Bnd 6: 660-680nm Bnd 7: 745-785nm Bnd 8: 845-885nm	daily
MODIS	1999 - present & 2002 - present	near-polar sun-synchronous 705km	250m (bnds 1&2) 500m (bnds 3-7) 1km (bnds 8-36)	12 bit	36 Bands (wavelength groupings)	daily
MERIS	Mar-02 to present		300m locally & 1.2km globally		up to 15 programmable (390 - 1040nm)	daily
AIRBORNE SENSORS						
CASI	1994 to present	N/A	varies with altitude	12 bit	up to 288 bands, range: 405-950nm	N/A

bands, but has a better spatial resolution of ~0.3km at nadir (ESA, 2005). Its mission not only includes the quantifying of phytoplankton distributions in the open oceans and coastal waters, but also the quantification of vegetation on the land surface (Rast *et al.*, 1999). MERIS shows improvement over SeaWiFS for the retrieval of Chl-*a* in turbid waters due to the inclusion of a band for the detection of the red/NIR edge (Gons *et al.*, 2002).

2.3.2 Developed Detection Techniques

Morel and Gordon (1980) categorized the different approaches used for the remote derivation of water parameter concentrations into three categories, including: (i) *analytical*; (ii) *empirical*; and, (iii) *semi-empirical*.

An *analytical* approach is an *a priori* deduction method that incorporates the inherent and apparent optical properties as they relate to reflectance (Kirk, 1994). These properties can be used to model reflectance or inversely used to predict parameter concentrations, as in Gitelson and Kondratyev (1991), Ammenberg *et al.* (2002), and Sathyendranath *et al.* (2004). The advantage of this approach is the creation of multitemporal algorithms for each of the parameters of interest.

Both the *empirical* and *semi-empirical* approaches are based on finding a purely statistical relationship between the parameter concentrations measured *in situ*, with a single band's reflectance or multiple band reflectance ratio. The difference between these two approaches is that the former does not use any prior knowledge and looks at all mathematically possible combinations, while the latter is limited to the bands that are anticipated to show statistical relationships with the parameters of interest's concentrations. An empirical approach has been applied in this study; however, Dekker *et al.* (1995) comment that this approach may produce false results because causal relationships between parameters are not necessarily implied.

2.3.2.1 Phytoplankton

Previous researches have established four semi-empirical means of relating R or R_{rs} with Chl-*a* concentration, including: (i) changes in the near-IR; (ii) changes in the blue & green; (iii) spectral slope changes; and, (iv) fluorescence line height (FLH) technique.

The first means is the simplest, which is to treat the remote sensing of Chl-*a* as a special case of suspended solids and associate any increased R or R_{rs} in the near-IR with an increase in biomass (Kirk, 1994). George and Malthus (2001) found a significant correlation (R^2=0.72) between Chl-*a* and a longer red band of a CASI sensor 10nm wide band centred on 685nm, for a series of lakes in north Wales.

Similarly, the second method associates increased absorption in the blue region with increased biomass. George and Malthus also noted a second significant correlation (R^2=0.75) between Chl-*a* and a 10nm wide blue band centre on 440nm, for the same series of lakes. This

method makes use of the fact that photosynthetic pigments absorb greatly at short wavelengths in the blue region of the visible range and decrease spectral reflectance. This approach is used regularly in open ocean waters where changes in optical absorption can be solely attributed to fluctuations of Chl-*a*. Clarke *et al.* (1970) measured Chl-*a*, ranging in value from <0.1 to 3.0mgm^{-3}, from low-flying aircraft using the spectral distribution of emergent flux from different regions of the Northwest Atlantic. In a review of amassed open ocean data sets containing coincident *in situ* Chl-*a* and R_{rs} measurements, O'Reilly *et al.* (1998) chose a blue/green ratio algorithm called the ocean chlorophyll 2 algorithm (OC2) as the at-launch SeaWiFS operational Chl-*a* algorithm. This algorithm was based on the principles of this empirical method and has been updated to the presently employed OC4 algorithm.

The third method associates localized changes to the shape of the spectral curve with changes in biomass. This method is similar to the red/near-IR and blue/green changes targeted in the previous two methods, however, is performed for all the bands available and can be carried out through examination of the first and second derivatives of the spectral curve for areas of major variation (Goodin *et al.*, 1993). In a tank experiment where the Chl-*a* concentration was incrementally diluted and spectra recorded, Goodin *et al.* (1993) noted a correlation between Chl-*a* concentration and the 2nd derivative at 660nm and 695nm with an R^2=0.89.

These first three methods make use of the fact that algal cells absorb light in certain regions of the spectrum, while the fourth semi-empirical method instead makes use of the fact that they also emit light. Algal cells re-emit about 1% of the light a photosynthesizing cell absorbs as *in vivo* fluorescence, with a peak at about 685nm, which can be seen in the upwelling spectrum (Kirk, 1994). Borstad *et al.* (1985) demonstrated that this peak could be used to map Chl-*a* from an airborne imaging spectrometer. Neville and Gower (1977) showed that *R* and Chl-*a* concentrations, ranging from 1-20μg/L, had an R^2=0.85 for British Columbia coastal waters using the FLH technique. Matthews *et al.* (2001a) comment that this FLH technique alleviates two of the problems encountered with the previously discussed methods. Firstly, since the fluorescence feature is narrow (~20nm wide), atmospheric effects do not alter greatly around the feature and do not cause major interference to the fluorescence from atmospheric absorption. Secondly, the fluorescence peak occurs in a part of the spectrum where reflectance from water and suspended sediments is low. Therefore, the FLH can still be employed in areas with high TSS loadings, such as coastal and inland waters. However, it is likely that this does not remain true in areas of extremely high concentrations of TSS, as absorption by TSS would then begin to play a role in reflectance attenuation.

2.3.2.2 Colour Dissolved Organic Matter

No empirically based study results were found directly relating CDOM with *R* or R_{rs}. It is believed that, since CDOM concentration is typically low in most marine waters and difficult to

distinguish from the total attenuance spectra, it has been omitted from Case II empirical water studies in favor of detection through *a priori* detection methods or by relating CDOM with measurements of salinity or DOC. Coble *et al.* (2004) indicate that as rivers are the main source of CDOM in coastal regions, there is often an inverse correlation between CDOM concentration and salinity, which results in high CDOM where salinity is low. Ferrari *et al.* (1996) showed that CDOM's natural fluorescent property of absorbing UV light and fluorescing blue light was highly correlated with DOC concentration.

2.3.2.3 Total Dissolved Solids

In a study of the southern coastal waters of Lake Superior, Warrington *et al.* (2002) employed SeaWiFS' band 5 (555nm) to empirically relate *in situ* water sample's TSS concentrations with simultaneously collected satellite R_{rs}. A linear regression line was fit to $R_{rs}(555)$ vs. *in situ* TSS with a resultant R^2 value of 0.94. This relationship was used to reveal a productive southern coastal corridor from Duluth Harbour to the tip of the Keweenaw Peninsula during spring and summer months, through the examination of time series satellite images of Lake Superior from 1998 to 1999.

Similarly, Jorgensen and Edelvang (2000) established another single band relationship between data collected with a CASI sensor and TSS *in situ* measurements, also using a green wavelength of λ=544nm. Sampling was conducted as part of a monitoring program during the construction of a combined tunnel and bridge across the coastal waters separating Denmark and Sweden. Dredging spills were creating a water plume dominated by TSS where Chl-*a* and CDOM were considered inconsequential on the developed single band relationship. The resultant algorithm, which was tested on both waters inside and outside of the plume, produced maps with an accuracy of R^2=0.97.

Prior to these studies, Kirk (1994) warned that the quest for a universal algorithm for TSS is never likely to come about no matter what band or combination of bands is used, as the scattering efficiency of suspended particles per unit weight is a function of size, which is variable with both time and place. He notes several Landsat studies from differing regions of the world with contradicting optimal wavelengths being reported (Table 2.2). Therefore any developed algorithms tend to be site specific.

TABLE 2.2: Previous Landsat vs. TSS studies

Study	Location	Landsat band correlated with TSS concentration
Ritchie *et al.* (1976)	Mississippi reservoirs, USA	700-800nm
Klemas *et al.* (1973)	Delaware Bay, USA	600-700nm
Brakel (1984)	Coastal waters, Kenya	700-800nm
Munday and Alfoldi (1979)	Bay of Fundy, Canada	600-700nm & 700-800nm
Bukata *et al.* (1974)	Lake Ontario, Canada	600-700nm
Ritchie *et al.* (1987) & Schiebe *et al.* (1992)	Moon Lake & Lake Chicot, USA	700-800nm

3.0 STUDY SITE

The study site consists of two individual water bodies: (i) Lake Cowichan, a fresh water inland environment; and, (ii) Cowichan Bay, a marine coastal environment. Although studied individually, these two water bodies are a part of the same watershed, with the former flowing into the latter via a 47 km length of river. This chapter commences by describing the watershed to which these two water bodies belong. It then describes both the lake and the bay individually in terms of their physiography, hydrography, biology, and socio-economics. Particular attention is focused on each water body's state in late August, as this time period coincides with the two-day intensive field campaign conducted for this study in late August 2003.

The Cowichan watershed was selected as to better understand a system subject to significant anthropogenic use. Heavy logging, mining and urban development began in the watershed approximately 150 years ago (Town of Lake Cowichan, 2003). In recent years, the extraction of natural resources has been scaled back and the harvesting of shellfish and crab closed due to concerns about contamination (Rideout *et al.*, 2000). A better understanding of such a system might help in future watershed management planning for similar watersheds around Vancouver Island and along British Columbia's coastline.

3.1 Cowichan Watershed

The optical properties of inland and coastal waters are influenced by many physical aspects of their surrounding watershed areas, such as topography, vegetation, hydrology, geology, and land use. Each of these components can be influential on the presence or absence of the parameters of interest (Meybeck, 1982) and thus a history of the watershed is presented.

The Cowichan watershed is a relatively undeveloped, but heavily logged, 940km^2 watershed on the south end of Vancouver Island, British Columbia, Canada. Located 30km north of Victoria (48.50° North latitude; 123.00° West longitude), the watershed sits in a glacial valley. The watershed consists of a large freshwater lake which outflows along a river into an estuary and eventually a neighbouring marine bay (Figure 3.1). The lake, river and bay are all situated lengthwise along the glacial valley's direction of strike. A valley with this geophysical layout is said to be *subsequent* in geological terms (Carl, 1953).

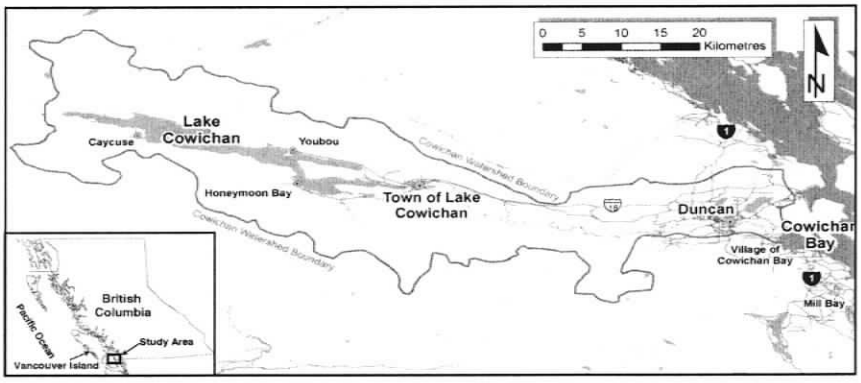


FIGURE 3.1: **The Cowichan Watershed is a subsequent valley that covers 940km^2 and drains into Cowichan Bay.**

3.1.1 Climate

The climate of the area is characteristic of British Columbia's mild and moist coastal region. Figure 3.2 shows the 30-year normal temperatures recorded by Environment Canada at monitoring stations near both Lake Cowichan and Cowichan Bay. There is little difference between the temperatures at these two locations, with only a slightly cooler (~0.5-1°C) temperature being recorded during summer and early autumn months at the bay. Generally throughout the watershed, summer air temperature rarely exceeds 28°C and winter temperatures only occasionally reach freezing temperatures, tending to favor a few degrees above 0°C. The annual average temperature for the watershed is 9.8°C, while it averages 17.7°C during the month of August. Despite these mild conditions, ice has been known to form on rare occasions in some areas of the surface of Lake Cowichan (Carl, 1953).

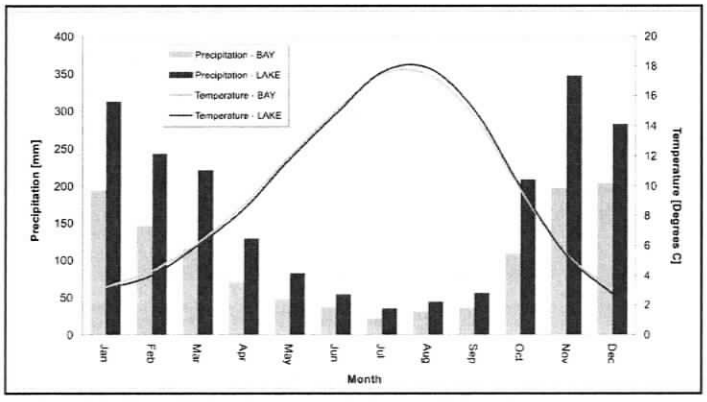


FIGURE 3.2: Cowichan watershed temperature and precipitation annual distributions (DATA SOURCE: Environment Canada 30-year normal data 1974-2003; BAY – *Duncan Forest* station @ 48° 46'N, 123° 40'W for 1974-1989 & *Duncan Kelvin Creek* station @ 48° 43'N, 123° 43'W for 1990-2003; LAKE – *Cowichan Lake Village* station @ 48° 49'N, 124° 03'W).

Precipitation patterns in the watershed are also characteristic of BC coastal region. The rainy season occurs during the winter months, between October and March (Figure 3.2). Precipitation falls as snow at the higher altitudes of the watershed and snow pack accumulation occurs. This accumulation contributes to an increased runoff input to the watershed's water bodies in the spring months with snowmelt. There is significantly more precipitation recorded at the lake station than at the bay station (~40% more monthly). The annual average precipitation fall is 2020mm at the lake and only 1211mm at the bay. August is the second driest month of the year at both stations, with an average rainfall of 44.4mm and 30.8mm at the lake and bay, respectively. July sees the least rainfall annually in both locations with low averages of only 35.8mm and 22.2mm at the lake and bay, respectively.

3.2 Lake Cowichan

3.2.1 Physiography

Lake Cowichan is a large oligotrophic lake located at an elevation of 162m above mean sea level. The lake has a surface area of 62km^2, an overall mean depth of 51m, and a maximum depth of 150m (Carl, 1953). The south arm is relatively shallow, with a maximum depth of 48 metres (Ministry of Environment, 1990). The lake bathymetry can be found in Appendix A. The lake sits at the most westerly extreme of the watershed and drains an area of 596km^2. It is a deep and narrow water body (approximately 34km long by 0.4-4km wide) and is the second largest freshwater lake on Vancouver Island (Lavin and McPhail, 1985) (Figure 3.3).

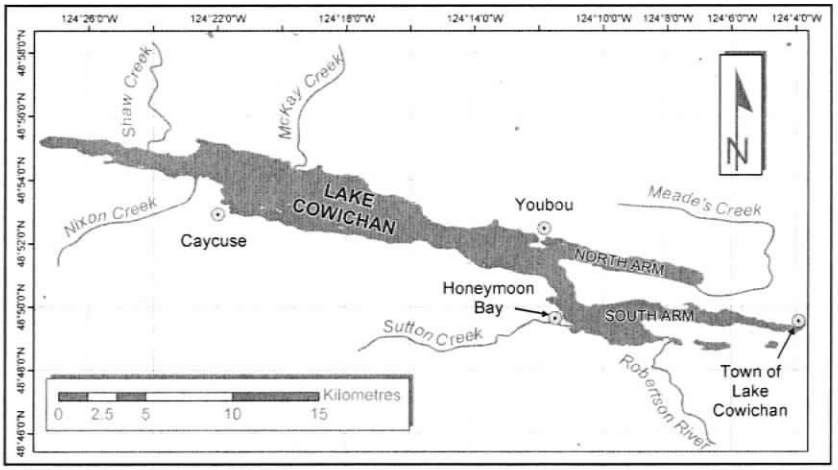


FIGURE 3.3: Lake Cowichan is a long and narrow oligotrophic lake located at an elevation of 162 metres above mean sea level.

3.2.2 Hydrography

Lake Cowichan is fed by five creeks (Shaw, Nixon, McKay, Sutton, and Meade's Creek) and one river (Robertson River). These surface water inputs are widely separated around the shores

of the lake and are characteristic of mountain streams, with gravelly reaches and swift, cold water (Carl, 1953). They tend to flood in the rainy season, moving gravel and boulders along their bottoms, and are reduced to trickles in the dry season, often with their relatively flat bottom reaches remaining completely dry. As the surrounding steep valley walls do not allow for much infiltration, there is very little contribution from groundwater input to the lake in the summer months. Carl (1953) does note the existence of a couple of submerged springs along the northern shore of the north arm of the lake. Direct precipitation interception by the lake is also a contributing factor due to the lake's large surface area.

Lake Cowichan flows out at a mean annual discharge of $53m^3/s$ through a provincially controlled weir structure, located in the Town of Lake Cowichan, and down the length of the Cowichan River (Rideout *et al.*, 2000). River discharge then passes through the Cowichan Estuary, remaining within a distinct flow channel, before spilling into the coastal marine environment of Cowichan Bay.

The lake's hydrograph indicates a slight time lag for river discharge response to precipitation events in 2003 (Figure 3.4). The lake's discharge remains relatively high through the month of April despite a decrease in precipitation, indicating the contribution from spring melt of the high altitude snow pack accumulation. August is the time when the watershed experiences its baseflow condition, however these baseflows, which represent solely groundwater contributions, are relatively negligible. Also evident from Figure 3.4 is that precipitation was also at its lowest during August 2003 with only 1mm of rain being measured. It should be noted that the hundred-year storm occurred in the month of October and is evident in the plot by the sharp peaks in both precipitation and discharge.

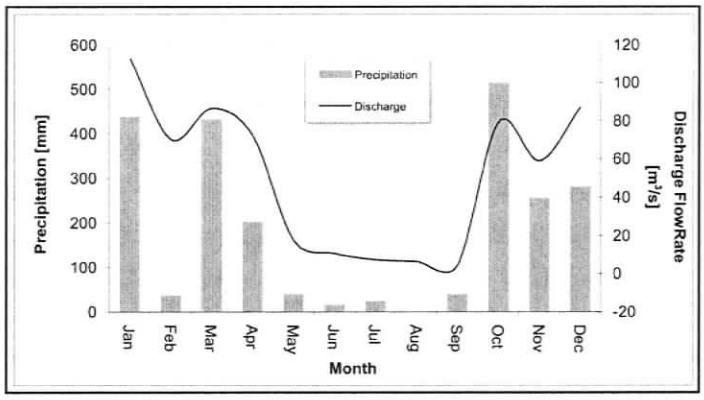


FIGURE 3.4: Lake Cowichan 2003 hydrograph (DATA SOURCE: Environment Canada, PRECIPITATION – *Cowichan Lake Village* station @ 48° 49'N, 124° 03'W & DISCHARGE – *Cowichan Lake Dam* station).

3.2.3 Biology

Potential contaminants to the Lake Cowichan water quality originate from a sawmill located at Youbou, a small abandoned base metal mine on the lake's north shore, public wharves near the outlet of the lake and direct sewage discharges into the lake from cottages and boat ballasts. Each of these potential contamination inputs could increase the concentrations of the parameters of interest study and subsequently the rate of eutrophication. Although no governmental water quality objectives have been set for the lake itself, a set of bacteriological criteria were invoked in 1989 for the Cowichan River water quality at the lake's outlet (Rideout *et al.*, 2000). These regulations were established due to the fact that the river is widely used between the lake and Island Highway bridge as a drinking water source and for primary contact recreation.

Only one study of this lake's biological conditions could be found. Carl (1953) summarizes the biological conditions observed in 1940 at Lake Cowichan. The author notes that although the results of a single year's sampling cannot be accepted as conclusive, they do indicate that the plankton productivity of the lake was low. Generally, the most abundant organisms, which included several types of protozoans, rotifers, copepods, and cladocera, exhibited peak conditions twice in a season: once in the late spring between April and June, and a second less pronounced peak in the fall. These two peak periods seem to coincide with the onset and deterioration of the summer stagnation period of the lake.

As Lake Cowichan rarely freezes, there are two primary temperature seasons, winter circulation and summer stagnation (Carl, 1953). The onset of thermal stratification in the lake usually begins between May and June, and the loss of stratification usually occurs in early December. The conditions in August 2003 were those of summer stagnation and together with the potential contaminant inputs described above and high summer temperatures, it was anticipated that the stagnate water body would contain reasonably high concentrations of plankton. The low precipitation of July and August 2003 (Figure 3.2) meant less contribution to the lake's TSS from land runoff sources.

3.3 Cowichan Bay

3.3.1 Physiography

Cowichan Bay is long and narrow in shape, and has a surface area of 13.5km^2. It sits with its elongated length following the Cowichan Valley's direction of strike and extends from the outlets of the Cowichan and Koksilah rivers to an imaginary line drawn between Separation and Cherry Points (Rideout *et al.*, 2000) (Figure 3.5). The westernmost 4.9 km^2 surface area is intertidal and considered the Cowichan Estuary, while the remainder is subtidal and the focus area for this study, where bottom reflection is not a concern.

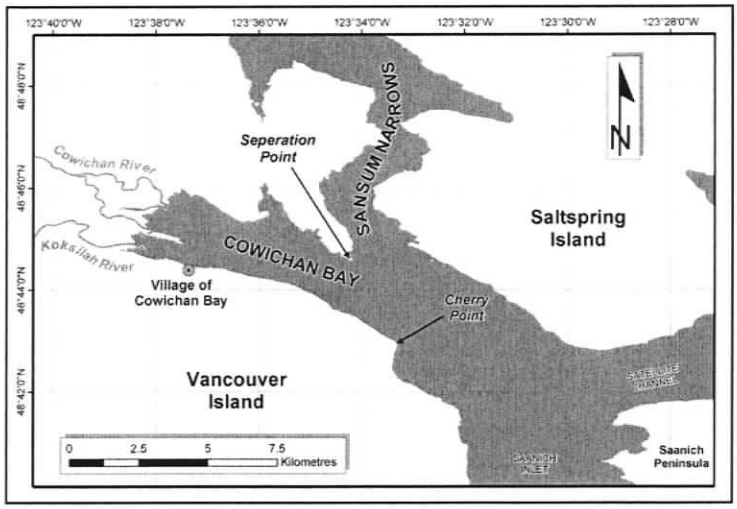


FIGURE 3.5: Cowichan Bay is a long and narrow coastal environment that sits at the outfall of both the Cowichan and Koksilah rivers.

3.3.2 Hydrography / Oceanography

Bell and Kallman (1979) found the waters of Cowichan Bay to be generally vertically stratified, with brackish waters overlaying salt waters. They attribute this to the combination of the bay being protected from the marine environment of the Strait of Georgia by the Gulf Islands, along with the bay's two prominent freshwater inputs, the Cowichan and Koksilah rivers. The majority of the bay's fresh water input comes from Lake Cowichan via the Cowichan River. The Koksilah watershed is a relatively small watershed that provides only a secondary freshwater input into the bay.

Unlike the lake's inputs, the Cowichan and Koksilah rivers do not dry up in the summer months. The Cowichan River monitoring station located at the river's confluence with the bay indicated that August 2003's average discharge was 4.47m^3/s. This flow is 28.4% below the 30-year normal August flow of 6.24m^3/s. The August 2003 average discharge from the Koksilah was not available, but given the diminished flow of the Cowichan, is presumed to have been similarly less than its 30-year normal August flow of 0.445m^3/s.

The average tidal volume represents approximately eleven percent of the volume of the bay (Rideout *et al.*, 2000). Unlike the neighbouring Saanich Inlet, Cowichan Bay does not have a submerged sill at its mouth and this allows for a good exchange of water with Satellite Channel. This exchange is further enhanced by the freshwater inputs of the Cowichan and Koksilah rivers. Rideout *et al.* (2000) also explain that although the mixing of surface waters and waters at depth is complicated, the primary source of new water to the bay is from Satellite Channel, while the two rivers are considered secondary sources. Hence, contaminants entering the bay from the

two rivers will tend to remain inshore to a greater degree in summer when river flows are lower and wind induced mixing is decreased.

3.3.3 Biology

Possible contamination sources to Cowichan Bay include those delivered via the Cowichan and Koksilah rivers as well as those located directly on the shores of the bay and on its surrounding lands. These sources include bacterial contamination from dairy farms near Dougan Lake, contaminants from the Cowichan Valley Regional District incinerator/landfill and gravel washing operations near Duncan. All of these possible contamination inputs could increase the parameters of interest within the bay.

Bell and Kallman (1979) found that there is very little information on the marine plankton concentrations and speciation of Cowichan Bay. However, they suspect that both the estuarine and marine plankton would be similar to those present in the nearby Fraser river outflow, which is also located in the southern Strait of Georgia.

Harrison *et al.* (1991) conducted a study of nutrient and plankton dynamics, including vertical profiling of temperature, salinity, fluorescence, nutrients, zooplankton, phytoplankton and bacterial biomass, for the Fraser River outflow into the Strait of Georgia. They found that primary productivity was highest in the outer part of the estuarine river plume and lowest in the riverine plume. They also found no variation in speciation with depth, where the primary phytoplankton observed, in terms of relative biovolume (72%), were the diatoms *Skeletonema costatum* and *Chaetoceros*. With sampling stations located inside and outside of the river plume, they determined that low primary production within the plume peaked in late July, while the higher primary production outside of the river plume occurred at a subsurface depth of 4-5m concurrently in late July.

Despite being physically closer to Cowichan Bay, a shallow sill at the opening of the Saanich Inlet (Thomson, 1981) compromises it as a dynamically different system and not necessarily an ideal point of comparison with Cowichan Bay's environment in terms of vertical distribution. However, Chl-*a* peaks in its surface waters have been considered potentially representative of Cowichan Bay's surface conditions.

Hobson (1980) and Takahashi *et al.* (1977) both observed that during 1975 and 1976 primary production in Saanich Inlet increased from a minimum in early spring to maximum values in summer, and then decreased to a minimum in the fall (Figure 3.6). In 1996, Sathyendranath *et al.* (2004) found Chl-*a* concentrations in the top 10m of the inlet were generally high, ranging from 3 to 22mg/m^3 during the spring and fall, with values of up to 40mg/m^3 being recorded during the summer months.

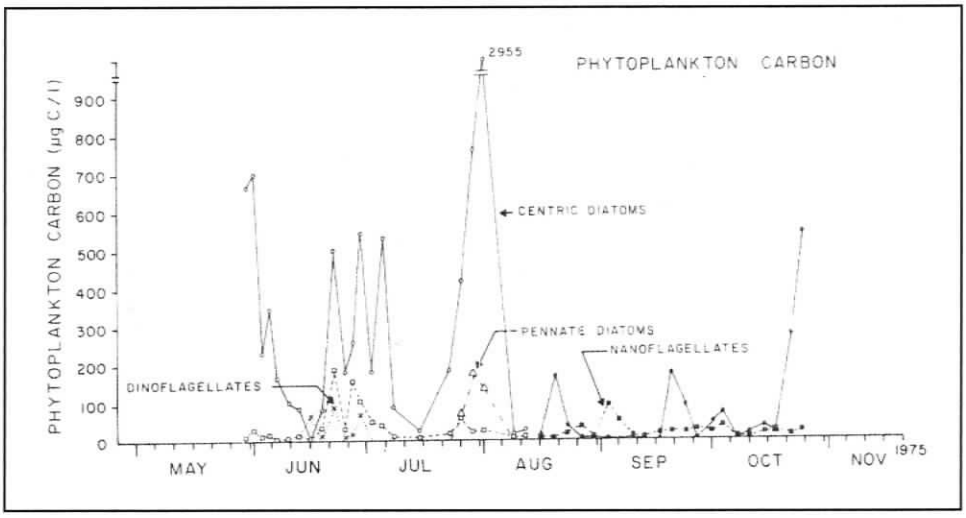


FIGURE 3.6: Phytoplankton carbon observations collected in 1975 Saanich Inlet from two stations (open vs closed symbols) indicated primary production in the top 10m of the water column increased from a minimum in early spring to maximum values in summer, and then decreased to a minimum in fall (adapted from Takahashi *et al.* 1977).

Predominantly southward tidal currents through the Sansum Narrows dictate that any bacteriological and nutrient inputs from the Cowichan and Koksilah watersheds are pushed southeasterly. Due to a very low river inflow and a weak tidal motion from the Saanich Inlet, as well as the sill separating the inlet from Satellite Channel, the majority of nutrients are then pushed through Satellite Channel and out towards the Strait of Georgia.

4.0 DATA COLLECTION AND ANALYSIS

A two-day field campaign was conducted in late August 2003, with sampling of Lake Cowichan on August 27th and sampling of Cowichan Bay on August 28th. This period was chosen for sampling as it has historically been the month with the least cloud coverage (Figure 4.1), a requirement for both CASI image acquisition and *in situ* spectral measurements. August is the month with the second least precipitation (Figure 3.2) and experiences elevated chlorophyll levels (Figure 3.6). The conditions during the field campaign and the preceding two weeks were similar to those recorded historically and no precipitation events were recorded. This chapter describes the data collected and the methodology used for its collection, as well as the analysis undertaken to extract useful information from the raw data.

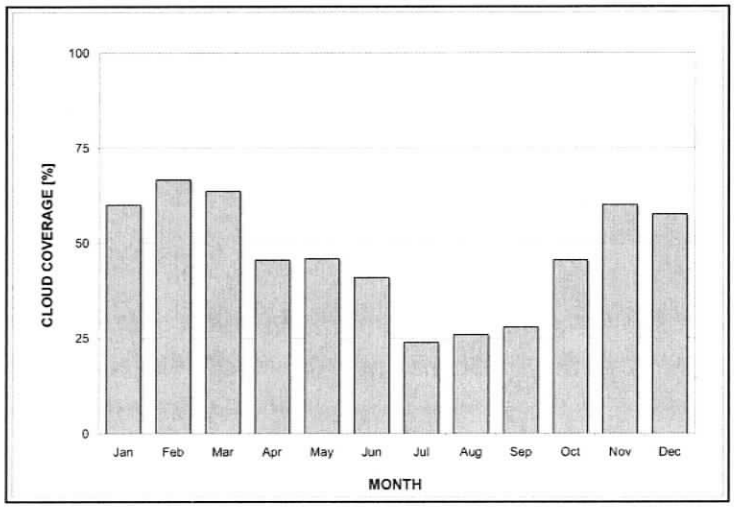


FIGURE 4.1: Historical average cloud coverage by month (DATA SOURCE: Canadian Centre for Remote Sensing - Earth Observation Catalogue, Landsat 5 and 7 preview imagery for 1997-2003).

The raw data consisted of concurrently collected datasets: (i) *in situ* surface water spectra; (ii) water samples; and, (iii) CASI imagery. Each of these datasets was collected for both study sites, Lake Cowichan and Cowichan Bay, under clear skies, between 9am and 4pm. Several teams were employed in order to minimize the time difference between the datasets for each of these dynamic study sites. Minimal time difference is crucial so that illumination conditions match between the collected *in situ* spectra and the CASI imagery, and also so that the water sample locations are as close as possible to CASI extracted spectra from the coincident coordinates.

4.1 *In situ* Spectra Collection

In situ spectra were collected using a Satlantic HyperSAS radiometer. The HyperSAS instrument measures spectra in the visible and near-infrared regions (VNIR) of the

electromagnetic spectrum, between 300-800nm at 3.3nm band widths. It collects: (i) *downwelling irradiance* (E_d); (ii) *downwelling* (indirect sky) *radiance* (L_d); and, iii) *upwelling* (total) *radiance* (L_u). The latter two were collected at 40° from zenith and nadir, respectively, as shown in Figure 4.2. The entire instrument was positioned looking at an azimuth (ϕ) angle of 90° away from the solar plane, where the azimuth is the angle between the directional bearing to the sun and a reference bearing, typically the North-South plane.

Proprietary software (Prosoft v7.7 a Matlab module developed by Satlantic Inc.) was used to deduce the data into 1nm bandwidth continuous spectra of spectral radiance units (SRU; $\mu W \bullet cm^{-1} \bullet sr^{-1} \bullet nm^{-1}$).

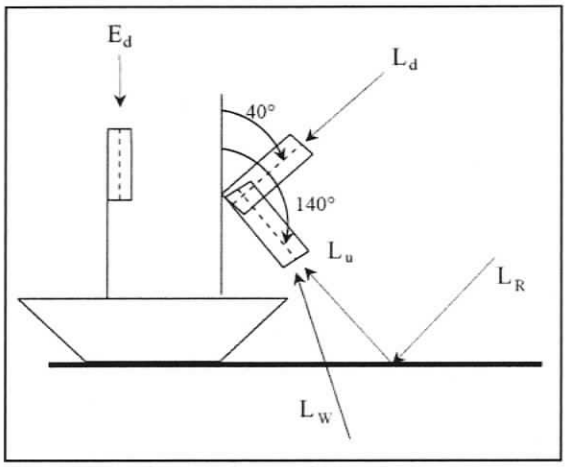


FIGURE 4.2: Satlantic HyperSAS configuration onboard research vessel. The recorded upwelling radiance (L_u) is the total of the radiance reflected by the water surface (L_R) and by the flux emerging from the water (L_W) (adapted from Gallagher, 2004).

Three *in situ* water spectra were collected from the surface of Lake Cowichan and five were collected from Cowichan Bay and the surrounding waters (Sansum Narrows, Satellite Channel, and Saanich Inlet) (Figures 4.3 and 4.4). Both sample sets were collected within three hours of their respective CASI image acquisitions. Two non-water spectra were also collected as potential future calibration targets. These targets include pavement in a local parking lot and recently cut grass in neighbouring lawn in the Village of Cowichan Bay. Due to logistics, these spectra were not collected until August 29th, one day and two days after collection over the lake and the bay. These measurements were made at the same time of day and under the same meteorological and solar conditions as present during the CASI acquisition. According to Smith and Milton (1999) this delay does not introduce any potential harmful effects, as pavement and grass are both spectrally stable over time.

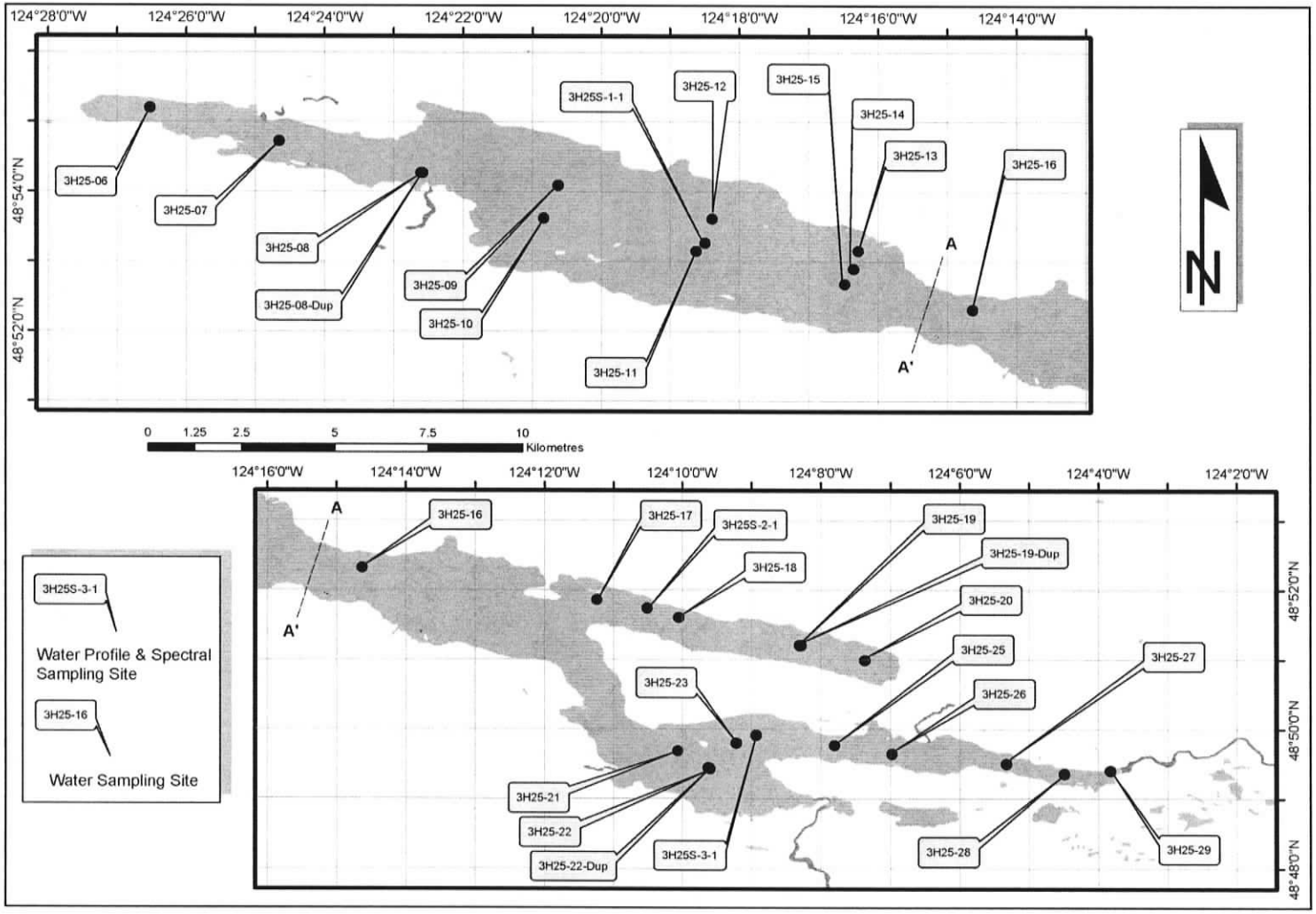


FIGURE 4.3: Sampling sites on Lake Cowichan; Date of collection August 27th, 2003.

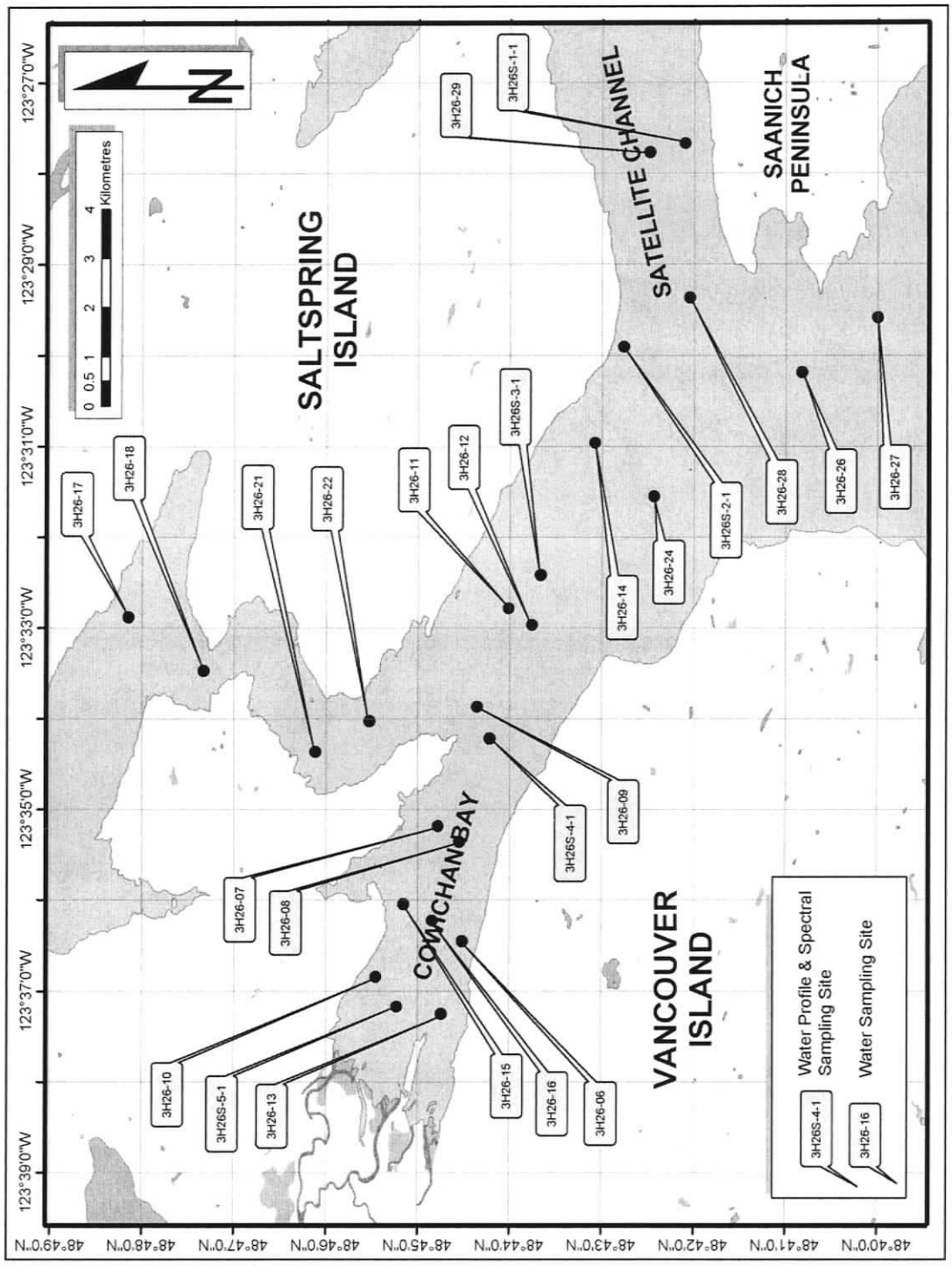


FIGURE 4.4: Sampling sites on Cowichan Bay; Date of collection August 28th, 2003.

4.2 Water Sampling

Horizontally distributed water samples were collected from Lake Cowichan, Cowichan Bay and its outlying waters. Sampling included thirty spatially distributed as indicated in Figures 4.3 and 4.4. Vertical profiling of Lake Cowichan confirmed the existence of the historically recorded temperature stratification (Figure 4.5a). For Cowichan Bay the historical vertical stratification of brackish waters overlaying salt waters was only narrowly evident (Figure 4.5b). This is most likely due to the seasonally low input of fresh waters from the Cowichan and Koksilah rivers.

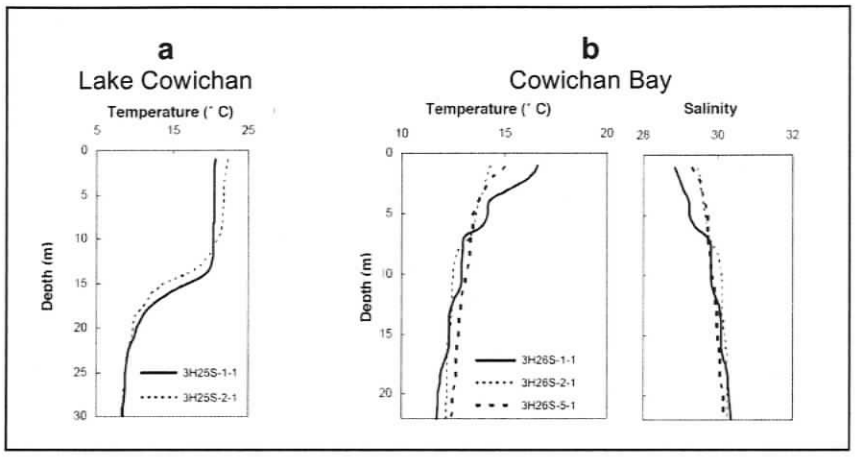


FIGURE 4.5: Vertical profile conditions in Lake Cowichan (a) and Cowichan Bay (b) in August 2003 (adapted from Gallagher, 2004).

4.2.1 Collection Methods

All water samples were collected within ~4 hours of image acquisition. The samples were collected using a reaching arm from a depth of approximately 0.5-1m below the water surface to avoid occasional surface debris floating on top of the water. One-litre high-density polyethylene (HDPE) Nalgene bottles were used for the collection and transportation of the water samples. These bottles are unreactive and reduce absorption to the surface walls of the bottle.

Prior to the field campaign all of the bottles were rinsed three times with de-ionized (DI) water. Rinsing ensured the removal of possible contaminants adhering to the container walls that could affect sampling results. Since the same containers were required for collection from both sample sites, sampling of the freshwaters of Lake Cowichan was conducted prior to sampling of the marine waters of Cowichan Bay. This order minimized the potential for site cross-contamination. Limited DI and time did not allow for re-rinsing of the containers between sampling of the two sites.

To further minimize potential for sample contamination, each of the sample collection containers was rinsed three times in the field with sample water prior to filling. The filled containers were then immediately stored in tupperware containers packed with ice. This storage

isolated the containers from direct sunlight and kept the samples chilled to minimize any changes in phytoplankton population within the containers. Filtering, preservation and transfer to fridge storage were conducted as soon as possible following return to shore. Completion of these processes was never longer than 12 hours from sampling for any of the samples.

All glassware and tweezers for the filtration system were thoroughly cleaned with DI prior to the field campaign. Careful measures were taken to ensure cleanliness was maintained during the filtration process. These measures included rinsing of the glassware and tweezers with DI between the filtering of samples. The filtration system included five filtration setups connected to two vacuum pumps. Each filtration setup consisted of a 1000mL glass collection flask, 300mL glass funnel, glass frit, and sealing clamp.

4.2.2 Laboratory Analysis

The methods of analysis employed are those found in *Standard Methods for the Examination of Water and Wastewater* (Clesceri *et al.*, 1998; hereon referred to as the "Standard Methods") and are described in the following subsections. The results of the laboratory analysis are available in Appendix B.

4.2.2.1 Chlorophyll-*a* (*Phytoplankton Proxy*)

Chlorophyll-*a* was determined spectrophotometric. For spectrophotometric analysis, sample water is filtered and the filter is stored in cold and dark conditions until analysis. This precaution is taken as any brief exposure to light during storage will alter chlorophyll values. For the analysis, the pigment is extracted from the filter and the resultant sample is then analyzed optically using a spectrophotometer. This instrument detects the magnitude of the chlorophyll absorption peak and determines the concentration present in a sample based on this value. The spectrophotometer uses narrow bandwidths of 0.5 to 2.0nm for detection of the absorption peak. Wider bandwidths may underestimate the Chl-*a* concentration (Clesceri *et al.*, 1998).

Procedure: Immediately following field sample collection, 1000mL of sample were passed through a 0.7μm glass-fiber filter (GF/F) using a standard vacuum setup. The filters were collected in falcon tubes, immediately covered with aluminum foil to prevent exposure to light, transferred to an airtight ziplock bag, and stored in a -20°C freezer. All falcon tubes were rinsed three times with DI prior to the field campaign. This rinsing ensured minimal contamination of samples when stored in the tubes.

For transportation from the field to the laboratory the filters had to be temporarily removed from the freezer and transferred in an ice packed cooler. The time spent in the cooler, prior to being transferred back to a –20°C freezer in the laboratory, was approximately three hours.

Analysis: Pigment extraction was carried out in a subdued light environment to avoid sample degradation. The pigments were extracted using a tissue grinder, because the chlorophyll

removal from cells varies considerably with different algae (Clesceri *et al.*, 1998) and a mechanical disruption of the cells is necessary. Due to their glass fiber makeup the use of GF/F filters assisted in breaking the cells during grinding.

The filter was then placed in the tissue grinder, covered with 2 to 3mL of 90% aqueous acetone solution and macerated for one minute. The sample was then transferred to a centrifuge tube and the grinder rinsed with a few milliliters of 90% aqueous acetone into the tube. The volume of the centrifuge tube was adjusted to a total volume of 10mL prior to being capped. The samples were then steeped at 4°C for a period of 2 hours. Following this the samples were clarified by centrifuge for a 20min period at 500*g* and extract decanted into a clean 15mL screw-cap centrifuge tube and the total volume was measured.

Optical density (OD) readings at 750, 664, 647, and 630nm were measured using a spectrophotometer to estimate chlorophyll-*a* in natural phytoplankton. The 750nm OD reading was considered a turbidity reading and subtracted from the other three OD readings as a means of turbidity correction.

Calculations: The concentration of Chl-*a* in the extract was calculated according to Jeffrey and Humphrey (1975) as follows:

$$C_a = 11.85(OD664) - 1.54(OD647) - 0.08(OD630) \quad \textbf{(4.1)}$$

After determining the concentration of pigment in the extract, the amount of pigment per unit volume was calculated as follows:

$$\text{Chlorophyll-}a\ [\text{mg/m}^3] = \frac{C_a \times \text{extract volume [L]}}{\text{volume of sample [m}^3\text{]}} \quad \textbf{(4.2)}$$

4.2.2.2 Colour Dissolved Organic Matter

CDOM was measured by determining the absorbance of filtered water at 440nm, using a spectrophotometer. This value is referred to as the samples g_{440} absorption (Kirk, 1994).

Procedure: Immediately following field sample collection, 1000mL of sample were passed through a GF/F filter using a standard vacuum setup. The filtrate was collected in HDPE sample bottles, which had been pre-rinsed with DI water three times to avoid sample contamination. The filled bottles were then stored in a refrigerator at 4°C until lab analysis could be conducted.

Analysis: Sample analysis was conducted using a spectrophotometer. Sample was transferred to a 1cm pathlength cuvette and the OD at 440nm was read. This analysis was conducted in a subdued light environment to avoid misreadings by the spectrophotometer.

Calculations: CDOM is reported as an absorption coefficient of water at 440nm (g_{440}), where the 'g' refers to one of CDOM's alternative names, *gilvin*. The absorption coefficient is reported as absorption per metre and calculated as follows:

$$g_{440} = 2.303 \times 100 \times OD440 \quad \textbf{(4.3)}$$

4.2.2.3 Total Suspended Solids

For the analysis of TSS, water sample is filtered through a GF/F of known weight. The filter and retained solids are dried to a constant weight and weighed. The difference in weight is attributed to the solids retained by the filter and represents the total suspended solids. Interferences can arise from large floating particles or submerged agglomerates of nonhomogeneous materials, which should be excluded if it is determined that their inclusion is not representative. Although no detection limit is listed in the Standard Methods (Clesceri *et al.*, 1998), sample size should yield 200mg residue to avoid the creation of a water-entrapping crust on the filter during filtration.

Procedure: The HVLP filters are known to lose part of their material makeup when subject to vacuum filtration. In order to minimize the loss of material during actual TSS sampling, the filters were subject to a prewash with DI prior to the field campaign. This prewash included the recording of the filter's initial "out-of-package weight", after which the filter was subject to a vacuum and wash with three successive 20mL portions of DI. These filters were then dried for a 1hr-time period at 80°C and cooled to room temperature in a desiccator. Their weights were read again and recorded as the filter's "initial weight". They were then stored in prepared aluminum foil envelopes. If these prewashings were not conducted, the loss of filter material could potentially be greater than the amount of TSS retained by the filter, resulting in false negative values.

Immediately following field sample collection, 1000mL of sample were passed through the prepared and pre-weighed HVLP filters using a standard vacuum setup. The used disk filters were twice folded into half to create a quarter circle shape. The filters were then returned to their aluminum foil envelopes with their pointed end down, so that any solids that might detach themselves through drying would remain inside the filter. The aluminum foil envelopes were kept in a vertical orientation to further ensure this prevention of material loss.

Analysis: The TSS sample aluminum foil envelopes were transferred to a drying oven with their flaps open for the drying of their contents. Drying was conducted for an hour at 80°C and the samples allowed to cool to room temperature. The filters were removed, weighed, and returned to their sample envelopes all the time in their upright orientation. The weight readings were recorded as the sample's "final weight". The samples were retained for potential future analysis of the sediments.

Calculation:

$$\text{mg total suspended solids/L} = \frac{(A-B)\times 1000}{\text{sample volume [mL]}} \qquad \textbf{(4.4)}$$

where, A = final weight, [mg] (weight of filter + dried residue)

B = initial weight, [mg] (weight of filter after prewash)

4.3 Airborne Imagery

Airborne imagery was acquired under clear sky conditions for both study sites. The data obtained by the sensor had to be corrected for the atmospheric contributions to the signal, as well as geometric issues. The following subsections describe the imagery's acquisition and preprocessing in detail.

4.3.1 Image Acquisition

CASI imagery was acquired by the Halifax based company Hyperspectral Data International (HDI). For this water investigation the sensor was flown at an altitude of 1500m and configured to collect data with a spatial resolution of $2m^2$, across 48 evenly distributed bands of approximately equal bandwidth (~11.5nm), between 417 and 952nm (Table 4.1). This configuration was used for the imaging of both Lake Cowichan and Cowichan Bay.

TABLE 4.1: Band configuration for CASI image acquisition

BAND	Centre Wavelength [nm]	Width (+/-) [nm]	BAND	Centre Wavelength [nm]	Width (+/-) [nm]
1	417.3	5.7	25	687.2	5.9
2	428.3	5.7	26	698.6	5.9
3	439.4	5.7	27	710.0	5.9
4	450.5	5.7	28	721.5	5.9
5	461.6	5.7	29	732.9	5.9
6	472.7	5.7	30	744.4	5.9
7	483.8	5.7	31	755.9	5.9
8	495.0	5.8	32	767.3	5.9
9	506.2	5.8	33	778.8	5.9
10	517.4	5.8	34	790.3	5.9
11	528.6	5.8	35	801.8	5.9
12	539.8	5.8	36	813.3	5.9
13	551.1	5.8	37	824.8	5.9
14	562.3	5.8	38	836.3	5.9
15	573.6	5.8	39	847.8	5.9
16	584.9	5.8	40	859.4	5.9
17	596.2	5.8	41	870.9	5.9
18	607.6	5.8	42	882.4	5.9
19	618.9	5.8	43	893.9	5.9
20	630.2	5.8	44	905.5	5.9
21	641.6	5.8	45	917.0	5.9
22	653.0	5.8	46	928.5	5.9
23	664.4	5.8	47	940.1	5.9
24	675.8	5.9	48	951.6	5.9

Two non-overlapping flightlines were acquired over Lake Cowichan, between 10 and 11am local time. Seven overlapping flightlines were used to encompass Cowichan Bay and its outlying waters (Figures 4.6 & 4.7), between 9 and 11am local time. Those flightlines directly over the bay were flown along parallel headings with approximately 40% overlap.

4.3.2 Image Processing

Before a comparison between imagery and water quality could be conducted, the CASI imagery had to be manipulated into a usable or processed form. Several steps were necessary to bring the raw data collected by the sensor to its processed state. Two remote sensing

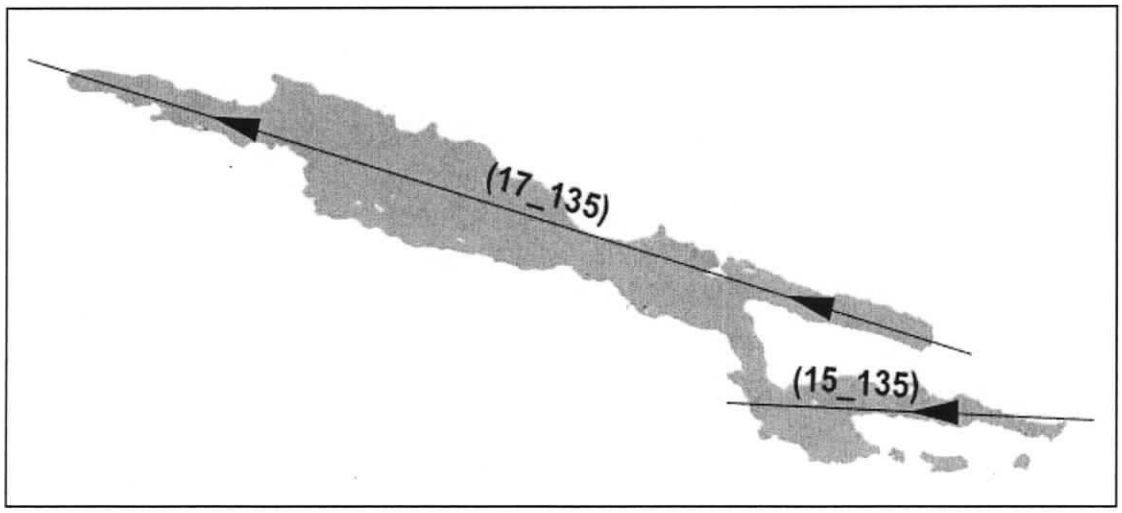


FIGURE: 4.6: CASI flightline # and location for acquisition over Lake Cowichan.

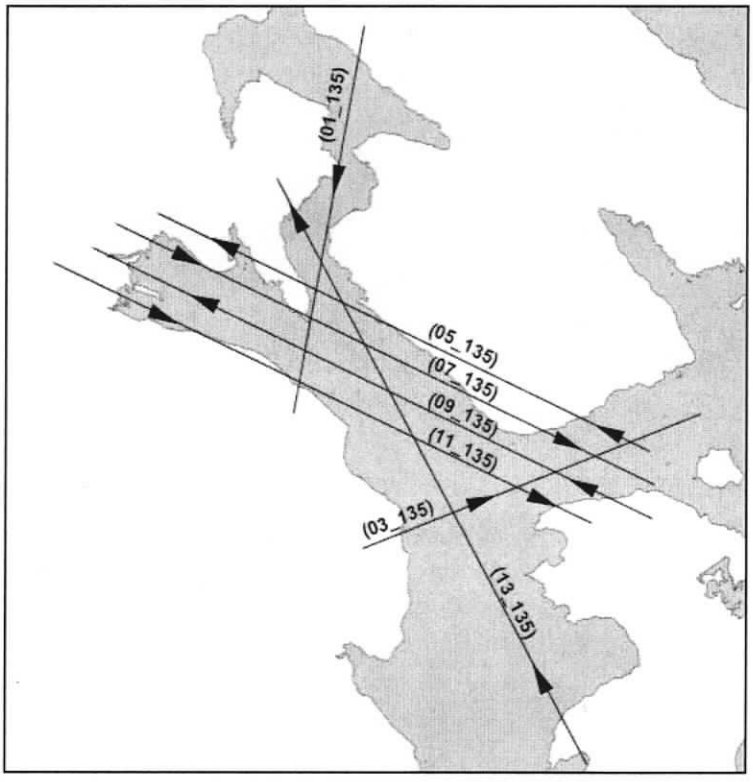


FIGURE: 4.7: CASI flightline # and location for acquisition over Cowichan Bay and its outlying waters.

software packages were used interchangeably for the various processing steps, (i) PCI Incorporated's Geomatica V9.1 and (ii) Research Systems Incorporated's ENVI 3.4.

Flightlines were processed individually prior to being arranged into final mosaics for both the lake and the bay. The majority of flightlines were delivered as two part files, for ease of data shipping, from HDI. Therefore, prior to any processing, the initial step was to rejoin the two sections of each two-part flightline into single files. A flow diagram outlining the steps taken in processing the CASI imagery is available in Appendix C.

4.3.2.1 Geometric Correction

Geometric correction is performed to register the image to a known co-ordinate system, which is accomplished through resampling of that image. This processing step was initially performed prior to data delivery by the acquisition consultants, HDI. However, the accuracy of their correction was found to be insufficient for sampling site location and mosaicking purposes, and was therefore re-performed. Östlund *et al.* (2001) experienced the same issue with CASI data collected by an outside consultant.

Geometric correction is a two-step process, including: (i) spatial; and, (ii) intensity interpolation. Spatial interpolation shifts a pixel's location in the uncorrected image (x',y') to its proper position in accordance with a geocorrected reference (x,y). A geocorrected reference is typically another image or a map already associated with a known co-ordinate system. The association is conducted through the identification of a set of ground control points (GCP) that are easily identifiable in both the uncorrected image and the geocorrected reference of the same area. These GCP are then used to develop a polynomial equation for the calculation of each pixel's relocation. According to Jensen (1996), for moderate distortions in a relatively small area, as is the case with this data, a first-order, six parameter, affine transformation is sufficient to rectify the imagery to a geographic frame of reference and is calculated as follows:

$$x' = a_0 + a_1x + a_2y \quad \& \quad y' = b_0 + b_1x + b_2y \qquad \textbf{(4.5 \& 4.6)}$$

where, a_0, a_1, a_2, b_0, b_1, and b_2 are constants describing the transformation functions.

Spatial interpolation was preformed on each flightline individually using a minimum of nine GCP. Land based GCP, which will not change position over time, were collected from orthorectified aerial photographs of the study area (Province of British Columbia, 2003). These aerial photos were defined in the Universal Transverse Mercator (UTM) coordinate system, using North American Datum 1983 (NAD83). To evaluate the accuracy of each correction, four extra "check GCPs" were collected from each flightline. The transformation equations were then applied to these GCP and the root-mean-square error (RMS_{error}) for each flighline was calculated.

$$RMS_{error} = \frac{\sum_{i=1}^{n} \sqrt{(x_i' - x_{i,orig})^2 + (y_i' - y_{i,orig})^2}}{n} \quad (4.7)$$

where, n is the number of "check GCP"

x_{orig} is the original image line

y_{orig} is the original image pixel

Table 4.2 summarizes the associated RMS_{error} with the geocorrection of each flightline. The resultant errors range from 4.88 to 9.20 pixels, which translates to a potential maximum positional error of approximately 18m. This amount of error is acceptable to this study because it is relatively small when compared to the accumulated errors due to GPS sample site location and time lags between image acquisition and sample collection. Also variability of the water parameters of interest over this distance would be too insignificant.

TABLE 4.2: Geometric correction RMS_{error} per flightline

Flight Line		RMS_{error}
ID	'NAME'	
- Lake Cowichan -		
15_135	South Arm	6.26
17_135	North Arm	4.88
- Cowichan Bay -		
01_135	Sansum Narrows	5.65
03_135	Satellite Channel	5.28
05_135	Cowichan Bay 1	6.96
07_135	Cowichan Bay 2	6.41
09_135	Cowichan Bay 3	9.20
11_135	Cowichan Bay 4	7.09
13_135	Saanich Inlet	4.97

The second step to geometric correction is intensity interpolation, which is commonly referred to as resampling. A first order nearest neighbour interpolation was selected for the resampling of the imagery, as it assigns pixel values of the nearest pixel in the input image to the pixel in the output image. The nearest neighbour algorithm keeps the original image information intact without any altering of pixel values.

4.3.2.2 Attenuation Correction

Each flightline was then calibrated for attenuance using ENVI's empirical line calibration. The ELC method of correction was selected over radiative transfer model packages because it was found that these commercially available models required variables, such as water vapour measurements and atmosphere visibility, which were not recorded in the field. An attempt to apply one of these model packages, ACORN, to the CASI data was attempted by HDI. They used generalized values for the input variables required by the model. It was found that the resultant CASI imagery was unusable for a water study, as the corrected spectra from water targets had been overcorrected. The spectra produced by the ACORN model did not exhibit the

expected shape of a water spectral distribution and much of the spectra was negative in value. This is a result of the reality that 95% of the radiance received by a satellite sensor over deep water may be due to atmospheric scattering. Verbyla (1995) describes the problem as analogous to attempting to take clear photographs on a foggy or smoky day. The ACORN model therefore nullified the targeted subtle spectral distribution originating from the water.

Alternatively, by using *in situ* above water spectra as reference input to an ELC, the CASI imagery was calibrated to a known spectrum of absolute R_{rs}. Above water spectra, collected coincident with the CASI acquisition for both Lake Cowichan and Cowichan Bay, were converted to R_{rs} and used as the reference *in situ* input for the ELC. This process was done separately for each set of flightlines from the lake and the bay. In both cases only one *in situ* reference target was used as reference spectra for the ELC. That *in situ* spectrum which was closest in time difference to CASI acquisition was considered as the most favourable reference target selection, as it represented the desired spectrum just above the water surface. However, these recorded surface spectra include both the radiance reflected off the water surface (L_R) and that emergent from below the water surface (L_W), where the latter is all that is desired (Figure 4.2).

The *in situ* spectra, hereon referred to as the *reference spectra*, were corrected for surface water reflectance by subtracting the reflection portion from the spectra in accordance to Mobley (1999). Mobley indicates that the surface water reflectance is calculated by multiplying the downwelling (indirect sky) radiance by a reflectance factor (ρ). This factor relates the radiance measured when the detector views the sky to the reflected sky radiance measured when the detector views the sea surface. It is sometimes called the *Fresnel coefficient*, which is incorrect as it only depends on this coefficient, but is not necessarily equal to it (Mobley, 1999). Therefore, ρ accounts for both the water surface conditions as well as the solar zenith angle, and R_{rs} can be calculated as follows:

$$R_{rs} = \frac{L_u - \rho L_d}{E_d} \qquad \textbf{(4.8)}$$

where, L_u is the total measured radiance

L_d is the indirect downwelling radiance

Post ELC, the corrected flightlines are considered to be above water R_{rs} spectra in units of per steradian, where the effects of both atmospheric attenuation and surface water reflection have been removed. It should be noted that the number of bands in these corrected flightlines was reduced during the ELC. This reduction in bands was due to the limitation of the *in situ* radiometer detection range of 300-800nm. Therefore CASI data beyond 800nm could not be corrected and bands 35-48 (refer to Table 4.1 for band configuration) were removed. The final band configuration for the atmospherically corrected CASI flightlines was limited to the first 34 bands collected.

4.3.2.3 Line-to-line Correction

Although individually corrected, those flightlines still exhibited subtle differences in radiometric levels and required normalization to one another. This was achieved by identifying one of the flightlines as the "master" and normalizing the others to its radiometric levels. This correction was preformed using the ELC application a second time, on the "secondary" flightlines, using areas of overlap with the master line to derive the necessary ELC coefficients. The line-to-line correction was only preformed on the set of flightlines for Cowichan Bay. It was not necessary for the two flight lines collected over the lake, as these were collected with an insignificant time lapse between them (~8min) and along roughly the same flight directional heading. The two flightlines did not share any overlapping coverage for R_{rs} matching purposes.

The CASI acquisition period over Cowichan Bay and its outlying waters took significantly longer (~70min) and therefore marine cycles were a concern. However, during the acquisition period the area's waters were in the process of shifting from an inward to an outward tide and currents were at a minimum, leading to minimal water shifting. As a result, distinct water masses could be easily identified in neighbouring flightlines. Spectra from these differing water masses, coincident to overlapping flightlines, were used as the reference inputs for the line-to-line correction of these flightlines. These spectra were extracted from the individual radiometrically corrected flightlines by collecting the mean average for a 10x10 pixel window for comparison.

Eight coincident spectra of varying R_{rs} brightness levels were extracted for each line-to-line correction. Four of these spectra were used to perform the ELC and the remainder used for evaluating the resultant line-to-line correction. This evaluation was performed by means of a statistical comparison of the "master" versus "secondary" spectra. The sums of the differences between the two spectra were calculated as follows:

$$\text{Sums of Diff.} = \sqrt{\frac{\sum_{i=1}^{n}\left(y_i - y'_i\right)^2}{n}} \qquad \textbf{(4.9)}$$

where, $y_i = R_{rs}$ for CASI band "i" in 'master' flightline

$y'_i = R_{rs}$ for CASI band "i" in 'secondary' flightline

n = total number of CASI bands

In order to present as percentages, the sums of differences were divided by a pooled average (Equation 4.11), where the pooled average was calculated as follows:

$$\text{Pooled Avg.} = \frac{\left(\sum_{i=1}^{n} y_i + \sum_{i=1}^{n} y'_i\right)}{2n} \qquad \textbf{(4.10)}$$

$$\text{Sums of Differences as \%} = \frac{\text{Sums of Differences}}{\text{Pooled Avgerage}} \quad (4.11)$$

Table 4.3 outlines the line-to-line radiometric correction results. The consistent decreases of sums of differences for each check spectra within each flightline indicates favorable radiometric matching to the master flightline. Line-to-line radiometric correction was not preformed on the "Satellite Channel" and "Cowichan Bay 1" flightlines (03_135 & 05_135), as they did not contain any water sample collection sites and therefore would not be necessary for comparison with CASI spectra.

TABLE 4.3: Line-to-line radiometric correction results; where flightline 'Cowichan Bay 3' (09_135) was used as the master to which all others were corrected.

Check Spectra #	Sums of Differences [%]	
	Prior to Line-to-line	Post Line-to-line
Flightline: 'Sansum Narrows' (01_135)		
1	15.0%	2.0%
2	11.7%	0.9%
3	14.1%	1.6%
4	10.5%	1.1%
Flightline: 'Cowichan Bay 2' (07_135)		
1	7.6%	1.7%
2	12.0%	5.5%
3	10.4%	3.7%
4	10.2%	3.9%
Flightline: 'Cowichan Bay 4' (11_135)		
1	2.9%	2.0%
2	3.1%	2.9%
3	5.4%	0.9%
4	4.9%	2.6%
Flightline: 'Saanich Inlet' (13_135)		
1	10.4%	1.8%
2	9.8%	0.8%
3	7.2%	4.2%
4	11.0%	3.4%

4.3.2.4 Mosaicking

Once the corrections were completed, the flightlines were mosaicked into image files of Lake Cowichan and Cowichan Bay (Figures 4.8 & 4.9). Where there was flightline overlap in the Cowichan Bay mosaic, it was ensured that the master flightline was the last to be overlain, to ensure its R_{rs} values remained the most valid.

4.3.2.5 Spectra Extraction

In order to draw a comparison between the CASI detected spectra and water quality, the spectral distributions for each water sampling location were extracted from the processed imagery. A 5x5 filtering extraction window was centred over the field recorded GPS coordinates collected at each of the sampling locations, as performed by Östlund *et al.*'s (2001).

Despite minimal movement by both Lake Cowichan and Cowichan Bay surface waters during data collection, the GPS coordinates for each sampling site's matching spectra provided only an

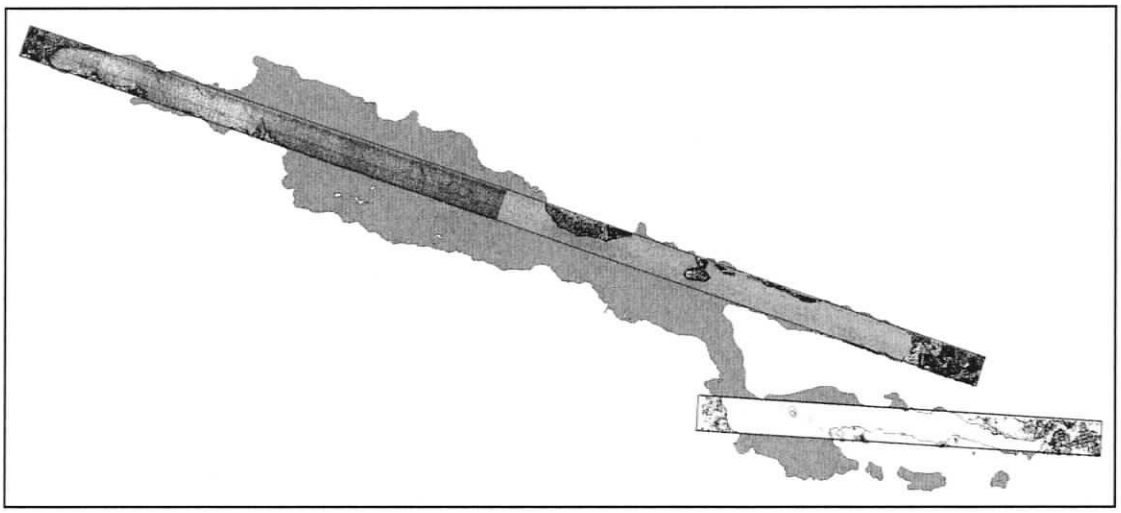


FIGURE: 4.8: Lake Cowichan mosaic of CASI flightlines.

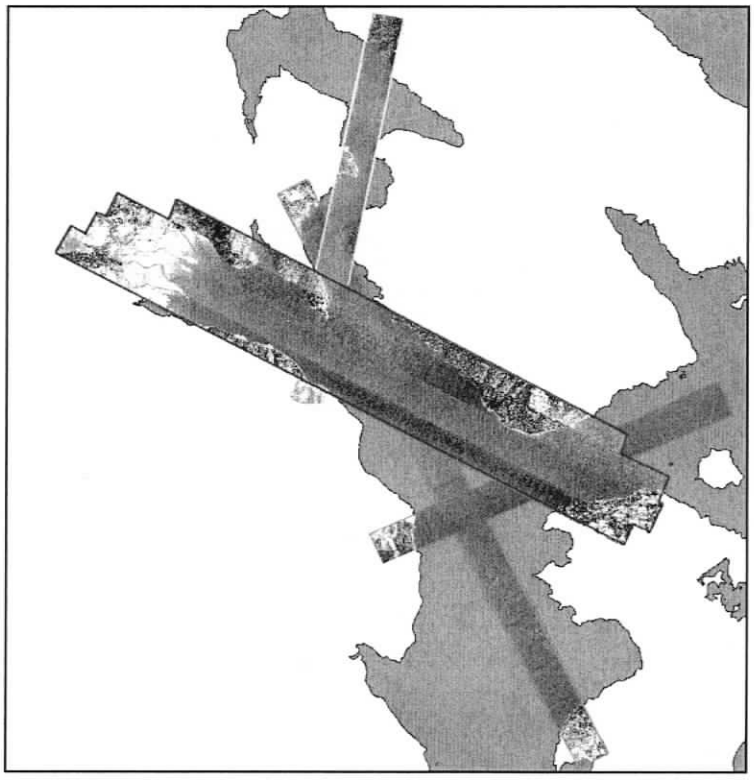


FIGURE: 4.9: Cowichan Bay mosaic of CASI flightlines.

initial indication of the location of the water mass from which the sample was collected. Some of the sample spectra windows had to be shifted slightly from the field recorded coordinates to fall within actual water masses sampled, which had shifted between sample collection and CASI acquisition.

The shifting of spectral extraction windows was guided by the strongest direct correlation initially observed between the parameters of interest and a single band R_{rs}. This initial correlation was performed using the extracted spectra from the field recorded coordinate locations. By allowing these initial trends to guide the shifting of the spectral extraction windows, an acceptance that the initially extracted spectra were generally representative of the actual correlations between the parameters of interest and the corrected imagery was necessary. The results of these initial correlations are presented in Appendix D for both the lake and the bay. The regression lines from the highest correlations, according to their scatter plot coefficient of determinations (R^2), were considered as the initial models, where the R^2 value represents the model's fit (Burt and Barber, 1996).

4.3.2.5.1 Lake Cowichan

Initially, a statistically significant correlation was achieved for the water parameter TSS at the 95% level of confidence, while none were found for either Chl-*a* nor for CDOM. Using this relationship as a guide, spectral extraction windows were then shifted slightly to accommodate higher or lower R_{rs} in the correlated bands. For example, the geographic position of those sample sites that were standing apart from the TSS regression line were shifted to locations nearby in the imagery from where the site sample was more likely to have been collected. These shifts were small in distance and generally were never more than 50 pixels or the equivalent of a maximum 100m on the ground. Upon completion of these shifts, the locations were considered the actual sample sites and correlation between all bands and the parameters of interest were examined.

The finalized spectral extraction windows produced statistically significant relationships for the prediction of each of the parameters of interest from a single CASI band. Each of these linear relationships exhibited the correct trend in terms of slope as was anticipated for the constituent and wavelength being considered. The final single band relationships for Lake Cowichan are available in Appendix D.

4.3.2.5.2 Cowichan Bay

Initially, statistically significant relationships were found for both the constituents Chl-*a* and TSS, while CDOM did not correlate well with any of the individual CASI bands. Upon completion of the shifting of spectral extraction windows the correlation trends observed for Chl-*a* and TSS

were as anticipated and CDOM remained uncorrelated with any individual CASI band. TSS correlated with R_{rs}462nm to produce a positive slope, favourable of the fact that an increase in TSS concentration is accompanied by an increased reflectance at 462nm. Similarly, the Chl-*a* trend produced a negative slope, favourable of the fact that an increased Chl-*a* concentration is accompanied by an increased absorption and therefore, decreased R_{rs}451nm. The final single band relationships for Cowichan Bay are available in Appendix D.

4.3.2.5.3 Finalized Spectra

To ensure that each of the final spectral extraction window positions produced representative mean spectra of a homogeneous water mass, the standard deviation (SD) and coefficient of variation (CV) were calculated, in accordance with Equations 4.12 & 4.13 (Burt and Barber, 1996), for each CASI band within each sample spectra. The finalized spectra, as well as their associated SD and CV, values are available in Appendix E, for both Lake Cowichan and Cowichan Bay.

$$SD = \sqrt{\frac{\sum_{i=1}^{i=5}\sum_{j=1}^{j=5}\left(X_{ij} - \overline{X}\right)^2}{24}} \qquad \textbf{(4.12)}$$

$$CV = \frac{SD}{\overline{X}} \qquad \textbf{(4.13)}$$

where, X = remote sensing reflectance (R_{rs}) value

Generally, the CV, which is a statistical measure of the deviation of a variable from its mean, ranged between a low of 1% and a high of 10% across all sample site spectra, indicating little variability. Consistently throughout all the extracted spectra, the CV was found to be lowest in the 450 - 650nm range and then increase as the wavelength increased into the NIR region, where the R_{rs} signal is small due to the strong water absorption bands. Due to this and relatively high CV values associated within the NIR region (around ~780nm) in more than one sample, the focus of this investigation was limited to a range of 400 - 750nm where CV values were found to be acceptable.

5.0 RESULTS AND DISCUSSION

This chapter presents and discusses the *in situ* spectra measurements, the laboratory analysis and extracted CASI spectra. It then summarizes the development of the final detection models for the parameters of interest. This is followed with statistical validation of these final models, along with their implementation and discussion thereof.

5.1 *In Situ* Spectra

The field collected *in situ* water surface spectra were used to atmospherically correct the CASI spectra to units of R_{rs} using the ELC technique. One water surface spectrum from the lake and one from the bay were used as input to the two ELC corrections. Figures 5.1a and 5.1b show the initial CASI spectra radiance versus their corrected R_{rs}. A reduction of the scattering process is clearly evident by the change in the blue and green regions of the curves. Overlain onto these two figures are the matching *in situ* surface spectra. Perfect correspondence is evident between the paired CASI and *in situ* R_{rs} spectra used as the ELC reference. The remaining spectra show proximity across the visible wavelengths, indicating favourable correction of the CASI spectra.

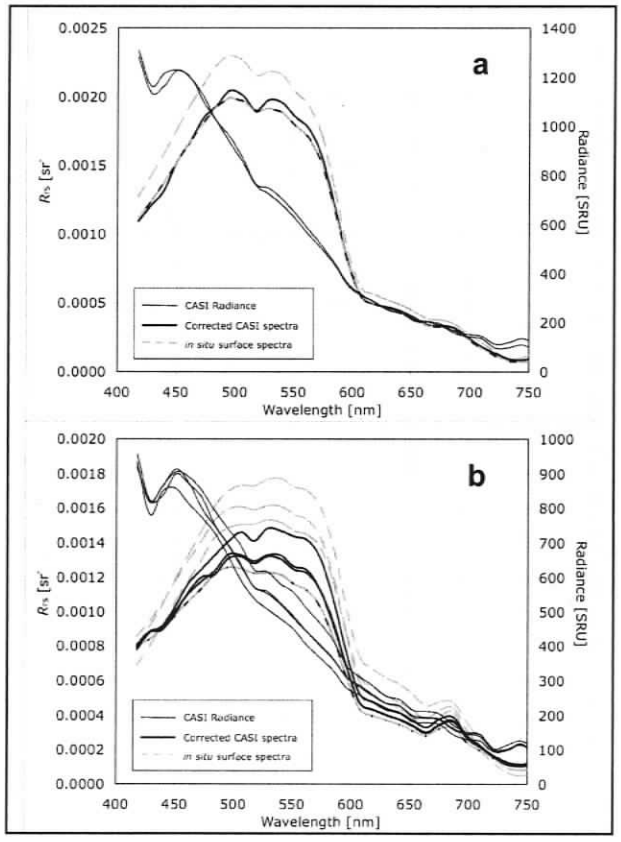


FIGURE: 5.1: Comparison of *in situ* water surface spectra, with matching CASI radiance and R_{rs} spectra; Lake Cowichan (a) and Cowichan Bay (b)

5.2 Water Quality

All results of the water quality laboratory analysis along with their associated errors are available in Appendix B. Replicate samples, reference samples and blank samples were employed in evaluating the analytical errors associated with these measurements. High errors were recorded for both Chl-*a* and CDOM measurements (±43% and ±57%, respectively). Recorded errors for TSS were relatively small (±9%).

Chl-*a* ranged between a low of 0.19μg/L and a high of 0.9μg/L in Lake Cowichan and between 0.75μg/L and 3.46μg/L in Cowichan Bay. While TSS ranged between 0.02 - 1.16mg/L and 4.41 - 6.69mg/L for the lake and the bay, respectively. Lastly, CDOM absorption at 440nm ranged between 0.12 - 1.57m^{-1} and 0.7 - 1.89m^{-1} for the lake and the bay, respectively. These measurements represent both low concentrations and small ranges. When combined with the high analytical errors for Chl-*a* and CDOM, the water sampling results indicate similar water quality throughout both the lake and the bay (Figures 5.2 and 5.3).

5.2.1 Parameter Correlations

Simple correlation coefficients between each of these parameters as well as with secchi disk measurements were calculated in order to detect any possible correlation between the parameters (Tables 5.1a & b). All relationships, except for two, were found to be insignificant at the 95% confidence level. The two cases of significance included (i) Secchi vs. TSS for the Lake Cowichan samples and (ii) Secchi vs. CDOM for the Cowichan Bay samples.

TABLE 5.1: Matrix of correlation coefficients for parameters of interest, plus secchi disk measurements: a. Lake Cowichan samples, b. Cowichan Bay samples; Values: R^2 and number of samples in brackets. * indicates those correlations significant at the 95% confidence level.

a

	Chl-*a*	CDOM	TSS	Secchi
Chl-*a*		0.001 (24)	0.019 (26)	0.016 (25)
CDOM			0.095 (25)	0.117 (24)
TSS				0.173* (26)
Secchi				

b

	Chl-*a*	CDOM	TSS	Secchi
Chl-*a*		0.010 (22)	0.006 (24)	0.120 (21)
CDOM			0.001 (21)	0.263* (18)
TSS				0.010 (20)
Secchi				

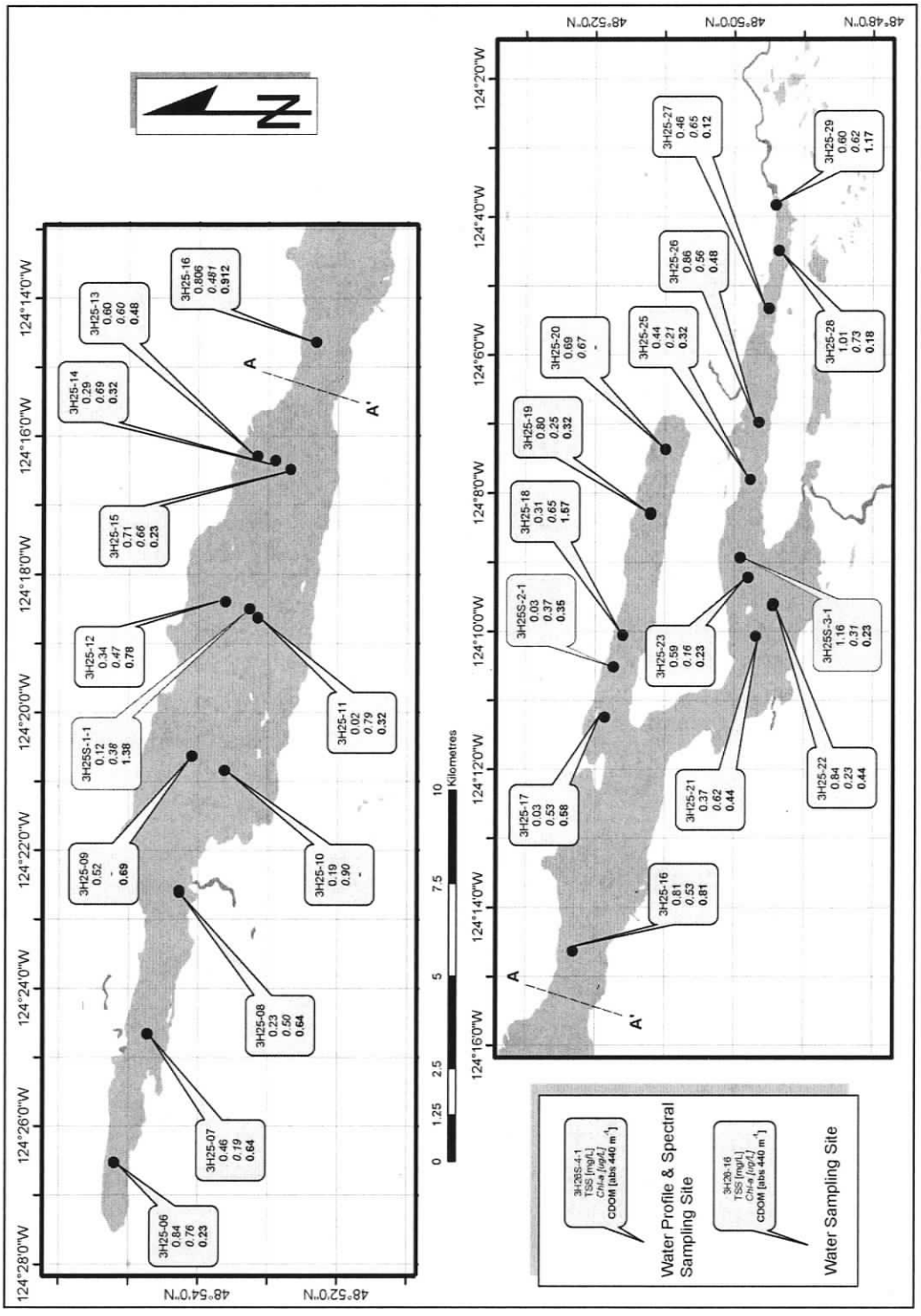


FIGURE 5.2: Sampling results for Lake Cowichan; Date of collection August 27th, 2003.

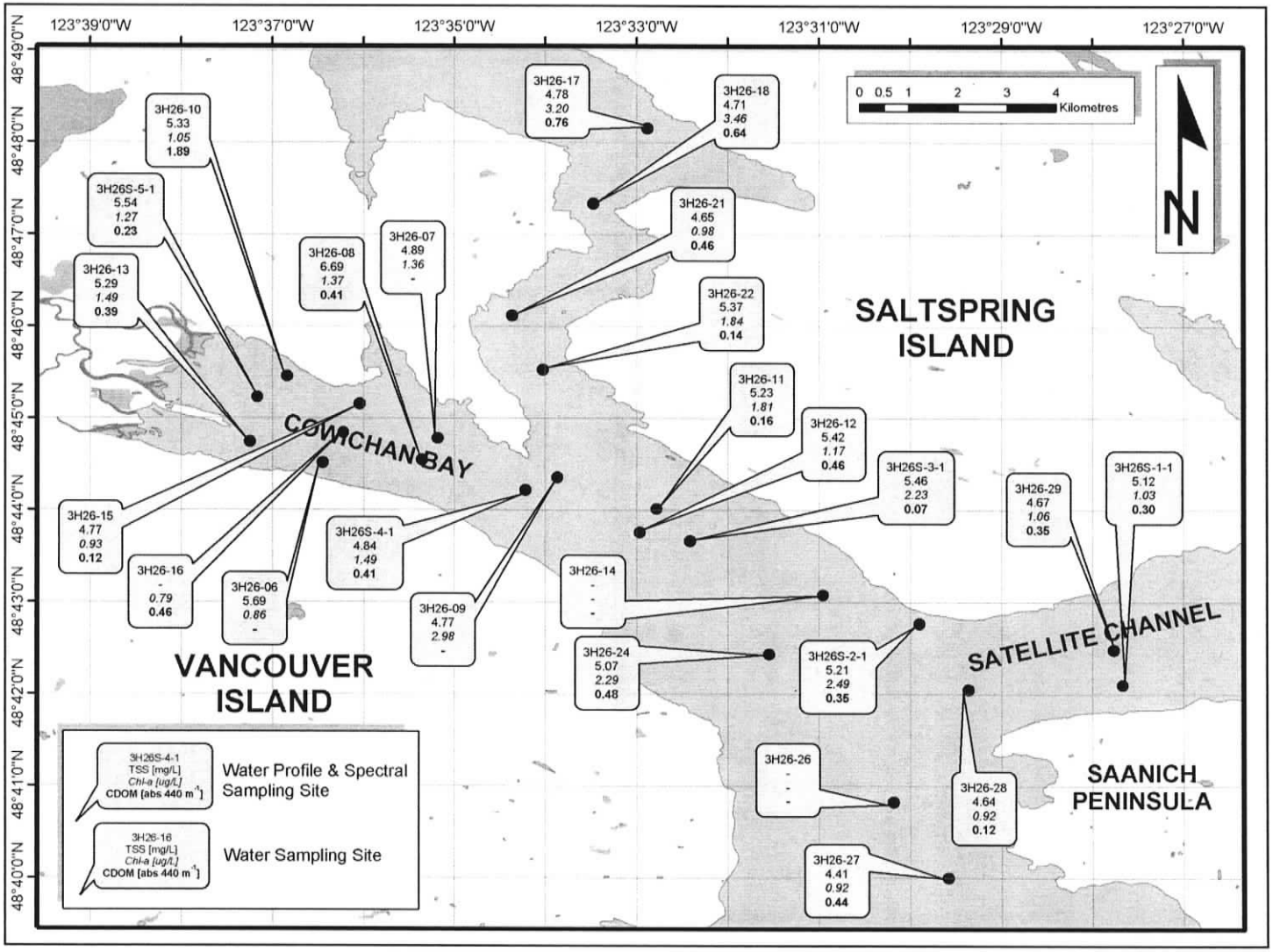


FIGURE 5.3: Sampling results for Cowichan Bay; Date of collection August 28th, 2003.

Statistically significant correlations between TSS and secchi measurements have been observed by researchers including Thiemann and Kaufmann (2002) and Lathrop (1992). Therefore, the correlation observed with the Lake Cowichan samples (Figure 5.4a) might be an indication of a potential alternative means of detecting TSS via the detection of secchi depths, where the above authors have successfully correlated secchi measurements with R_{rs} measurements.

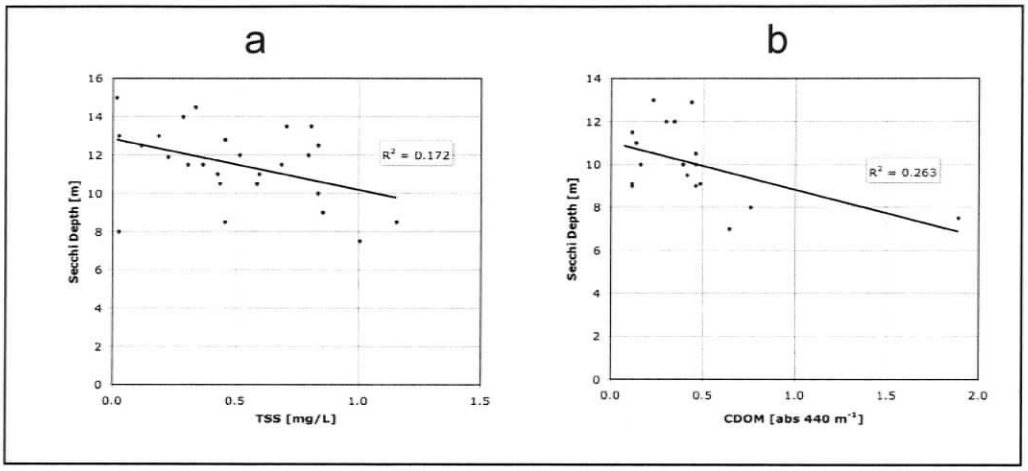


FIGURE: 5.4: Correlations of (a) secchi depth vs. TSS for Lake Cowichan samples and (b) secchi depth vs. CDOM for Cowichan Bay samples.

Upon closer examination of the significant correlation between the bay's secchi and CDOM measurements, it was found that the sample with the highest recorded CDOM absorption (Sample#: 3H26-10) was well removed from the cluster of all other samples and influencing the correlation significantly (Figure 5.4b). Without the inclusion of this one particular sample the correlation was found to no longer be significant.

5.2.2 Spatial Distribution

The low values and small range for each of the three parameters of interest for Lake Cowichan samples are indicative of a homogeneous surface distribution. It was anticipated that elevated levels of Chl-*a* and TSS would be detected in the lake's south arm and especially towards the eastern extreme due to the concentration of urban settlement along the shores of this area. However, the surface water quality did not vary and remained consistent with oligotrophic levels throughout the lake. These low levels and small range of values are likely a result of the lack of precipitation during the preceding month. This lack of precipitation meant that delivery of chemical nutrients and land based solids through runoff was limited and the lake's surface waters remained homogeneous and evenly distributed by natural causes, such as wind mixing.

Similar conditions of homogenous surface distributions were observed from the resultant Cowichan Bay samples. However, these samples did exhibit higher values and greater range of both Chl-*a* and TSS concentrations. These differences are an indication of the higher level of productivity in the bay. Despite the lack of precipitation in the weeks leading up to the study site sampling and the resultant same lack of land runoff, the bay receives a replenishment of the necessary chemical nutrients for productivity from the tidal induced exchange of waters with the surrounding marine environment waters (Satellite Channel and Sansum Narrows). Also contributing to the homogeneity of the bay's surface water quality was the low flow freshwater inputs from both the Cowichan and Koksilah rivers, which are a result of the aforementioned low precipitation. The observed Chl-*a* concentration values in the bay were slightly lower than those recorded in a detailed July and August survey of the nearby Strait of Georgia, which produced values from 3 to >5μg/L (Parsons *et al.* 1981). While Takahashi *et al.* (1977) recorded Chl-*a* concentrations in the neighbouring Saanich Inlet ranging from 3 to 22μg/L during the spring and the fall with Gower (1980) observing concentrations as high as 40μg/L in the inlet during the summer months.

The CDOM levels in both Lake Cowichan and Cowichan Bay were consistently low in concentration value and variability. The average CDOM value in Lake Cowichan was $0.53m^{-1}$, which is much less than averages recorded by Jewson and Taylor (1978) for lakes in Ireland, as well as lower than the average of $0.90m^{-1}$ recorded by Weidemann and Bannister (1986) for Lake Ontario. Relative to other coastal studies, the average CDOM value of $0.41m^{-1}$ recorded in Cowichan Bay is on par with observations reported by Gallegos *et al.* (1990) for Chesapeake Bay, as well as Kowalczuk *et al.* (2005) and Jerlov (1976) for coastal areas of the Baltic Sea. The recorded CDOM values showed very little variability with spatial distribution, giving no indication of regions of higher or lower concentration. In general, the average concentration levels were found to be slightly higher in the lake than in the bay, which is indicative that there is possibly greater decomposition of organic matter in the lake. Of note is the location of the highest CDOM recorded in Cowichan Bay, which is significantly higher than all other concentrations recorded in the bay and is coincident with the location of the Westcan Terminal log sorting plant. The decaying of logs stored in floating booms and the pieces of woody debris scattered in the water near this sampling location would account for the higher source of CDOM concentration.

5.3 CASI Spectra

A difference in spectral response between Lake Cowichan and Cowichan Bay waters is immediately evident upon examination of Figure 5.5, where all extracted CASI spectra have been plotted for both the lake and bay. Grouping of each water body's spectra is clearly seen with the bay's curves generally appearing flatter with a smaller overall range in R_{rs} and lower maxima. Through a simulation of above-water R_{rs} spectra from this study's dataset, Gallagher (2004) notes

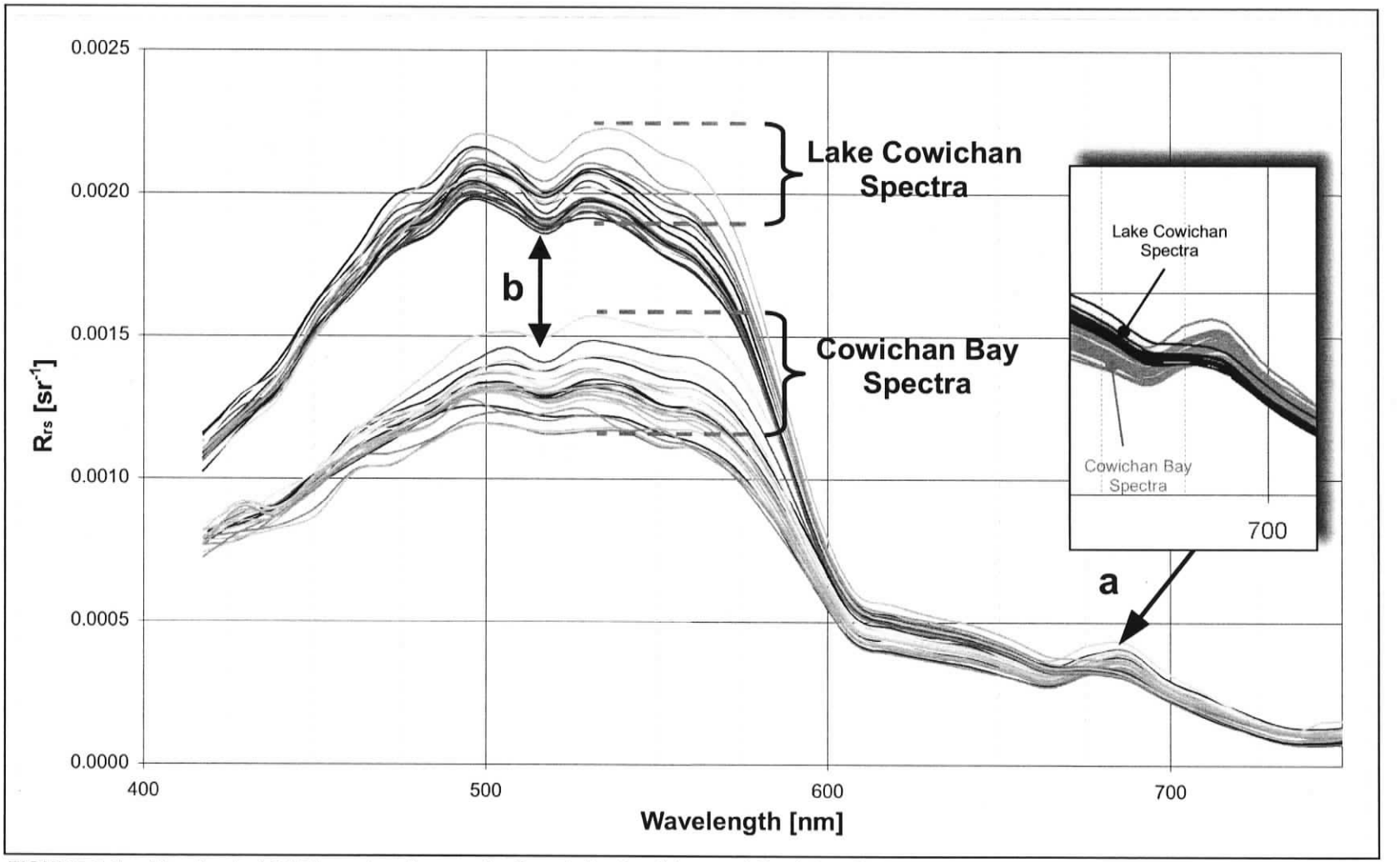


FIGURE 5.5: All extracted CASI spectra; the spectra from Lake Cowichan and Cowichan Bay are clustered together to form two distinct sets of spectra, where the lake spectra are generally brighter than those collected over the bay due to the higher concentrations of Chl-*a* and TSS found in the bay, which decrease R_{rs} through absorption.

that the total absorption is two orders of magnitude greater than total backscattering in both the lake and coastal waters. This is an indication that changes in total absorption tend to dominate the R_{rs} signal more so than changes in total backscattering. With higher TSS values recorded in the bay, it is expected that the two groupings be reversed with the bay spectra appearing brighter. However, the grouping configuration was recorded by three distinct instruments, including: (i) the CASI imager; (ii) the above water spectroradiometer; and, (iii) an in water spectroradiometer. All three of these instruments had been calibrated prior to the field campaign, where the in water spectroradiometer data were a part of Gallagher (2004). No determination of the percentages of organic versus inorganic TSS was conducted. It is probable that the majority of the TSS was in fact organic and increased total absorption, while it decreased total backscattering. Beyond 650nm the spectra from both the lake and the bay begin to coincide. However, the absorption by water at these wavelengths is so great that all spectra remain relatively low in signal strength.

Location 'a' in Figure 5.5 is an indication of the higher Chl-*a* in the bay's water. The two distinct groups of spectra have been uniformly coloured in the expanded window frame so that the increased absorption peak at 665nm is clearly identifiable in the bay spectra. Similarly, the fluorescence peak at 685nm is also made more identifiable as compared to any peak in the lake spectra. This fluorescence peak was also noted by Sathyendranath *et al.* (2004) in the neighbouring Saanich Inlet.

The impacts of absorption by CDOM on the spectra shape is made clear at location 'b' (Figure 5.5). At $\lambda \approx 518$nm a distinct valley in the spectra is identifiable in the Lake Cowichan spectra and not in the Cowichan Bay spectra. Pozdnyakov and Grassl (2003) indicate that this valley is a result of low CDOM in an experiment where chlorophyll and suspended sediments were maintained at constant low concentrations and CDOM was varied. The absorption by CDOM is in fact greater at wavelengths less than 518nm, however due to the relatively stronger absorption by Chl-*a* at these shorter wavelengths its effects are imperceptible. At wavelengths greater than 518nm, the absorption by CDOM is relatively weak and again indistinguishable in the R_{rs} spectra. Absorption by Chl-*a* is also responsible for the CDOM absorption valley feature at 518nm being evident only in the lake spectra and not in the bay spectra. The higher levels of Chl-*a* in Cowichan Bay dominate the absorption of R_{rs} at 518nm and therefore any absorption by CDOM, which exhibits equally low concentrations as detected in the lake, remains undetectable.

Variations within the groupings due to the parameters of interest were investigated. Individual plots of those spectra corresponding with the four lowest and four highest parameter concentrations are available in Appendix F. From these plots the general trends associated with increased CDOM and TSS are evident. The higher concentration CDOM spectra fall below the lower concentration spectra across the entire visible range due to increased absorptions. The higher concentration TSS spectra increase scattering and their spectra appear brighter between 480 to 570 nm then the lower observed TSS samples in both Lake Cowichan and Cowichan Bay.

5.4 Parameters of Interest Models

The development of the parameter of interest models was conducted separately for Lake Cowichan and Cowichan Bay. This decision was made due to the low ranges in water quality parameter concentrations and the fact that the collected CASI spectra were clustered into two distinct groups. The low ranges and small variability of parameter concentrations also led to the investigation of several modelling methods to check which would be more applicable to these conditions.

5.4.1 Model Development

The initial starting point for the empirical models' developments were the single band correlations with each of the parameters of interest discussed at the conclusion of chapter 4. These single band algorithms presented the highest direct correlations between the CASI bands collected and the parameter concentrations from each pair of sampling sites. Stepwise linear regression was conducted to potentially provide greater predictability then the single band algorithms. Also considered for model development are the techniques discussed in chapter 2, section 2.3.2, which include band ratios, derivative analysis, the FLH algorithm, and the OC4 algorithm. These last two only apply to the detection of Chl-*a*.

5.4.1.1 Single Band Linear Regression

Tables 5.2 and 5.3 summarize the strongest single band regression models as discussed at the conclusion of chapter 4.

TABLE 5.2: Lake Cowichan parameters of interest single band linear regression models.

PARAMETER	MODEL	R^2	SIGNIFIGANCE
Chl-*a*	= 2168.54(R_{rs}462) – 3.146465	0.172	Y (95%)
CDOM	= -2832.144(R_{rs}529) + 6.238066	0.348	Y (99%)
TSS	= 16727.97(R_{rs}699) – 3.452005	0.301	Y (99%)

Despite its statistical significance at the 95% level of confidence, the model for Chl-*a* in Lake Cowichan has not been considered as it has an incorrect direction of slope. The relationship between Chl-*a* concentration and 462nm should produce a negative slope where an increase in Chl-*a* would increase the absorption at 462nm and see a concurrent decrease in reflectance at this wavelength (Bukata *et al.*, 1995). According to the above Chl-*a* model, the opposite would occur given its positive slope. This unexpected slope may be the result of the small range in variability of the Chl-*a* concentrations between 0.16 and 0.9μg/L, which produces a tight cluster of results and decreases the chance for detecting a representative correlation.

The models for CDOM and TSS produce appropriate relationships with their respective wavelengths. According to Jerlov (1968), increased CDOM will increase adsorption at 529nm and therefore decrease reflectance at this wavelength, generating the negative slope exhibited by the model. Correlation with a shorter wavelength was anticipated in accordance with the absorption profile of CDOM (Figure 2.4). Bukata *et al.* (1995) note that even a small increase of TSS can substantially increase reflectance due to scattering in the longer visible wavelengths such as 699nm. In fact, reflectance is increased across the entire visible range due to TSS increases, with the reflection increase mounting towards longer wavelengths. This relationship was evident when all single band versus TSS correlations were examined in selecting the above TSS model and the highest R^2 values were associated with the longer wavelengths, where the relationship with 699nm produced the highest R^2.

TABLE 5.3: Cowichan Bay parameters of interest single band linear regression models.

PARAMETER	MODEL	R^2	SIGNIFIGANCE
Chl-*a*	= -12202.55(R_{rs}451) + 13.70614	0.388	Y (99%)
CDOM	= -3709.298(R_{rs}439) + 3.7342	0.097	N
TSS	= 8216.289(R_{rs}462) – 3.994347	0.523	Y (99%)

Bukata *et al.* (1995) show that the largest changes in reflectance due to changes in Chl-*a* occur in the 430-460nm range. The strongest single band Chl-*a* model produced for the bay was found to be within this range at 451nm. The statistically significant model has predicted a negative slope as is to be expected for the relationship between Chl-*a* concentration and this wavelength.

No statistically significant single band model could be found for the prediction of CDOM in the bay, which may be a result of the low absorption values recorded in the bay. The CDOM model listed in Table 5.3 is that of the band producing the highest correlation, but is not considered because of its lack of significance.

The above TSS model was not expected as it shows a significant relationship with a shorter wavelength. This is most likely due to the higher levels of Chl-*a* present in the bay, relative to the lake, which can change the overall attenuance curve to the degree that TSS is not necessarily best correlated with the longer wavelengths.

5.4.1.2 Stepwise Linear Regression

Stepwise linear regression was applied to the data set to determine if a multiple regression model employing more than a single band might provide stronger predictability of each of the parameters of interest. The stepwise regression technique can be applied in either a forward or reverse direction, where the available independent variables (in this case the individual CASI

bands) are either added or removed, respectively, to or from the prediction model based upon their contribution to the model's predictability (Hair *et al.*, 1998).

SPSS for Windows, version 11.0.1, was employed in a forward stepwise regression, where CASI bands 1 through 31 were considered as the available variables for the regression model. With each step the most statistically significant term, that with the lowest P-value, was added until there were no significant terms left. The P-value is an indication of the independent term's ability to predict the dependent variable. It is also possible to start with a subset of all the terms and then add significant terms; therefore, the single bands outlined in section 5.4.1.1 were assigned as the starting subset for each parameter of interest. The resultant regression models for both the lake and the bay parameters of interest are presented in Tables 5.4 and 5.5.

TABLE 5.4: Lake Cowichan parameters of interest model results of stepwise regression.

PARAMETER	MODEL	R^2	SIGNIFIGANCE
Chl-*a*	$= 2168.54(R_{rs}462) - 3.146465$	0.172	Y (95%)
CDOM	$= -15747.4(R_{rs}529) + 15202.491(R_{rs}517) - 6292.969(R_{rs}417) + 9.629$	0.632	Y (99%)
TSS	$= 16727.97(R_{rs}699) - 3.452005$	0.301	Y (99%)

The stepwise regression lake models only improved upon the CDOM model, where no further significant variables were added to either the TSS or Chl-*a* models. The two bands added to the CDOM model were both of wavelengths less than 529nm, which is to be expected as absorption by CDOM increases with shorter wavelengths. There were no additions to the other two models, most likely due to high correlation between the R_{rs} of the individual CASI bands. Again, because of its incorrect slope direction, the Chl-*a* model is not considered despite its statistical significance.

TABLE 5.5: Cowichan Bay parameters of interest model results of stepwise regression.

PARAMETER	MODEL	R^2	SIGNIFIGANCE
Chl-*a*	$= -18365.8(R_{rs}451) + 6369.098(R_{rs}585) - 23228.4(R_{rs}756) + 16.474$	0.537	Y (99%)
CDOM	-	-	-
TSS	$= 8216.289(R_{rs}462) - 3.994347$	0.523	Y (99%)

The stepwise regression bay models only improved upon the Chl-*a* model, where a green (585nm) and a NIR (756nm) band were added to the regression model. The green band coincides with an absorption minimum in the Chl-*a* absorption spectra, thus making it a good prediction band. Similarly, the NIR band added is coincident with the second absorption minimum. As wavelength is increased from red further into the NIR region, absorption by Chl-*a* decreases significantly (Jensen, 2000). In this instance, 756nm represents the longest

wavelength from the range being considered (417–756nm) and reflects the overall absorption minima within this range. No further significant variables were included in the TSS model, again most likely due to high correlation between the individual bands. Also, no significant variables were found for a CDOM model.

5.4.1.3 Band Ratios

All possible band ratios were correlated with each of the parameters of interest in hopes of finding a suitable ratio for prediction purposes, as the use of reflectance ratios has been shown to reduce the effects of changes in illumination conditions (Doxaran *et al.*, 2002a). Band ratio models have been successfully applied in the detection of TSS in coastal waters by Matthews *et al.* (2001b), as well as in the detection of Chl-*a* in turbid reservoir waters by Han and Rundquist (1997). The correlation coefficient between the ratio of each pair of bands and a parameter's concentration can be visualized using a two-dimensional correlation matrix. This type of figure aids in the identification of those ratios that provide the strongest correlation with the parameter's concentration. These correlation matrices can be found in Appendix G.

Tables 5.6 and 5.7 summarize the most significant band ratio to parameters of interest relationships, made evident by examination of the correlation matrices.

TABLE 5.6: Lake Cowichan parameters of interest model results of band rationing technique.

PARAMETER	MODEL	R^2	SIGNIFIGANCE
Chl-*a*	= -15.291(R_{rs}630/R_{rs}608) + 13.508	0.301	Y (99%)
CDOM	= 22.244(R_{rs}517/R_{rs}529) - 20.887	0.414	Y (99%)
TSS	= -5.7175(R_{rs}506/R_{rs}574) + 7.6824	0.353	Y (99%)

Band ratio models for Chl-*a* and TSS produced statistically stronger relationships than the previous single and multiple band regression models of sections 5.4.1.1 and 5.4.1.2. The ratio of 630:608nm takes advantage of the rising slope towards the second peak at ~665nm in the Chl-*a* absorption spectrum to provide a statistically stronger model. The ratio of 506:574nm falls within the range of ratios showing correlation with suspended sediment concentrations as noted in Matthews *et al.* (2001b). The multiple regression model for CDOM prediction remains as the statistically strongest model.

TABLE 5.7: Cowichan Bay parameters of interest model results of band rationing technique.

PARAMETER	MODEL	R^2	SIGNIFIGANCE
Chl-*a*	= 12.651(R_{rs}417/R_{rs}451) - 8.462	0.413	Y (99%)
CDOM	= 25.566(R_{rs}722/R_{rs}439) - 4.1452	0.381	Y (99%)
TSS	= 14.944(R_{rs}540/R_{rs}517) - 10.052	0.360	Y (99%)

Examination of the bay's strongest resultant band ratio models indicates that the technique did not provide statistically stronger models for either Chl-*a* or TSS. However, it did provide a statistically significant model for CDOM, where one could not be found through either single or multiple band regression. When the discovered ratio is compared to the correlation between CDOM concentration and its g_{440} value, the above NIR to blue ratio of 722:439nm reveals similarities. The ratio accounts for absorption at 439nm and also at 722nm, where the latter should show no absorption in the CDOM absorption spectra and therefore act as a baseline comparison point in this ratio.

5.4.1.4 Derivative Analysis

Derivative analysis techniques enhance minute fluctuations in reflectance spectra and separate closely related absorption features (Louchard *et al.*, 2002). An example of this is the use of derivative analysis by analytical chemists working in remote sensing to reduce background signal and to resolve overlapping features (Goodin *et al.*, 1993).

The first derivative is the slope of the R_{rs} spectrum as a function of wavelength and has a value of zero at wavelengths that correspond to maxima and minima in the original spectrum. Similarly, the second derivative has a value of zero where the first derivative reaches a minimum or maximum. These points correspond to points of inflection in the original curve and thus aid in identifying features that characterize the spectra. The first derivatives' spectra and their parent sample spectra are available in Appendix E. Where the first derivative for the n^{th} band in each sample spectrum has been calculated in accordance with Equation 5.1 (Louchard *et al.*, 2002).

$$\left.\frac{\partial R_{rs}}{\partial \lambda}\right|_n \approx \frac{R_{rs,n+1} - R_{rs,n}}{\lambda_{n+1} - \lambda_n} \qquad \textbf{(5.1)}$$

As was performed in sections 5.4.1.1 and 5.4.1.2, linear and stepwise linear regression analysis was then carried out with the first derivative spectrum replacing the sampled spectrum for each sampling location. Tables 5.8 and 5.9 summarize the resultant models found through derivative analysis.

TABLE 5.8: Lake Cowichan parameters of interest model results from derivative analysis; where "Dev670" refers to the first derivative at the wavelength 670nm.

PARAMETER	MODEL	R^2	SIGNIFIGANCE
Chl-*a*	= -333487(Dev670) + 0.4534	0.255	Y (95%)
	= -250917(Dev670) - 439769(Dev613) - 193951(Dev625) + 38232.69(Dev591) + 48567.535(Dev456) - 1.409	0.785	Y (99%)
CDOM	= -119657(Dev523) + 1.335	0.444	Y (99%)
	= -145945(Dev523) + 255688.3(Dev647) + 116992.6(Dev545) + 75814.2(Dev501) + 3.853	0.688	Y (99%)
TSS	= -72058(Dev579) - 1.9636	0.277	Y (99%)
	= -72324.9(Dev579) - 891671(Dev727) + 354882.5(Dev670) - 5.074	0.454	Y (99%)

The multiple regression models produced using the first derivative spectra for the lake show statistically stronger relationships for each of the three parameters of interest over the previously developed single band, multi-band, and band ratio models. The above single derivative Chl-*a* prediction model is reflective of the rising slope of the Chl-a fluorescence peak centred at 685nm. Fraser (1998) predicted Chl-*a* with the use of Dev695, which targets the same feature in the reflectance of chlorophyll, but on its downward slope. A variety of shorter wavelength derivatives were added in the step-wise regression analysis, indicating that several distinct minute features exist in the R_{rs} spectra.

The above single band CDOM prediction focuses on the change in slope in a relatively flat region of the CDOM absorption spectra. It is not known why this derivative was resultant as the derivative at shorter wavelength was anticipated, where the slope changes in the CDOM absorption curve are greater. Even the additional derivatives included during the step-wise analysis fall within the red and NIR regions. This might be an indication that very minute changes in curve inflections, which are only visible through derivative analysis, exist in this region of the CDOM reflection curve.

Fraser (1998) also managed to use derivative analysis in the development of two separate regression models for the prediction of TSS, where the most significant single derivative models were based on Dev429 and Dev628. Although site specific for its study site, Fraser's research indicates TSS correlates with both derivatives in the shortwave blue region of the electromagnetic spectrum and with the longer wave red wavelengths. In the above single derivative TSS prediction equation, the model focuses on the relatively large descent in the TSS scattering cross-section. Longer wavelength derivatives were added in the step-wise regression.

In general, all of the above models have the highest correlation of the models considered thus far, due to the low parameter concentrations in Lake Cowichan. Already the water leaving R_{rs} is only a small fraction of the signal recorded at the sensor, so with these low concentrations the changes to the water leaving R_{rs} due to the parameters of interest will be even more difficult to detect. These low concentrations and small variability in ranges do not allow for the most

expectant correlations to be dominant and correlations through a derivative analysis technique is therefore more apt to detect the very subtle changes in the R_{rs} spectra.

TABLE 5.9: Cowichan Bay parameters of interest model results from derivative analysis; where "Dev445" refers to the first derivative at the wavelength 445nm.

PARAMETER	MODEL	R^2	SIGNIFIGANCE
Chl-*a*	= -174804(Dev445) + 3.2185	0.238	Y (99%)
	No further improvements by multiple linear regression		
CDOM	= -62199(Dev434) + 0.582	0.338	Y (99%)
	= -57539.2(Dev434) + 439357.3(Dev636) +1.395	0.422	Y (99%)
TSS	= 144259(Dev523) + 4.6477	0.280	Y (99%)
	No further improvements by multiple linear regression		

In Cowichan Bay the concentrations of both Chl-*a* and TSS were much higher than those of the lake and, therefore, no statistically stronger models for the prediction of either parameter were found through derivative analysis. However, the multiple regression model for the prediction of CDOM in the bay was found to be statistically stronger than any of the previously developed models. This again is most likely due to the very low concentrations and ranges of CDOM recorded in the bay.

5.4.1.5 Fluorescence Line Height

The FLH is calculated from the peak in the reflectance spectrum centred around 682nm, which is a result of chlorophyll fluorescence (Gower, 1980). Gower *et al.* (1999) calculate the FLH in accordance with equation 5.2, where the height of the peak is measured from a baseline defined by the signals of two adjacent wavelengths (Figure 5.6), which are less influenced by chlorophyll fluorescence (664 & 699nm). An average of CASI bands 24 and 25 (675.8nm & 687.2nm) was used for λ_2, as none of the collected bands were centred at 682nm. CASI bands 23 and 26 (664.4nm and 698.6nm) were used for λ_1 and λ_3, respectively. In this study, R_{rs} has been used in place of water-leaving radiance to account for the type of spectra extracted from the CASI imagery.

$$\mathrm{FLH} = R_{rs}(\lambda_2) - R_{rs}(\lambda_1) - \left[R_{rs}(\lambda_3) - R_{rs}(\lambda_1)\right] \times \frac{(\lambda_2 - \lambda_1)}{(\lambda_3 - \lambda_1)} \qquad \textbf{(5.2)}$$

where, $\lambda_1 = 664\text{nm}$

$\lambda_2 = 682\text{nm}$

$\lambda_3 = 699\text{nm}$

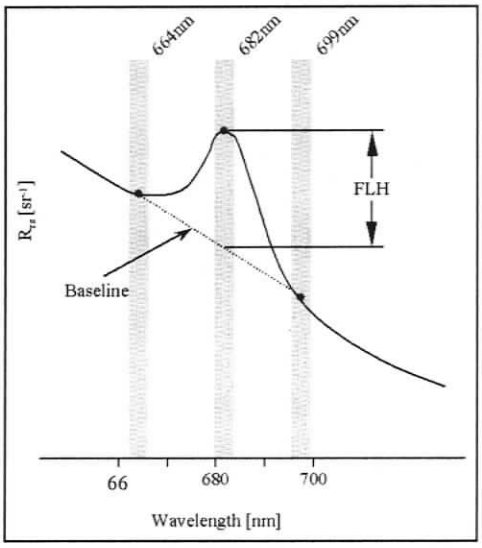


FIGURE: 5.6: Calculation of fluorescence line height; where FLH is the height of the peak centred at 682nm, above the baseline.

The relationships between the Chl-*a* concentrations and the calculated FLH values did not produce statistically strong enough models to warrant their consideration over previously developed models. It is of note that the relationship for the lake dataset did produce a statistically significant relationship at the 95% confidence level. The results of the FLH algorithm applied to the Lake Cowichan and Cowichan Bay datasets can be found in Appendix H.

Chl-*a* concentrations and FLH values for both study sites were combined for an investigation of the FLH technique to the overall dataset (Figure 5.7). Despite a statistically significant relationship and overlapping ranges in Chl-*a* concentration ranges, it is evident that the calculated FLH values are clustered according to their respective study sites. The cluster of lower FLH values are those of Lake Cowichan, where the lower Chl-*a* concentrations were recorded, indicating a less pronounced fluorescence signal. This clustering is likely due to the lack of radiometric correction between the flightlines from the two study sites and the cause of the algorithm's statistical significance.

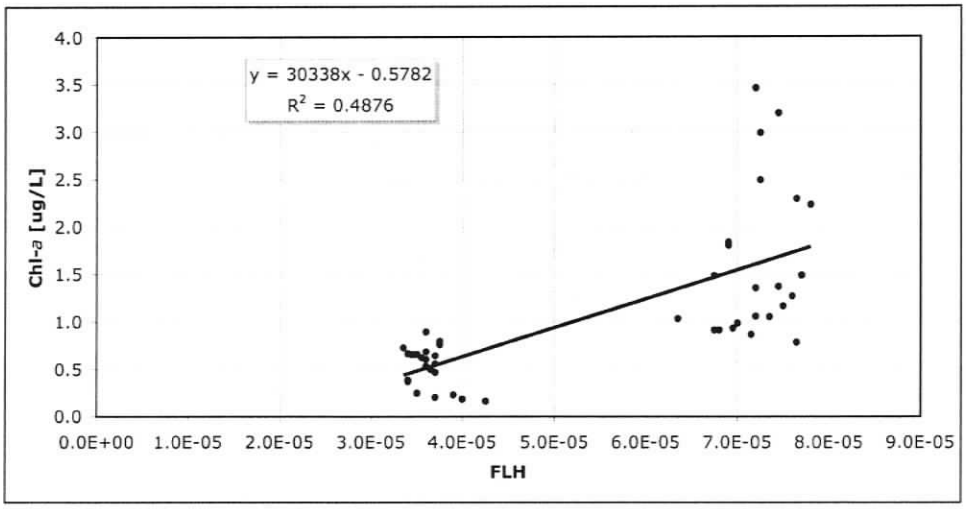


FIGURE: 5.7: Chl-*a* concentrations versus fluorescence line height values for both the lake and the bay study sites; despite a statistically significant correlation, clustering of the data indicates that the relationship is not favourable.

5.4.1.6 Ocean Colour 4 Algorithm

The ocean chlorophyll 4 (OC4) is a four band (443, 490, 510, 555 nm), maximum band ratio formula developed to determine Chl-*a* concentration from remotely sensed R_{rs} values. The algorithm initially calculates a band ratio as follows:

$$\text{Band Ratio} = \log\left[\frac{(R_{rs}443 > R_{rs}490 > R_{rs}510)}{R_{rs}555}\right] \quad \textbf{(5.3)}$$

where the highest R_{rs} value of either $R_{rs}(410)$, $R_{rs}(490)$, or R_{rs} (510) is used in the numerator. This band ratio is then applied in a modified cubic polynomial (Eqn 5.4) to predict Chl-*a* concentration.

$$\text{Chl-}a = 10^{(a0+a1\cdot R+a2\cdot R^2+a3\cdot R^3)} + a4 \quad \textbf{(5.4)}$$

where a0 = 0.4708

$a1$ = -3.8469

$a2$ = 4.5338

$a3$ = -2.4434

$a4$ = -0.0414

R = Band Ratio from Eqn 5.3

This algorithm was applied separately to both the Lake Cowichan and Cowichan Bay datasets. As the collected CASI bands did not include bands centred at any of the four required wavelengths, averages of the appropriate bands were calculated in accordance with Table 5.10.

TABLE 5.10: Summary of the band averaging necessary as input for the OC4 algorithm; none of the bands collected by CASI were centred on the required wavelengths.

Required Wavelength	Available from CASI		Averaged Wavelength
	Band	Wavelength	
443 nm	3	439.4	445.0
	4	450.5	
490 nm	7	483.8	489.4
	8	495.0	
510 nm	9	506.2	511.8
	10	517.4	
555 nm	13	551.1	556.7
	14	562.3	

The OC4 algorithm was unsuccessful in predicting Chl-*a* concentrations for both the lake and the bay. Figure 5.8a and 5.8b show the predicted versus observed Chl-*a* concentrations for both study sites. It is evident that in neither case do the paired concentrations fall along the 1:1 line, nor do they contain a statistically significant relationship, therefore, neither of these models was considered further. This result was expected as the model was developed using data from open ocean samples and rarely applies to coastal and inland waters (O'Reilly *et al.*, 1998).

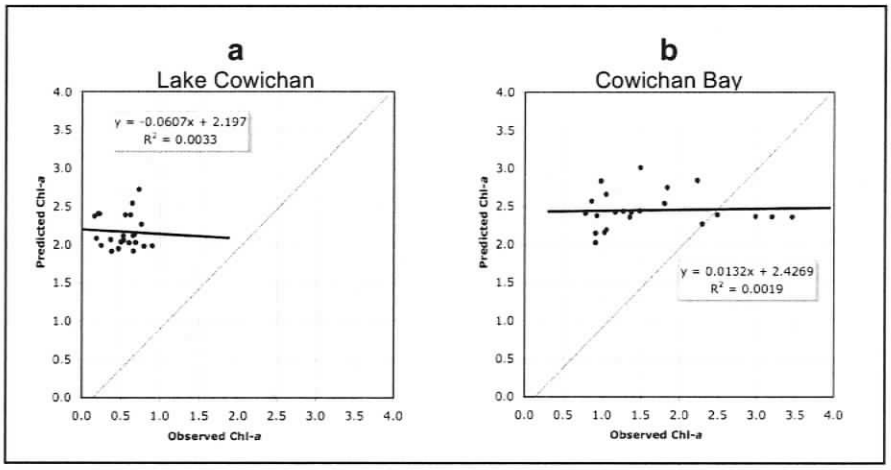


FIGURE: 5.8: Results of the OC4 algorithm as applied to the Lake Cowichan data (a) and the Cowichan Bay data (b); Chl-*a* concentrations as predicted by the OC4 algorithm versus observed concentrations indicate poor correlation.

5.4.2 Model Statistical Validations

Model validation is possibly the most important step in the model building process. Those models from section 5.4.1 producing the statistically strongest relationships between R_{rs} and the parameters of interest, based upon R^2, have been considered as potential final models. However, complete reliance on a high R^2 value is insufficient, as this does not guarantee that the model fits the data well. Therefore, they have been subject to validation tests.

Model validation usually involves checking the model against independent data (Neter *et al.*, 1990). The best means of doing this is through the collection of new data, however this was logistically impossible. Therefore, for each model its available dataset was randomly divided into two equally sized subsets: (i) a "model building dataset" and (ii) a "validation dataset". A regression model was then built from the "model building dataset", in accordance with the model structure exemplifying the strongest R^2 in section 5.4.1. This model was then applied to the "validation dataset" to examine whether it was still applicable for the validation data. Further assurance is possible through the development of a second model using the "validation dataset". Comparison between these two models should indicate consistent regression coefficients. This type of model validation procedure is often called *cross-validation*, where the splitting of the data effectively simulates partial or complete replication of the study (Neter *et al.*, 1990).

Both of these models should also be assessed by means of a one-way analysis of variance (ANOVA). An ANOVA evaluates whether a model's predictive capabilities are causal or simple chance. The ANOVA analysis uses an F-test to determine significance or non-significance of a null hypothesis, which for the models being evaluated is: that none of the independent variables predicts the dependent variable. This F-test reflects three things: the difference of means, group sample sizes, and the group variances. Eventual output of the test is a calculated F ratio value (F-statistic), which is then compared against a predetermined critical F value (F_{crit}) to decide on acceptance ($F > F_{crit}$) or rejection ($F < F_{crit}$) of the null hypothesis. The F_{crit} value is determined based on the degrees of freedom and the confidence level of the ANOVA analysis. The F-statistic is calculated as follows:

$$F = \frac{MS_B}{MS_W} \qquad \textbf{(5.5)}$$

where MS_B and MS_W represent independent estimates of population, where MS_B is estimate of variance between the groups and MS_W is estimate of variance within the groups. Therefore, the F-statistic is a measure of how much variance is attributable to the different treatments versus the variance expected from random sampling.

Once cross-validation and the ANOVA tests are completed and the model accepted, it is customary practice to then use the complete dataset ("model building" + "validation" datasets) to determine the final regression model. This should decrease the variances of the estimated regression coefficients.

5.4.2.1 Lake Cowichan Models

Table 5.11 summarizes those models from section 5.4.1 that produced the highest R^2 values for the relationships between R_{rs} and each of the parameters of interest.

TABLE 5.11: Lake Cowichan parameter of interest models to be validated.

PARAMETER	MODEL	R^2	SIGNIFIGANCE
Chl-*a*	= -250917(Dev670) - 439769(Dev613) - 193951(Dev625) + 38232.69(Dev591) + 48567.535(Dev456) - 1.409	0.785	Y (99%)
CDOM	= -145945(Dev523) + 255688.3(Dev647) + 116992.6(Dev545) + 75814.2(Dev501) + 3.853	0.688	Y (99%)
TSS	= -72324.9(Dev579) - 891671(Dev727) + 354882.5(Dev670) - 5.074	0.454	Y (99%)

5.4.2.1.1 Chlorophyll-*a*

The selected model for the prediction of Lake Cowichan's Chl-*a* concentrations was the multiple regression derivative analysis model, with an R^2=0.785. Models built on the "model building" and "validation" datasets are available in Appendix I. Regression coefficients were consistent between these two models, with all five independent variables being retained in both the "model building" and "validation" dataset models. As well, the F-statistic for both models exceeded their respective F_{crit}, and the null hypothesis was rejected in each case and the models accepted.

A measure of the actual predictability of the "model building dataset" model and the "validation dataset" model is possible via a comparison between the initial model's MS_W and the Mean Squared Prediction Error (MSPR). The MSPR is calculated by using the initial model to predict each case in the validation dataset, summing the differences, and dividing the total by the number of cases (Neter *et al.*, 1990).

$$\text{MSPR} = \frac{\sum_{i=1}^{n^*}\left(Y_i - Y_i'\right)^2}{n^*} \qquad \textbf{(5.6)}$$

where, Y_i is the Chl-*a* concentration of the *i*th validation case

Y'_i is the predicted Chl-*a* concentration for the *i*th validation case based on the "model building dataset" model

n^* is the number of validation cases

If the MSPR is close to the MS_W, then the latter gives a good predictability of the model. Alternatively, if the MSPR is much larger than the MS_W, it is then better to rely on the MSPR as an indication of how well the selected regression model will predict Chl-*a*. A comparison between the "model building" and "validation" dataset models indicates little difference between the MSPR and the MS_W. However, as the final Chl-*a* model is determined based upon the complete dataset it remains as that listed in Table 5.11.

5.4.2.1.2 Colour Dissolved Organic Matter

The selected model for the prediction of Lake Cowichan's CDOM concentrations was also its multiple regression derivative analysis model, with an R^2=0.688. The "model building" and

"validation" dataset models are available in Appendix I. Regression coefficients were consistent between these two models, with all four independent variables being retained in both models. Again the F-statistics for each model exceeded their respective F_{crit}, and the null hypothesis was rejected in each case and the models accepted. Therefore, the final model for CDOM was determined from the complete dataset and remains as listed in Table 5.11.

5.4.2.1.3 Total Suspended Solids

The selected model for the prediction of Lake Cowichan's TSS concentrations was also its multiple regression derivative analysis model, with an R^2=0.454. The developed models based upon the "model building" and "validation" datasets both returned a regression coefficient of zero for one of the three independent variables (Dev727), meaning that that variable was no longer included in the prediction model. Therefore, this variable was removed and the two models were developed a second time based solely upon the first two independent variables (Dev579 & Dev670). Once again both models returned a regression coefficient of zero for one of the two independent variables (Dev670). However, the removal of both Dev727 and Dev670 for model development would result in the single derivative analysis model developed in section 5.4.1.4 with an R^2 less than that of the band ratio model developed for TSS in section 5.4.1.3. Therefore, the TSS model listed in Table 5.11 was found to be invalid and the band ratio model was tested instead, as it was found to be the model with the next highest R^2 value of 0.324.

Band ratio models based upon the "model building" and the "validation" datasets were developed and they produced consistent regression coefficients. These models are available in Appendix I. The F-statistics for each model exceeded their respective F_{crit}, and the null hypothesis was rejected in each case and the models accepted. Therefore, the final model for TSS is not that listed in Table 5.11, but rather that of equation 5.7.

$$TSS = -5.7175\left[\frac{R_{rs}506}{R_{rs}574}\right] + 7.6824 \qquad \textbf{(5.7)}$$

5.4.2.2 Cowichan Bay Models

Table 5.12 summarizes those models from section 5.4.1 that produced the highest R^2 values for the relationships between R_{rs} and each of the parameters of interest.

TABLE 5.12: Cowichan Bay parameter of interest models to be validated.

PARAMETER	MODEL	R^2	SIGNIFIGANCE
Chl-*a*	= -18365.8(R_{rs}451) + 6369.098(R_{rs}585) – 23228.4(R_{rs}756) + 16.474	0.537	Y (99%)
CDOM	= -57539.2(Dev434) + 439357.3(Dev636) +1.395	0.422	Y (99%)
TSS	= 8216.289(R_{rs}462) – 3.994347	0.523	Y (99%)

5.4.2.2.1 Chlorophyll-*a*

The selected model for the prediction of Cowichan Bay's Chl-*a* concentrations was the multiple regression model, with an R^2=0.537. Models built on the "model building" and "validation" datasets are available in Appendix I. Regression coefficients were consistent between these two models, with all three independent variables being retained in both the "model building" and "validation" dataset models. As well, the F-statistics for both models exceeded their respective F_{crit}, and the null hypothesis was rejected in each case and the models accepted. The final Chl-*a* prediction model for the bay was determined using the complete dataset and remains as listed in Table 5.12.

5.4.2.2.2 Colour Dissolved Organic Matter

The selected model for the prediction of Cowichan Bay's CDOM concentrations was the multiple regression derivative analysis model, with an R^2=0.422. Models built on the "model building" and "validation" datasets are available in Appendix I. Regression coefficients were consistent between these two models, with the two independent variables being retained in both the "model building" and "validation" dataset models. As well, the F-statistics for both models exceeded their respective F_{crit}, and the null hypothesis was rejected in each case and the models accepted. The final CDOM prediction model for the bay was determined using the complete dataset and remains as listed in Table 5.12.

5.4.2.2.3 Total Suspended Solids

The selected model for the prediction of Cowichan Bay's TSS concentrations was the single band regression model, with an R^2=0.523. Models built on the "model building" and "validation" datasets are available in Appendix I. Regression coefficients were consistent between these two models. As well, the F-statistics for both models exceeded their respective F_{crit}, and the null hypothesis was rejected in each case and the models accepted. The final TSS prediction model for the bay was determined using the complete dataset and remains as listed in Table 5.12.

5.4.3 Model Implementation

The six models developed and validated in sections 5.4.1 and 5.4.2, respectively, have been applied herein and their outputs presented in Figures 5.9 and 5.10. Although each of these models was found to be statistically sound, it is evident from their visual outputs that there are several problematic issues, which can be clearly and consistently identified for each flightline within both the lake and the bay mosaics. The list of issues includes: (i) image striping and

speckling; (ii) gradient concentration variations across-track; and, (iii) preference for along-track concentration values accompanied by sharp concentration gradients
along the edges of each flightline. Each of these issues can be tied back to reflectance variations and therefore, are born of poor image collection or insufficient image preprocessing.

Upon delivery of the CASI imagery from the imagery acquisition consultant, the issues of image striping and speckle were immediately evident (Figure 5.11), which is fairly common due to 80-100% of reflectance recorded at the sensor originating from the atmosphere rather than the water (Kirk, 1994). A preliminary attempt to remove the striping through the use of the Fourier Forward Transform was made. However, during this attempt, it was found that the technique was too complex and time consuming to be implemented within the time available for the study, as the issues of incorrect geometric correction and reflectance variations between neighboring flightlines were of higher priority. Therefore, the striping removal was abandoned and the investigation continued with the hope that it would not have an adverse effect on the final model's outcome. However, as is evident from the resultant model output, this issue remained problematic.

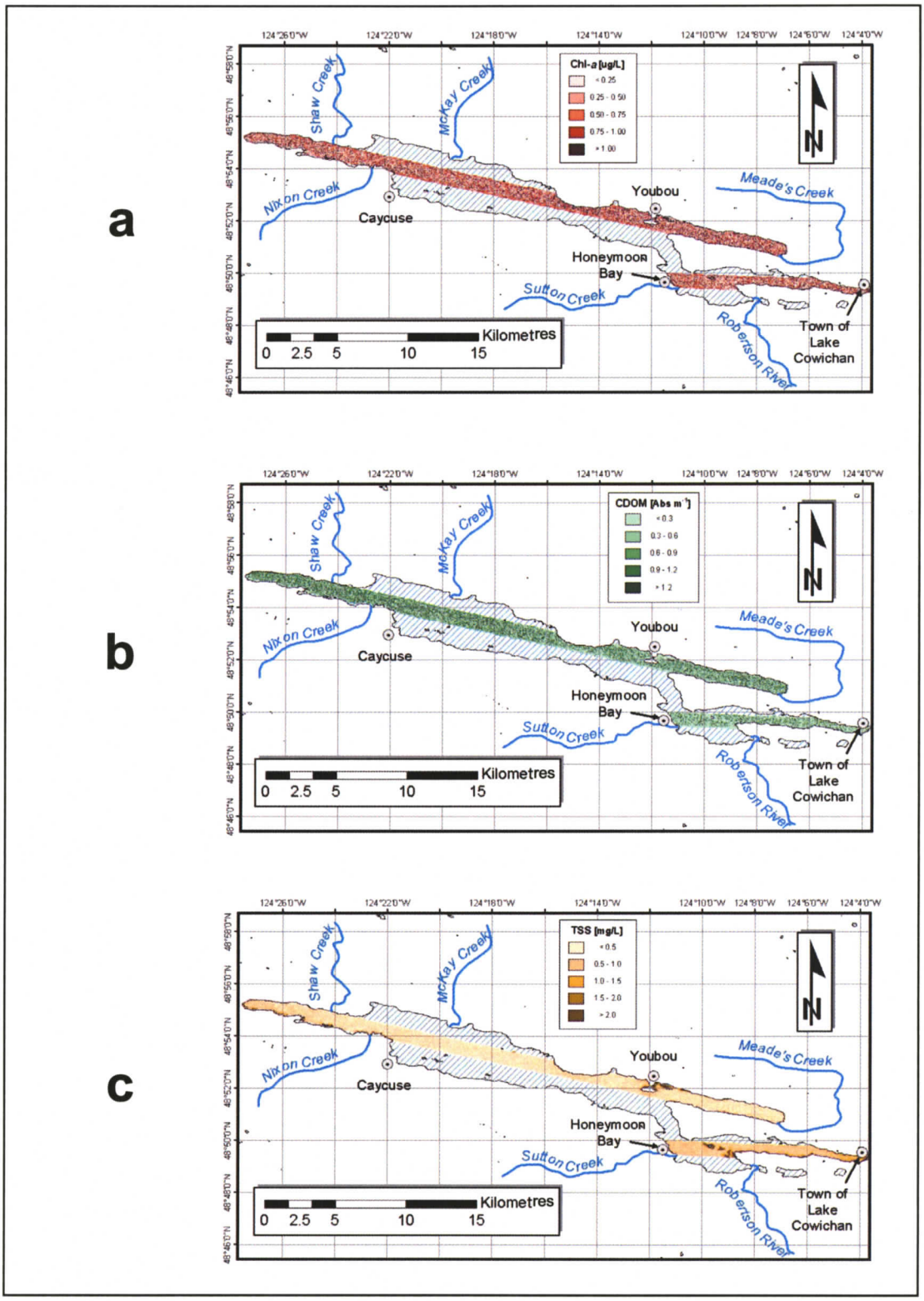


FIGURE 5.9: Lake Cowichan model outputs for (a) Chl-*a*, (b) CDOM, and (c) TSS.

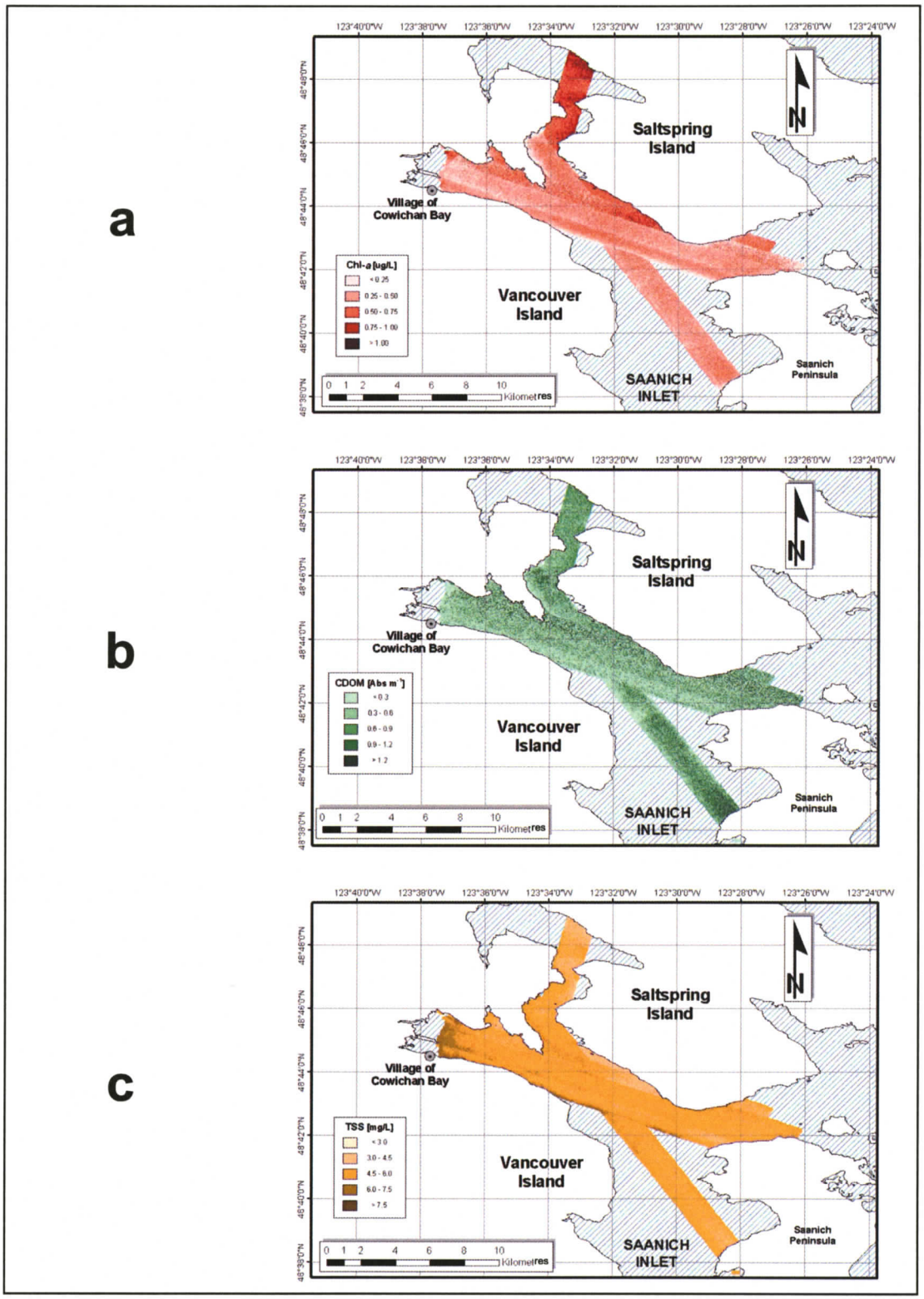


FIGURE 5.10: Cowichan Bay model outputs for (a) Chl-*a*, (b) CDOM, and (c) TSS.



FIGURE: 5.11: Problematic issues of speckle and striping in the collected CASI imagery are evident in flightline "Cowichan Bay 4," as well as throughout all other collected imagery.

From Figure 5.12, a variation in the R_{rs} across-track of the swath can be seen in both the original CASI imagery and subsequently in concentrations of the parameters of interest from the final model outputs. Generally, higher R_{rs} at all wavelengths is evident along the borders of each flightline. Cross-section R_{rs} profiles, as seen in Figure 5.12, displayed similar trends throughout all flightlines, regardless of directional heading of the acquiring aircraft, where the red band was relatively dark and flat due to absorption by water. These across-track gradient variations are therefore not representative of actual concentration gradients, but simply a result of the lighting variations across the swath width at the time of CASI acquisition.

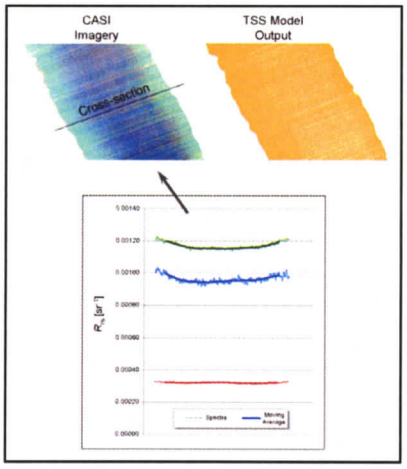


FIGURE: 5.12: **Across-track variations in original imagery are evident in model outputs; CASI imagery – R: 653 G: 551 B:451, Model Output: Final TSS model output.**

In an attempt to compensate for these problematic issues, both mosaics were resampled to 10x10m spatial resolution, as the models were developed based upon the average spectra from a 10x10m area. The nearest neighbour averaging filter was used with a 5x5 pixel kernel for this resampling, as it returns the mean average for the kernel with a 10x10m spatial resolution. It remains consistent with the mean average of a 5x5 filter window used in the extraction of the sample site spectra for model development. The effects of this resampling are demonstrated by a comparison of Figures 5.13a & 5.13b. To aid with visual improvement a 15x15 median averaging filter was applied to the model results to produce a smoother visual output, while retaining the 10x10m spatial resolution (Figure 5.13c). The median filter is good for removing image speckle by replacing each centre pixel with the median value of the kernel neighbourhood specified (Research Systems Incorporated, 2001).

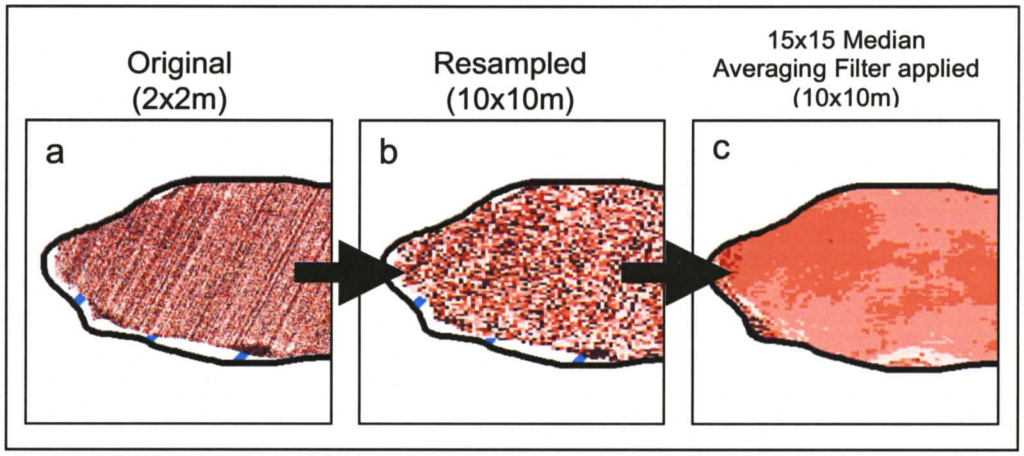


FIGURE: 5.13: Comparison of the progressive output resolution using Chl-*a* model output for Lake Cowichan; (a) original imagery, (b) resized imagery, and (c) median averaging filter applied.

Another problematic issue is that of a preference for along-track patterns, which is made all the more evident once the image resizing and filtering have been applied (Figure 5.14). The final model outputs, presented in the following two subsections, display concentration plumes parallel to the aircraft's flight-heading in each flightline. It is unlikely that these parallel concentration plumes existed in reality and their development is most likely connected to the collected R_{rs} and not to the models. As the previous across-track illumination issue would lead to the development of these along-track concentration plumes, concentration gradients can again be seen along the edges of each flightline.

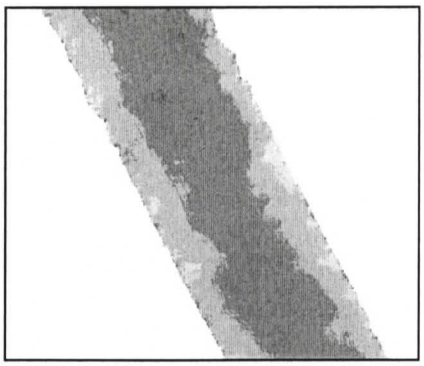


FIGURE: 5.14: As a result of insufficient across-track illumination correction, along-track plumes can be seen in the final model outputs as evident in this greyscale version of Cowichan Bay CDOM model output along flightline 'Saanich Inlet'.

5.4.3.1 Lake Cowichan Model Outputs

Figures 5.15, 5.16, and 5.17 are the final outputs from the Chl-*a*, CDOM, and TSS models for Lake Cowichan. Each map has had its parameter of interest categorized into five concentration classes, where the ranges were selected to best represent the average concentration value present, plus and minus three times its standard deviation. As with the spatially distributed water samples collected, the results of the models show low concentrations for each of the parameters of interest and also small ranges in values.

The range in Chl-*a* values across the surface of Lake Cowichan (Figure 5.15) is small and the distribution homogenous in nature according to the final model. The majority of the lake surface appears to be within the range of 0.25 and 0.75μg/L, with only the occasional small area showing concentrations above or below this range. Areas showing higher Chl-*a* concentrations include the north shore of the narrow section of lake 1.5km west of Youbou and the eastern side of the Youbou peninsula. These two areas of increased Chl-*a* are attributable to a public campground and the Youbou marina, respectively. The campground most likely sees heavy usage during the summer months of July and August. Probable Chl-*a* sources could be introduced to the lake due to recreational activities along the campground shore and potential groundwater seepage into the lake, originating or passing through the campground area. In Youbou's marina, ballast leakages or discharges must certainly contribute to elevating the Chl-*a* concentrations, as well as the delivery of other productivity nutrients to the lake through heavy human usage of the marina waters.

The problem issue of along-track pattern development is most evident in the output of the CDOM model. From Figure 5.16 it appears that CDOM presence is most prevalent along the centre axes of both flightlines and is coincident with the flightline direction. Although this is unlikely the actual case, the general distribution of CDOM shows higher concentrations in the lake's North arm with the highest levels occurring in the western half, where the majority of the

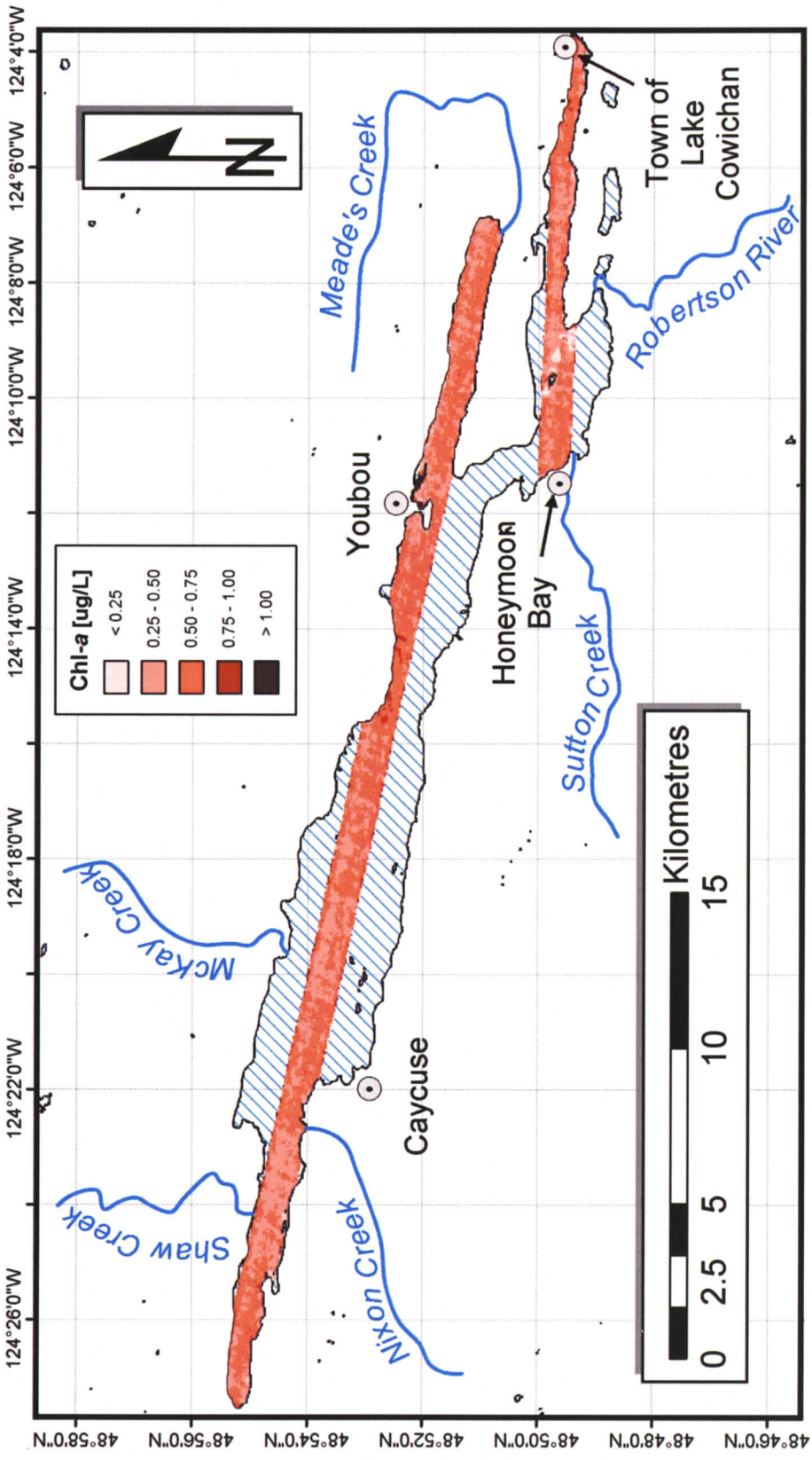


FIGURE 5.15: Lake Cowichan Chl-*a* distribution in accordance to final model application on CASI imagery.

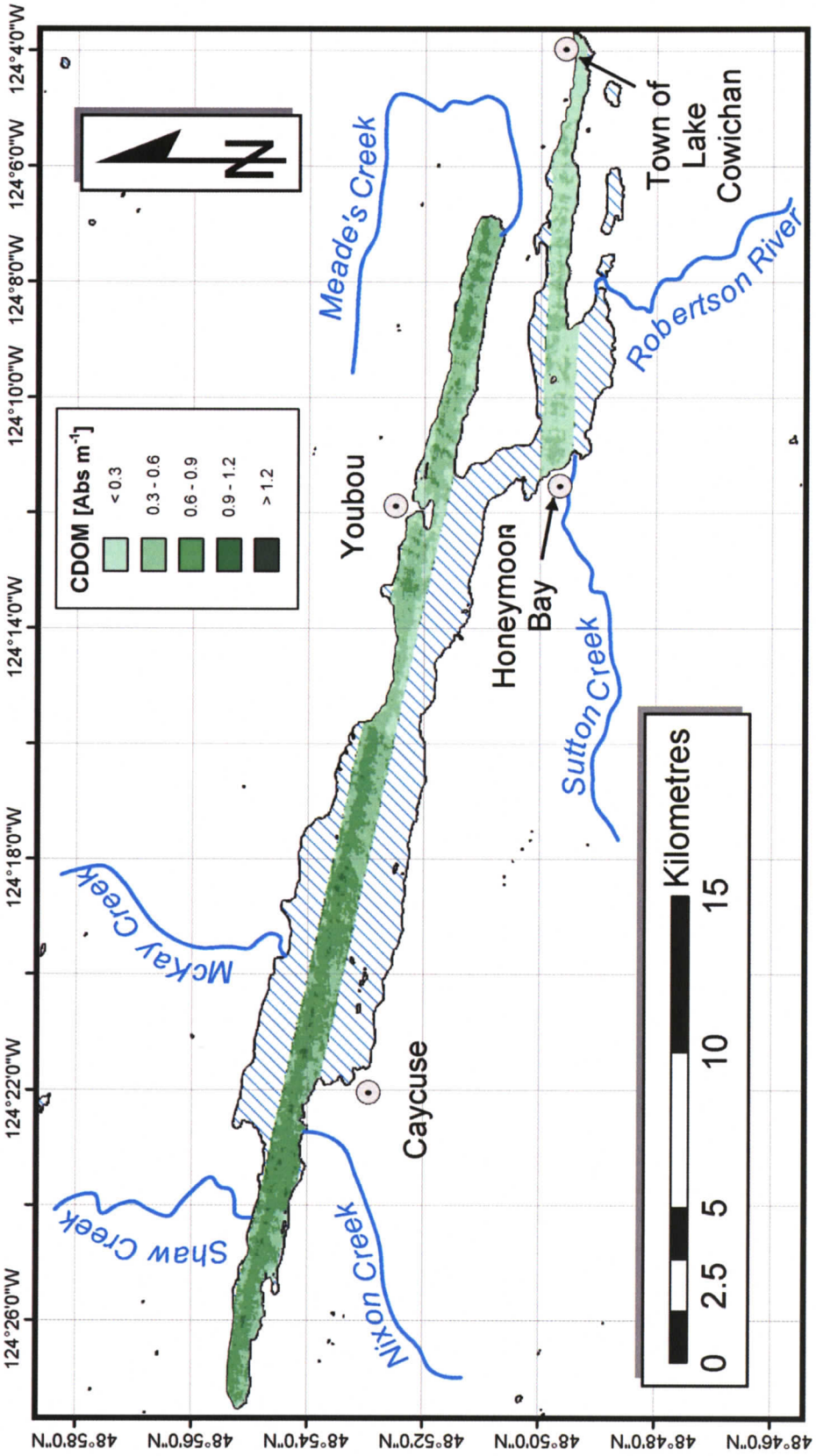


FIGURE 5.16: Lake Cowichan CDOM distribution in accordance to final model application on CASI imagery.

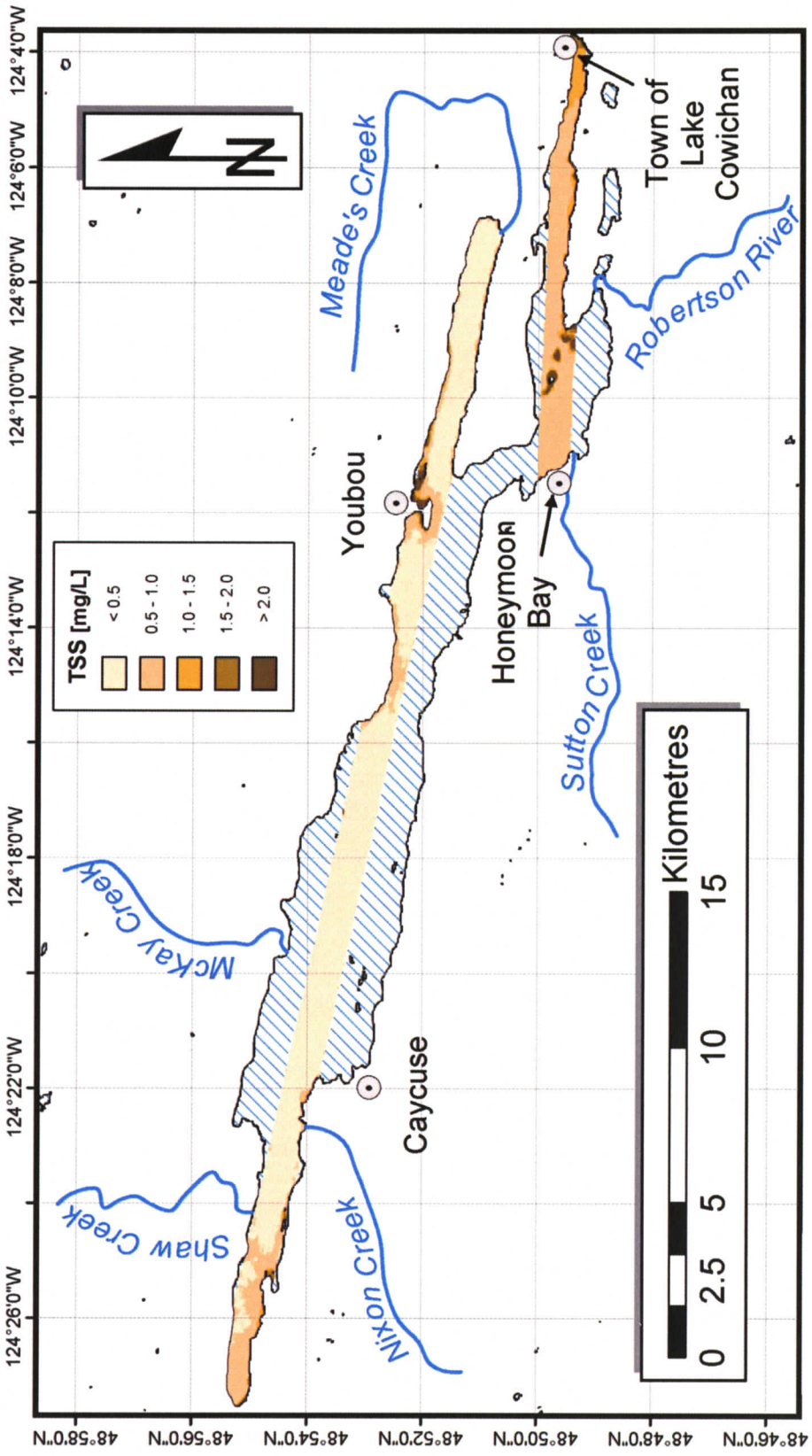


FIGURE 5.17: Lake Cowichan TSS distribution in accordance to final model application on CASI imagery.

historically intense logging and mining took place on the surrounding mountain sides. The lower concentration shown in the lake's south arm may be a result of a lack of line-to-line radiometric correction between the lake's two flightlines or a result of the dampening effects of the presence of TSS.

The TSS model output appears to be the least affected by the aforementioned problematic image issues (Figure 5.17). This is most likely due to its relatively large concentration range of TSS (0.5 - 2.0mg/L). The majority of the lake's North arm has a very low presence of TSS, while areas of increased TSS appear at its western extreme, immediately around the aforementioned campground shores and the Youbou marina. The lake's South arm shows a uniform increase in TSS relative to the North arm. The uniform increased level of TSS in this arm may again be a result of the lack of line-to-line reflectance correction between the lake's two flightlines. Although the South arm is relatively shallow as compared to the remainder of the lake it is unlikely that bottom reflection is the reason for this TSS distribution difference as the mean depth of the South arm is below its euphotic zone. However, the differences within the South arm flightline can be accounted for where increased TSS at the arm's eastern extreme is coincident with the most developed area of the lake's shores and coincident with the lake's dam and the preceding log booms. These two structures may act as stoppage for surface solids, creating a solids plume through its backwater effect on the surface layer.

5.4.3.2 Cowichan Bay Model Outputs

Figures 5.18, 5.19, and 5.20 are the final outputs from the Chl-*a*, CDOM, and TSS models for Cowichan Bay, respectively. As with the Lake Cowichan model outputs, each map has had its parameter of interest categorized into five concentration classes, where the ranges were selected to best represent the average concentration value present, plus and minus three times its standard deviation. As with the spatially distributed water samples collected, the results of the models show low concentrations for each of the parameters of interest and also small ranges in values.

Although the bay and its surrounding waters were determined to have higher levels of Chl-*a* than Lake Cowichan, the range in concentration is still small, with the majority of the bay, Satellite Channel and Saanich Inlet falling within the 0.25 to 0.50μg/L concentration range. In Figure 5.18 varying concentration ranges are evident between flightlines, with sharp changes in concentration where the flightlines overlap. These differences are most likely due to insufficient line-to-line correction of the imagery and not actual Chl-*a* differences. These differences indicated that the final Chl-*a* model exaggerates the differences of the low R_{rs} signal from that of the surface water, despite the previous attempt to correct them through line-to-line radiometric correction. In general, the area of lowest Chl-*a* concentration is at the estuary end of Cowichan Bay, which coincides with the fresh water inputs from both the Cowichan and Koksilah rivers. The area of

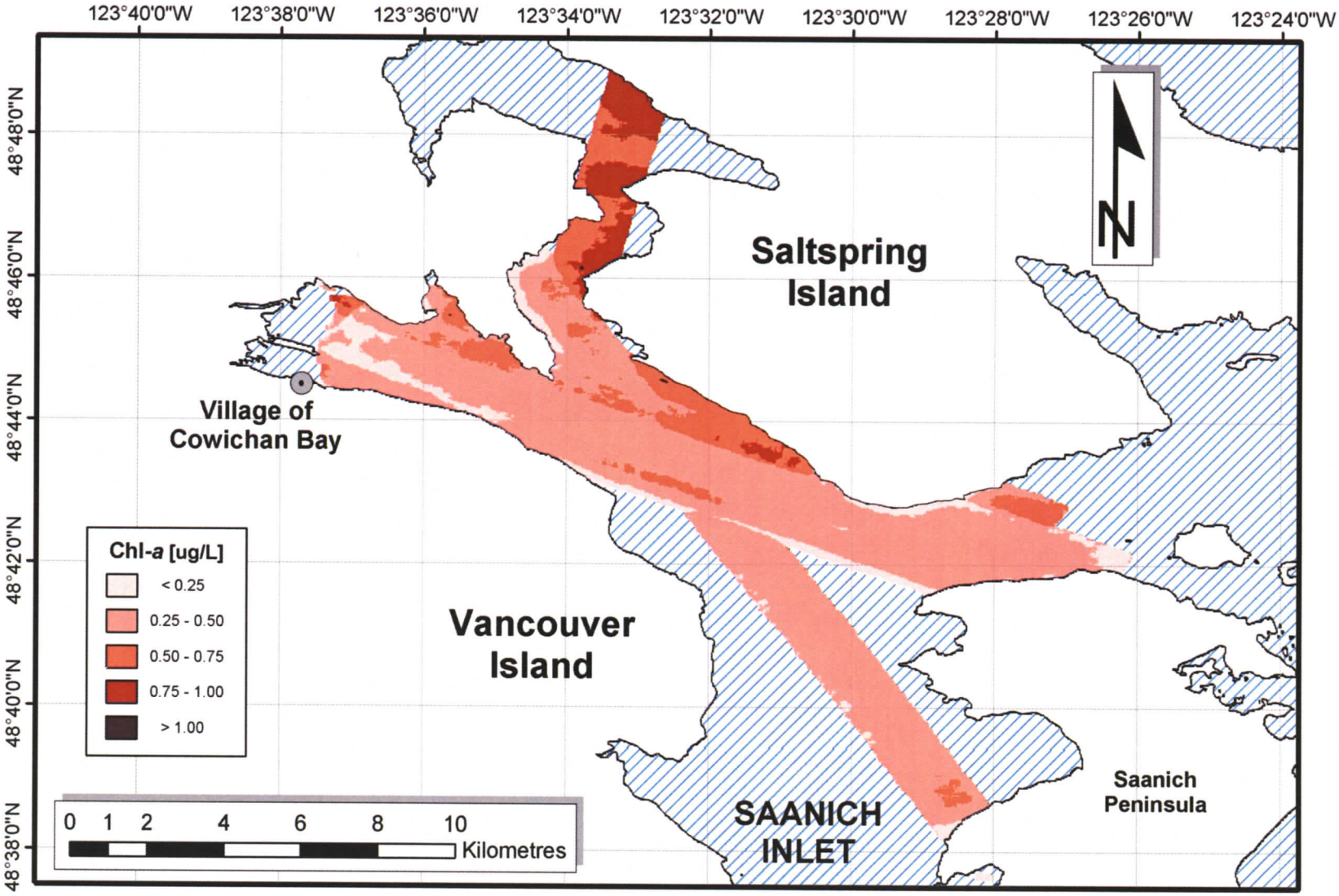


FIGURE 5.18: Cowichan Bay Chl-*a* distribution in accordance to final model application on CASI imagery.

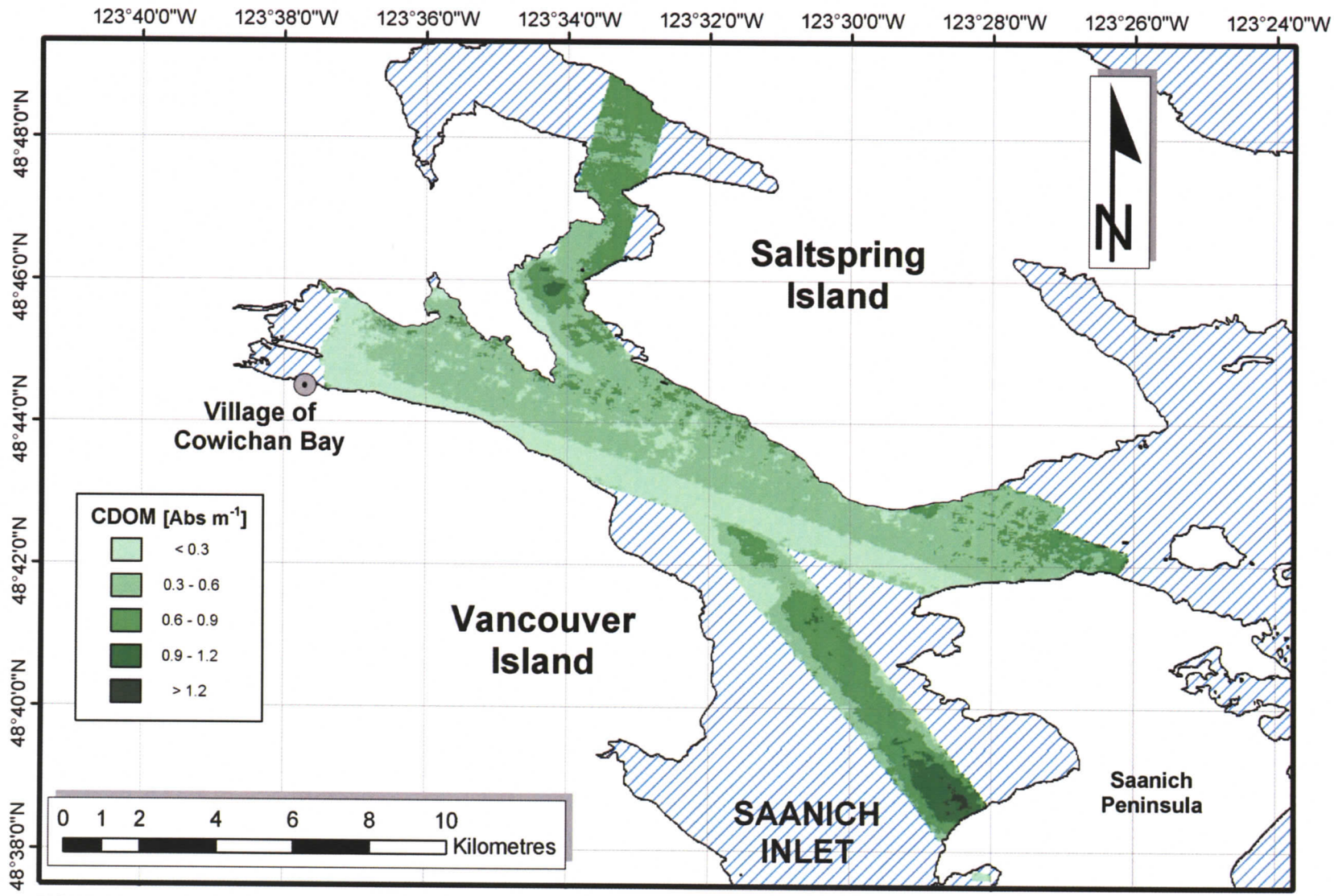


FIGURE 5.19: Cowichan Bay CDOM distribution in accordance to final model application on CASI imagery.

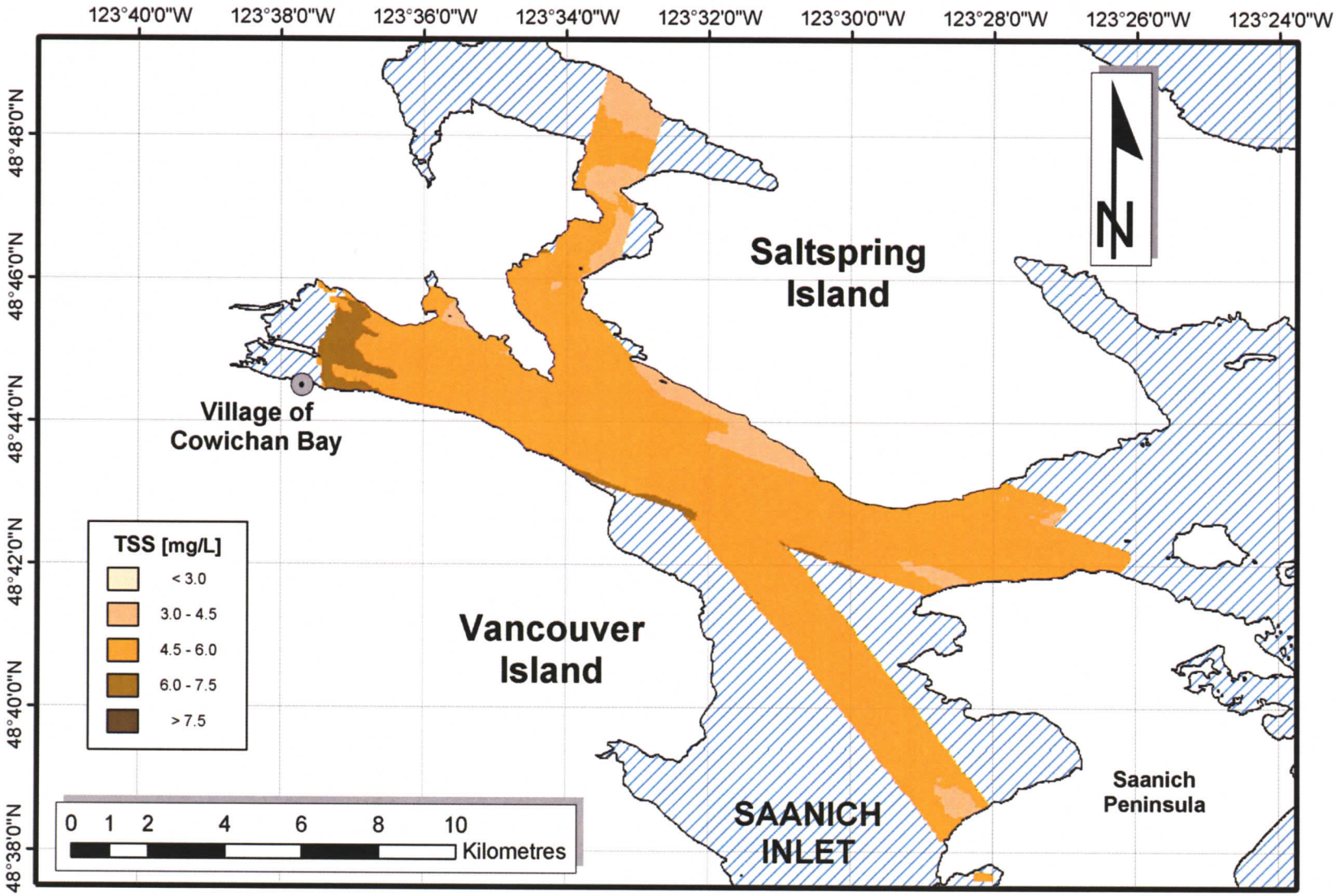


FIGURE 5.20: Cowichan Bay TSS distribution in accordance to final model application on CASI imagery.

highest Chl-*a* concentration is in the Sansum Narrows. These high concentrations may be related to the industrial plant in Crofton and the fish farm, located at the north end of the Sansum narrows, or possibly the southward flow of nutrient rich Strait of Georgia waters entering the narrows from North of Saltspring Island.

As with the CDOM model for Lake Cowichan, Figure 5.19 shows that the CDOM model for Cowichan Bay is also sensitive to the across-track variations in the CASI imagery and results in along-track plumes of CDOM. Despite these patterns, the general distribution of CDOM indicates higher concentrations in the Saanich Inlet and Sansum Narrows. Cowichan Bay and Satellite channel exhibit lower absorption by CDOM.

The TSS model output (Figure 5.20) indicates almost an identical spatial distribution as that of the Chl-*a* model, but opposite in concentration levels, with the highest concentrations of TSS present at the estuary end of Cowichan Bay and the lowest concentrations in the Sansum Narrows. These similar spatial patterns are most likely related to the inclusion of short wavelengths in both the Chl-*a* and TSS models. Table 5.12 indicates that the TSS model uses the λ=462nm and the Chl-*a* model uses λ=451nm. These two wavelengths are likely correlated and as such would generate similar parameter of interest distribution patterns being for the two models. The opposite concentration levels are most likely due to those areas of high TSS masking absorption by Chl-*a* through R_{rs} scattering. The TSS distribution of higher concentrations in the estuary and lower concentrations towards the Strait of Georgia was anticipated and is considered real, as the greater industrial and recreational use of the bay, as well as land run-off through river discharge would increase TSS and be mixed and diluted towards the strait.

5.5 Recommendations

For future work it is recommended that further attempts be made for more accurate CASI data, to ensure that the imagery is a true representation of the water leaving radiance and subsequently correct R_{rs}. To attain this, improvements to CASI calibration are necessary. It is recommended these improvements include proper across-track lighting variation corrections and removal of the evident line striping, either through Fast Fourier Transform or some alternative method. In addition, more accurate atmospheric correction would be beneficial. This could be attained through the use of an increased number of reference targets, if an ELC method were employed again, where the targets would be of both light and dark spectra, such as reference tarps. An alternative option for improved atmospheric correction would be the *in situ* collection of the necessary meteorological variables required by the atmospheric model to be applied.

One of the objectives of this research was to assist in the isolation and recommendation of bands for future remote sensors dedicated to inland and coastal water monitoring. The primary wavelength of the Cowichan Bay Chl-*a* prediction model (451nm) indicates close proximity to that

of the standard MERIS band configuration targeting Chl-*a* absorption (442.5nm). Although there is no exact overlap, the proximity indicates that both the model and the MERIS band configuration are targeting the same phenomena. This 15 band configuration of the programmable MERIS sensor (Table 5.13) has seen success in inland and coastal waters for research by Gower *et al.* (1999), Östlund *et al.* (2001) and Sathyendranath *et al.* (2004) where the first and last of these researchers conducted their work within the neighbouring Saanich Inlet.

TABLE 5.13: Band configuration for the MERIS spaceborne sensor, which was designed to target coastal Chl-*a* and TSS concentrations (table adapted from Gower *et al.*, 1999).

Band	Centre Wavelength [nm]	Bandwidth [nm]	Primary Purpose
1	412.5	10	DOM absorption
2	442.5	10	Chlorophyll absorption
3	490	10	Pigment absorption
4	510	10	Seston/phyto scattering
5	560	10	Seston/phyto scattering
6	620	10	Seston/phyto scattering
7	665	10	Fluorescence baseline
8	681.25	5	Fluorescence
9	705	10	Fluorescence baseline
10	753.75	7.5	Oxygen/aerosols
11	760	2.5	Oxygen absorption (R band)
12	775	12.5	Aerosol scattering
13	865	10	Aerosol scattering
14	890	10	Water vapour reference
15	900	10	Water vapour absorption

It is recommended that the standard band configuration of the MERIS sensor be examined more closely in future inland and coastal water quality studies in and around Southern Vancouver Island. In addition to the similar Chl-*a* correlation phenomena noted above, this configuration also accounts for potential Chl-*a* concentration prediction through the FLH technique, CDOM detection at the shortwave 412.5nm, as well as aerosol scattering and water vapour absorption for the purposes of proper atmospheric correction. Presumably CDOM concentrations would need to be higher than those recorded within Lake Cowichan and Cowichan Bay for detection with this band configuration.

6.0 CONCLUSIONS

Although inland and coastal water quality is still monitored by traditional *in situ* methods, this attempt to develop a means of remotely detecting the parameters of Chl-*a*, CDOM and TSS provides encouraging results that this alternative method has potential with further research and method development. Through the building of these empirical prediction models for both the inland water of Lake Cowichan and the coastal water of Cowichan Bay, this research has aided in the isolation of the more significant wavelengths.

Field studies were conducted for both Lake Cowichan and Cowichan Bay separately in late August of 2003. The results of these field campaigns indicated both the lake and the bay to be of oligotrophic status. Water analysis indicated the range of Chl-*a* to be 0.19 - 0.9μg/L and 0.75 – 3.46μg/L for the lake and the bay, respectively. CDOM ranged 0.12 – 1.57m^{-1} in the lake and 0.7 – 1.89m^{-1} in the bay. Lastly, TSS was found to range 0.02 – 1.16mg/L and 4.41 – 6.69mg/L in the lake and the bay, respectively. High analytical errors were recorded for both Chl-*a* and CDOM (±43% and ±57%, respectively), while that for TSS remained relatively low (±9%). Although each of these parameter ranges is both small and also low, statistically significant relationships with the concurrently collected CASI spectra were found for each at both study sites.

From this research it is difficult to definitively conclude as to whether the empirically derived prediction models are in fact causal or due to simple chance. Based upon an understanding of the phenomena being researched, it is believed that the resultant models for both Chl-*a* and TSS over Cowichan Bay are real, while no certainty can be made for the remaining four models (Chl-*a* & TSS for Lake Cowichan; CDOM for both the lake and the bay). Both the Chl-*a* and TSS models for Cowichan Bay, which correlated with short wave blue wavelengths, agree with previously developed relationships between their parameter and the features of their respective attenuance cross-sectional spectra. Chl-*a* primarily correlated with absorption at 451nm (R^2=0.537), while TSS correlated with scattering at 462nm (R^2=0.523). All remaining models relate with relatively low parameter concentrations and have returned relationships that have not been previously recognized. The high analytical errors associated with these low concentrations also indicate that these measurements are all similar. Therefore, the developed models were built for a limited range in parameter concentrations. Follow-up research to confirm or dismiss these relationships is necessary. Regardless of their confidence, it should be noted each of these models can only be used to predict water quality parameter concentrations within, or close to those observed in the field. Also these models are limited to use under similar field conditions over the same region. Beyond these conditions, the models may not hold up and the predicted concentrations may result in erroneous values. This limitation is due to the empirical nature of the findings and a less site-specific model would have to be identified by means of analytical analysis.

Although confident prediction models were not the end result for each of the parameters of interest in this case, the final outcome of this research is encouragingly positive. The remote detection of water quality from Vancouver Island's inland and coastal waters is possible. The knowledge gained through the processes employed herein will be an asset to the development of future methods for research in this area employing improved CASI data quality.

7.0 REFERENCES

Ammenberg, P., Flink, P., Lindell, T., Pierson, D., and Strömbeck, N., 2002. Bio-optical modelling combined with remote sensing to assess water quality, *International Journal of Remote Sensing*, 23:1621-1638.

Aronoff, S., 1995. *Geographic Information Systems – A Management Perspective*, WDL Publications, Ottawa.

Babey, S.K., and Anger, C.D., 1989. *A Compact Airborne Spectrographic Imager*, Proceedings IGARSS '89/Twelfth Canadian Symposium on Remote Sensing, IEEE, 2, 1028-1031.

Bell, L.M. and Kallman, R.J., 1979. The Cowichan-Chemainus river estuaries status of environmental knowledge to 1975, report to estuary working group, *Special Estuary Series* No.4.

Ben-Dor, E., Kruse, F.A., Lefkoff, A.B., and Banin, A., 1994. Comparison of three calibration techniques for utilization of GER 63-channel aircraft scanner data of Makhtesh Ramon, Negev, Israel, *Photogrammetric Engineering and Remote Sensing*, 60:1339-1354.

Bird, P.M., and Rapport, D.J., 1986. *State of the Environment Report for Canada*, Minister of Supply and Services Canada, Ottawa, Ontario.

Borstad, G.A., Gower, J.F.R., Edel, H.R., and Hollinger, A.B., 1985. Analysis of test and flight data from the Fluorescence Line Imager, *Canadian Special Publication of Fisheries and Aquatic Sciences, No. 83*, 38pp.

Bukata, R.P., Burton, J.E., and Jerome, J.H., 1985. *Application of Direct Measurements of Optical Parameters to the Estimation of Lake Water Quality Indicators*, Environment Canada, Inland Waters Directorate, National Water Research Inst., Canada Centre for Inland Waters, Burlington, Ontario Scientific Series No. 140, 35pp.

Bukata, R.P., Jerome, J.H., Kondratyev, K.Y., and Pozdnyakov, D.V., 1995. *Optical Properties and Remote Sensing of Inland and Coastal Waters*, CRC Press, New York, 362pp.

Burt, J.E., and Barber, G.M., 1996. *Elementary Statistics for Geographers*, The Guilford Press, 2nd edition, New York, NY, 640pp.

Campbell, J., 2000. *Map Use and Analysis*, McGraw-Hill Higher Education, 4th edition, Toronto, Ontario, 384pp.

Carl, G.C., 1953. Limnobiology of Lake Cowichan, B.C., *Journal of the Fisheries Research Board of Canada*, 9:417-449.

Carpenter, D. J., and Carpenter, S. M., 1983. Modeling inland water quality using Landsat data, *Remote Sensing of Environment*, 13:345 352.

Chandrasenkhar, S., 1960. *Radiative Transfer*, Dover Publications, New York, 393pp.

Clark, R., Swayze, G., Livo, E., Kokaly, R., King, T., Dalton, B., Vance, S., Rockwell, B., Hoefen, T., and McDougal, R., 2002. *Surface Reflectance Calibration of Terrestrial Imaging Spectroscopy Data: A Tutorial Using AVIRIS*, Jet Propulsion Laboratory (JPL) AVIRIS Workshop, Pasadena, California, USA.

Clarke, G.K., Ewing, G.C., and Lorenzen, C.J., 1970. Spectra of backscattered light from the sea obtained from aircraft as a measure of chlorophyll concentration, *Science*, 167:1119-1121.

Clesceri, L.S., Greenberg, A.E., and Eaton, A.D., (Eds.), 1998. *Standard Methods for the Examination of Water and Wastewater*, American Public Health Association, Washington, DC.

Coble, P., Hu., C., Gould Jr., R.W., Chang, G., and Wood, A.M., 2004. Colored dissolved organic matter in the coastal ocean, *Oceanography*, 17:50-59.

Davies, J.M., and Mazumder, A., 2003. Health and environmental policy issues in Canada: the role of watershed management in sustaining clean drinking water quality at surface sources, *Journal of Environmental Management*, 68:273-286.

Dekker, A.G., 1993. *Detection of Optical Water Quality Parameters for Eutrophic Waters by High Resolution Remote Sensing*, Ph.D. thesis, Vrije Universiteit, Amsterdam, The Netherlands, 219pp.

Dekker, A.G., Malthus, T.J., and Hoogenboom, H.J., 1995. The remote sensing of inland water quality, - in: Danson and Plummer, (Eds.): *Advances in Remote Sensing*, John Wiley and Sons Ltd., 123-142.

Dekker, A.G., and Bukata, R.P., 2002. Remote sensing of inland and coastal waters, - in: Hallikainen, MT, (Eds.): *Review of radio science 1999-2003*, IEEE Press, Piscataway, NJ, USA, 519-534.

DeVilliers, M., 1999. *Water*, Stoddart Publishing Co. Limited, Toronto, 413pp.

Dierberg, F.E., and Carrlker, N.E., Field testing two instruments for remotely sensing water quality in the Tennessee Valley, *Environmental Science and Technology*, 28:16-25.

Doxaran, D., Froidefond, J,-M., and Castaing, P., 2002a. A reflectance band ratio used to estimate suspended matter concentrations in sediment-dominated coastal waters, *International Journal of Remote Sensing*, 23:5079-5085.

Doxaran, D., Froidefond, J,-M., Lavender, S., and Castaing, P., 2002b. Spectral signature of highly turbid waters, Application with SPOT data to quantify suspended particulate matter concentrations, *Remote Sensing of Environment*, 81:149-161.

ESA – European Space Agency MERIS Webpage, 2005. http://envisat.esa.int/instruments/meris/

Ferrari, G.M., Dowell, M.D., Grossi, S., and Targal, C., 1996. Relationship between the optical properties of chromophoric dissolved organic matter and total concentration of dissolved organic carbon in the southern Baltic Sea region, *Marine Chemistry*, 55:299-316.

Fraser, R.N. 1998. Hyperspectral remote sensing of turbidity and chlorophyll a among Nebraska sand hills lakes, *International Journal of Remote Sensing*, 19:1579-1589.

Gallagher, L.C., 2004. *Hyperspectral Remote Sensing of Suspended Minerals, Chlorophyll and Coloured Dissolved Organic Matter in Coastal and Inland Waters, British Columbia, Canada*, M.Sc. thesis, University of Victoria, Victoria, Canada, 108pp.

Gallegos, C.L., Correll, D.L., and Pierce, J.W., 1990. Modelling spectral diffuse attenuation, absorption, and scattering coefficients in a turbid estuary, *Limnology and Oceanography*, 35:1486-1502.

Gallie, E.A., and Murtha, P.A., 1992. Specific absorption and backscattering spectra for suspended minerals and chlorophyll-a in Chilko Lake, British Columbia, *Remote Sensing of Environment*, 39:103-118.

George, D.G., and Malthus, T.J., 2001. Using a compact airborne spectrographic imager to monitor phytoplankton biomass in a series of lakes in north Wales, *The Science of the Total Environment*, 268:215-226.

Gin, K.Y.-H., Koh, S.T., and Lin, I.-I., 2003. Spectral irradiance profiles of suspended marine clay for the estimation of suspended sediment concentration in tropical waters, *International Journal of Remote Sensing*, 24:3235-3245.

Gitelson, A.A., and Kondratyev, K.Ya., 1991. Optical models of mesotrophic and eutrophic water bodies, *International Journal of Remote Sensing*, 12:373-385.

Gladden, J.B., 2003. 2002 *Hyperspectral Analysis of Hazardous Waste Sites on the Savannah River Site*, Technical Report, US Department of Energy, US, 57pp.

Goel, P.K., Prasher, S.O., Landry, R.M., Patel, R.M., Viau, A.A., and Miller, J.R., 2003. Estimation of crop biophysical parameters through airborne and field hyperspectral remote sensing, *Transactions of the ASAE*, 46:1235-1246.

Gons, H.J., Machteld, R., and Ruddick, K.G., 2002. A chlorophyll-retrieval algorithm for satellite imagery (Medium Resolution Imaging Spectrometer) of inland and coastal waters, *Journal of Plankton Research*, 24:947-951.

Goodin, D.G., Han, L., Fraser, R.N., Rundquist, D.C., Stebbins, W.A., and Schalles, J.F., 1993. Analysis of suspended solids in water using remotely sensed high resolution derivative spectra, *Photogrammetric Engineering 7 Remote Sensing*, 59:505-510.

Gordon, H.R., Clark, D.K., Brown, J.W., Brown, O.B., Evans, R.H., and Broenkow, W.W., 1983. Phytoplankton pigment concentrations in the middle Atlantic bight: Comparison of ship determinations and coastal zone colour scanner measurements, *Applied Optics*, 22:20-36.

Gower, J.F.R., 1980. Observations of *in situ* fluorescence of chlorophyll-*a* in Saanich Inlet, *Boundary-Layer Meteorology*, 18:235-245.

Gower, J.F.R., Doerffer, R., and Borstad, G.A., 1999. Interpretation of the 685nm peak in water-leaving radiance spectra in terms of fluorescence, absorption and scattering, and its observation by MERIS, *International Journal of Remote Sensing*, 20:1771-1786.

Hair, J.F.Jr., Anderson, R.E., Tatham, R.L., and Black, W.C., 1998. *Multivariate Data Analysis*, Prentice Hall, 2nd edition, Upper Saddle River, New Jersey, 730pp.

Hakvoort, H., de Hann, J., Jordans, R., Vos, R., Peters, S., and Rijkeboer, M., 2002. Towards airborne remote sensing of water quality in The Netherlands – validation and error analysis, *Journal of Photogrammetry and Remote Sensing*, 57:171-183.

Hamilton, M.K, Davis, C.O., Rhea, W.J., Pilorz, S.H., and Carder, K.L., 1993. Estimating chlorophyll content and bathymetry of Lake Tahoe using AVIRIS data, *Remote Sensing of Environment*, 44:217-230.

Han L.H., and Rundquist D.C., 1997. Comparison of NIR/RED ratio and first derivative of reflectance in estimating algal-chlorophyll concentration: A case study in a turbid reservoir, *Remote Sensing of Environment*, 62: 253-261.

Harper, D., 1983. *Eye In The Sky, Introduction to Remote Sensing*, Multiscience Publications Limited, 2nd edition, Montreal, Canada, 252pp.

Harrison, P.J., Clifford, P.J., Cochlan, W.P., Yin, K., St, John, M.A, Thompson, P.A., Sibbald, M.J., and Albright, L.J., 1991. Nutrient and plankton dynamics in the Fraser River plume, Strait of Georgia, British Columbia, M*arine Ecology Progress Series*, 70:291-304.

Hobson, L.A. 1980. Phytoplankton biology of Saanich Inlet, B.C., - in: Freeland, Farmer, and Levings, (Eds.): *Fjord Oceanography*, Plenum Press, 423-427.

Hu, B.X., Inannen, K., and Miller, J.R., 2000. Retrieval of leaf area index and canopy closure from CASI data over the BOREAS flux tower sites, *Remote Sensing of Environment*, 74:255-274.

Jacques, A., O'Neill, N.T., and Therriault, J.-C., 1998. Chlorophyll remote sensing potential in pigment-poor moderately turbid case II waters: lower St. Lawrence estuary, *Canadian Journal of Remote Sensing*, 24:194-199.

Jeffrey, S.W., and Humphrey, G.F., 1975. New spectrophotometric equations for determining chlorophyll *a*, *b*, and *c*, in higher plants, algae and natural phytoplankton, *Biochemie und Physiologie der Pflanzen*, 167:191-194.

Jensen, J.R., 1996. *Introductory Digital Image Processing, a Remote Sensing Perspective*, Prentice Hall, 2nd edition, New Jersey, 318pp.

Jensen, J.R., 2000. *Remote Sensing of the Environment: An Earth Resource Perspective*, Prentice Hall, Upper Saddle River, New Jersey, 544pp.

Jerlov, N.G., 1968. *Optical Oceanography*, Elsevier Publishing Company, Amsterdam, 194pp.

Jerlov, N.G., 1976. *Marine Optics*, Elsevier Scientific Publishing Company, Amsterdam, 231pp.

Jerome, J.H., and Bukata, R.P., 1994. Colours of natural waters: 2. Observations of spectral variations in British Columbia rivers, *Northwest Science*, 68:53 64.

Jewson, D.H., and Taylor, J.A., 1978. The influence of turbidity on net phytoplankton photosynthesis in some Irish lakes, *Freshwater Biology*, 8:573-584.

Jorgensen, P.V., and Edelvang, K., 2000. CASI data utilized for mapping suspended matter concentrations in sediment plumes and verification of 2-D hydrodynamic modelling, *International Journal of Remote Sensing*, 21:2247-2258.

Kirk, J.T.O., 1994. *Light and Photosynthesis in Aquatic Ecosystems*, Cambridge, 509pp.

Kloiber, S.M., Brezonik, P.L., Olmanson, L.G., and Bauer, M.E., 2002. A procedure for regional lake water clarity assessment using Landsat multispectral data, *Remote Sensing of Environment*, 82:38 47.

Kowalczuk, P., Olszewski, J., Darecki, M., and Kaczmarek, S., 2005. Empirical relationships between coloured dissolved organic matter (CDOM) absorption and apparent optical properties in Baltic Sea waters, *International Journal of Remote Sensing*, 26:345-370.

Kunzig, R., 2002. *Mapping the Deep: The Extraordinary Story of Ocean Science*, W.W. Norton & Company, New York, 345pp.

Lathrop, R.G., 1992. Landsat Thematic Mapper monitoring of turbid inland water-quality, *Photogrammetric Engineering and Remote Sensing*, 58:465-470.

Lavin, P.A. and McPhail, J.D., 1985. The evolution of freshwater diversity in the threespine stickleback (gasterosteus aculeatus): site-specific differentiation of trophic morphology, *Canadian Journal of Zoology*, 63:2632-2638.

Louchard, E.M., Reid, R.P., Stephens, C.F., Davis, C.O., Leathers, R.A., and Downes, T.V., 2002. Derivative analysis of absorption features in hyperspectral remote sensing data of carbonate sediments, *Optics Express*, 10:1573-1584.

Manahan, S.E., 1994. *Environmental Chemistry*, CRC Press Inc., 6th edition, Florida, 811pp.

Mather, P.M., 2004. *Computer Processing of Remotely-Sensed Images: An Introduction*, John Wiley and Sons Ltd., 3rd edition, West Sussex, England, 342pp.

Matthews, A.M., Duncan, A.G., and Davison, R.G., 2001a. An assessment of validation techniques for estimating chlorophyll-a concentration from airborne multispectral imagery, *International Journal of Remote Sensing*, 22:429-447.

Matthews, A.M., Duncan, A.G., and Davison, R.G., 2001b. Error assessment of validation techniques for estimating suspended particulate matter concentration from airborne multispectral imagery, *International Journal of Remote Sensing*, 22:449-469.

Ministry of Environment, 1990. *Cowichan Lake*, 1:24 000, Province of British Columbia, Recreational Fisheries Branch – Habitat Management Section.

Meybeck, M., 1982. Carbon, nitrogen, and phosphorus transport by world rivers, *American Journal of Science*, 282:401-450.

Mobley, C.D., 1994. *Light and Water, Radiative Transfer in Natural Waters*, Academic Press, San Diego, 592pp.

Mobley, C.D., 1999. Estimation of the remote-sensing reflectance from above-surface measurements, *Applied Optics*, 38:7442-7455.

Morel, A.Y., and Prieur, L., 1977. Analysis of variations in ocean colour, *Limnology and Oceanography*, 22:707-722.

Morel, A.Y., and Gordon, H.R., 1980. Report of the working group on water colour, *Boundary-Layer Meteorology*, 18:343-355.

NASA – National Aeronautics and Space Administration MODIS webpage, 2005. http://modis.gsfc.nasa.gov/

Neter, J., Wasserman, W., and Kutner, M.H., 1990. *Applied Linear Statistical Models: Regression, Analysis of Variance, and Experimental Designs*, Irwin, 3rd edition, Homewood, Il, 1181pp.

Neville, R.A., and Gower, J.F.R., 1977. Passive remote sensing of phytoplankton via chlorophyll *a* in fluorescence, *Journal of Geophysical Research*, 82:3487-3493.

O'Reilly, J.E, Maritorena, S., Mitchell, B.G., Siegel, D.A., Carder, K.L., Garver, S.A., Kahru, M., and McClain, C., 1998. Ocean color chlorophyll algorithms for SeaWiFS, *Journal of Geophysical Research*, 103:24,937-24,953.

Östlund, C., Flink, P., Strombeck, N., Pierson, D., and Lindell, T., 2001. Mapping of the water quality of Lake Erken, Sweden, from imaging spectrometry and Landsat Thematice Mapper, *The Science of the Total Environment*, 268:139-154.

Parsons, T.R., Stronach, J., Borstad, GA., Louttit, G., and Perry, R.I., 1981. Biological fronts in the Strait of Georgia, British Columbia, and their relation to recent measurements of primary productivity, *Marine Ecology-Progress Series*, 6:237-242.

Pozdnyakov, D., and Grassl, H., 2003. *Colour of Inland and Coastal Waters: A Methodology for its Interpretation*, Praxis Publishing, United Kingdom, 170pp.

Price, R., Anger, C.D., and Mah, S., 1995. *Preliminary Evaluation of CASI Preprocessing Techniques*, Proceedings of the 17th Canadian Symposium on Remote Sensing, June 12-15, Saskatoon, Canada.

Province of British Columbia, 1980. *Cowichan Estuary Task Force Report*, Environment and Land Use Committee Secretariat, Victoria.

Province of British Columbia, 2003. Provincial aerial photograph database, 1:10000, Ministry of Sustainable Resources, Victoria.

Rast, M., Bezy, J.L., and Bruzzi, S., 1999. The ESA Medium Resolution Imaging Spectrometer MERIS – a review of the instrument and its mission, *International Journal of Remote Sensing*, 20:1681-1702.

Research Systems Incorporated, *2001. The Environment for Visualizing Images (ENVI) User's Guide*, Version 3.4.

Rideout, P., Taekema, B., Deniseger, J., Liboiron, R., and McLaren, D., 2000. *A Water Quality Assessment of the Cowichan and Koksilah Rivers and Cowichan Bay*, Ministry of Environment, Lands and Parks, Province of British Columbia, Pollution Prevention, Vancouver Island Region, 109pp.

Sathyendranath, S., Stuart, V., Cota, G., Maass, H., and Platt, T., 2001. Remote sensing of phytoplankton pigments: A comparison of empirical and theoretical approaches, *International Journal of Remote Sensing*, 22:249 273.

Sathyendranath, S., Platt, T., Irwin, B., Horne, E., Borstad, G., Stuart, V., Payzant, L., Maass, H., Kepkay, P., Li, W.K.W., Spry, J., and Gower, J., 2004. A multispectral remote sensing study of coastal waters off Vancouver Island, *International Journal of Remote Sensing*, 25:893-919.

Schofield, O, Arnone, R.A., Bissett, W.P., Dickey, T.D., Davis, C.O., Finkel, Z., Oliver, M., and Moline, M.A., 2004. Watercolors in the coastal zone, what can we see?, *Oceanography*, 17:24-31.

SERC - Smithsonian Environmental Research Center, 1999. http://www.serc.si.edu/Index.htm.

Shafique, N.A., Autrey, B.C., Fulk, F., and Cormier, S.M., 2001. Hyperspectral narrow wavebands selection for optimizing water quality monitoring on the Great Miami River, Ohio, *Journal of Spatial Hydrology*, 1:1-22.

Shrubsole, D.A., 1990. Integrated water management strategies in Canada – in: Mitchell (Ed.): *Integrated Water Management, International Experiences and Perspectives*, Belhaven Press, New York, 88-118.

Smith, G.M., and Milton, E.J., 1999. The use of empirical line method to calibrate remotely sensed data to reflectance, *International Journal of Remote Sensing*, 20:2653-2662.

Smith, R.L., 1992. *Elements of Ecology*, HarperCollins Publishers Inc., 3rd edition, New York, 617pp.

Takahashi, M., Seibert, D.L., and Thomas, W.H., 1977. Occasional blooms of phytoplankton during summer in Saanich Inlet, B.C., Canada, *Deep-Sea Research*, 24:775-780.

Tchobanoglous, G., and Schroeder, E.D., 1987. *Water Quality, Characteristics, Modelling, Modification*, Addison-Wesley Publishing Company, Don Mills, Ontario, 768pp.

Teillet, P.M., Slater, P.N., Ding, Y., Santor, R.P., Jackson, R.D., and Moran, M.S., 1990. Three methods for the absolute calibration of the NOAA AVHRR sensors in-flight, *Remote Sensing of Environment*, 31:105-120.

Thieman, S. and Kaufmann, H., 2002. Lake water quality monitoring using hyperspectral airborne data – A semiemperical multisensor and multitemporal approach for the Mecklenburg Lake District, Germany, *Remote Sensing of Environment*, 81:228 237.

Thomson, R.E., 1981. Oceanography of the British Columbia coast, *Canadian Special Publications of Fisheries and Aquatic Science*, No. 56, 291pp.

Town of Lake Cowichan, 2003. http://www.town.lakecowichan.bc.ca.

USEPA - U.S. Environmental Protection Agency, 1987. *Quality Criteria for Water*, EPA Publication 440/5-86- 001, U.S. Government, Washington D.C.

Verbyla, D.L., 1995. *Satellite Remote Sensing of Natural Resources*, CRC Lewis Publishers, 198pp.

Warrington, D.S., Budd, J.W., Stumpf, R.P., and Green, S.A., 2002. *Satellite-Based Chlorophyll and Turbidity Estimates Using SeaWiFS Imagery of Lake Superior*, American Society of Limnology and Oceanography Conference, Honolulu, Hawaii.

Weidemann, A.D., and Bannister, T.T., 1986. Absorption and scattering coefficients in Irondequoit Bay, *Limnology and Oceanography*, 31:567-583.

Wentzell-Brehme, C., 1999. *A Guide to Remote Sensing: An Overview of the Science and its Application to the Coastal and Marine Environment*, Island Institute, 29pp.

::: APPENDIX A :::

Lake Cowichan Bathymetry



Adapted from Ministry of Environment, 1990



Adapted from Ministry of Environment, 1990

::: APPENDIX B :::

Water Quality
Sample Analysis Results

LAKE COWICHAN

SAMPLE ID	Chl-a (w Pheo) [µg/L] ±43%	CDOM [abs 440 m^{-1}] ±57%	TSS [mg/L] ±9%	Secchi [m]	Bottom Depth [m]	Sampling Time	CASI Acquisition	Time Lapse	NOTES
3H25S-1-1	0.38	1.38	0.12	12.5			10:21		
3H25S-2-1	0.37	0.35	0.03	8.0			10:37		
3H25S-3-1	0.31	0.23	1.16	8.5			10:37		
3H25S-4-1									No Sample Collected
3H25S-5-1									No Sample Collected
3H25-06	0.76	0.23	0.84	10.0	53.3	13:33	10:37	2:56	Sample collected two days prior to CASI flight & other samples
3H25-07	0.19	0.64	0.46	12.8	77.4	14:04	10:37	3:27	Sample collected two days prior to CASI flight & other samples
3H25-08	0.50	0.64	0.23	11.9	41.1	14:20	10:37	3:43	Sample collected two days prior to CASI flight & other samples
3H25-09		0.69	0.52	12.0	45.4	15:00	10:37	4:23	Sample collected two days prior to CASI flight & other samples
3H25-10	0.90		0.19	13.0	69.2	15:15	10:37	4:38	Sample collected two days prior to CASI flight & other samples
3H25-11	0.79	0.32	0.02	15.0	>85.3	10:46	10:37	0:09	
3H25-12	0.47	0.78	0.34	14.5	56.7	11:02	10:37	0:25	
3H25-13	0.60	0.48	0.60	11.0	9.8	11:17	10:37	0:40	
3H25-14	0.69	0.32	0.29	14.0	78.0	11:25	10:37	0:48	
3H25-15	0.66	0.23	0.71	13.5	>85.3	11:33	10:37	0:56	
3H25-16	0.53	0.81	0.81	13.5	>85.3	11:46	10:37	1:09	
3H25-17	0.53	0.58	0.03	13.0	44.2	12:02	10:37	1:25	
3H25-18	0.65	1.57	0.31	11.5	62.8	12:15	10:37	1:38	
3H25-19	0.25	0.32	0.80	12.0	>85.3	12:27	10:37	1:50	
3H25-20	0.67		0.69	11.5	64.0	12:49	10:37	2:12	
3H25-21	0.62	0.44	0.37	11.5	26.5	13:14	10:21	2:53	
3H25-22	0.23	0.44	0.84	12.5	46.3	13:25	10:21	3:04	
3H25-23	0.16	0.23	0.59	10.5	20.7	13:43	10:21	3:22	
3H25-24	0.40	0.32	0.43	11.0	47.55	13:55	10:21	3:34	Only Northing recorded, no Easting
3H25-25	0.21	0.32	0.44	10.5	47.9	14:06	10:21	3:45	
3H25-26	0.56	0.48	0.86	9.0	42.7	14:22	10:21	4:01	
3H25-27	0.65	0.12	0.46	8.5	38.1	14:41	10:21	4:20	
3H25-28	0.73	0.18	1.01	7.5	19.8	14:50	10:21	4:29	
3H25-29	0.62	1.17	0.60		5.2	15:03	10:21	4:42	
3H25-30									No Sample Collected

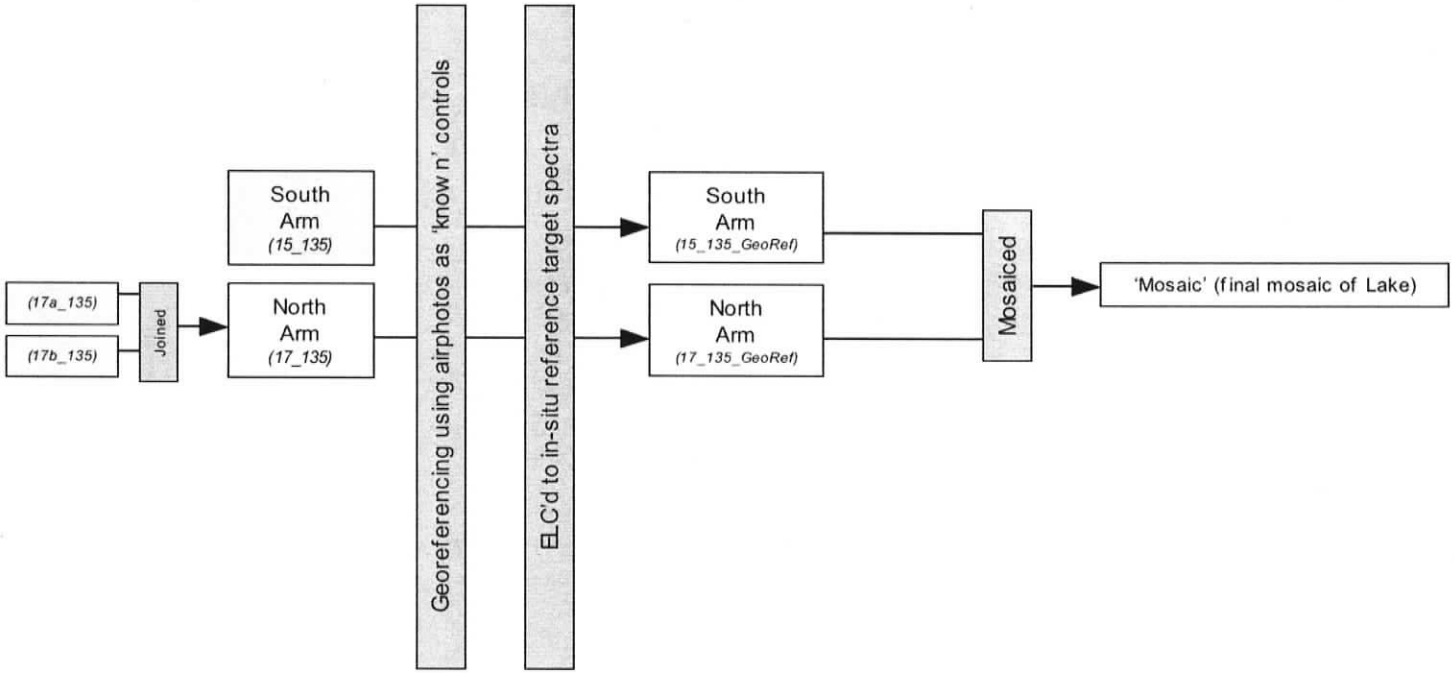
COWICHAN BAY

SAMPLE ID	Chl-a (w Pheo) [µg/L] ±43%	CDOM [abs 440 m^{-1}] ±57%	TSS [mg/L] ±9%	Secchi [m]	Bottom Depth [m]	Sampling Time	CASI Acquisition	Time Lapse	NOTES
3H26S-1-1	1.03	0.30	5.12	12.0			9:44		
3H26S-2-1	2.49	0.35	5.21				9:44		
3H26S-3-1	2.23	0.07	5.46				9:44		
3H26S-4-1	1.49	0.41	4.84				0.41		
3H26S-5-1	1.27	0.23	5.54				0.41		
3H26-06	0.86		5.69	8.5	44.5	14:48	9:56	4:52	
3H26-07	1.36		4.89	10.0	>85.3	13:55	9:28	4:27	
3H26-08	1.37	0.41	6.69	9.5		15:20	9:44	5:36	
3H26-09	2.98		4.77	11.0	>85.3	13:42	9:28	4:14	
3H26-10	1.05	1.89	5.33	7.5	40.8	14:23	9:28	4:55	
3H26-11	1.81	0.16	5.23	10.0	>85.3	13:30	9:28	4:02	
3H26-12	1.17	0.46	5.42	10.5	63.4	13:16	9:44	3:32	
3H26-13	1.49	0.39	5.29	10.0	37.8	14:36	9:56	4:40	
3H26-14				11.5	64.6	12:56	9:44	3:12	
3H26-15	0.93	0.12	4.77	9.0	60.4	14:11	9:28	4:43	
3H26-16	0.79	0.46		10.0	58.5	14:59	9:44	5:15	
3H26-17	3.20	0.76	4.78	8.0	>85.3	16:19	9:02	7:17	
3H26-18	3.46	0.64	4.71	7.0	54.3	16:46	9:02	7:44	
3H26-19									No Sample Collected
3H26-20									No Sample Collected
3H26-21	0.98	0.46	4.65	9.0	>85.3	17:02	10:13	6:49	
3H26-22	1.84	0.14	5.37	11.0	56.1	16:01	10:13	5:48	
3H26-23									No Sample Collected
3H26-24	2.29	0.48	5.04	9.1	>85.3	12:40	10:13	2:27	
3H26-25	0.75	0.12	4.65	9.1	70.1	11:35			No spectral distribution to associate with
3H26-26				10.1	>85.3	11:57			No Sample Collected
3H26-27	0.92	0.44	4.41	12.9	>85.3	12:10	10:13	1:57	
3H26-28	0.92	0.12	4.64	11.5	79.2	11:10	9:56	1:14	
3H26-29	1.06	0.35	4.67	12.0	60.4	10:55	9:28	1:27	
3H26-30	1.31	0.23	5.42	13.0	>85.3	10:30			No spectral distribution to associate with

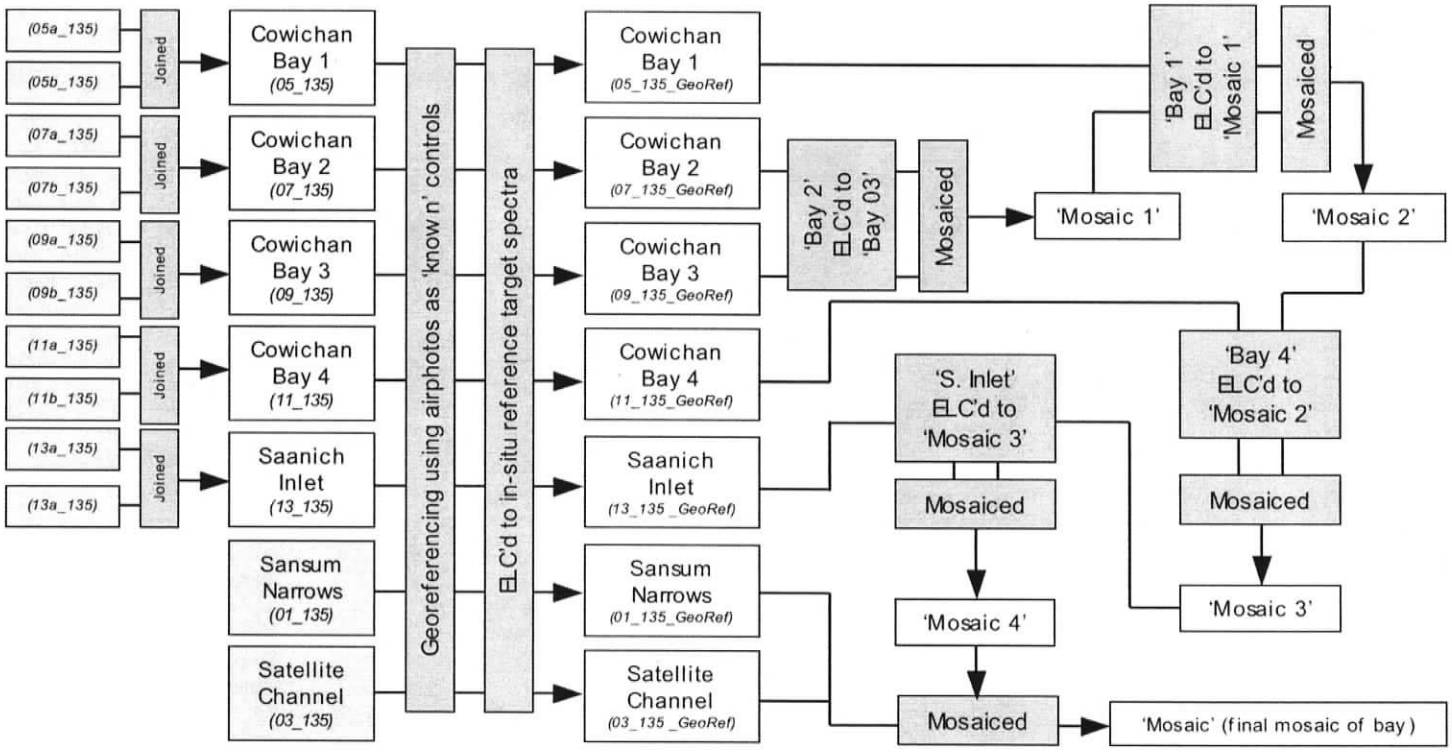
::: APPENDIX C :::

Data Processing Flow Diagrams

LAKE COWICHAN: Data Processing Flow Diagram



COWICHAN BAY: Data Processing Flow Diagram

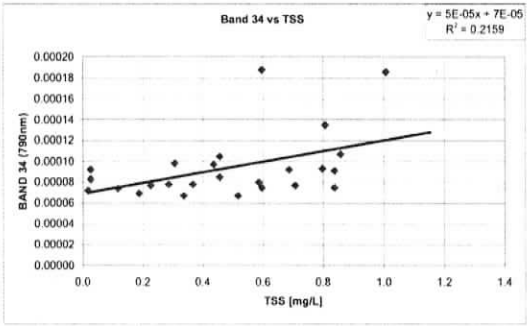


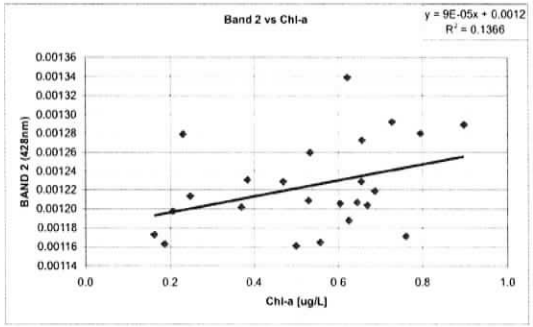
::: APPENDIX D :::

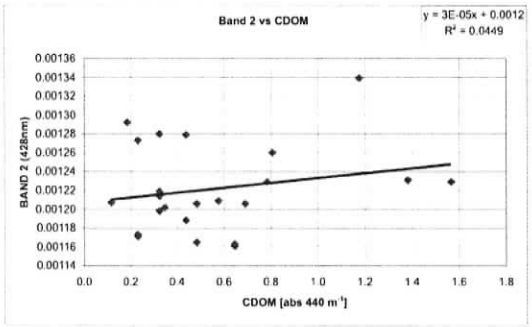
Spectral Extractions

LAKE COWICHAN – *Initial Spectra*

* Significance at 95% confidence level
** Significance at 99% confidence level





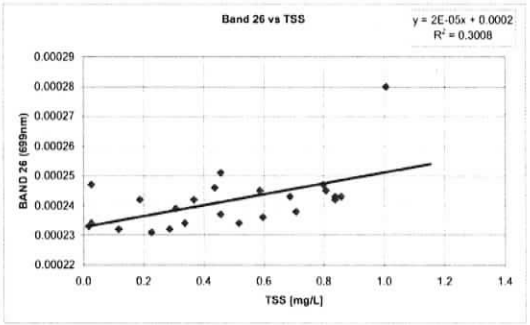


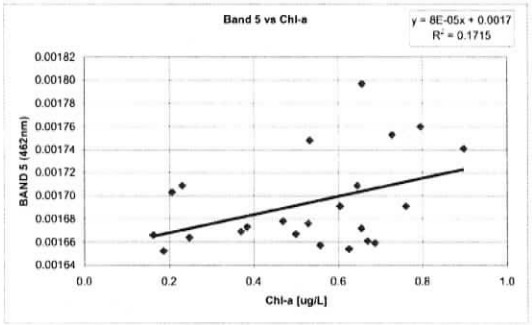
BAND	W.L. [nm]	TSS (N = 25)	CHL_A (N = 24)	CDOM (N = 23)
01	417	0.056	0.321	0.077
02	428	0.082	0.370	0.212
03	439	0.145	0.162	0.135
04	451	0.201	0.206	0.053
05	462	0.274	0.246	-0.009
06	473	0.277	0.158	-0.012
07	484	0.305	0.201	0.108
08	495	0.320	0.128	-0.025
09	506	0.331	0.122	0.001
10	517	0.327	0.114	0.024
11	529	0.355	0.097	0.001
12	540	0.346	0.098	0.023
13	551	0.341	0.098	0.065
14	562	0.350	0.098	0.051
15	574	0.348	0.092	0.074
16	585	0.348	0.084	0.060
17	596	0.361	0.131	0.057
18	608	0.385	0.172	0.048
19	619	0.377	0.139	0.064
20	630	0.398*	0.115	0.044
21	642	0.377	0.115	0.025
22	653	0.379	0.113	0.106
23	664	0.384	0.137	0.065
24	676	0.422*	0.095	0.108
25	687	0.423*	0.123	0.059
26	699	0.407*	0.121	0.134
27	710	0.427*	0.120	0.132
28	722	0.441*	0.139	0.117
29	733	0.417*	0.142	0.119
30	744	0.427*	0.140	0.103
31	756	0.418*	0.174	0.100
32	767	0.433*	0.175	0.108
33	779	0.428*	0.161	0.088
34	790	0.465*	0.158	0.106

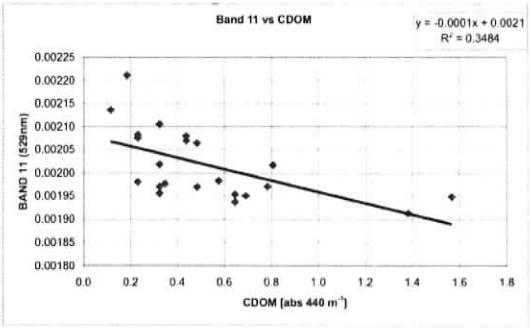
INITIAL SPECTRA
All spectra are those from original ROI's, determined using field recorded UTM Coord.

LAKE COWICHAN – *Final Spectra*

* Significance at 95% confidence level
** Significance at 99% confidence level







BAND	W.L. [nm]	TSS (N = 24)	CHL_A (N = 23)	CDOM (N = 22)
01	417	-0.268	0.405	0.026
02	428	-0.200	0.391	0.070
03	439	-0.079	0.322	-0.015
04	451	0.093	0.266	-0.196
05	462	0.188	0.414*	-0.248
06	473	0.180	0.231	-0.325
07	484	0.291	0.208	-0.316
08	495	0.305	0.181	-0.513*
09	506	0.278	0.149	-0.468*
10	517	0.374	0.136	-0.458*
11	529	0.409*	0.084	-0.590**
12	540	0.429*	0.065	-0.548**
13	551	0.451*	0.050	-0.505*
14	562	0.436*	0.075	-0.509*
15	574	0.477*	0.059	-0.512*
16	585	0.434*	0.035	-0.504*
17	596	0.443*	0.108	-0.498*
18	608	0.477*	0.241	-0.570**
19	619	0.470*	0.105	-0.522*
20	630	0.517**	0.076	-0.577**
21	642	0.452*	0.093	-0.561**
22	653	0.516**	0.122	-0.479*
23	664	0.443*	0.167	-0.464*
24	676	0.522**	0.013	-0.473*
25	687	0.527**	0.046	-0.505*
26	699	0.548**	0.055	-0.397
27	710	0.506*	0.074	-0.291
28	722	0.527**	0.060	-0.349
29	733	0.451*	0.023	-0.293
30	744	0.470*	0.037	-0.304
31	756	0.412*	0.088	-0.305
32	767	0.483*	0.093	-0.304
33	779	0.455*	0.075	-0.301
34	790	0.516**	0.085	-0.304

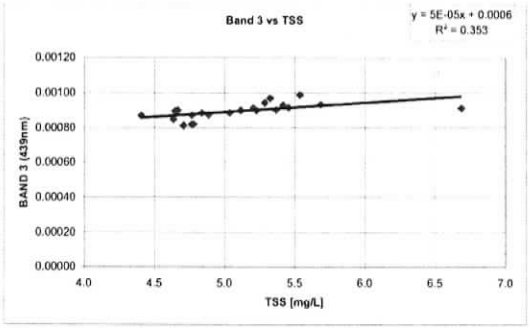
FINAL SPECTRA

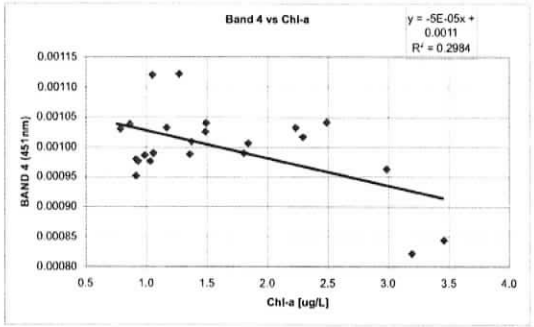
Darkened:
18 (Trial 03)
22 (Trial 03)
28 (Trial 03)

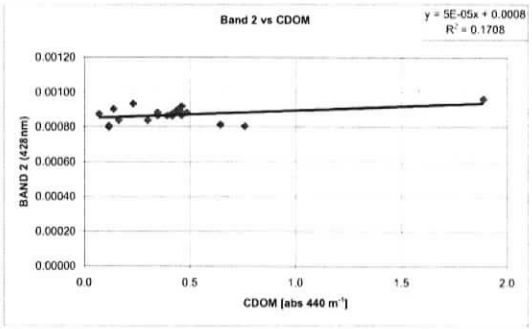
Brightened:
06 (Trial 03)
07 (Trial 03)
08 (Trial 03)
09 (Trial 03)
12 (Trial 03)

COWICHAN BAY – *Initial Spectra*

* Significance at 95% confidence level
** Significance at 99% confidence level





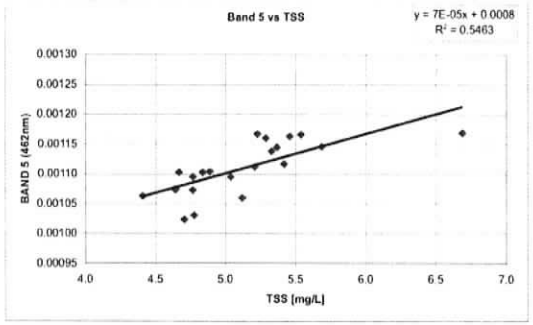


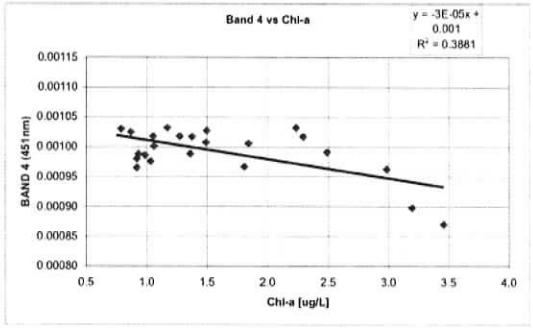
BAND	W.L. [nm]	TSS (N = 22)	CHL_A (N = 23)	CDOM (N = 20)
01	417	0.363	0.109	0.234
02	428	0.270	-0.284	0.413
03	439	0.594**	-0.425*	0.215
04	451	0.465*	-0.546**	0.136
05	462	0.578**	-0.327	0.117
06	473	0.531*	-0.390	0.146
07	484	0.458*	-0.355	0.207
08	495	0.509*	-0.319	0.165
09	506	0.530*	-0.297	0.159
10	517	0.490*	-0.288	0.149
11	529	0.478*	-0.308	0.127
12	540	0.528*	-0.240	0.154
13	551	0.477	-0.292	0.132
14	562	0.502	-0.224	0.112
15	574	0.475	-0.195	0.134
16	585	0.483	-0.171	0.180
17	596	0.480	-0.170	0.242
18	608	0.472	-0.213	0.274
19	619	0.462*	-0.210	0.287
20	630	0.433*	-0.224	0.276
21	642	0.437*	-0.185	0.297
22	653	0.439*	-0.193	0.313
23	664	0.445*	-0.227	0.304
24	676	0.443*	-0.204	0.307
25	687	0.440*	-0.119	0.336
26	699	0.461*	-0.168	0.305
27	710	0.492*	-0.141	0.362
28	722	0.485*	-0.208	0.321
29	733	0.414	-0.161	0.384
30	744	0.199	-0.197	0.073
31	756	0.232	-0.274	0.072
32	767	0.437*	-0.348	0.183
33	779	0.024	-0.183	0.048
34	790	0.187	0.371	0.311

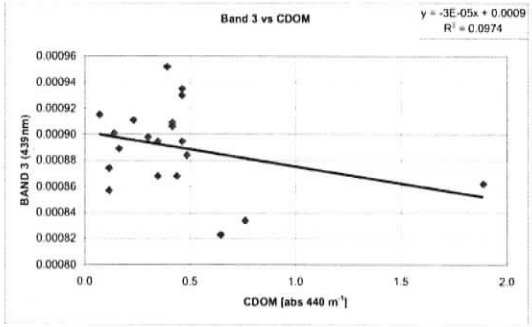
INITIAL SPECTRA
All spectra are those from original ROI's, determined using field recorded UTM Coord.

COWICHAN BAY – *Final Spectra*

* Significance at 95% confidence level
** Significance at 99% confidence level







BAND	W.L. [nm]	TSS (N = 22)	CHL_A (N = 23)	CDOM (N = 20)
01	417	0.291	0.136	0.146
02	428	0.300	-0.282	0.308
03	439	0.544**	-0.431*	-0.312
04	451	0.506*	-0.623**	-0.075
05	462	0.739**	-0.328	-0.092
06	473	0.535*	-0.390	0.010
07	484	0.534*	-0.305	-0.040
08	495	0.486*	-0.314	-0.064
09	506	0.514*	-0.271	-0.123
10	517	0.449*	-0.276	-0.076
11	529	0.478*	-0.276	-0.107
12	540	0.520*	-0.193	-0.074
13	551	0.464*	-0.226	-0.049
14	562	0.451*	-0.158	-0.041
15	574	0.459*	-0.122	-0.047
16	585	0.463*	-0.110	-0.006
17	596	0.483*	-0.076	0.062
18	608	0.505*	-0.157	0.117
19	619	0.471*	-0.149	0.147
20	630	0.454*	-0.184	0.137
21	642	0.430*	-0.129	0.193
22	653	0.452*	-0.105	0.170
23	664	0.468*	-0.170	0.164
24	676	0.481*	-0.124	0.167
25	687	0.467*	-0.040	0.221
26	699	0.441*	-0.097	0.207
27	710	0.443*	-0.103	0.251
28	722	0.422	-0.186	0.365
29	733	0.384	-0.101	0.224
30	744	0.175	-0.193	0.074
31	756	0.174	-0.242	0.100
32	767	0.337	-0.294	0.088
33	779	0.003	-0.167	-0.014
34	790	0.139	0.358	0.264

FINAL SPECTRA

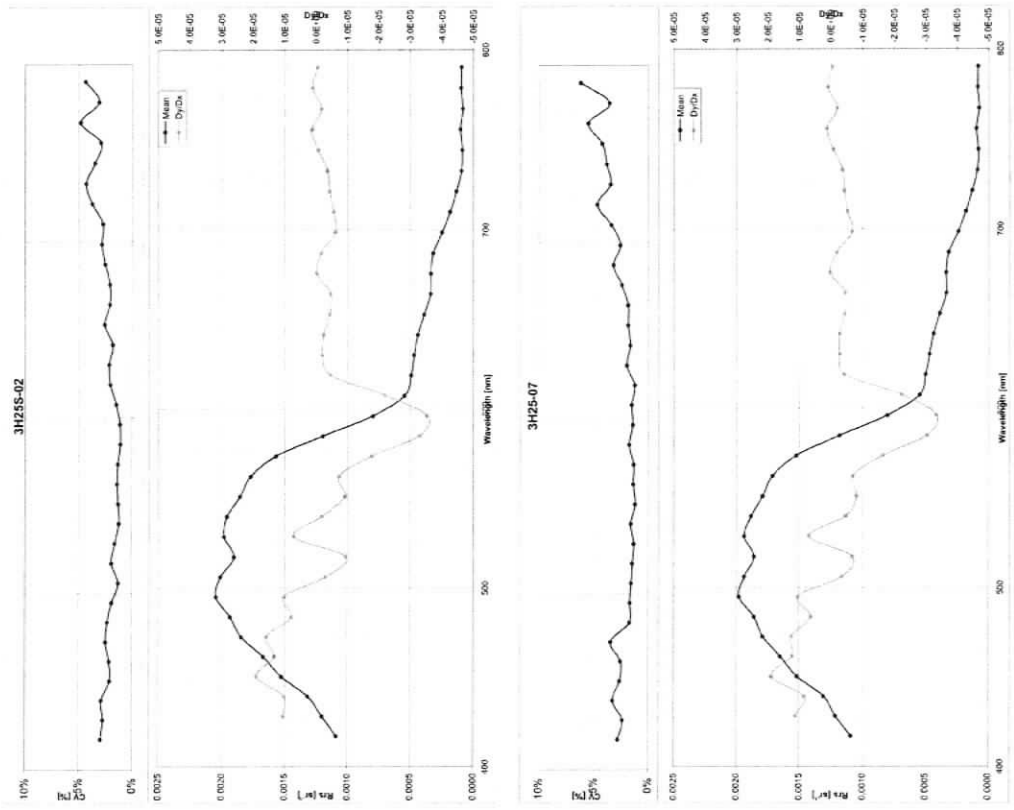
Brightened:

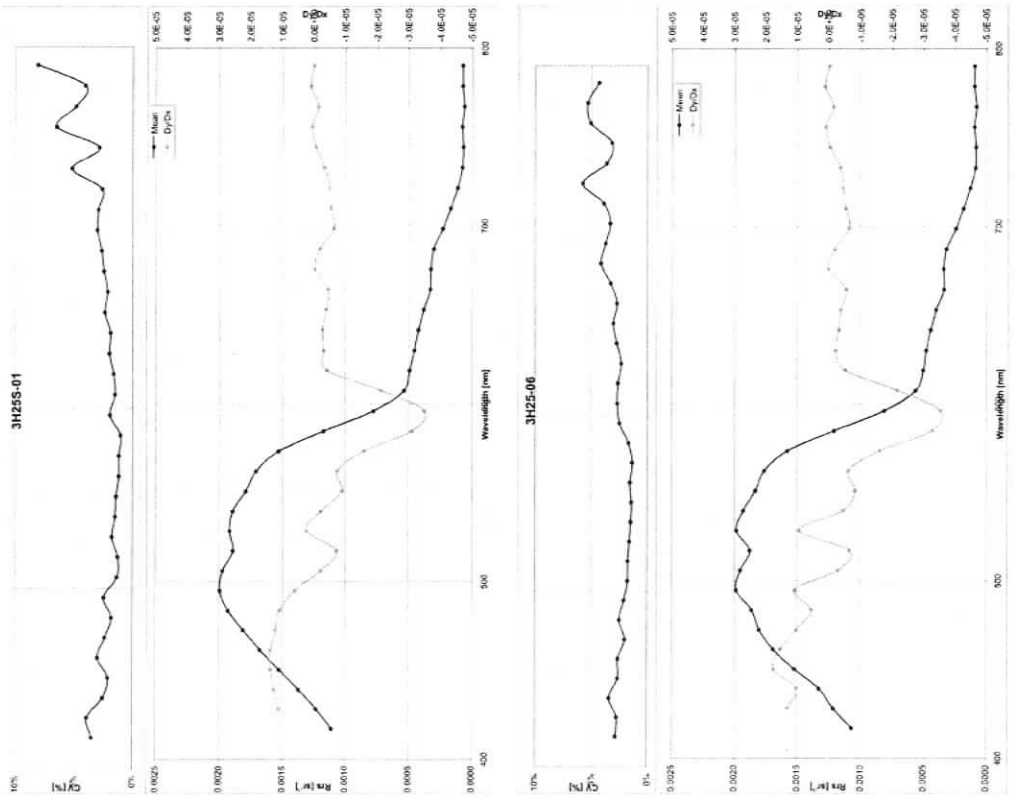
Darkened:
05 (Try 05)
06 (Try 02)
13 (Try 02)

::: APPENDIX E :::

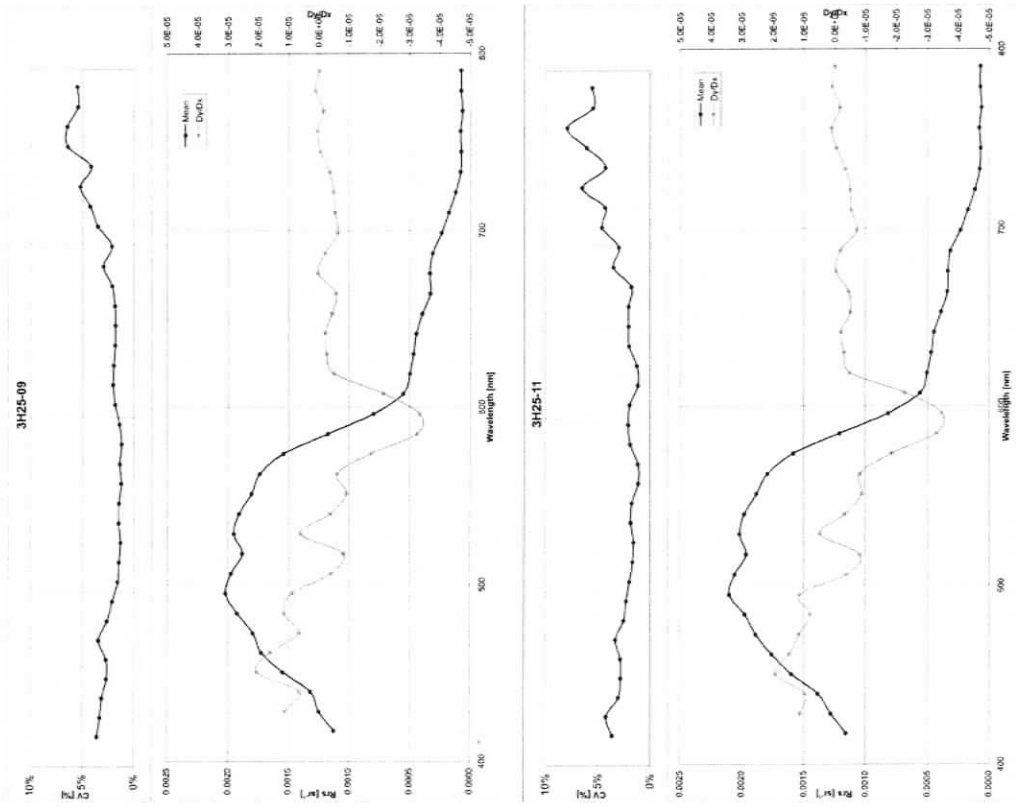
Final Extracted Spectra

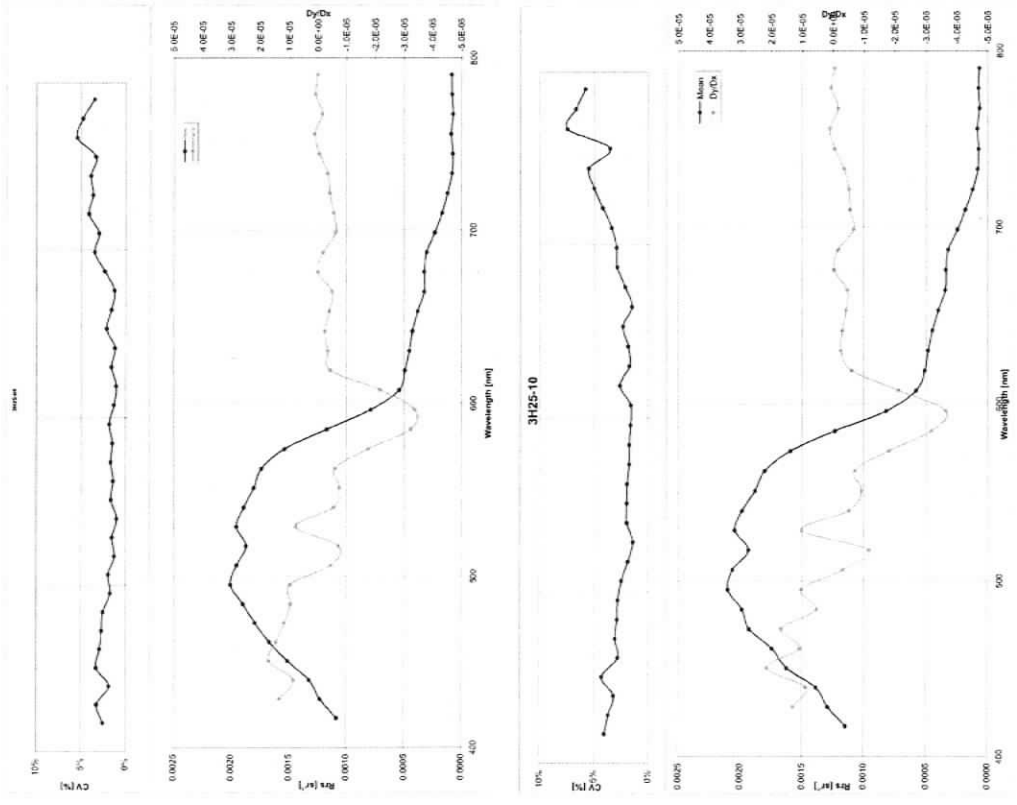
Band	WL	3H25S-01				3H25S-02				3H25-06				3H25-07			
		Mean	SD	CV	Dy/Dx	Mean	SD	CV	Dy/Dx	Mean	SD	CV	Dy/Dx	Mean	SD	CV	Dy/Dx
1	417	0.00111	3.9E-05	4%	-	0.00109	3.2E-05	3%	-	0.00107	3.0E-05	3%	-	0.00109	3.0E-05	3%	-
2	428	0.00123	4.8E-05	4%	1.1E-05	0.00120	3.3E-05	3%	1.0E-05	0.00121	3.3E-05	3%	1.3E-05	0.00121	2.8E-05	2%	1.1E-05
3	439	0.00137	3.5E-05	3%	1.3E-05	0.00131	3.8E-05	3%	1.0E-05	0.00133	4.5E-05	3%	1.0E-05	0.00131	4.2E-05	3%	8.6E-06
4	451	0.00152	3.2E-05	2%	1.4E-05	0.00152	3.2E-05	2%	1.9E-05	0.00152	4.0E-05	3%	1.8E-05	0.00152	3.9E-05	3%	1.9E-05
5	462	0.00167	5.0E-05	3%	1.4E-05	0.00167	3.6E-05	2%	1.3E-05	0.00169	4.4E-05	3%	1.5E-05	0.00165	4.1E-05	2%	1.2E-05
6	473	0.00181	4.3E-05	2%	1.2E-05	0.00184	4.6E-05	2%	1.6E-05	0.00180	3.6E-05	2%	1.0E-05	0.00179	6.1E-05	3%	1.2E-05
7	484	0.00193	3.5E-05	2%	1.1E-05	0.00193	4.5E-05	2%	7.7E-06	0.00186	4.6E-05	2%	5.4E-06	0.00186	3.1E-05	2%	6.3E-06
8	495	0.00199	4.9E-05	2%	6.0E-06	0.00204	3.9E-05	2%	1.0E-05	0.00198	4.1E-05	2%	1.1E-05	0.00198	3.2E-05	2%	1.0E-05
9	506	0.00197	2.6E-05	1%	-2.1E-06	0.00201	2.6E-05	1%	-3.1E-06	0.00195	3.4E-05	2%	-3.0E-06	0.00194	2.9E-05	1%	-3.7E-06
10	517	0.00189	2.4E-05	1%	-7.2E-06	0.00190	3.7E-05	2%	-9.6E-06	0.00188	3.2E-05	2%	-6.6E-06	0.00186	2.6E-05	1%	-6.8E-06
11	529	0.00191	3.4E-05	2%	2.3E-06	0.00198	3.2E-05	2%	7.0E-06	0.00198	3.1E-05	2%	9.4E-06	0.00194	2.5E-05	1%	6.9E-06
12	540	0.00189	2.8E-05	1%	-2.2E-06	0.00196	2.4E-05	1%	-2.0E-06	0.00193	2.8E-05	1%	-4.6E-06	0.00188	2.9E-05	2%	-4.8E-06
13	551	0.00179	2.5E-05	1%	-8.9E-06	0.00185	2.4E-05	1%	-9.2E-06	0.00183	2.6E-05	1%	-8.4E-06	0.00179	2.1E-05	1%	-8.1E-06
14	562	0.00170	2.0E-05	1%	-7.4E-06	0.00177	2.5E-05	1%	-7.4E-06	0.00176	2.7E-05	2%	-6.3E-06	0.00171	2.3E-05	1%	-7.0E-06
15	574	0.00153	1.8E-05	1%	-1.6E-05	0.00157	2.1E-05	1%	-1.8E-05	0.00158	2.1E-05	1%	-1.6E-05	0.00153	2.0E-05	1%	-1.7E-05
16	585	0.00117	1.2E-05	1%	-3.1E-05	0.00120	1.3E-05	1%	-3.3E-05	0.00121	2.0E-05	2%	-3.3E-05	0.00118	2.0E-05	2%	-3.1E-05
17	596	0.00078	1.5E-05	2%	-3.5E-05	0.00080	9.0E-06	1%	-3.5E-05	0.00081	2.0E-05	2%	-3.5E-05	0.00080	1.1E-05	1%	-3.4E-05
18	608	0.00054	8.0E-06	1%	-2.1E-05	0.00054	8.0E-06	1%	-2.2E-05	0.00056	1.5E-05	3%	-2.2E-05	0.00055	8.0E-06	1%	-2.2E-05
19	619	0.00049	8.0E-06	2%	-4.1E-06	0.00049	1.0E-05	2%	-4.7E-06	0.00050	1.3E-05	3%	-5.2E-06	0.00050	6.0E-06	1%	-4.2E-06
20	630	0.00046	9.0E-06	2%	-3.2E-06	0.00047	1.0E-05	2%	-2.0E-06	0.00048	1.1E-05	2%	-2.1E-06	0.00047	9.0E-06	2%	-2.7E-06
21	642	0.00043	8.0E-06	2%	-2.7E-06	0.00044	8.0E-06	2%	-2.5E-06	0.00044	1.2E-05	3%	-3.2E-06	0.00043	7.0E-06	2%	-2.8E-06
22	653	0.00038	9.0E-06	2%	-3.9E-06	0.00039	1.0E-05	3%	-4.3E-06	0.00040	1.2E-05	3%	-3.8E-06	0.00038	7.0E-06	2%	-4.4E-06
23	664	0.00033	7.0E-06	2%	-4.5E-06	0.00034	7.0E-06	2%	-4.6E-06	0.00033	9.0E-06	3%	-5.5E-06	0.00033	6.0E-06	2%	-4.6E-06
24	676	0.00033	8.0E-06	2%	-3.5E-07	0.00034	7.0E-06	2%	-1.8E-07	0.00034	1.1E-05	3%	1.8E-07	0.00034	8.0E-06	2%	2.6E-07
25	687	0.00030	8.0E-06	3%	-1.9E-06	0.00032	8.0E-06	3%	-1.7E-06	0.00032	1.3E-05	4%	-1.8E-06	0.00031	1.0E-05	3%	-1.8E-06
26	699	0.00023	7.0E-06	3%	-6.3E-06	0.00025	7.0E-06	3%	-6.1E-06	0.00024	9.0E-06	4%	-6.4E-06	0.00024	6.0E-06	3%	-6.8E-06
27	710	0.00017	5.0E-06	3%	-5.4E-06	0.00018	5.0E-06	3%	-5.6E-06	0.00018	6.0E-06	3%	-5.4E-06	0.00018	6.0E-06	3%	-5.2E-06
28	722	0.00012	3.0E-06	3%	-4.9E-06	0.00013	5.0E-06	4%	-4.3E-06	0.00013	5.0E-06	4%	-4.5E-06	0.00013	6.0E-06	5%	-4.3E-06
29	733	0.00008	4.0E-06	5%	-3.3E-06	0.00009	4.0E-06	4%	-3.6E-06	0.00009	5.0E-06	6%	-3.7E-06	0.00009	3.0E-06	3%	-3.7E-06
30	744	0.00007	2.0E-06	3%	-6.1E-07	0.00009	3.0E-06	3%	-6.1E-07	0.00008	3.0E-06	4%	-3.5E-07	0.00008	3.0E-06	4%	-7.0E-07
31	756	0.00008	5.0E-06	6%	6.1E-07	0.00010	3.0E-06	3%	1.4E-06	0.00010	3.0E-06	3%	1.0E-06	0.00010	4.0E-06	4%	1.4E-06
32	767	0.00006	3.0E-06	5%	-1.3E-06	0.00008	4.0E-06	5%	-1.7E-06	0.00008	4.0E-06	5%	-1.4E-06	0.00007	4.0E-06	5%	-1.9E-06
33	779	0.00007	3.0E-06	4%	1.0E-06	0.00010	3.0E-06	3%	1.2E-06	0.00009	5.0E-06	5%	1.3E-06	0.00009	3.0E-06	4%	1.0E-06
34	790	0.00007	6.0E-06	8%	0.0E+00	0.00009	4.0E-06	4%	-4.3E-07	0.00009	4.0E-06	4%	-8.7E-08	0.00008	5.0E-06	6%	-3.5E-07


3H25S-02
3H25-07
Mean
Dy/Dx
Wavelength [nm]


3H25S-01
3H25-06
Mean
Dy/Dx
Wavelength [nm]

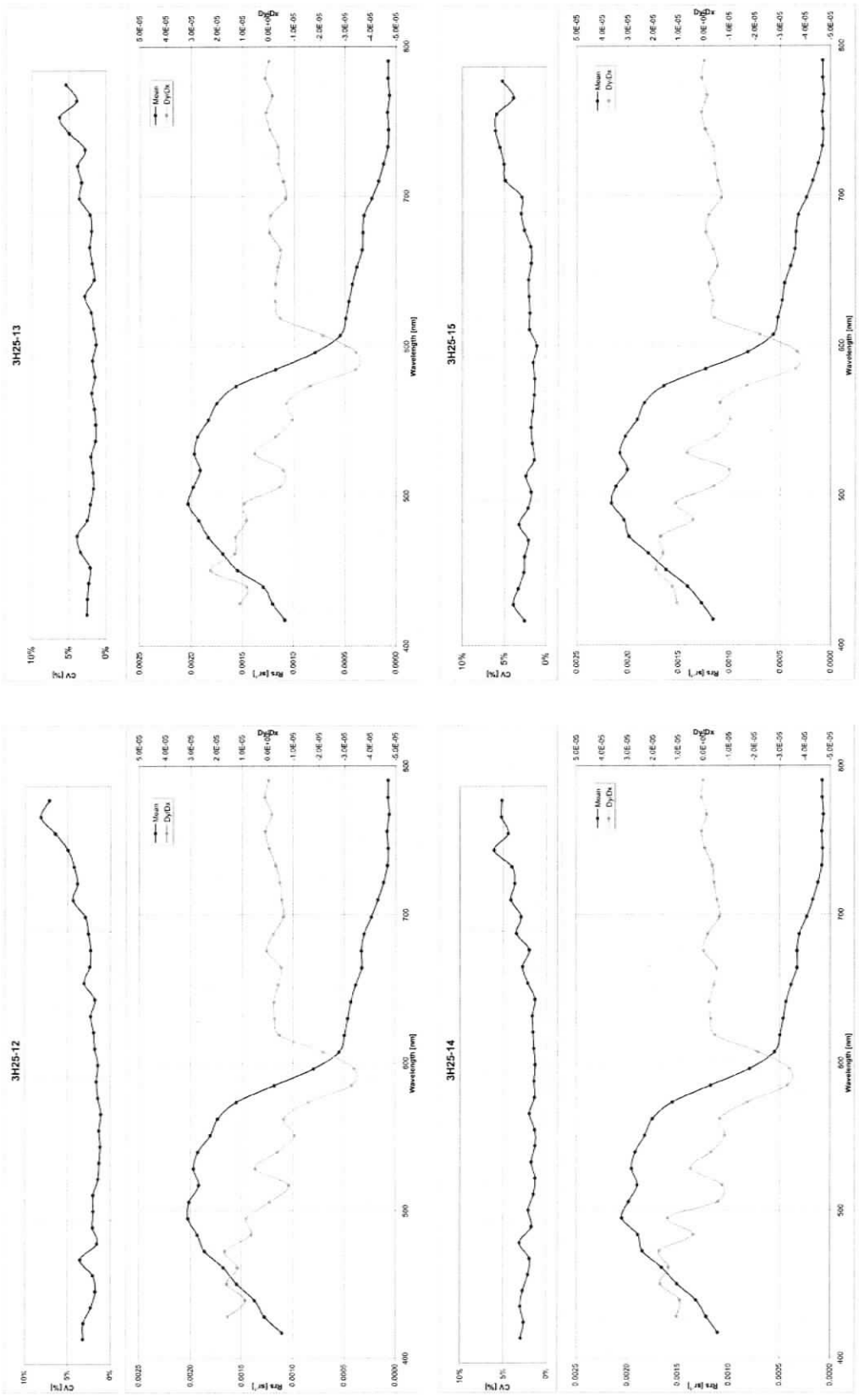
Band	WL	3H25-08				3H25-09				3H25-10				3H25-11			
		Mean	SD	CV	Dy/Dx	Mean	SD	CV	Dy/Dx	Mean	SD	CV	Dy/Dx	Mean	SD	CV	Dy/Dx
1	417	0.00108	2.7E-05	2%	-	0.00113	4.0E-05	4%	-	0.00115	4.6E-05	4%	-	0.00116	4.2E-05	4%	-
2	428	0.00123	3.9E-05	3%	1.3E-05	0.00125	4.1E-05	3%	1.1E-05	0.00129	4.7E-05	4%	1.3E-05	0.00128	5.4E-05	4%	1.1E-05
3	439	0.00132	2.4E-05	2%	8.3E-06	0.00132	4.1E-05	3%	6.3E-06	0.00139	4.4E-05	3%	8.7E-06	0.00139	4.2E-05	3%	9.5E-06
4	451	0.00151	4.9E-05	3%	1.7E-05	0.00155	4.1E-05	3%	2.0E-05	0.00162	6.9E-05	4%	2.1E-05	0.00160	4.5E-05	3%	1.9E-05
5	462	0.00167	4.8E-05	3%	1.4E-05	0.00172	4.6E-05	3%	1.6E-05	0.00174	4.8E-05	3%	1.1E-05	0.00176	5.0E-05	3%	1.5E-05
6	473	0.00179	4.7E-05	3%	1.1E-05	0.00180	6.1E-05	3%	6.5E-06	0.00193	5.8E-05	3%	1.7E-05	0.00189	6.3E-05	3%	1.2E-05
7	484	0.00190	4.7E-05	2%	9.4E-06	0.00192	5.0E-05	3%	1.1E-05	0.00198	5.6E-05	3%	5.2E-06	0.00198	5.0E-05	3%	7.9E-06
8	495	0.00201	3.4E-05	2%	9.6E-06	0.00202	4.2E-05	2%	8.8E-06	0.00210	5.8E-05	3%	1.0E-05	0.00210	4.8E-05	2%	1.1E-05
9	506	0.00195	3.7E-05	2%	-4.7E-06	0.00197	3.1E-05	2%	-4.1E-06	0.00206	5.0E-05	2%	-3.3E-06	0.00206	4.1E-05	2%	-3.9E-06
10	517	0.00187	2.3E-05	1%	-7.3E-06	0.00188	2.7E-05	1%	-8.1E-06	0.00193	3.5E-05	2%	-1.2E-05	0.00197	3.3E-05	2%	-8.1E-06
11	529	0.00195	2.9E-05	1%	7.5E-06	0.00195	2.5E-05	1%	6.1E-06	0.00204	2.8E-05	1%	1.0E-05	0.00202	3.2E-05	2%	4.6E-06
12	540	0.00189	1.8E-05	1%	-5.6E-06	0.00191	2.8E-05	1%	-3.8E-06	0.00198	3.8E-05	2%	-5.3E-06	0.00198	3.7E-05	2%	-3.4E-06
13	551	0.00181	2.9E-05	2%	-7.6E-06	0.00181	2.6E-05	1%	-9.1E-06	0.00188	3.6E-05	2%	-9.3E-06	0.00188	3.3E-05	2%	-8.8E-06
14	562	0.00174	2.4E-05	1%	-6.1E-06	0.00174	2.1E-05	1%	-6.2E-06	0.00180	3.4E-05	2%	-7.1E-06	0.00179	2.1E-05	1%	-8.1E-06
15	574	0.00154	2.5E-05	2%	-1.8E-05	0.00154	2.1E-05	1%	-1.7E-05	0.00159	2.7E-05	2%	-1.8E-05	0.00158	1.9E-05	1%	-1.8E-05
16	585	0.00117	1.7E-05	1%	-3.2E-05	0.00117	1.4E-05	1%	-3.3E-05	0.00123	2.1E-05	2%	-3.2E-05	0.00121	2.3E-05	2%	-3.3E-05
17	596	0.00079	1.4E-05	2%	-3.4E-05	0.00080	1.1E-05	1%	-3.3E-05	0.00082	1.3E-05	2%	-3.7E-05	0.00082	1.7E-05	2%	-3.5E-05
18	608	0.00054	7.0E-06	1%	-2.2E-05	0.00055	1.0E-05	2%	-2.1E-05	0.00058	9.0E-06	2%	-2.1E-05	0.00056	1.1E-05	2%	-2.3E-05
19	619	0.00049	5.0E-06	1%	-4.3E-06	0.00050	1.0E-05	2%	-5.0E-06	0.00051	1.3E-05	3%	-6.0E-06	0.00050	6.0E-06	1%	-4.9E-06
20	630	0.00045	7.0E-06	2%	-3.5E-06	0.00047	9.0E-06	2%	-2.7E-06	0.00048	8.0E-06	2%	-2.6E-06	0.00047	6.0E-06	1%	-3.0E-06
21	642	0.00043	5.0E-06	1%	-2.4E-06	0.00044	8.0E-06	2%	-2.1E-06	0.00044	8.0E-06	2%	-3.1E-06	0.00045	9.0E-06	2%	-2.0E-06
22	653	0.00038	8.0E-06	2%	-4.0E-06	0.00039	7.0E-06	2%	-4.3E-06	0.00039	9.0E-06	2%	-4.3E-06	0.00039	8.0E-06	2%	-5.0E-06
23	664	0.00032	5.0E-06	2%	-4.9E-06	0.00033	6.0E-06	2%	-5.7E-06	0.00034	5.0E-06	1%	-4.6E-06	0.00034	7.0E-06	2%	-4.5E-06
24	676	0.00032	4.0E-06	1%	8.8E-08	0.00033	7.0E-06	2%	2.6E-07	0.00034	7.0E-06	2%	-3.5E-07	0.00033	6.0E-06	2%	-4.4E-07
25	687	0.00030	7.0E-06	2%	-1.8E-06	0.00031	9.0E-06	3%	-2.1E-06	0.00032	9.0E-06	3%	-1.7E-06	0.00031	1.1E-05	4%	-1.8E-06
26	699	0.00023	8.0E-06	3%	-6.3E-06	0.00023	5.0E-06	2%	-6.3E-06	0.00024	7.0E-06	3%	-6.7E-06	0.00023	7.0E-06	3%	-7.0E-06
27	710	0.00017	5.0E-06	3%	-5.4E-06	0.00017	6.0E-06	3%	-5.4E-06	0.00018	6.0E-06	3%	-5.5E-06	0.00017	8.0E-06	5%	-5.3E-06
28	722	0.00012	5.0E-06	4%	-4.1E-06	0.00012	5.0E-06	4%	-4.8E-06	0.00012	5.0E-06	4%	-5.1E-06	0.00012	5.0E-06	4%	-5.0E-06
29	733	0.00008	3.0E-06	4%	-3.4E-06	0.00008	4.0E-06	5%	-3.6E-06	0.00008	4.0E-06	5%	-3.5E-06	0.00008	5.0E-06	6%	-3.4E-06
30	744	0.00008	3.0E-06	4%	-5.2E-07	0.00007	3.0E-06	4%	-4.3E-07	0.00007	4.0E-06	5%	-6.1E-07	0.00007	3.0E-06	4%	-6.1E-07
31	756	0.00009	3.0E-06	3%	1.2E-06	0.00008	5.0E-06	6%	5.2E-07	0.00009	3.0E-06	4%	1.0E-06	0.00008	5.0E-06	6%	1.0E-06
32	767	0.00007	4.0E-06	5%	-1.5E-06	0.00006	4.0E-06	6%	-1.4E-06	0.00007	5.0E-06	7%	-1.6E-06	0.00006	5.0E-06	8%	-1.7E-06
33	779	0.00008	4.0E-06	5%	8.7E-07	0.00007	4.0E-06	5%	1.0E-06	0.00008	5.0E-06	7%	7.0E-07	0.00007	4.0E-06	5%	8.7E-07
34	790	0.00009	3.0E-06	3%	1.7E-07	0.00007	4.0E-06	5%	-8.7E-08	0.00007	4.0E-06	6%	-5.2E-07	0.00007	4.0E-06	6%	-8.7E-08


3H25-09
CV [%]
Rrs [sr⁻¹]
Dy/Dx
Mean
Wavelength [nm]

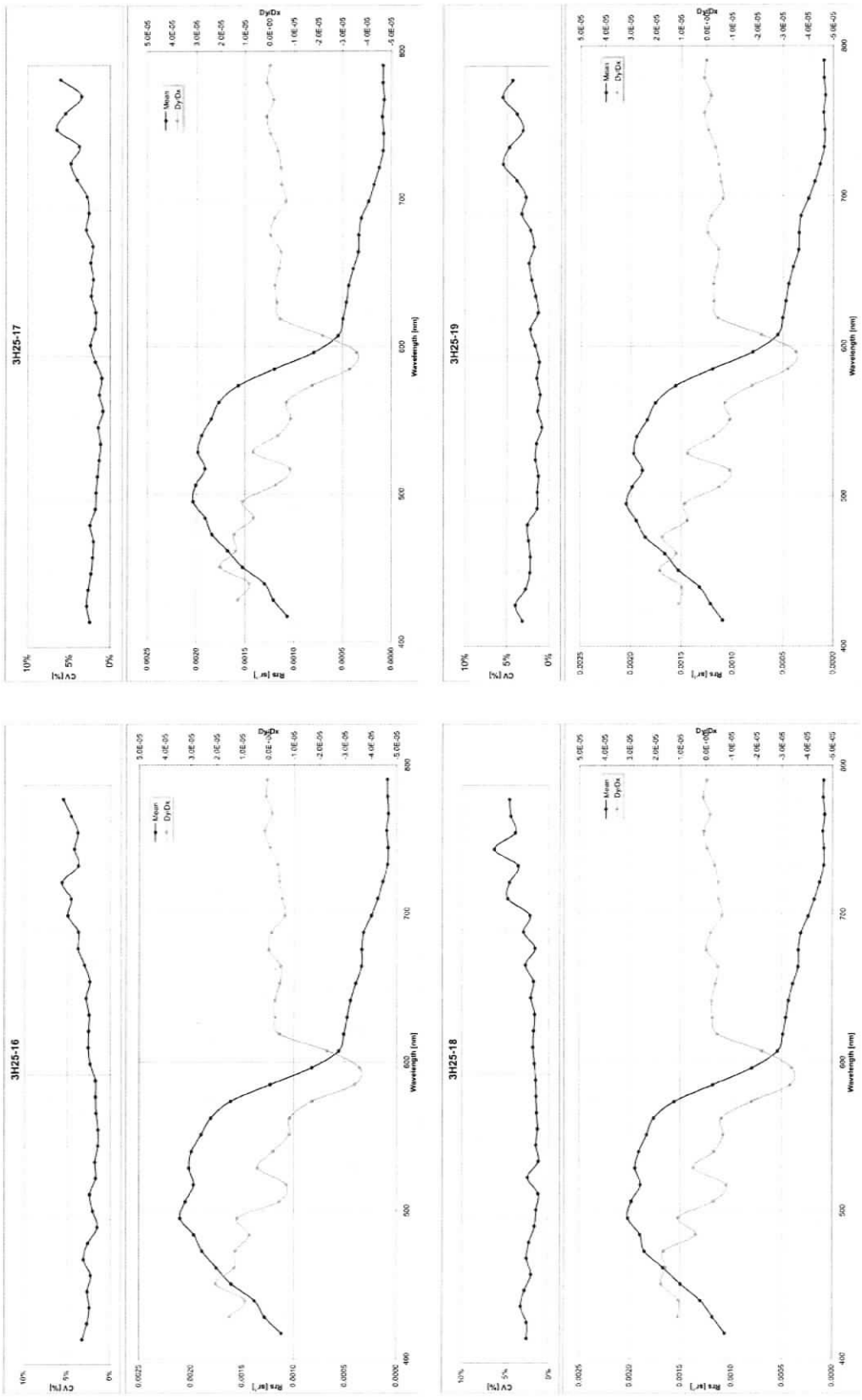

3H25-10
CV [%]
Rrs [sr⁻¹]
Dy/Dx
Mean
Wavelength [nm]

3H25-11
CV [%]
Rrs [sr⁻¹]
Dy/Dx
Mean
Wavelength [nm]

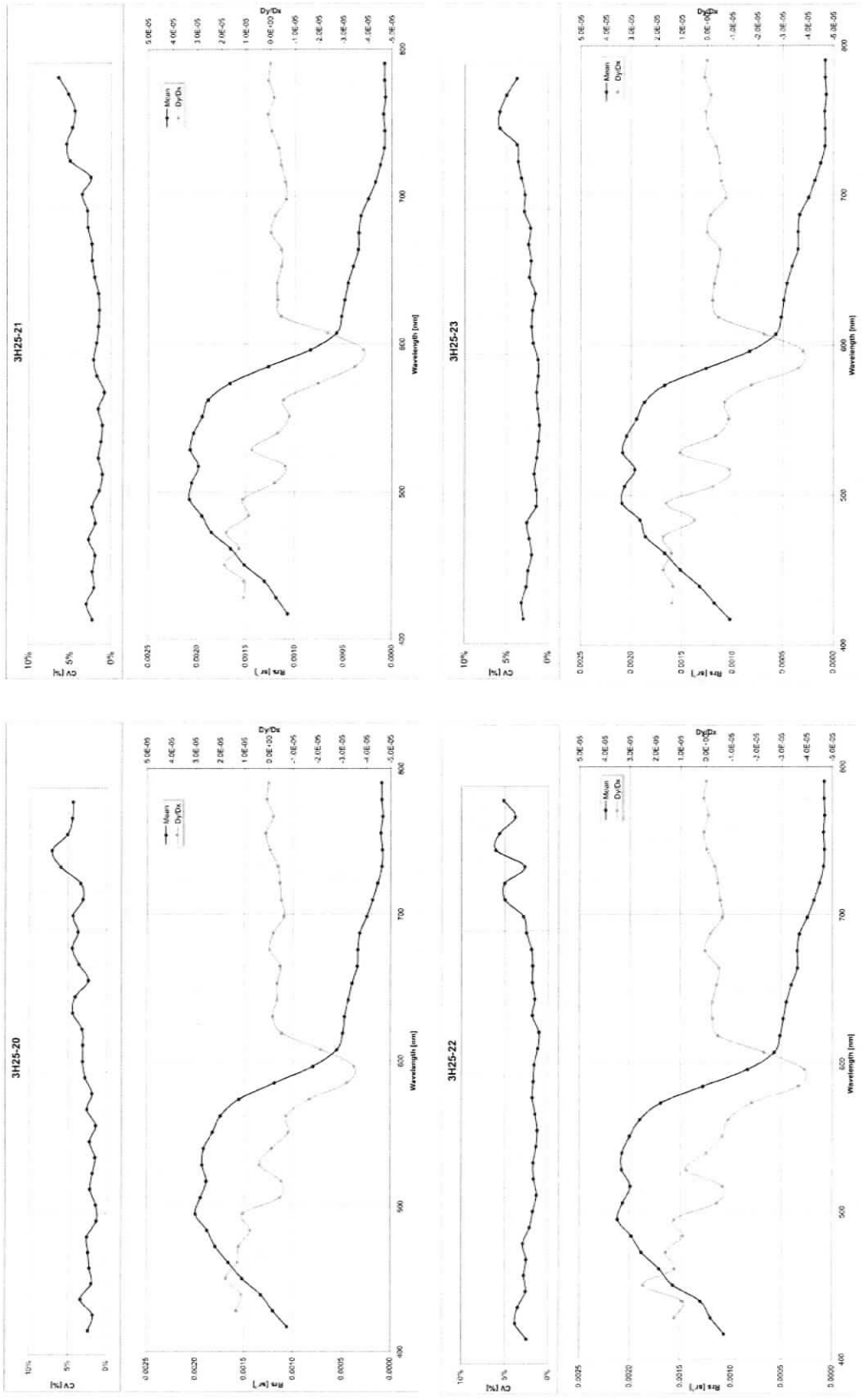
Band	WL	3H25-12				3H25-13				3H25-14				3H25-15			
		Mean	SD	CV	Dy/Dx	Mean	SD	CV	Dy/Dx	Mean	SD	CV	Dy/Dx	Mean	SD	CV	Dy/Dx
1	417	0.00111	3.5E-05	3%	-	0.00109	2.7E-05	2%	-	0.00111	3.3E-05	3%	-	0.00116	2.9E-05	3%	-
2	428	0.00128	4.0E-05	3%	1.5E-05	0.00121	2.9E-05	2%	1.1E-05	0.00122	3.2E-05	3%	1.0E-05	0.00127	4.9E-05	4%	1.1E-05
3	439	0.00137	3.1E-05	2%	8.6E-06	0.00130	2.9E-05	2%	8.2E-06	0.00132	4.0E-05	3%	9.2E-06	0.00141	4.6E-05	3%	1.2E-05
4	451	0.00155	2.7E-05	2%	1.6E-05	0.00155	3.2E-05	2%	2.3E-05	0.00151	4.1E-05	3%	1.7E-05	0.00162	4.2E-05	3%	1.9E-05
5	462	0.00168	3.4E-05	2%	1.2E-05	0.00169	5.7E-05	3%	1.3E-05	0.00166	3.5E-05	2%	1.4E-05	0.00180	4.5E-05	3%	1.6E-05
6	473	0.00186	6.5E-05	3%	1.6E-05	0.00183	7.0E-05	4%	1.3E-05	0.00185	3.6E-05	2%	1.7E-05	0.00199	4.1E-05	2%	1.7E-05
7	484	0.00193	3.0E-05	2%	6.3E-06	0.00193	4.7E-05	2%	8.4E-06	0.00189	5.9E-05	3%	4.0E-06	0.00203	6.5E-05	3%	4.3E-06
8	495	0.00202	4.1E-05	2%	8.2E-06	0.00203	4.1E-05	2%	9.4E-06	0.00205	3.5E-05	2%	1.4E-05	0.00216	4.5E-05	2%	1.1E-05
9	506	0.00201	4.0E-05	2%	-9.8E-07	0.00198	3.2E-05	2%	-4.6E-06	0.00198	4.1E-05	2%	-6.0E-06	0.00211	3.6E-05	2%	-3.9E-06
10	517	0.00192	3.8E-05	2%	-8.4E-06	0.00191	3.2E-05	2%	-5.9E-06	0.00190	2.8E-05	1%	-7.4E-06	0.00200	4.7E-05	2%	-9.9E-06
11	529	0.00197	2.8E-05	1%	4.7E-06	0.00197	3.9E-05	2%	5.2E-06	0.00196	2.5E-05	1%	5.0E-06	0.00208	2.8E-05	1%	6.5E-06
12	540	0.00193	2.5E-05	1%	-3.8E-06	0.00194	2.6E-05	1%	-2.9E-06	0.00192	3.3E-05	2%	-3.1E-06	0.00202	3.2E-05	2%	-4.7E-06
13	551	0.00181	2.1E-05	1%	-1.1E-05	0.00183	2.4E-05	1%	-9.4E-06	0.00183	2.3E-05	1%	-8.5E-06	0.00191	3.3E-05	2%	-1.0E-05
14	562	0.00174	2.3E-05	1%	-6.3E-06	0.00175	2.6E-05	1%	-7.2E-06	0.00175	2.3E-05	1%	-6.7E-06	0.00183	2.8E-05	2%	-6.4E-06
15	574	0.00155	1.7E-05	1%	-1.6E-05	0.00157	2.9E-05	2%	-1.6E-05	0.00155	3.0E-05	2%	-1.8E-05	0.00164	2.2E-05	1%	-1.7E-05
16	585	0.00118	1.7E-05	1%	-3.3E-05	0.00118	1.7E-05	1%	-3.4E-05	0.00118	1.6E-05	1%	-3.3E-05	0.00123	1.6E-05	1%	-3.6E-05
17	596	0.00080	1.3E-05	2%	-3.4E-05	0.00079	1.4E-05	2%	-3.4E-05	0.00079	1.1E-05	1%	-3.4E-05	0.00082	1.2E-05	1%	-3.7E-05
18	608	0.00055	8.0E-06	1%	-2.2E-05	0.00055	7.0E-06	1%	-2.1E-05	0.00055	7.0E-06	1%	-2.1E-05	0.00057	6.0E-06	1%	-2.2E-05
19	619	0.00050	9.0E-06	2%	-4.7E-06	0.00049	8.0E-06	2%	-4.8E-06	0.00050	7.0E-06	1%	-4.7E-06	0.00052	1.0E-05	2%	-4.1E-06
20	630	0.00047	9.0E-06	2%	-2.8E-06	0.00046	9.0E-06	2%	-2.7E-06	0.00046	7.0E-06	2%	-2.9E-06	0.00048	9.0E-06	2%	-3.7E-06
21	642	0.00044	1.0E-05	2%	-2.5E-06	0.00043	1.2E-05	3%	-2.9E-06	0.00043	7.0E-06	2%	-2.5E-06	0.00046	9.0E-06	2%	-2.1E-06
22	653	0.00039	7.0E-06	2%	-4.1E-06	0.00039	6.0E-06	2%	-3.8E-06	0.00039	5.0E-06	1%	-4.2E-06	0.00039	8.0E-06	2%	-5.4E-06
23	664	0.00033	1.0E-05	3%	-5.3E-06	0.00033	6.0E-06	2%	-4.7E-06	0.00033	7.0E-06	2%	-5.2E-06	0.00035	6.0E-06	2%	-3.8E-06
24	676	0.00033	8.0E-06	2%	2.6E-07	0.00033	7.0E-06	2%	-5.3E-07	0.00033	9.0E-06	3%	-8.8E-08	0.00034	6.0E-06	2%	-8.8E-07
25	687	0.00031	7.0E-06	2%	-2.4E-06	0.00031	6.0E-06	2%	-9.6E-07	0.00031	6.0E-06	2%	-1.8E-06	0.00032	8.0E-06	3%	-2.1E-06
26	699	0.00023	6.0E-06	3%	-6.2E-06	0.00024	5.0E-06	2%	-6.8E-06	0.00023	8.0E-06	3%	-6.4E-06	0.00024	7.0E-06	3%	-6.9E-06
27	710	0.00017	5.0E-06	3%	-5.5E-06	0.00017	6.0E-06	4%	-5.9E-06	0.00017	5.0E-06	3%	-5.4E-06	0.00018	5.0E-06	3%	-5.5E-06
28	722	0.00012	5.0E-06	4%	-4.9E-06	0.00012	4.0E-06	3%	-4.0E-06	0.00012	5.0E-06	4%	-4.3E-06	0.00012	6.0E-06	5%	-4.4E-06
29	733	0.00008	3.0E-06	4%	-3.2E-06	0.00008	3.0E-06	4%	-3.9E-06	0.00008	3.0E-06	4%	-3.5E-06	0.00008	4.0E-06	5%	-3.9E-06
30	744	0.00007	3.0E-06	4%	-6.1E-07	0.00007	2.0E-06	3%	-6.1E-07	0.00008	3.0E-06	4%	-6.1E-07	0.00007	4.0E-06	5%	-6.1E-07
31	756	0.00008	4.0E-06	5%	8.7E-07	0.00008	4.0E-06	5%	7.8E-07	0.00008	5.0E-06	6%	7.0E-07	0.00008	5.0E-06	6%	8.7E-07
32	767	0.00006	4.0E-06	6%	-1.7E-06	0.00006	4.0E-06	6%	-1.5E-06	0.00007	3.0E-06	4%	-1.3E-06	0.00007	4.0E-06	6%	-1.3E-06
33	779	0.00007	6.0E-06	8%	1.0E-06	0.00008	3.0E-06	4%	1.1E-06	0.00008	4.0E-06	5%	7.8E-07	0.00008	3.0E-06	4%	8.7E-07
34	790	0.00007	5.0E-06	7%	-3.5E-07	0.00008	4.0E-06	5%	-1.7E-07	0.00008	4.0E-06	5%	8.7E-08	0.00008	4.0E-06	5%	-8.7E-08


3H25-13
3H25-15
3H25-12
3H25-14
CV [%]
Rrs [sr⁻¹]
Wavelength [nm]
Mean
DyDx

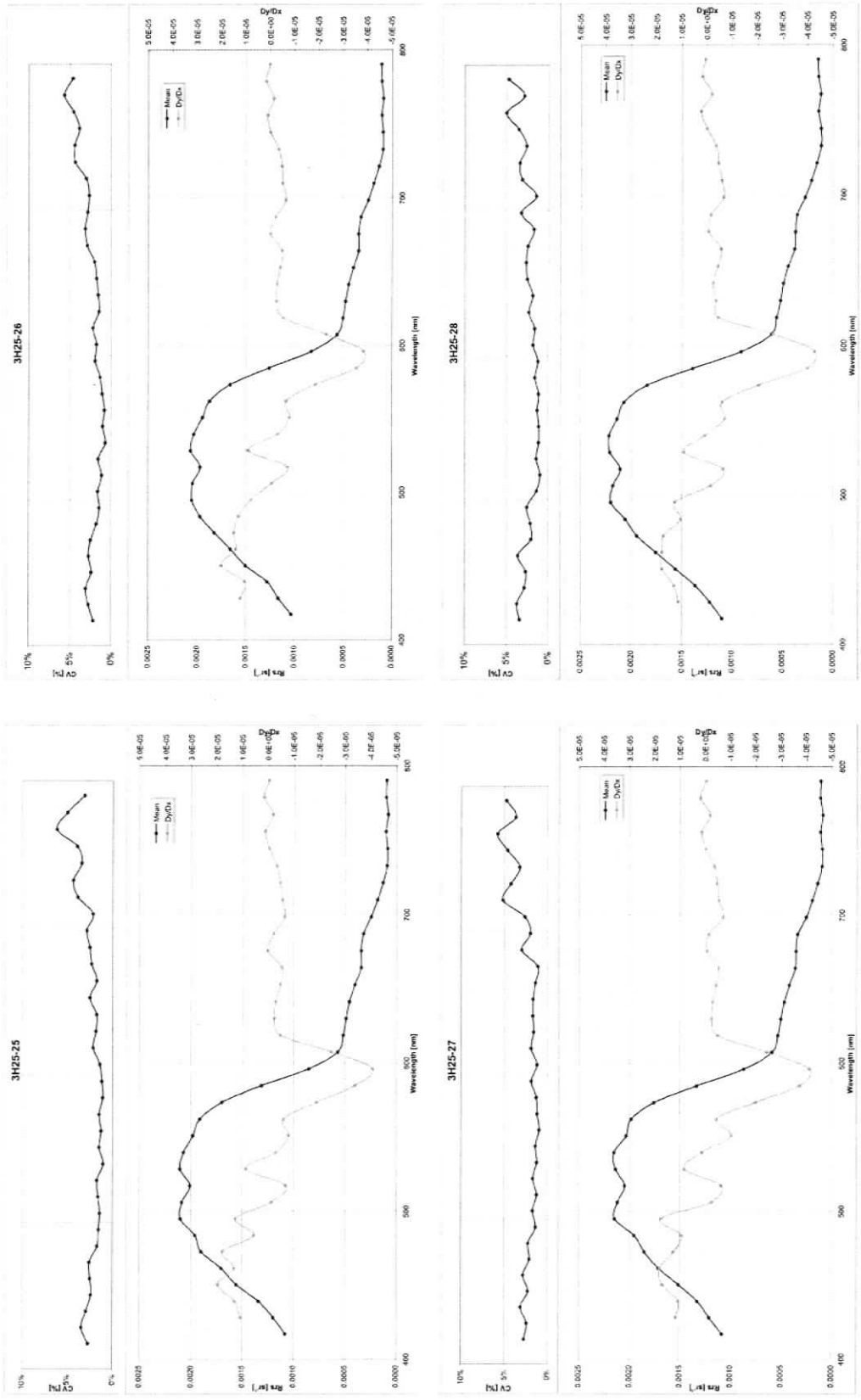
Band	WL	3H25-16				3H25-17				3H25-18				3H25-19			
		Mean	SD	CV	Dy/Dx	Mean	SD	CV	Dy/Dx	Mean	SD	CV	Dy/Dx	Mean	SD	CV	Dy/Dx
1	417	0.00112	3.6E-05	3%	-	0.00107	2.6E-05	2%	-	0.00106	2.7E-05	3%	-	0.00109	3.4E-05	3%	-
2	428	0.00128	3.4E-05	3%	1.5E-05	0.00121	3.4E-05	3%	1.3E-05	0.00118	3.0E-05	3%	1.1E-05	0.00121	4.8E-05	4%	1.1E-05
3	439	0.00138	3.3E-05	2%	8.8E-06	0.00130	3.4E-05	3%	8.2E-06	0.00130	4.2E-05	3%	1.1E-05	0.00132	3.6E-05	3%	9.8E-06
4	451	0.00160	4.2E-05	3%	2.0E-05	0.00152	3.5E-05	2%	2.0E-05	0.00150	4.2E-05	3%	1.8E-05	0.00153	3.4E-05	2%	1.9E-05
5	462	0.00175	3.9E-05	2%	1.3E-05	0.00168	3.5E-05	2%	1.4E-05	0.00167	3.4E-05	2%	1.6E-05	0.00166	3.6E-05	2%	1.2E-05
6	473	0.00189	5.8E-05	3%	1.3E-05	0.00184	3.7E-05	2%	1.4E-05	0.00186	4.7E-05	3%	1.7E-05	0.00186	4.4E-05	2%	1.8E-05
7	484	0.00197	5.1E-05	3%	7.2E-06	0.00191	4.6E-05	2%	6.5E-06	0.00190	4.3E-05	2%	3.9E-06	0.00195	4.9E-05	3%	7.7E-06
8	495	0.00210	3.1E-05	1%	1.2E-05	0.00203	3.6E-05	2%	1.1E-05	0.00202	3.3E-05	2%	1.1E-05	0.00204	2.8E-05	1%	8.8E-06
9	506	0.00205	4.1E-05	2%	-4.5E-06	0.00200	3.4E-05	2%	-2.5E-06	0.00199	2.9E-05	1%	-3.1E-06	0.00199	2.7E-05	1%	-4.9E-06
10	517	0.00197	4.7E-05	2%	-7.1E-06	0.00191	2.9E-05	2%	-8.5E-06	0.00190	2.3E-05	1%	-8.1E-06	0.00189	2.3E-05	1%	-9.0E-06
11	529	0.00202	3.4E-05	2%	4.0E-06	0.00198	2.6E-05	1%	6.6E-06	0.00195	4.7E-05	2%	4.8E-06	0.00197	3.1E-05	2%	7.5E-06
12	540	0.00199	3.5E-05	2%	-2.1E-06	0.00194	2.2E-05	1%	-3.5E-06	0.00191	2.3E-05	1%	-3.3E-06	0.00194	2.8E-05	1%	-2.7E-06
13	551	0.00190	2.7E-05	1%	-8.3E-06	0.00185	2.6E-05	1%	-8.7E-06	0.00183	2.7E-05	1%	-6.9E-06	0.00184	1.5E-05	1%	-9.1E-06
14	562	0.00181	2.5E-05	1%	-8.5E-06	0.00177	1.5E-05	1%	-7.1E-06	0.00176	2.3E-05	1%	-6.3E-06	0.00176	2.3E-05	1%	-7.1E-06
15	574	0.00161	2.6E-05	2%	-1.7E-05	0.00157	2.0E-05	1%	-1.7E-05	0.00156	2.2E-05	1%	-1.8E-05	0.00156	1.6E-05	1%	-1.8E-05
16	585	0.00123	2.1E-05	2%	-3.4E-05	0.00120	1.2E-05	1%	-3.3E-05	0.00118	1.7E-05	1%	-3.4E-05	0.00119	1.7E-05	1%	-3.2E-05
17	596	0.00083	1.4E-05	2%	-3.6E-05	0.00079	1.4E-05	2%	-3.6E-05	0.00080	1.2E-05	2%	-3.4E-05	0.00080	9.0E-06	1%	-3.5E-05
18	608	0.00056	1.3E-05	2%	-2.3E-05	0.00055	1.3E-05	2%	-2.2E-05	0.00054	9.0E-06	2%	-2.2E-05	0.00055	9.0E-06	2%	-2.2E-05
19	619	0.00051	1.3E-05	3%	-4.4E-06	0.00050	9.0E-06	2%	-4.4E-06	0.00049	9.0E-06	2%	-4.7E-06	0.00050	1.1E-05	2%	-4.3E-06
20	630	0.00048	1.2E-05	3%	-2.8E-06	0.00046	8.0E-06	2%	-3.0E-06	0.00046	8.0E-06	2%	-2.7E-06	0.00047	6.0E-06	1%	-2.8E-06
21	642	0.00045	1.1E-05	2%	-2.8E-06	0.00044	1.0E-05	2%	-2.3E-06	0.00043	7.0E-06	2%	-2.3E-06	0.00044	7.0E-06	2%	-2.5E-06
22	653	0.00040	1.1E-05	3%	-4.6E-06	0.00039	8.0E-06	2%	-3.9E-06	0.00039	8.0E-06	2%	-3.8E-06	0.00040	8.0E-06	2%	-3.9E-06
23	664	0.00034	8.0E-06	2%	-4.9E-06	0.00034	8.0E-06	2%	-4.6E-06	0.00034	6.0E-06	2%	-4.7E-06	0.00034	8.0E-06	2%	-4.6E-06
24	676	0.00034	1.0E-05	3%	-2.6E-07	0.00033	7.0E-06	2%	-4.4E-07	0.00033	9.0E-06	3%	-1.8E-07	0.00034	6.0E-06	2%	-2.6E-07
25	687	0.00032	1.2E-05	4%	-1.4E-06	0.00031	9.0E-06	3%	-2.0E-06	0.00031	5.0E-06	2%	-1.9E-06	0.00032	7.0E-06	2%	-1.7E-06
26	699	0.00025	9.0E-06	4%	-6.6E-06	0.00023	6.0E-06	3%	-6.8E-06	0.00024	7.0E-06	3%	-6.3E-06	0.00025	8.0E-06	3%	-6.4E-06
27	710	0.00018	9.0E-06	5%	-5.4E-06	0.00018	5.0E-06	3%	-4.9E-06	0.00018	4.0E-06	2%	-5.0E-06	0.00018	5.0E-06	3%	-5.5E-06
28	722	0.00013	6.0E-06	5%	-4.4E-06	0.00012	5.0E-06	4%	-4.7E-06	0.00013	6.0E-06	5%	-4.8E-06	0.00013	5.0E-06	4%	-4.6E-06
29	733	0.00009	5.0E-06	6%	-3.8E-06	0.00008	4.0E-06	5%	-3.5E-06	0.00009	4.0E-06	5%	-3.4E-06	0.00009	5.0E-06	5%	-3.4E-06
30	744	0.00008	3.0E-06	4%	-7.0E-07	0.00008	3.0E-06	4%	-3.5E-07	0.00008	3.0E-06	4%	-3.5E-07	0.00009	4.0E-06	5%	-6.1E-07
31	756	0.00010	4.0E-06	4%	1.3E-06	0.00009	6.0E-06	6%	1.1E-06	0.00010	6.0E-06	6%	9.6E-07	0.00010	3.0E-06	3%	1.0E-06
32	767	0.00008	3.0E-06	4%	-1.5E-06	0.00007	4.0E-06	5%	-1.7E-06	0.00008	3.0E-06	4%	-1.6E-06	0.00008	3.0E-06	4%	-1.6E-06
33	779	0.00009	4.0E-06	5%	7.8E-07	0.00009	3.0E-06	3%	1.0E-06	0.00009	4.0E-06	4%	1.2E-06	0.00009	5.0E-06	5%	1.0E-06
34	790	0.00009	5.0E-06	5%	2.6E-07	0.00008	5.0E-06	6%	-2.6E-07	0.00009	4.0E-06	5%	-2.6E-07	0.00009	4.0E-06	4%	1.7E-07


3H25-17
3H25-19
3H25-16
3H25-18
CV [%]
Rrs [sr⁻¹]
Wavelength [nm]
Mean
DyDx

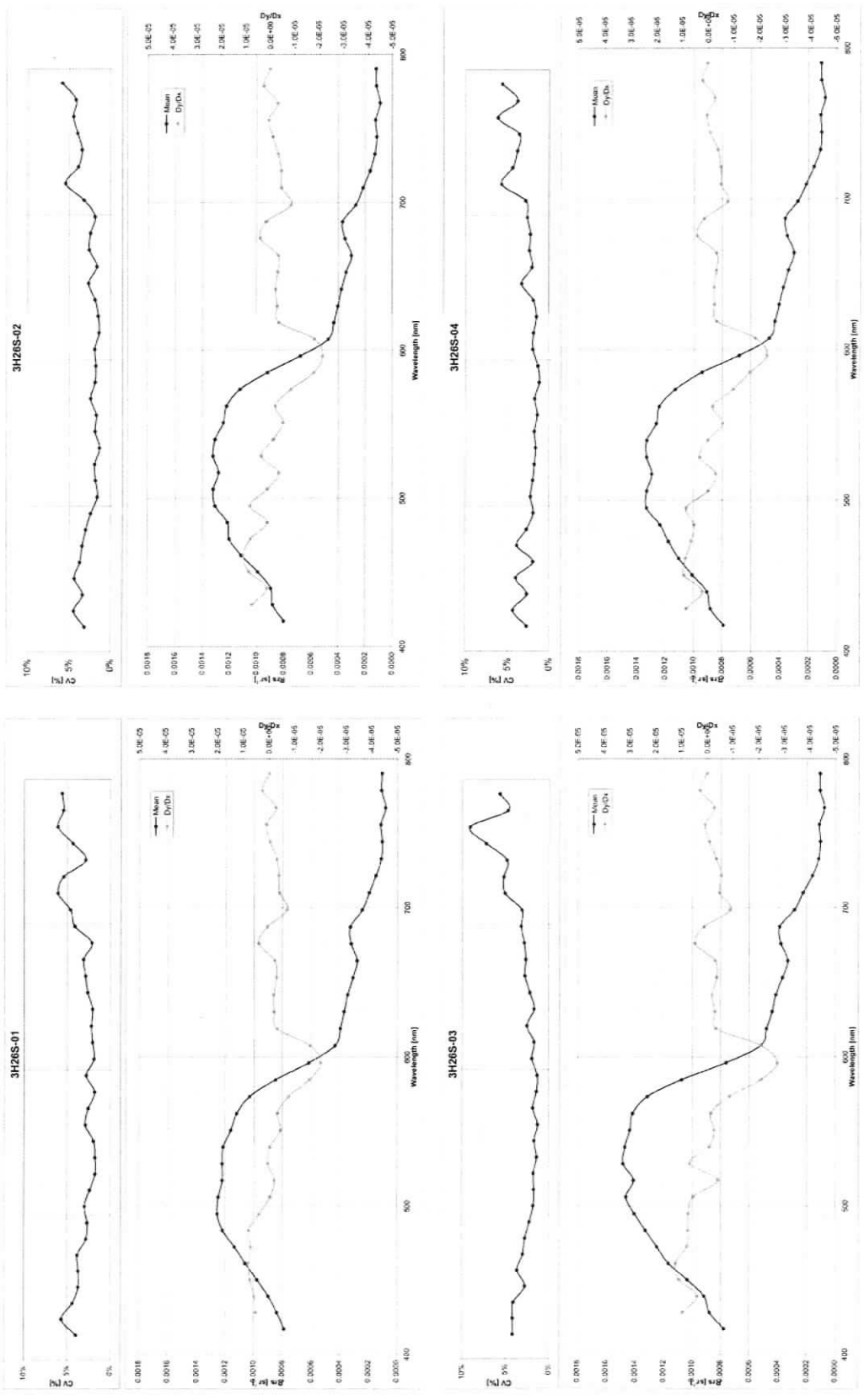
Band	WL	3H25-20				3H25-21				3H25-22				3H25-23			
		Mean	SD	CV	Dy/Dx	Mean	SD	CV	Dy/Dx	Mean	SD	CV	Dy/Dx	Mean	SD	CV	Dy/Dx
1	417	0.00106	2.5E-05	2%	-	0.00107	2.4E-05	2%	-	0.00106	2.6E-05	2%	-	0.00102	3.0E-05	3%	-
2	428	0.00120	2.1E-05	2%	1.3E-05	0.00119	3.5E-05	3%	1.1E-05	0.00120	4.5E-05	4%	1.2E-05	0.00117	3.7E-05	3%	1.4E-05
3	439	0.00133	4.4E-05	3%	1.1E-05	0.00131	2.7E-05	2%	1.1E-05	0.00130	4.5E-05	3%	9.1E-06	0.00132	3.4E-05	3%	1.3E-05
4	451	0.00152	2.9E-05	2%	1.7E-05	0.00151	3.4E-05	2%	1.9E-05	0.00157	4.0E-05	3%	2.5E-05	0.00151	3.6E-05	2%	1.7E-05
5	462	0.00166	3.6E-05	2%	1.3E-05	0.00165	3.2E-05	2%	1.3E-05	0.00171	4.7E-05	3%	1.2E-05	0.00167	3.2E-05	2%	1.4E-05
6	473	0.00180	4.2E-05	2%	1.2E-05	0.00185	5.0E-05	3%	1.8E-05	0.00188	4.7E-05	2%	1.6E-05	0.00186	4.1E-05	2%	1.7E-05
7	484	0.00188	4.7E-05	3%	7.5E-06	0.00195	3.7E-05	2%	8.8E-06	0.00198	5.7E-05	3%	9.0E-06	0.00191	4.8E-05	3%	4.9E-06
8	495	0.00200	2.6E-05	1%	1.1E-05	0.00208	4.8E-05	2%	1.1E-05	0.00212	4.4E-05	2%	1.2E-05	0.00209	2.9E-05	1%	1.6E-05
9	506	0.00195	2.7E-05	1%	-4.6E-06	0.00206	2.9E-05	1%	-1.9E-06	0.00207	3.6E-05	2%	-4.6E-06	0.00206	2.9E-05	1%	-2.4E-06
10	517	0.00189	4.0E-05	2%	-5.2E-06	0.00199	2.1E-05	1%	-6.2E-06	0.00199	2.6E-05	1%	-6.7E-06	0.00196	3.2E-05	2%	-8.9E-06
11	529	0.00193	3.5E-05	2%	3.7E-06	0.00207	3.2E-05	2%	7.5E-06	0.00208	3.4E-05	2%	7.7E-06	0.00208	2.8E-05	1%	1.1E-05
12	540	0.00192	2.8E-05	1%	-1.3E-06	0.00204	2.5E-05	1%	-3.0E-06	0.00208	3.5E-05	2%	-3.6E-07	0.00204	2.3E-05	1%	-3.5E-06
13	551	0.00183	4.0E-05	2%	-8.1E-06	0.00195	2.1E-05	1%	-7.8E-06	0.00200	2.7E-05	1%	-6.7E-06	0.00195	2.0E-05	1%	-8.7E-06
14	562	0.00174	2.4E-05	1%	-7.2E-06	0.00189	3.0E-05	2%	-5.4E-06	0.00190	2.3E-05	1%	-9.0E-06	0.00187	2.3E-05	1%	-7.1E-06
15	574	0.00155	3.9E-05	3%	-1.7E-05	0.00166	1.4E-05	1%	-2.0E-05	0.00169	2.5E-05	1%	-1.8E-05	0.00167	2.3E-05	1%	-1.8E-05
16	585	0.00119	2.2E-05	2%	-3.2E-05	0.00127	2.2E-05	2%	-3.5E-05	0.00128	2.3E-05	2%	-3.7E-05	0.00126	1.5E-05	1%	-3.6E-05
17	596	0.00079	2.2E-05	3%	-3.5E-05	0.00084	1.8E-05	2%	-3.8E-05	0.00083	1.4E-05	2%	-3.9E-05	0.00083	1.0E-05	1%	-3.8E-05
18	608	0.00055	1.7E-05	3%	-2.1E-05	0.00057	1.0E-05	2%	-2.4E-05	0.00057	9.0E-06	2%	-2.3E-05	0.00057	1.0E-05	2%	-2.3E-05
19	619	0.00049	1.5E-05	3%	-5.3E-06	0.00052	8.0E-06	2%	-4.5E-06	0.00051	6.0E-06	1%	-4.9E-06	0.00052	1.0E-05	2%	-4.6E-06
20	630	0.00047	1.5E-05	3%	-1.6E-06	0.00048	7.0E-06	1%	-3.0E-06	0.00048	5.0E-06	1%	-2.8E-06	0.00049	9.0E-06	2%	-2.3E-06
21	642	0.00043	1.9E-05	4%	-3.4E-06	0.00045	7.0E-06	2%	-2.9E-06	0.00045	8.0E-06	2%	-2.7E-06	0.00046	7.0E-06	2%	-3.0E-06
22	653	0.00039	1.6E-05	4%	-3.4E-06	0.00040	8.0E-06	2%	-4.6E-06	0.00040	6.0E-06	2%	-4.5E-06	0.00041	9.0E-06	2%	-4.4E-06
23	664	0.00034	8.0E-06	2%	-4.7E-06	0.00034	8.0E-06	2%	-4.6E-06	0.00034	6.0E-06	2%	-5.3E-06	0.00035	7.0E-06	2%	-5.2E-06
24	676	0.00034	1.2E-05	4%	-3.5E-07	0.00034	8.0E-06	2%	-3.5E-07	0.00034	6.0E-06	2%	1.8E-07	0.00035	8.0E-06	2%	0.0E+00
25	687	0.00032	1.4E-05	4%	-1.8E-06	0.00032	9.0E-06	3%	-2.0E-06	0.00032	6.0E-06	2%	-1.9E-06	0.00033	7.0E-06	2%	-1.4E-06
26	699	0.00024	9.0E-06	4%	-6.3E-06	0.00024	7.0E-06	3%	-6.6E-06	0.00024	6.0E-06	2%	-6.7E-06	0.00025	7.0E-06	3%	-7.5E-06
27	710	0.00018	8.0E-06	4%	-5.2E-06	0.00017	6.0E-06	4%	-6.3E-06	0.00018	5.0E-06	3%	-5.8E-06	0.00018	5.0E-06	3%	-5.6E-06
28	722	0.00013	4.0E-06	3%	-4.6E-06	0.00012	3.0E-06	3%	-4.3E-06	0.00012	6.0E-06	5%	-4.9E-06	0.00012	4.0E-06	3%	-5.0E-06
29	733	0.00009	3.0E-06	3%	-3.7E-06	0.00008	4.0E-06	5%	-3.5E-06	0.00008	4.0E-06	5%	-3.6E-06	0.00008	3.0E-06	4%	-3.6E-06
30	744	0.00008	5.0E-06	6%	-4.3E-07	0.00007	4.0E-06	5%	-5.2E-07	0.00008	2.0E-06	3%	-4.3E-07	0.00008	3.0E-06	4%	-2.6E-07
31	756	0.00010	7.0E-06	7%	1.3E-06	0.00009	4.0E-06	5%	9.6E-07	0.00008	5.0E-06	6%	7.0E-07	0.00009	5.0E-06	6%	5.2E-07
32	767	0.00008	4.0E-06	5%	-1.8E-06	0.00007	3.0E-06	4%	-1.5E-06	0.00007	4.0E-06	6%	-1.1E-06	0.00007	4.0E-06	6%	-1.5E-06
33	779	0.00009	4.0E-06	4%	9.6E-07	0.00008	4.0E-06	5%	7.8E-07	0.00008	3.0E-06	4%	7.0E-07	0.00008	4.0E-06	5%	9.6E-07
34	790	0.00009	4.0E-06	4%	1.7E-07	0.00008	5.0E-06	6%	8.7E-08	0.00008	4.0E-06	5%	-8.7E-08	0.00008	3.0E-06	4%	0.0E+00


3H25-21
3H25-23
3H25-20
3H25-22
CV [%]
Rrs [sr⁻¹]
Dy/Dx
Mean
Wavelength [nm]

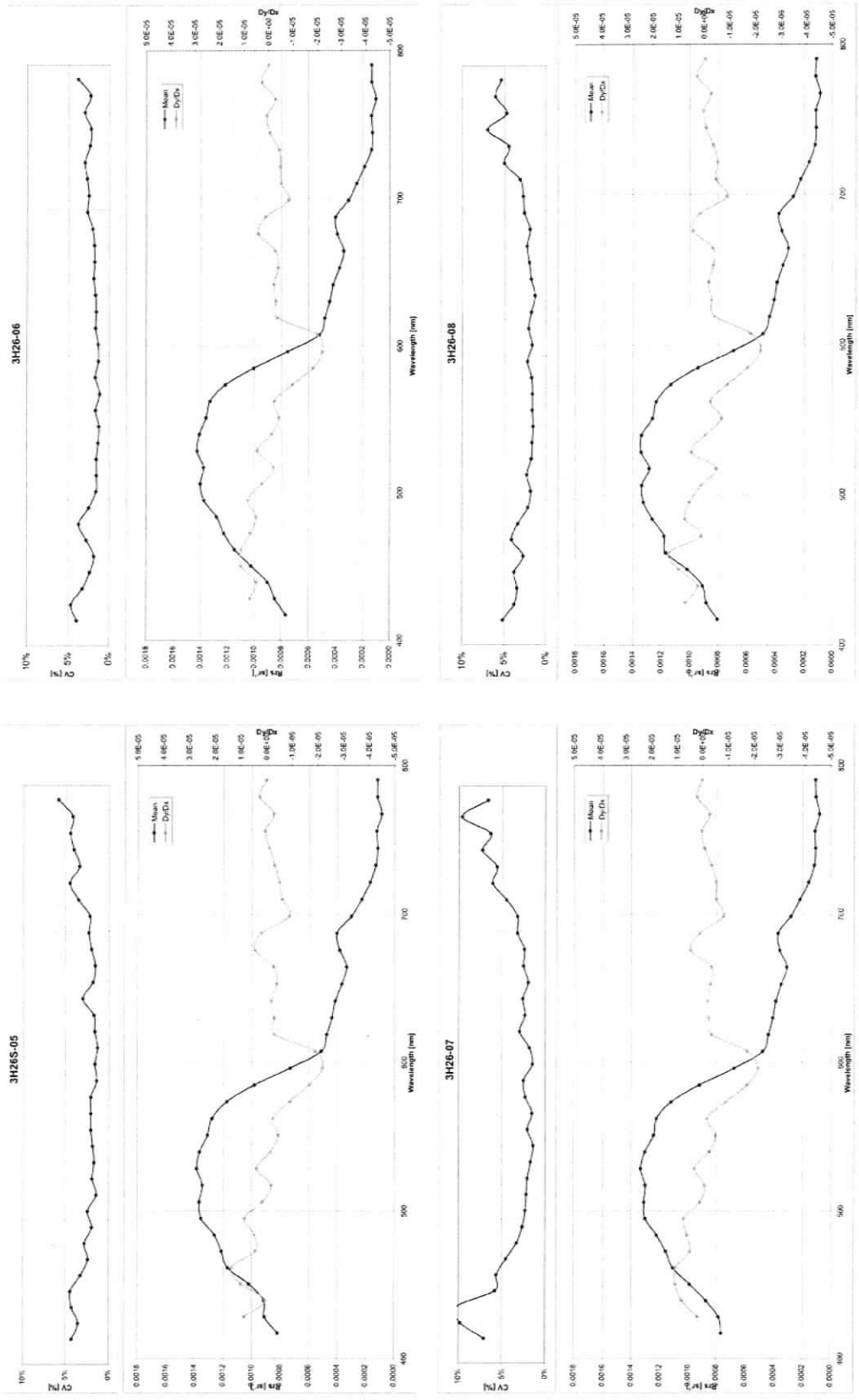
Band	WL	3H25-25				3H25-26				3H25-27				3H25-28			
		Mean	SD	CV	Dy/Dx	Mean	SD	CV	Dy/Dx	Mean	SD	CV	Dy/Dx	Mean	SD	CV	Dy/Dx
1	417	0.00108	2.9E-05	3%	-	0.00103	2.2E-05	2%	-	0.00108	2.9E-05	3%	-	0.00110	3.7E-05	3%	-
2	428	0.00120	4.1E-05	3%	1.1E-05	0.00117	3.2E-05	3%	1.2E-05	0.00121	2.9E-05	2%	1.2E-05	0.00122	4.5E-05	4%	1.1E-05
3	439	0.00134	3.9E-05	3%	1.3E-05	0.00128	3.9E-05	3%	1.0E-05	0.00132	4.1E-05	3%	1.1E-05	0.00136	3.8E-05	3%	1.3E-05
4	451	0.00156	3.7E-05	2%	2.0E-05	0.00150	3.6E-05	2%	2.0E-05	0.00151	3.4E-05	2%	1.7E-05	0.00156	4.1E-05	3%	1.8E-05
5	462	0.00170	4.2E-05	2%	1.3E-05	0.00166	4.5E-05	3%	1.4E-05	0.00171	4.8E-05	3%	1.8E-05	0.00175	6.3E-05	4%	1.8E-05
6	473	0.00190	4.8E-05	3%	1.8E-05	0.00182	4.5E-05	2%	1.5E-05	0.00185	3.8E-05	2%	1.2E-05	0.00194	3.9E-05	2%	1.7E-05
7	484	0.00196	3.3E-05	2%	5.4E-06	0.00197	3.5E-05	2%	1.3E-05	0.00195	4.3E-05	2%	9.4E-06	0.00206	4.3E-05	2%	1.0E-05
8	495	0.00210	3.2E-05	2%	1.3E-05	0.00205	2.9E-05	1%	7.9E-06	0.00215	2.9E-05	1%	1.7E-05	0.00220	5.5E-05	3%	1.3E-05
9	506	0.00209	2.9E-05	1%	-1.3E-06	0.00205	3.3E-05	2%	-6.3E-07	0.00212	3.6E-05	2%	-2.6E-06	0.00218	3.0E-05	1%	-1.7E-06
10	517	0.00201	3.2E-05	2%	-6.9E-06	0.00197	2.2E-05	1%	-7.2E-06	0.00204	2.5E-05	1%	-6.4E-06	0.00211	2.0E-05	1%	-6.4E-06
11	529	0.00211	3.6E-05	2%	8.6E-06	0.00207	3.2E-05	2%	8.9E-06	0.00214	3.6E-05	2%	8.2E-06	0.00221	3.1E-05	1%	9.1E-06
12	540	0.00207	2.1E-05	1%	-3.0E-06	0.00203	1.4E-05	1%	-3.0E-06	0.00215	2.6E-05	1%	1.3E-06	0.00222	2.5E-05	1%	8.0E-07
13	551	0.00198	2.9E-05	1%	-8.1E-06	0.00194	2.0E-05	1%	-7.8E-06	0.00203	2.8E-05	1%	-1.0E-05	0.00214	2.4E-05	1%	-7.0E-06
14	562	0.00191	2.4E-05	1%	-6.1E-06	0.00187	1.5E-05	1%	-6.5E-06	0.00198	1.9E-05	1%	-4.6E-06	0.00207	2.7E-05	1%	-6.1E-06
15	574	0.00170	2.5E-05	1%	-1.9E-05	0.00166	1.8E-05	1%	-1.8E-05	0.00176	2.1E-05	1%	-2.0E-05	0.00184	2.1E-05	1%	-2.0E-05
16	585	0.00131	1.4E-05	1%	-3.4E-05	0.00126	1.7E-05	1%	-3.5E-05	0.00133	1.7E-05	1%	-3.7E-05	0.00139	2.2E-05	2%	-4.0E-05
17	596	0.00085	1.0E-05	1%	-4.1E-05	0.00083	1.6E-05	2%	-3.8E-05	0.00087	1.6E-05	2%	-4.1E-05	0.00091	1.1E-05	1%	-4.3E-05
18	608	0.00057	8.0E-06	1%	-2.5E-05	0.00056	1.0E-05	2%	-2.3E-05	0.00059	7.0E-06	1%	-2.5E-05	0.00061	1.1E-05	2%	-2.6E-05
19	619	0.00052	1.1E-05	2%	-4.7E-06	0.00050	1.1E-05	2%	-5.3E-06	0.00053	1.0E-05	2%	-5.0E-06	0.00056	9.0E-06	2%	-4.4E-06
20	630	0.00049	9.0E-06	2%	-2.5E-06	0.00048	7.0E-06	1%	-2.5E-06	0.00050	8.0E-06	2%	-2.6E-06	0.00052	1.2E-05	2%	-3.6E-06
21	642	0.00046	8.0E-06	2%	-2.9E-06	0.00044	7.0E-06	2%	-2.7E-06	0.00047	8.0E-06	2%	-3.1E-06	0.00049	9.0E-06	2%	-2.5E-06
22	653	0.00040	1.0E-05	2%	-4.7E-06	0.00040	7.0E-06	2%	-4.1E-06	0.00042	7.0E-06	2%	-4.4E-06	0.00045	1.1E-05	2%	-4.2E-06
23	664	0.00034	6.0E-06	2%	-5.3E-06	0.00034	7.0E-06	2%	-4.8E-06	0.00036	5.0E-06	1%	-5.3E-06	0.00038	1.0E-05	3%	-5.6E-06
24	676	0.00034	8.0E-06	2%	8.8E-08	0.00034	1.0E-05	3%	0.0E+00	0.00035	4.0E-06	1%	-7.0E-07	0.00037	9.0E-06	2%	-7.0E-07
25	687	0.00032	8.0E-06	3%	-2.2E-06	0.00032	1.0E-05	3%	-2.2E-06	0.00033	1.0E-05	3%	-1.4E-06	0.00036	6.0E-06	2%	-1.6E-06
26	699	0.00025	7.0E-06	3%	-6.4E-06	0.00024	7.0E-06	3%	-6.5E-06	0.00025	5.0E-06	2%	-7.2E-06	0.00028	9.0E-06	3%	-6.6E-06
27	710	0.00018	4.0E-06	2%	-5.4E-06	0.00019	5.0E-06	3%	-5.0E-06	0.00019	5.0E-06	3%	-5.4E-06	0.00021	3.0E-06	1%	-5.9E-06
28	722	0.00013	5.0E-06	4%	-4.7E-06	0.00013	4.0E-06	3%	-4.8E-06	0.00014	7.0E-06	5%	-4.7E-06	0.00016	5.0E-06	3%	-4.6E-06
29	733	0.00009	4.0E-06	4%	-3.3E-06	0.00009	4.0E-06	4%	-3.5E-06	0.00009	4.0E-06	4%	-3.6E-06	0.00012	4.0E-06	3%	-3.7E-06
30	744	0.00009	3.0E-06	3%	-3.5E-07	0.00009	4.0E-06	4%	-8.7E-08	0.00009	3.0E-06	3%	-1.7E-07	0.00012	3.0E-06	3%	-8.7E-08
31	756	0.00010	4.0E-06	4%	1.2E-06	0.00010	4.0E-06	4%	1.1E-06	0.00011	5.0E-06	5%	1.4E-06	0.00014	5.0E-06	3%	2.3E-06
32	767	0.00008	5.0E-06	6%	-1.8E-06	0.00009	4.0E-06	5%	-1.4E-06	0.00009	5.0E-06	6%	-1.9E-06	0.00012	6.0E-06	5%	-1.9E-06
33	779	0.00010	5.0E-06	5%	1.7E-06	0.00011	6.0E-06	6%	1.6E-06	0.00011	4.0E-06	4%	1.9E-06	0.00014	4.0E-06	3%	1.8E-06
34	790	0.00010	3.0E-06	3%	-2.6E-07	0.00011	5.0E-06	5%	1.7E-07	0.00011	5.0E-06	5%	-2.6E-07	0.00015	7.0E-06	5%	6.1E-07


3H25-26
3H25-28
3H25-25
3H25-27
CV [%]
Mean
Dy/Dx
Wavelength [nm]

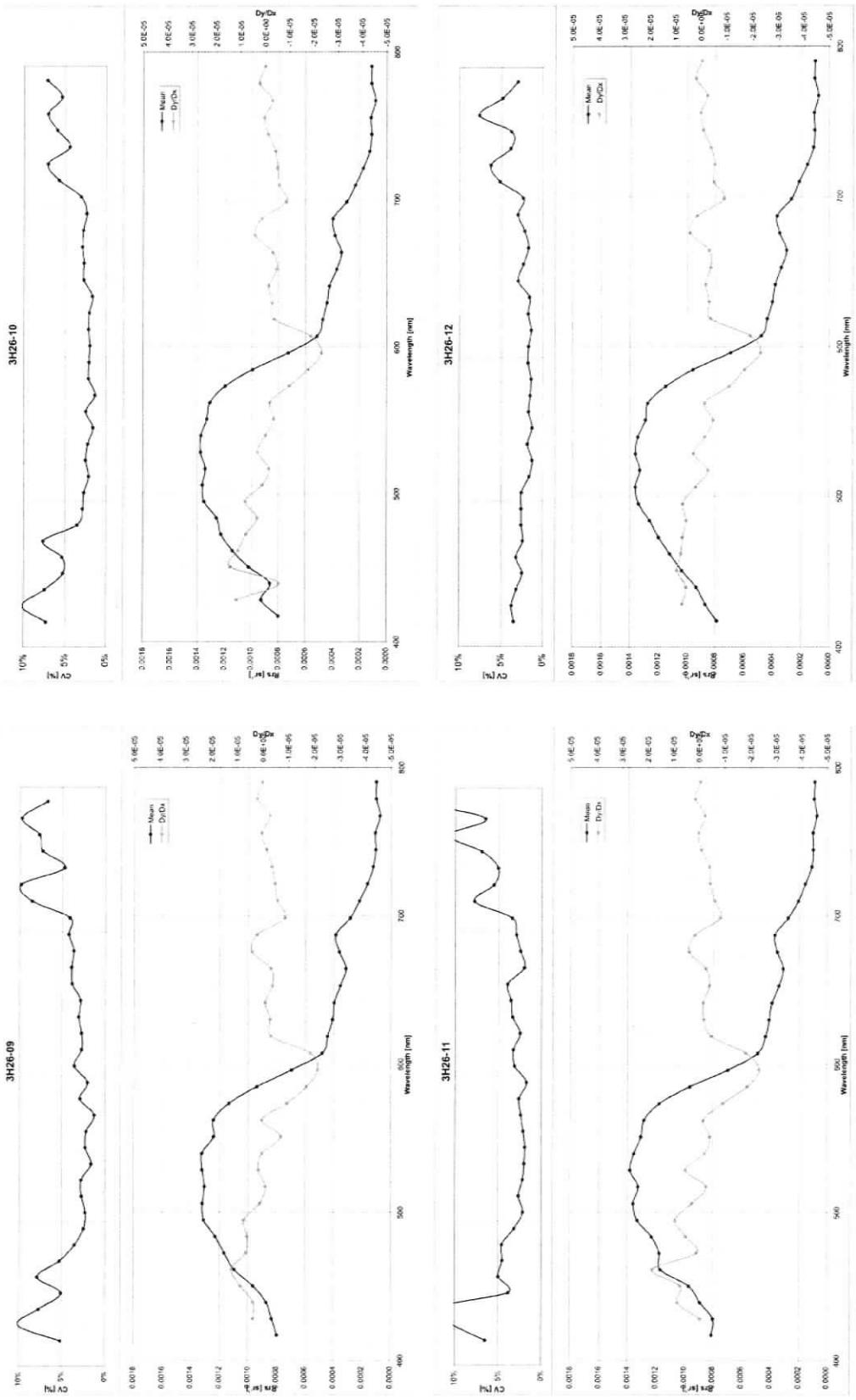
Band	WL	3H26S-1-1				3H26S-2-1				3H26S-3-1				3H26S-4-1			
		Mean	SD	CV	Dy/Dx	Mean	SD	CV	Dy/Dx	Mean	SD	CV	Dy/Dx	Mean	SD	CV	Dy/Dx
1	417	0.00079	3.1E-05	4%	-	0.00080	2.5E-05	3%	-	0.00078	3.2E-05	4%	-	0.00079	2.1E-05	3%	-
2	428	0.00084	4.7E-05	6%	4.6E-06	0.00088	3.9E-05	4%	7.3E-06	0.00088	3.6E-05	4%	9.2E-06	0.00088	3.8E-05	4%	8.4E-06
3	439	0.00090	3.9E-05	4%	5.4E-06	0.00090	3.0E-05	3%	1.4E-06	0.00092	3.7E-05	4%	3.5E-06	0.00091	2.4E-05	3%	2.1E-06
4	451	0.00098	3.6E-05	4%	7.0E-06	0.00099	4.3E-05	4%	8.6E-06	0.00103	2.8E-05	3%	1.1E-05	0.00101	4.0E-05	4%	9.2E-06
5	462	0.00106	3.9E-05	4%	7.6E-06	0.00111	4.1E-05	4%	1.1E-05	0.00116	4.2E-05	4%	1.2E-05	0.00110	2.1E-05	2%	8.6E-06
6	473	0.00113	4.3E-05	4%	6.7E-06	0.00120	4.1E-05	3%	7.9E-06	0.00125	3.7E-05	3%	7.5E-06	0.00118	4.5E-05	4%	6.5E-06
7	484	0.00122	3.4E-05	3%	7.5E-06	0.00121	3.6E-05	3%	1.2E-06	0.00133	3.6E-05	3%	7.1E-06	0.00124	3.3E-05	3%	5.4E-06
8	495	0.00126	3.3E-05	3%	3.4E-06	0.00131	3.1E-05	2%	8.2E-06	0.00140	3.1E-05	2%	7.0E-06	0.00133	2.5E-05	2%	8.4E-06
9	506	0.00125	3.7E-05	3%	-7.1E-07	0.00132	2.1E-05	2%	1.2E-06	0.00146	2.6E-05	2%	5.1E-06	0.00133	2.9E-05	2%	-1.8E-07
10	517	0.00122	2.9E-05	2%	-2.4E-06	0.00128	2.3E-05	2%	-3.5E-06	0.00141	2.4E-05	2%	-4.6E-06	0.00129	2.5E-05	2%	-3.1E-06
11	529	0.00122	2.1E-05	2%	8.9E-08	0.00132	2.5E-05	2%	3.6E-06	0.00148	2.6E-05	2%	6.5E-06	0.00133	2.3E-05	2%	3.1E-06
12	540	0.00121	2.1E-05	2%	-6.3E-07	0.00130	1.7E-05	1%	-1.3E-06	0.00147	2.0E-05	1%	-1.2E-06	0.00133	2.1E-05	2%	-8.9E-08
13	551	0.00116	2.2E-05	2%	-4.8E-06	0.00124	2.3E-05	2%	-5.3E-06	0.00144	2.4E-05	2%	-3.0E-06	0.00126	2.2E-05	2%	-5.8E-06
14	562	0.00112	3.2E-05	3%	-3.6E-06	0.00122	2.1E-05	2%	-2.1E-06	0.00142	1.8E-05	1%	-1.8E-06	0.00124	1.7E-05	1%	-2.0E-06
15	574	0.00103	2.6E-05	3%	-8.0E-06	0.00112	2.7E-05	2%	-8.6E-06	0.00131	2.4E-05	2%	-9.1E-06	0.00113	1.9E-05	2%	-9.9E-06
16	585	0.00085	1.5E-05	2%	-1.6E-05	0.00092	1.7E-05	2%	-1.8E-05	0.00107	1.5E-05	1%	-2.1E-05	0.00094	1.1E-05	1%	-1.7E-05
17	596	0.00062	1.7E-05	3%	-2.0E-05	0.00068	1.2E-05	2%	-2.2E-05	0.00076	1.0E-05	1%	-2.8E-05	0.00068	9.0E-06	1%	-2.3E-05
18	608	0.00043	8.0E-06	2%	-1.6E-05	0.00047	9.0E-06	2%	-1.8E-05	0.00052	1.0E-05	2%	-2.1E-05	0.00047	9.0E-06	2%	-1.8E-05
19	619	0.00040	8.0E-06	2%	-3.3E-06	0.00043	6.0E-06	1%	-3.5E-06	0.00048	8.0E-06	2%	-3.7E-06	0.00043	8.0E-06	2%	-3.5E-06
20	630	0.00037	8.0E-06	2%	-2.3E-06	0.00040	6.0E-06	2%	-2.8E-06	0.00044	1.1E-05	3%	-3.4E-06	0.00040	6.0E-06	1%	-2.7E-06
21	642	0.00035	7.0E-06	2%	-2.1E-06	0.00038	7.0E-06	2%	-2.2E-06	0.00041	7.0E-06	2%	-2.2E-06	0.00037	7.0E-06	2%	-2.5E-06
22	653	0.00031	8.0E-06	3%	-3.2E-06	0.00034	9.0E-06	3%	-3.1E-06	0.00037	8.0E-06	2%	-4.0E-06	0.00034	1.1E-05	3%	-3.3E-06
23	664	0.00028	8.0E-06	3%	-2.5E-06	0.00030	5.0E-06	2%	-3.3E-06	0.00033	9.0E-06	3%	-3.4E-06	0.00030	6.0E-06	2%	-3.3E-06
24	676	0.00032	1.0E-05	3%	3.8E-06	0.00035	9.0E-06	3%	4.0E-06	0.00038	1.0E-05	3%	4.4E-06	0.00034	8.0E-06	2%	4.1E-06
25	687	0.00033	7.0E-06	2%	3.5E-07	0.00037	9.0E-06	2%	1.7E-06	0.00039	1.1E-05	3%	7.9E-07	0.00036	8.0E-06	2%	1.4E-06
26	699	0.00024	1.0E-05	4%	-7.4E-06	0.00027	5.0E-06	2%	-8.7E-06	0.00028	9.0E-06	3%	-9.3E-06	0.00027	7.0E-06	3%	-7.7E-06
27	710	0.00019	9.0E-06	5%	-4.2E-06	0.00022	7.0E-06	3%	-4.6E-06	0.00023	7.0E-06	3%	-5.0E-06	0.00022	6.0E-06	3%	-5.0E-06
28	722	0.00015	9.0E-06	6%	-4.0E-06	0.00017	9.0E-06	5%	-4.4E-06	0.00016	8.0E-06	5%	-5.7E-06	0.00016	9.0E-06	6%	-4.9E-06
29	733	0.00011	6.0E-06	5%	-3.2E-06	0.00013	5.0E-06	4%	-3.2E-06	0.00012	6.0E-06	5%	-3.8E-06	0.00012	5.0E-06	4%	-3.9E-06
30	744	0.00011	3.0E-06	3%	-5.2E-07	0.00012	4.0E-06	3%	-1.0E-06	0.00010	5.0E-06	5%	-1.0E-06	0.00011	4.0E-06	4%	-7.8E-07
31	756	0.00012	5.0E-06	4%	8.7E-07	0.00012	5.0E-06	4%	7.0E-07	0.00011	8.0E-06	7%	6.1E-07	0.00011	4.0E-06	4%	5.2E-07
32	767	0.00008	5.0E-06	6%	-2.9E-06	0.00009	4.0E-06	4%	-3.1E-06	0.00008	7.0E-06	9%	-3.0E-06	0.00008	5.0E-06	6%	-2.6E-06
33	779	0.00011	6.0E-06	5%	2.4E-06	0.00012	5.0E-06	4%	2.6E-06	0.00011	5.0E-06	5%	2.6E-06	0.00011	4.0E-06	4%	2.2E-06
34	790	0.00011	6.0E-06	6%	-2.6E-07	0.00012	7.0E-06	6%	8.7E-08	0.00011	6.0E-06	6%	-8.7E-08	0.00011	6.0E-06	6%	8.7E-08


3H26S-02
3H26S-04
3H26S-01
3H26S-03
CV [%]
Mean
Dy/Dx
Wavelength [nm]

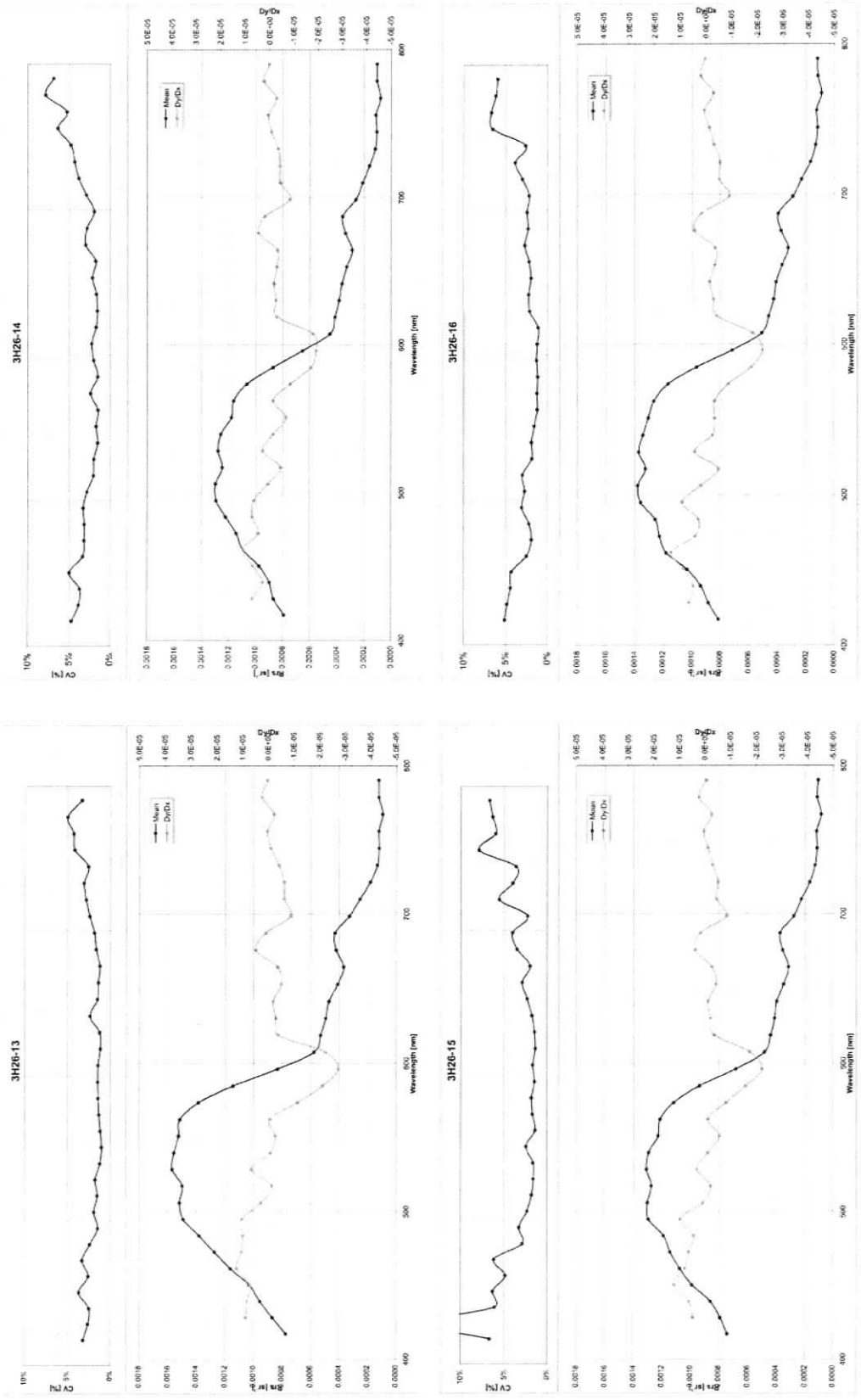
Band	WL	3H26S-5-1				3H26-06				3H26-07				3H26-08			
		Mean	SD	CV	Dy/Dx	Mean	SD	CV	Dy/Dx	Mean	SD	CV	Dy/Dx	Mean	SD	CV	Dy/Dx
1	417	0.00082	3.5E-05	4%	-	0.00077	3.0E-05	4%	-	0.00077	5.4E-05	7%	-	0.00080	4.1E-05	5%	-
2	428	0.00091	3.2E-05	4%	8.4E-06	0.00085	3.9E-05	5%	7.5E-06	0.00079	7.7E-05	10%	1.7E-06	0.00088	3.3E-05	4%	7.3E-06
3	439	0.00091	3.9E-05	4%	1.8E-07	0.00090	2.9E-05	3%	4.8E-06	0.00087	8.9E-05	10%	7.9E-06	0.00091	3.1E-05	3%	2.3E-06
4	451	0.00102	4.5E-05	4%	9.6E-06	0.00103	2.4E-05	2%	1.1E-05	0.00099	5.7E-05	6%	1.0E-05	0.00102	3.8E-05	4%	9.7E-06
5	462	0.00117	3.8E-05	3%	1.3E-05	0.00115	2.1E-05	2%	1.1E-05	0.00110	6.2E-05	6%	1.0E-05	0.00117	3.1E-05	3%	1.4E-05
6	473	0.00121	2.9E-05	2%	4.1E-06	0.00123	3.4E-05	3%	7.2E-06	0.00116	5.2E-05	4%	4.7E-06	0.00118	4.8E-05	4%	1.1E-06
7	484	0.00126	3.5E-05	3%	4.4E-06	0.00128	4.7E-05	4%	4.9E-06	0.00122	4.0E-05	3%	5.9E-06	0.00126	4.2E-05	3%	7.4E-06
8	495	0.00135	2.6E-05	2%	8.3E-06	0.00137	3.4E-05	2%	8.3E-06	0.00130	3.4E-05	3%	7.1E-06	0.00133	2.8E-05	2%	5.6E-06
9	506	0.00137	3.3E-05	2%	1.3E-06	0.00140	2.2E-05	2%	2.5E-06	0.00131	3.0E-05	2%	8.0E-07	0.00134	2.4E-05	2%	1.1E-06
10	517	0.00134	1.9E-05	1%	-2.1E-06	0.00138	2.1E-05	2%	-2.2E-06	0.00130	2.8E-05	2%	-8.9E-07	0.00129	2.9E-05	2%	-4.6E-06
11	529	0.00139	2.6E-05	2%	3.7E-06	0.00143	2.2E-05	2%	4.4E-06	0.00133	2.7E-05	2%	3.0E-06	0.00134	2.3E-05	2%	5.1E-06
12	540	0.00136	2.3E-05	2%	-1.9E-06	0.00141	1.9E-05	1%	-1.5E-06	0.00130	2.2E-05	2%	-2.8E-06	0.00134	2.2E-05	2%	-3.6E-07
13	551	0.00131	2.4E-05	2%	-4.9E-06	0.00136	1.7E-05	1%	-4.4E-06	0.00124	1.7E-05	1%	-5.2E-06	0.00126	1.9E-05	2%	-6.7E-06
14	562	0.00128	2.6E-05	2%	-2.8E-06	0.00133	2.2E-05	2%	-2.6E-06	0.00122	2.5E-05	2%	-1.9E-06	0.00124	2.0E-05	2%	-2.4E-06
15	574	0.00117	2.4E-05	2%	-9.3E-06	0.00122	1.4E-05	1%	-1.0E-05	0.00112	1.7E-05	2%	-9.2E-06	0.00113	1.8E-05	2%	-9.0E-06
16	585	0.00098	2.0E-05	2%	-1.7E-05	0.00101	1.7E-05	2%	-1.8E-05	0.00092	2.1E-05	2%	-1.7E-05	0.00094	1.6E-05	2%	-1.7E-05
17	596	0.00073	1.0E-05	1%	-2.2E-05	0.00075	1.0E-05	1%	-2.2E-05	0.00068	1.7E-05	3%	-2.2E-05	0.00069	1.5E-05	2%	-2.2E-05
18	608	0.00051	8.0E-06	2%	-1.9E-05	0.00052	7.0E-06	1%	-2.0E-05	0.00048	7.0E-06	1%	-1.8E-05	0.00049	8.0E-06	2%	-1.8E-05
19	619	0.00047	6.0E-06	1%	-3.4E-06	0.00048	8.0E-06	2%	-3.7E-06	0.00044	8.0E-06	2%	-3.5E-06	0.00044	9.0E-06	2%	-4.1E-06
20	630	0.00044	7.0E-06	2%	-3.2E-06	0.00045	7.0E-06	2%	-3.1E-06	0.00041	1.2E-05	3%	-2.6E-06	0.00041	7.0E-06	2%	-2.8E-06
21	642	0.00041	7.0E-06	2%	-2.0E-06	0.00042	7.0E-06	2%	-2.3E-06	0.00038	9.0E-06	2%	-2.0E-06	0.00039	5.0E-06	1%	-1.8E-06
22	653	0.00037	1.1E-05	3%	-4.1E-06	0.00037	7.0E-06	2%	-4.1E-06	0.00035	9.0E-06	3%	-3.2E-06	0.00035	6.0E-06	2%	-3.6E-06
23	664	0.00033	6.0E-06	2%	-3.0E-06	0.00034	6.0E-06	2%	-2.8E-06	0.00031	6.0E-06	2%	-3.6E-06	0.00031	6.0E-06	2%	-3.4E-06
24	676	0.00038	6.0E-06	2%	4.3E-06	0.00039	7.0E-06	2%	4.1E-06	0.00036	9.0E-06	3%	4.6E-06	0.00036	8.0E-06	2%	4.2E-06
25	687	0.00040	8.0E-06	2%	1.9E-06	0.00040	8.0E-06	2%	1.1E-06	0.00037	9.0E-06	2%	1.1E-06	0.00038	7.0E-06	2%	1.7E-06
26	699	0.00030	7.0E-06	2%	-9.0E-06	0.00030	8.0E-06	3%	-8.4E-06	0.00028	9.0E-06	3%	-8.1E-06	0.00027	7.0E-06	3%	-8.9E-06
27	710	0.00023	5.0E-06	2%	-6.3E-06	0.00024	6.0E-06	2%	-5.3E-06	0.00022	7.0E-06	3%	-5.4E-06	0.00022	6.0E-06	3%	-4.6E-06
28	722	0.00017	6.0E-06	4%	-5.1E-06	0.00019	5.0E-06	3%	-5.0E-06	0.00016	7.0E-06	5%	-5.4E-06	0.00016	5.0E-06	3%	-5.2E-06
29	733	0.00013	6.0E-06	5%	-3.3E-06	0.00014	4.0E-06	3%	-4.4E-06	0.00012	7.0E-06	6%	-3.5E-06	0.00012	6.0E-06	5%	-3.6E-06
30	744	0.00012	4.0E-06	3%	-1.2E-06	0.00013	3.0E-06	2%	-6.1E-07	0.00011	6.0E-06	6%	-7.0E-07	0.00011	5.0E-06	4%	-7.0E-07
31	756	0.00012	5.0E-06	4%	4.3E-07	0.00014	3.0E-06	2%	6.1E-07	0.00011	8.0E-06	7%	2.6E-07	0.00012	8.0E-06	7%	1.7E-07
32	767	0.00009	4.0E-06	4%	-3.0E-06	0.00010	3.0E-06	3%	-3.0E-06	0.00008	5.0E-06	6%	-2.7E-06	0.00009	4.0E-06	5%	-2.6E-06
33	779	0.00012	5.0E-06	4%	2.6E-06	0.00013	3.0E-06	2%	2.7E-06	0.00010	1.0E-05	10%	2.2E-06	0.00012	7.0E-06	6%	2.7E-06
34	790	0.00012	7.0E-06	6%	0.0E+00	0.00013	5.0E-06	4%	0.0E+00	0.00011	7.0E-06	7%	1.7E-07	0.00011	6.0E-06	5%	-3.5E-07


3H26-06
3H26-08
3H26S-05
3H26-07
CV [%]
Mean
Dy/Dx
Wavelength [nm]

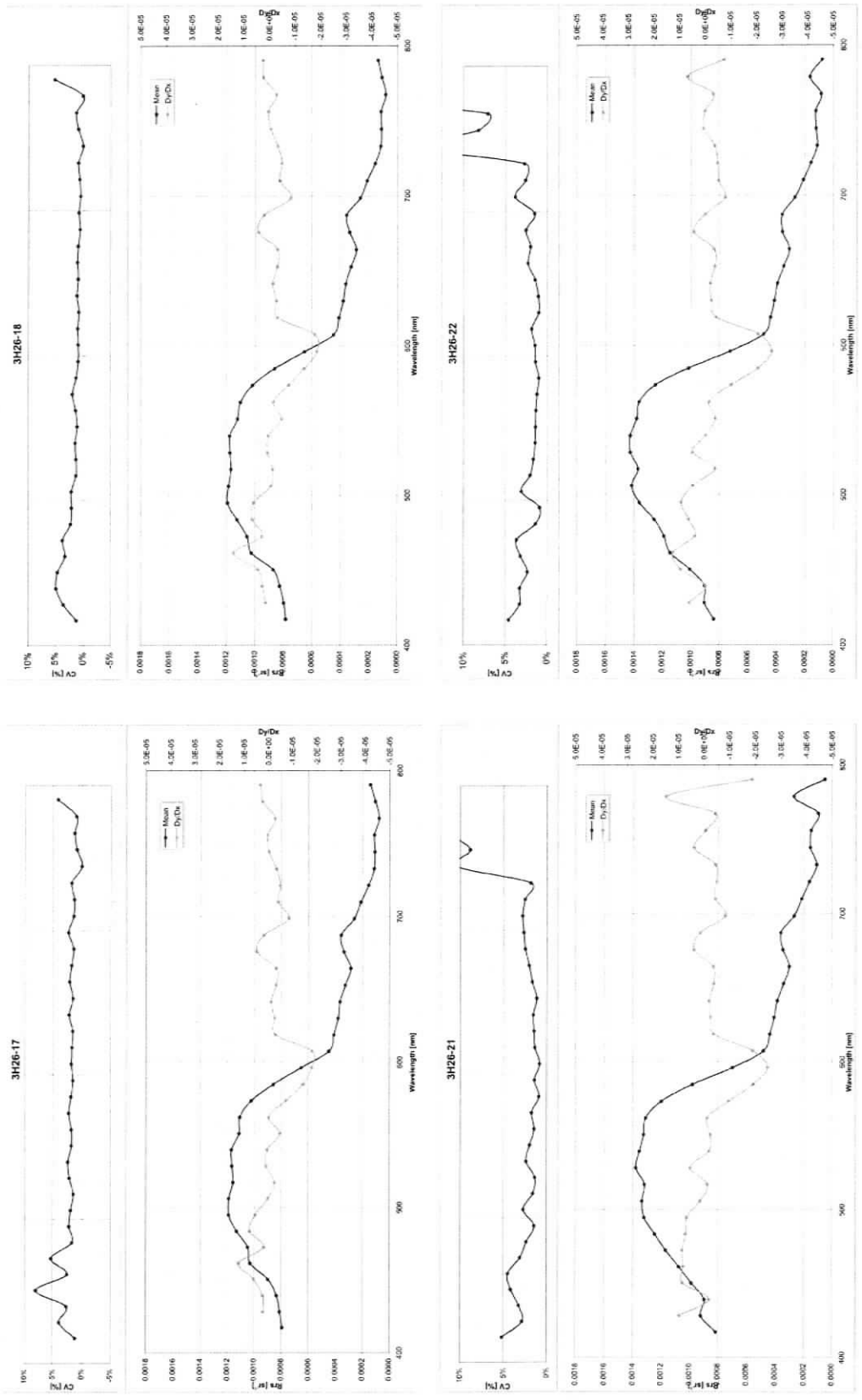
Band	WL	3H26-09				3H26-10				3H26-11				3H26-12			
		Mean	SD	CV	Dy/Dx	Mean	SD	CV	Dy/Dx	Mean	SD	CV	Dy/Dx	Mean	SD	CV	Dy/Dx
1	417	0.00079	4.1E-05	5%	-	0.00080	5.8E-05	7%	-	0.00081	5.2E-05	6%	-	0.00079	2.7E-05	3%	-
2	428	0.00083	8.4E-05	10%	3.5E-06	0.00093	9.4E-05	10%	1.2E-05	0.00080	8.2E-05	10%	-7.3E-07	0.00087	3.2E-05	4%	7.3E-06
3	439	0.00087	6.7E-05	8%	3.4E-06	0.00086	6.4E-05	7%	-5.8E-06	0.00089	1.1E-04	13%	8.2E-06	0.00093	2.9E-05	3%	5.7E-06
4	451	0.00096	4.9E-05	5%	8.4E-06	0.00102	5.3E-05	5%	1.4E-05	0.00097	3.7E-05	4%	7.0E-06	0.00103	2.5E-05	2%	9.2E-06
5	462	0.00110	8.6E-05	8%	1.2E-05	0.00114	6.0E-05	5%	1.1E-05	0.00117	5.8E-05	5%	1.8E-05	0.00112	3.5E-05	3%	7.7E-06
6	473	0.00117	6.1E-05	5%	6.3E-06	0.00122	9.3E-05	8%	7.7E-06	0.00118	5.3E-05	5%	7.2E-07	0.00120	2.8E-05	2%	7.1E-06
7	484	0.00123	4.3E-05	3%	5.8E-06	0.00126	4.4E-05	3%	3.2E-06	0.00123	5.6E-05	5%	4.8E-06	0.00126	3.2E-05	3%	5.7E-06
8	495	0.00131	3.2E-05	2%	7.1E-06	0.00135	3.8E-05	3%	8.0E-06	0.00133	4.2E-05	3%	9.1E-06	0.00134	3.4E-05	3%	7.0E-06
9	506	0.00132	3.0E-05	2%	8.9E-07	0.00136	3.6E-05	3%	1.1E-06	0.00136	2.9E-05	2%	2.5E-06	0.00136	3.4E-05	3%	2.1E-06
10	517	0.00130	3.5E-05	3%	-1.2E-06	0.00134	2.8E-05	2%	-1.7E-06	0.00132	3.5E-05	3%	-3.0E-06	0.00133	2.1E-05	2%	-2.8E-06
11	529	0.00132	3.6E-05	3%	1.5E-06	0.00138	3.4E-05	2%	3.0E-06	0.00138	3.0E-05	2%	5.1E-06	0.00136	1.7E-05	1%	2.8E-06
12	540	0.00132	2.1E-05	2%	8.9E-08	0.00137	3.0E-05	2%	-3.6E-07	0.00135	2.7E-05	2%	-2.4E-06	0.00134	2.4E-05	2%	-1.6E-06
13	551	0.00124	2.8E-05	2%	-7.3E-06	0.00133	2.1E-05	2%	-3.6E-06	0.00130	2.5E-05	2%	-4.4E-06	0.00129	1.6E-05	1%	-4.7E-06
14	562	0.00124	2.7E-05	2%	1.8E-07	0.00131	3.2E-05	2%	-2.1E-06	0.00128	2.7E-05	2%	-1.9E-06	0.00127	2.1E-05	2%	-1.4E-06
15	574	0.00113	1.4E-05	1%	-9.6E-06	0.00119	1.6E-05	1%	-1.0E-05	0.00118	2.8E-05	2%	-9.5E-06	0.00115	1.7E-05	1%	-1.1E-05
16	585	0.00094	2.7E-05	3%	-1.7E-05	0.00099	2.1E-05	2%	-1.8E-05	0.00096	2.5E-05	3%	-1.9E-05	0.00096	1.3E-05	1%	-1.7E-05
17	596	0.00069	1.4E-05	2%	-2.2E-05	0.00073	1.5E-05	2%	-2.3E-05	0.00070	1.2E-05	2%	-2.4E-05	0.00069	1.2E-05	2%	-2.3E-05
18	608	0.00048	1.7E-05	4%	-1.9E-05	0.00051	1.0E-05	2%	-1.9E-05	0.00049	1.5E-05	3%	-1.8E-05	0.00048	8.0E-06	2%	-1.9E-05
19	619	0.00044	1.2E-05	3%	-3.3E-06	0.00047	1.0E-05	2%	-3.6E-06	0.00043	1.4E-05	3%	-5.0E-06	0.00044	6.0E-06	1%	-3.6E-06
20	630	0.00041	1.1E-05	3%	-3.0E-06	0.00044	9.0E-06	2%	-2.8E-06	0.00041	1.0E-05	2%	-2.0E-06	0.00040	7.0E-06	2%	-3.1E-06
21	642	0.00040	1.2E-05	3%	-1.1E-06	0.00042	7.0E-06	2%	-1.5E-06	0.00039	1.3E-05	3%	-1.8E-06	0.00038	6.0E-06	2%	-1.8E-06
22	653	0.00035	1.0E-05	3%	-3.9E-06	0.00037	1.0E-05	3%	-4.7E-06	0.00034	1.2E-05	4%	-4.1E-06	0.00034	1.0E-05	3%	-3.8E-06
23	664	0.00031	1.2E-05	4%	-3.3E-06	0.00034	9.0E-06	3%	-3.1E-06	0.00031	1.2E-05	4%	-2.8E-06	0.00030	7.0E-06	2%	-3.2E-06
24	676	0.00036	1.4E-05	4%	4.0E-06	0.00038	1.1E-05	3%	4.1E-06	0.00035	7.0E-06	2%	3.9E-06	0.00035	6.0E-06	2%	4.3E-06
25	687	0.00038	1.4E-05	4%	2.1E-06	0.00040	1.1E-05	3%	1.3E-06	0.00037	9.0E-06	2%	1.5E-06	0.00037	8.0E-06	2%	1.6E-06
26	699	0.00029	1.2E-05	4%	-8.7E-06	0.00030	7.0E-06	2%	-8.8E-06	0.00027	8.0E-06	3%	-8.2E-06	0.00027	8.0E-06	3%	-8.9E-06
27	710	0.00022	9.0E-06	4%	-5.7E-06	0.00023	7.0E-06	3%	-5.7E-06	0.00020	7.0E-06	3%	-6.1E-06	0.00021	5.0E-06	2%	-4.7E-06
28	722	0.00016	1.4E-05	9%	-4.9E-06	0.00018	1.0E-05	6%	-5.0E-06	0.00015	1.2E-05	8%	-4.3E-06	0.00016	8.0E-06	5%	-5.1E-06
29	733	0.00012	1.2E-05	10%	-3.6E-06	0.00013	9.0E-06	7%	-4.2E-06	0.00011	6.0E-06	6%	-4.0E-06	0.00011	7.0E-06	6%	-3.8E-06
30	744	0.00011	5.0E-06	5%	-1.5E-06	0.00011	5.0E-06	4%	-1.2E-06	0.00010	5.0E-06	5%	-7.8E-07	0.00010	4.0E-06	4%	-7.0E-07
31	756	0.00011	8.0E-06	7%	3.5E-07	0.00012	7.0E-06	6%	4.3E-07	0.00010	7.0E-06	7%	1.7E-07	0.00011	4.0E-06	4%	1.7E-07
32	767	0.00008	6.0E-06	8%	-2.8E-06	0.00009	6.0E-06	7%	-2.9E-06	0.00007	8.0E-06	11%	-2.4E-06	0.00008	6.0E-06	8%	-2.4E-06
33	779	0.00010	1.0E-05	10%	2.2E-06	0.00011	6.0E-06	5%	2.3E-06	0.00009	6.0E-06	7%	1.6E-06	0.00010	5.0E-06	5%	2.1E-06
34	790	0.00010	7.0E-06	7%	8.7E-08	0.00011	8.0E-06	7%	0.0E+00	0.00009	1.3E-05	15%	-3.5E-07	0.00010	3.0E-06	3%	-1.7E-07


3H26-10
3H26-12
3H26-09
3H26-11
CV [%]
Mean
Dy/Dx
Wavelength [nm]

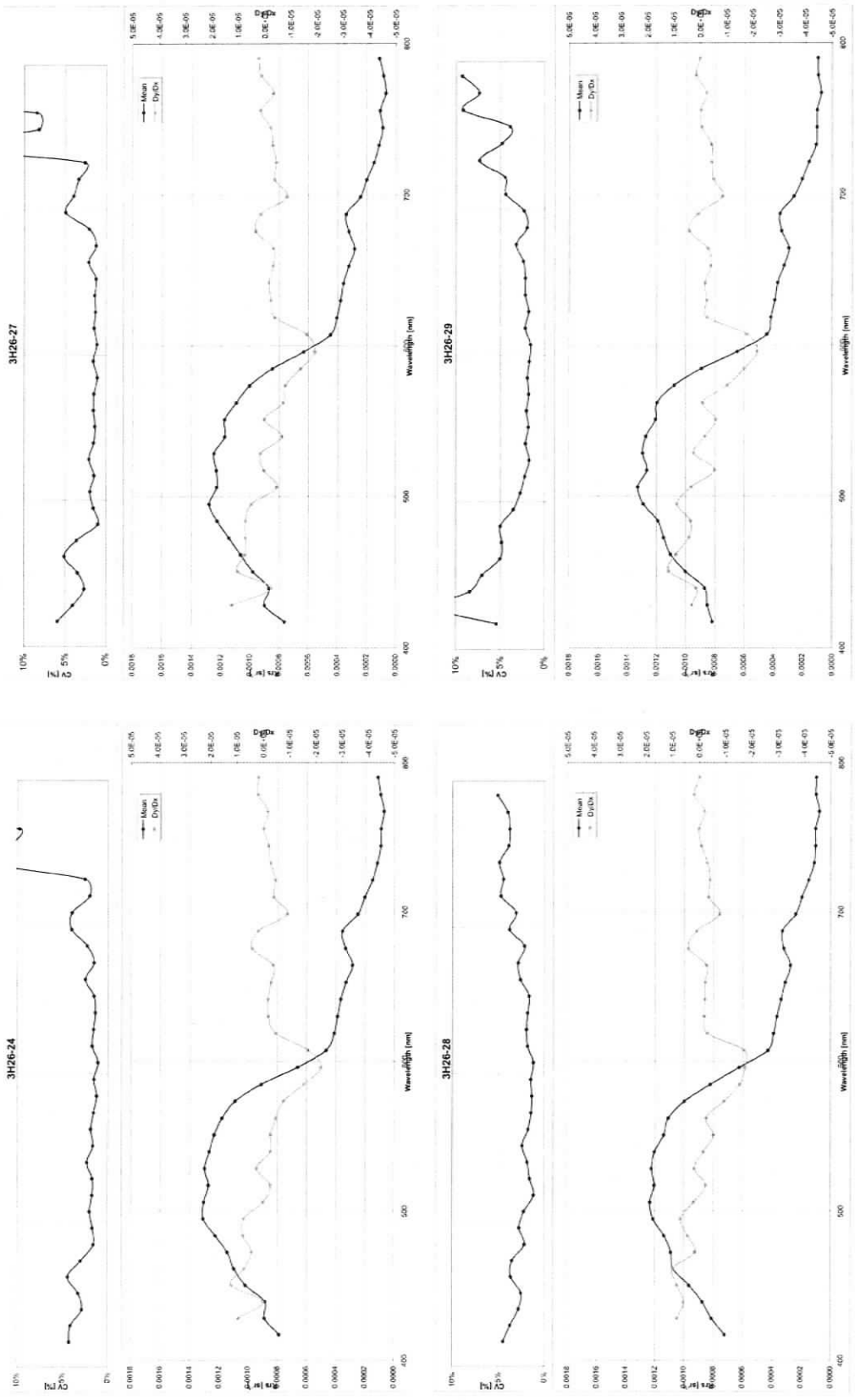
Band	WL	3H26-13				3H26-14				3H26-15				3H26-16			
		Mean	SD	CV	Dy/Dx	Mean	SD	CV	Dy/Dx	Mean	SD	CV	Dy/Dx	Mean	SD	CV	Dy/Dx
1	417	0.00077	2.4E-05	3%	-	0.00079	3.7E-05	5%	-	0.00074	4.9E-05	7%	-	0.00081	4.1E-05	5%	-
2	428	0.00087	2.2E-05	3%	8.5E-06	0.00087	3.3E-05	4%	7.0E-06	0.00079	1.2E-04	15%	4.5E-06	0.00088	4.2E-05	5%	6.4E-06
3	439	0.00095	2.3E-05	2%	7.8E-06	0.00090	3.3E-05	4%	2.8E-06	0.00086	5.2E-05	6%	6.0E-06	0.00094	4.1E-05	4%	4.9E-06
4	451	0.00103	3.7E-05	4%	6.8E-06	0.00097	4.8E-05	5%	6.8E-06	0.00099	6.2E-05	6%	1.2E-05	0.00103	4.4E-05	4%	8.6E-06
5	462	0.00116	2.9E-05	3%	1.2E-05	0.00109	3.6E-05	3%	1.1E-05	0.00107	5.2E-05	5%	7.7E-06	0.00118	2.9E-05	2%	1.3E-05
6	473	0.00127	4.1E-05	3%	1.0E-05	0.00114	3.6E-05	3%	4.5E-06	0.00114	7.0E-05	6%	6.1E-06	0.00122	2.3E-05	2%	4.1E-06
7	484	0.00138	3.2E-05	2%	9.5E-06	0.00122	3.8E-05	3%	6.9E-06	0.00119	3.4E-05	3%	4.1E-06	0.00125	2.7E-05	2%	2.8E-06
8	495	0.00149	2.1E-05	1%	9.9E-06	0.00129	4.2E-05	3%	6.3E-06	0.00129	4.2E-05	3%	9.5E-06	0.00136	4.1E-05	3%	9.1E-06
9	506	0.00152	2.8E-05	2%	2.4E-06	0.00130	3.6E-05	3%	5.4E-07	0.00130	3.0E-05	2%	5.4E-07	0.00138	3.7E-05	3%	1.9E-06
10	517	0.00150	2.2E-05	1%	-1.7E-06	0.00125	2.5E-05	2%	-4.6E-06	0.00127	2.3E-05	2%	-2.3E-06	0.00132	3.9E-05	3%	-4.9E-06
11	529	0.00157	2.7E-05	2%	6.4E-06	0.00128	2.5E-05	2%	2.8E-06	0.00131	2.1E-05	2%	2.9E-06	0.00137	2.5E-05	2%	4.3E-06
12	540	0.00156	1.8E-05	1%	-1.2E-06	0.00126	1.9E-05	2%	-1.8E-06	0.00129	2.1E-05	2%	-1.3E-06	0.00134	2.5E-05	2%	-2.6E-06
13	551	0.00152	1.5E-05	1%	-2.9E-06	0.00118	2.0E-05	2%	-6.8E-06	0.00123	3.0E-05	2%	-5.8E-06	0.00130	2.0E-05	2%	-3.5E-06
14	562	0.00151	1.7E-05	1%	-8.0E-07	0.00116	1.7E-05	1%	-1.5E-06	0.00121	1.7E-05	1%	-1.3E-06	0.00126	1.5E-05	1%	-3.4E-06
15	574	0.00138	1.8E-05	1%	-1.2E-05	0.00107	2.5E-05	2%	-8.7E-06	0.00112	1.9E-05	2%	-8.5E-06	0.00116	1.4E-05	1%	-8.8E-06
16	585	0.00114	1.6E-05	1%	-2.1E-05	0.00087	1.3E-05	1%	-1.7E-05	0.00093	1.7E-05	2%	-1.6E-05	0.00096	1.1E-05	1%	-1.8E-05
17	596	0.00083	1.2E-05	1%	-2.8E-05	0.00065	1.3E-05	2%	-1.9E-05	0.00068	1.0E-05	1%	-2.2E-05	0.00071	9.0E-06	1%	-2.2E-05
18	608	0.00057	8.0E-06	1%	-2.3E-05	0.00045	1.0E-05	2%	-1.8E-05	0.00048	8.0E-06	2%	-1.8E-05	0.00051	6.0E-06	1%	-1.8E-05
19	619	0.00053	6.0E-06	1%	-4.1E-06	0.00041	7.0E-06	2%	-3.1E-06	0.00044	6.0E-06	1%	-3.8E-06	0.00046	5.0E-06	1%	-4.3E-06
20	630	0.00049	6.0E-06	1%	-3.1E-06	0.00038	6.0E-06	2%	-2.7E-06	0.00041	6.0E-06	1%	-2.3E-06	0.00042	9.0E-06	2%	-3.0E-06
21	642	0.00047	1.1E-05	2%	-2.1E-06	0.00036	6.0E-06	2%	-1.9E-06	0.00039	7.0E-06	2%	-1.4E-06	0.00041	9.0E-06	2%	-1.6E-06
22	653	0.00041	6.0E-06	1%	-5.2E-06	0.00033	7.0E-06	2%	-3.2E-06	0.00034	8.0E-06	2%	-4.4E-06	0.00037	7.0E-06	2%	-3.6E-06
23	664	0.00037	5.0E-06	1%	-3.8E-06	0.00029	5.0E-06	2%	-3.3E-06	0.00031	9.0E-06	3%	-2.9E-06	0.00032	7.0E-06	2%	-3.8E-06
24	676	0.00042	5.0E-06	1%	4.6E-06	0.00034	1.0E-05	3%	4.3E-06	0.00035	7.0E-06	2%	3.7E-06	0.00037	1.0E-05	3%	4.4E-06
25	687	0.00043	7.0E-06	2%	7.0E-07	0.00036	1.0E-05	3%	1.8E-06	0.00037	1.3E-05	4%	1.6E-06	0.00039	9.0E-06	2%	1.8E-06
26	699	0.00033	6.0E-06	2%	-8.9E-06	0.00026	5.0E-06	2%	-8.5E-06	0.00027	1.1E-05	4%	-8.5E-06	0.00029	7.0E-06	2%	-9.0E-06
27	710	0.00025	6.0E-06	2%	-6.4E-06	0.00021	6.0E-06	3%	-4.5E-06	0.00022	5.0E-06	2%	-4.6E-06	0.00023	5.0E-06	2%	-5.2E-06
28	722	0.00018	5.0E-06	3%	-6.4E-06	0.00016	6.0E-06	4%	-4.3E-06	0.00016	9.0E-06	6%	-5.2E-06	0.00017	5.0E-06	3%	-5.5E-06
29	733	0.00013	4.0E-06	3%	-4.2E-06	0.00012	5.0E-06	4%	-3.7E-06	0.00013	5.0E-06	4%	-3.2E-06	0.00013	5.0E-06	4%	-3.2E-06
30	744	0.00012	3.0E-06	3%	-1.1E-06	0.00011	5.0E-06	5%	-9.6E-07	0.00011	4.0E-06	4%	-1.2E-06	0.00012	3.0E-06	3%	-1.2E-06
31	756	0.00012	5.0E-06	4%	1.7E-07	0.00011	7.0E-06	6%	4.3E-07	0.00011	9.0E-06	8%	2.6E-07	0.00012	8.0E-06	7%	6.1E-07
32	767	0.00009	4.0E-06	4%	-2.4E-06	0.00008	4.0E-06	5%	-3.0E-06	0.00008	5.0E-06	6%	-2.6E-06	0.00009	6.0E-06	7%	-2.9E-06
33	779	0.00012	6.0E-06	5%	2.3E-06	0.00010	8.0E-06	8%	2.3E-06	0.00011	7.0E-06	6%	2.3E-06	0.00011	7.0E-06	6%	2.1E-06
34	790	0.00012	4.0E-06	3%	8.7E-08	0.00010	7.0E-06	7%	0.0E+00	0.00011	7.0E-06	7%	-5.2E-07	0.00012	7.0E-06	6%	3.5E-07


3H26-14
3H26-16
3H26-13
3H26-15
CV [%]
Mean
Dy/Dx
Wavelength [nm]

Band	WL	3H26-17				3H26-18				3H26-21				3H26-22			
		Mean	SD	CV	Dy/Dx	Mean	SD	CV	Dy/Dx	Mean	SD	CV	Dy/Dx	Mean	SD	CV	Dy/Dx
1	417	0.00079	9.0E-06	1%	-	0.00078	9.0E-06	1%	-	0.00082	4.2E-05	5%	-	0.00084	3.8E-05	5%	-
2	428	0.00081	3.2E-05	4%	1.8E-06	0.00079	2.8E-05	4%	1.3E-06	0.00092	2.6E-05	3%	9.5E-06	0.00090	2.9E-05	3%	6.1E-06
3	439	0.00083	2.2E-05	3%	2.1E-06	0.00082	4.0E-05	5%	2.6E-06	0.00090	2.9E-05	3%	-2.2E-06	0.00090	2.9E-05	3%	-2.7E-07
4	451	0.00090	7.2E-05	8%	5.8E-06	0.00087	4.0E-05	5%	4.2E-06	0.00099	4.1E-05	4%	8.2E-06	0.00101	2.3E-05	2%	9.5E-06
5	462	0.00103	2.6E-05	3%	1.2E-05	0.00102	3.3E-05	3%	1.4E-05	0.00107	4.8E-05	4%	7.9E-06	0.00115	3.6E-05	3%	1.3E-05
6	473	0.00105	5.6E-05	5%	1.6E-06	0.00105	3.9E-05	4%	2.7E-06	0.00117	3.6E-05	3%	8.3E-06	0.00119	4.3E-05	4%	3.9E-06
7	484	0.00113	1.9E-05	2%	7.4E-06	0.00113	2.5E-05	2%	6.5E-06	0.00124	2.9E-05	2%	7.0E-06	0.00126	1.7E-05	1%	6.3E-06
8	495	0.00119	2.6E-05	2%	5.2E-06	0.00119	2.5E-05	2%	6.0E-06	0.00132	1.9E-05	1%	6.6E-06	0.00136	1.2E-05	1%	9.3E-06
9	506	0.00119	2.3E-05	2%	0.0E+00	0.00118	2.5E-05	2%	-8.0E-07	0.00133	3.6E-05	3%	1.3E-06	0.00142	4.3E-05	3%	4.7E-06
10	517	0.00116	1.7E-05	1%	-2.8E-06	0.00117	1.5E-05	1%	-1.4E-06	0.00132	2.1E-05	2%	-1.4E-06	0.00137	2.7E-05	2%	-3.8E-06
11	529	0.00117	2.5E-05	2%	7.1E-07	0.00117	1.5E-05	1%	6.2E-07	0.00138	1.9E-05	1%	5.3E-06	0.00143	2.3E-05	2%	4.8E-06
12	540	0.00117	2.8E-05	2%	2.7E-07	0.00118	1.7E-05	1%	1.8E-07	0.00135	3.2E-05	2%	-2.1E-06	0.00143	2.0E-05	1%	0.0E+00
13	551	0.00111	2.0E-05	2%	-5.0E-06	0.00112	1.2E-05	1%	-4.9E-06	0.00132	2.6E-05	2%	-2.6E-06	0.00138	1.9E-05	1%	-4.0E-06
14	562	0.00111	2.0E-05	2%	-4.5E-07	0.00110	1.5E-05	1%	-1.7E-06	0.00131	1.9E-05	1%	-1.3E-06	0.00136	1.8E-05	1%	-1.5E-06
15	574	0.00102	2.3E-05	2%	-7.5E-06	0.00102	2.0E-05	2%	-7.6E-06	0.00120	2.1E-05	2%	-9.7E-06	0.00125	1.5E-05	1%	-1.0E-05
16	585	0.00086	1.6E-05	2%	-1.5E-05	0.00086	1.1E-05	1%	-1.4E-05	0.00098	9.0E-06	1%	-1.9E-05	0.00102	1.0E-05	1%	-2.1E-05
17	596	0.00065	1.0E-05	2%	-1.8E-05	0.00065	6.0E-06	1%	-1.9E-05	0.00070	1.0E-05	1%	-2.5E-05	0.00073	1.0E-05	1%	-2.6E-05
18	608	0.00045	8.0E-06	2%	-1.8E-05	0.00045	4.0E-06	1%	-1.8E-05	0.00048	4.0E-06	1%	-1.9E-05	0.00049	7.0E-06	1%	-2.1E-05
19	619	0.00041	7.0E-06	2%	-3.1E-06	0.00041	4.0E-06	1%	-3.3E-06	0.00044	6.0E-06	1%	-3.8E-06	0.00044	8.0E-06	2%	-4.2E-06
20	630	0.00038	6.0E-06	2%	-2.7E-06	0.00038	3.0E-06	1%	-2.8E-06	0.00041	6.0E-06	1%	-2.7E-06	0.00042	4.0E-06	1%	-2.4E-06
21	642	0.00037	8.0E-06	2%	-1.3E-06	0.00036	4.0E-06	1%	-1.4E-06	0.00038	6.0E-06	2%	-2.1E-06	0.00039	4.0E-06	1%	-2.0E-06
22	653	0.00033	5.0E-06	2%	-3.4E-06	0.00033	3.0E-06	1%	-3.2E-06	0.00034	4.0E-06	1%	-3.9E-06	0.00035	5.0E-06	1%	-3.9E-06
23	664	0.00029	6.0E-06	2%	-3.5E-06	0.00029	3.0E-06	1%	-3.3E-06	0.00030	5.0E-06	2%	-3.6E-06	0.00031	7.0E-06	2%	-3.5E-06
24	676	0.00034	6.0E-06	2%	4.6E-06	0.00033	3.0E-06	1%	4.1E-06	0.00034	7.0E-06	2%	3.9E-06	0.00036	7.0E-06	2%	4.3E-06
25	687	0.00036	5.0E-06	1%	1.7E-06	0.00036	2.0E-06	1%	1.9E-06	0.00036	9.0E-06	3%	1.4E-06	0.00036	9.0E-06	3%	8.8E-08
26	699	0.00026	6.0E-06	2%	-8.5E-06	0.00026	2.0E-06	1%	-8.5E-06	0.00027	7.0E-06	3%	-8.3E-06	0.00027	4.0E-06	1%	-7.8E-06
27	710	0.00021	3.0E-06	1%	-4.2E-06	0.00021	1.0E-06	0%	-4.1E-06	0.00022	6.0E-06	3%	-4.4E-06	0.00021	8.0E-06	4%	-5.1E-06
28	722	0.00015	2.0E-06	1%	-5.0E-06	0.00016	1.0E-06	1%	-5.0E-06	0.00016	4.0E-06	3%	-4.9E-06	0.00016	4.0E-06	3%	-4.8E-06
29	733	0.00011	2.0E-06	2%	-3.5E-06	0.00012	1.0E-06	1%	-3.4E-06	0.00011	2.0E-06	2%	-4.5E-06	0.00011	3.0E-06	3%	-3.8E-06
30	744	0.00011	0.0E+00	0%	-4.3E-07	0.00011	0.0E+00	0%	-6.1E-07	0.00015	1.6E-05	10%	3.9E-06	0.00012	1.9E-05	16%	7.0E-07
31	756	0.00011	1.0E-06	1%	2.6E-07	0.00011	1.0E-06	1%	3.5E-07	0.00015	1.3E-05	9%	-5.2E-07	0.00012	1.0E-05	8%	8.7E-08
32	767	0.00008	1.0E-06	1%	-2.9E-06	0.00008	1.0E-06	1%	-2.8E-06	0.00010	1.1E-05	11%	-4.3E-06	0.00009	6.0E-06	7%	-3.2E-06
33	779	0.00011	1.0E-06	1%	2.3E-06	0.00011	0.0E+00	0%	2.3E-06	0.00027	3.0E-05	11%	1.5E-05	0.00016	3.9E-05	24%	6.8E-06
34	790	0.00014	6.0E-06	4%	3.3E-06	0.00014	7.0E-06	5%	2.4E-06	0.00005	1.0E-05	19%	-1.9E-05	0.00008	1.0E-05	13%	-7.3E-06

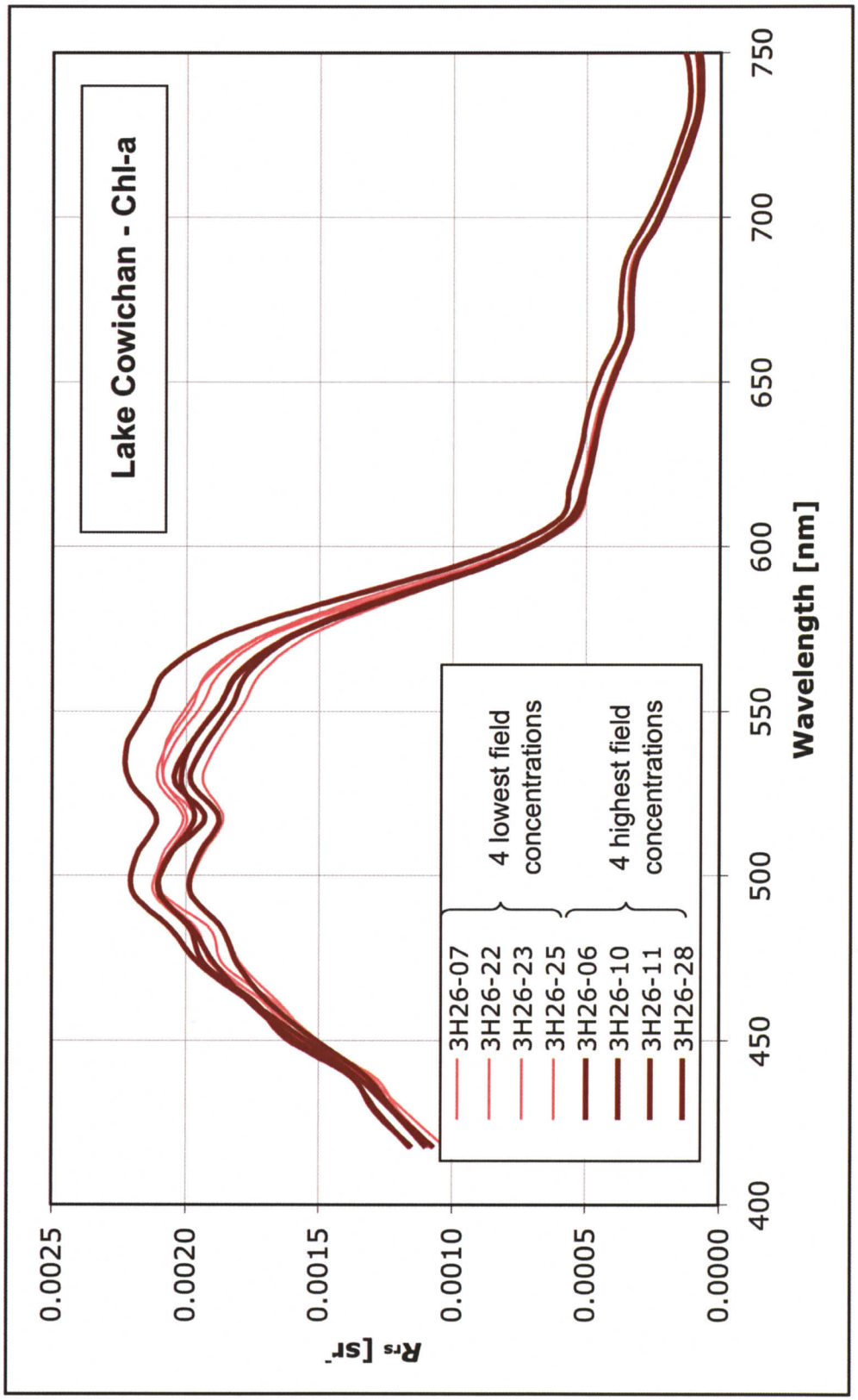

3H26-18
3H26-22
3H26-17
3H26-21
CV [%]
Mean
Dy/Dx
Wavelength [nm]

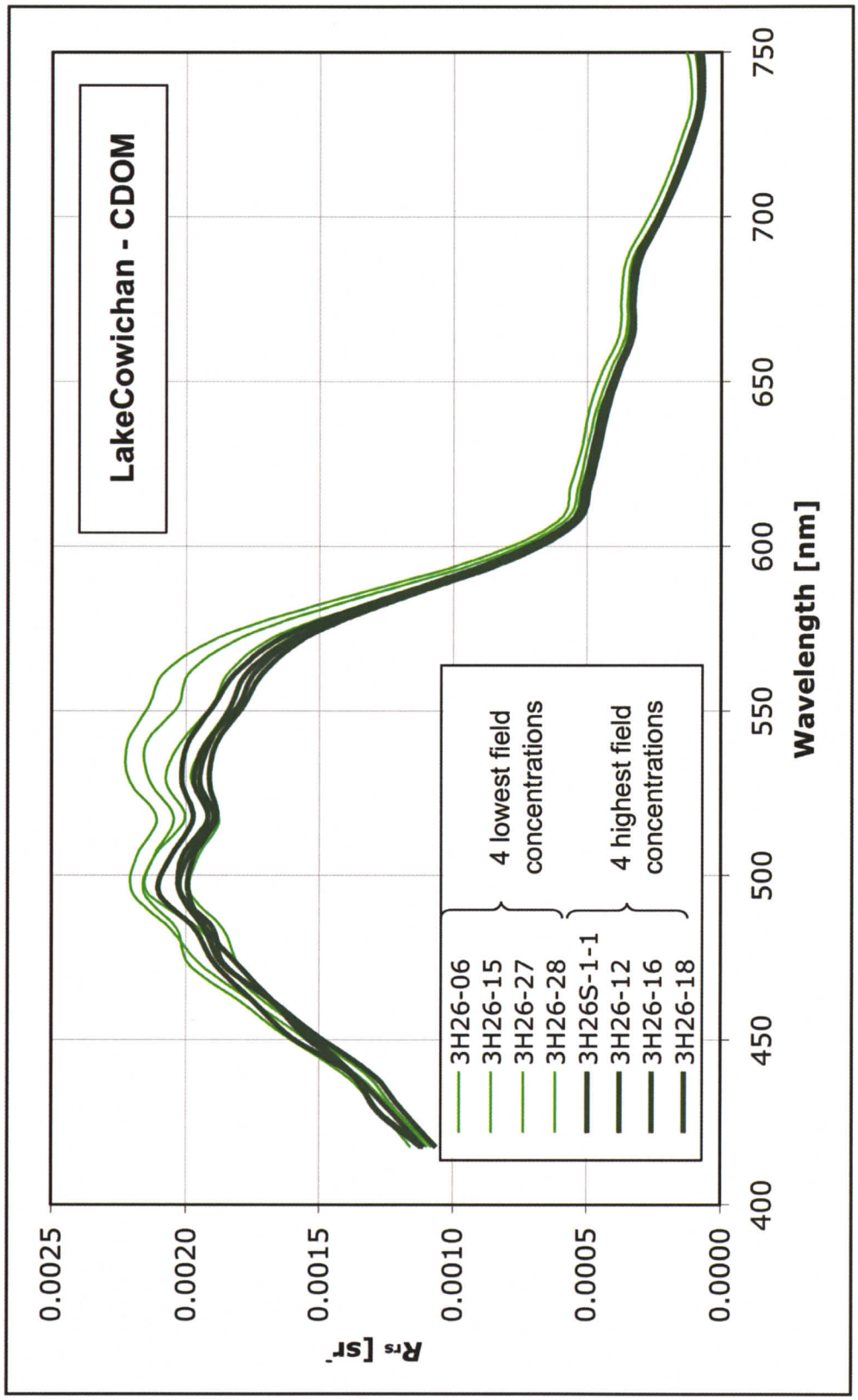
Band	WL	3H26-24				3H26-27				3H26-28				3H26-29			
		Mean	SD	CV	Dy/Dx	Mean	SD	CV	Dy/Dx	Mean	SD	CV	Dy/Dx	Mean	SD	CV	Dy/Dx
1	417	0.00079	3.3E-05	4%	-	0.00076	4.5E-05	6%	-	0.00072	3.2E-05	4%	-	0.00082	4.4E-05	5%	-
2	428	0.00089	3.6E-05	4%	9.2E-06	0.00090	3.6E-05	4%	1.2E-05	0.00081	3.0E-05	4%	8.1E-06	0.00085	1.1E-04	12%	3.1E-06
3	439	0.00088	2.5E-05	3%	-1.8E-07	0.00087	2.3E-05	3%	-2.7E-06	0.00087	2.4E-05	3%	5.7E-06	0.00087	7.3E-05	8%	1.5E-06
4	451	0.00102	3.3E-05	3%	1.2E-05	0.00098	3.4E-05	3%	1.0E-05	0.00097	2.4E-05	2%	8.2E-06	0.00100	7.0E-05	7%	1.2E-05
5	462	0.00110	4.8E-05	4%	7.0E-06	0.00106	5.4E-05	5%	7.5E-06	0.00107	3.9E-05	4%	9.8E-06	0.00110	5.5E-05	5%	9.2E-06
6	473	0.00114	3.4E-05	3%	4.2E-06	0.00114	4.1E-05	4%	7.2E-06	0.00109	3.8E-05	3%	1.4E-06	0.00115	5.5E-05	5%	4.2E-06
7	484	0.00123	1.9E-05	2%	7.5E-06	0.00122	1.2E-05	1%	7.2E-06	0.00114	2.4E-05	2%	4.1E-06	0.00119	5.9E-05	5%	3.7E-06
8	495	0.00131	2.2E-05	2%	7.2E-06	0.00128	2.0E-05	2%	4.9E-06	0.00121	3.3E-05	3%	6.9E-06	0.00129	4.5E-05	3%	8.8E-06
9	506	0.00130	2.6E-05	2%	-1.8E-07	0.00123	2.4E-05	2%	-4.6E-06	0.00123	2.7E-05	2%	1.9E-06	0.00133	3.6E-05	3%	3.3E-06
10	517	0.00127	2.2E-05	2%	-2.9E-06	0.00123	1.8E-05	1%	2.7E-07	0.00120	1.4E-05	1%	-2.7E-06	0.00127	2.8E-05	2%	-5.4E-06
11	529	0.00130	2.2E-05	2%	2.3E-06	0.00125	2.6E-05	2%	1.5E-06	0.00122	1.9E-05	2%	1.7E-06	0.00129	2.2E-05	2%	2.5E-06
12	540	0.00127	2.9E-05	2%	-2.9E-06	0.00117	1.8E-05	2%	-6.6E-06	0.00120	2.2E-05	2%	-1.9E-06	0.00127	2.7E-05	2%	-1.9E-06
13	551	0.00123	2.0E-05	2%	-2.9E-06	0.00117	1.6E-05	1%	8.8E-08	0.00114	2.7E-05	2%	-5.6E-06	0.00121	2.2E-05	2%	-5.8E-06
14	562	0.00118	2.2E-05	2%	-4.9E-06	0.00109	1.7E-05	2%	-7.1E-06	0.00111	1.9E-05	2%	-2.9E-06	0.00120	2.4E-05	2%	-8.9E-07
15	574	0.00109	1.7E-05	2%	-8.0E-06	0.00100	1.5E-05	1%	-8.0E-06	0.00100	1.4E-05	1%	-9.7E-06	0.00108	1.9E-05	2%	-1.0E-05
16	585	0.00091	1.1E-05	1%	-1.6E-05	0.00085	9.0E-06	1%	-1.4E-05	0.00082	1.1E-05	1%	-1.6E-05	0.00089	1.7E-05	2%	-1.7E-05
17	596	0.00066	1.0E-05	2%	-2.2E-05	0.00063	1.0E-05	2%	-1.9E-05	0.00062	9.0E-06	1%	-1.8E-05	0.00065	1.1E-05	2%	-2.2E-05
18	608	0.00047	5.0E-06	1%	-1.7E-05	0.00045	5.0E-06	1%	-1.6E-05	0.00043	5.0E-06	1%	-1.7E-05	0.00045	7.0E-06	2%	-1.8E-05
19	619	0.00041	7.0E-06	2%	-4.9E-06	0.00041	6.0E-06	1%	-3.9E-06	0.00039	7.0E-06	2%	-3.3E-06	0.00042	9.0E-06	2%	-2.5E-06
20	630	0.00039	6.0E-06	2%	-2.0E-06	0.00038	5.0E-06	1%	-2.3E-06	0.00036	7.0E-06	2%	-2.2E-06	0.00039	7.0E-06	2%	-2.4E-06
21	642	0.00037	5.0E-06	1%	-1.9E-06	0.00036	5.0E-06	1%	-1.7E-06	0.00034	6.0E-06	2%	-2.5E-06	0.00037	8.0E-06	2%	-1.8E-06
22	653	0.00033	5.0E-06	2%	-3.1E-06	0.00032	4.0E-06	1%	-3.2E-06	0.00031	5.0E-06	2%	-2.5E-06	0.00033	7.0E-06	2%	-3.9E-06
23	664	0.00029	7.0E-06	2%	-3.9E-06	0.00029	6.0E-06	2%	-3.3E-06	0.00027	7.0E-06	3%	-3.0E-06	0.00030	7.0E-06	2%	-2.7E-06
24	676	0.00033	5.0E-06	1%	4.2E-06	0.00032	4.0E-06	1%	3.4E-06	0.00032	9.0E-06	3%	3.9E-06	0.00034	1.1E-05	3%	4.3E-06
25	687	0.00036	8.0E-06	2%	1.8E-06	0.00034	7.0E-06	2%	1.5E-06	0.00033	7.0E-06	2%	8.8E-07	0.00036	7.0E-06	2%	9.6E-07
26	699	0.00025	1.0E-05	4%	-9.2E-06	0.00024	1.2E-05	5%	-8.5E-06	0.00024	9.0E-06	4%	-7.9E-06	0.00026	6.0E-06	2%	-8.3E-06
27	710	0.00020	8.0E-06	4%	-4.1E-06	0.00020	8.0E-06	4%	-3.8E-06	0.00020	6.0E-06	3%	-3.7E-06	0.00021	9.0E-06	4%	-4.8E-06
28	722	0.00015	3.0E-06	2%	-4.6E-06	0.00015	5.0E-06	3%	-4.3E-06	0.00015	7.0E-06	5%	-4.2E-06	0.00016	7.0E-06	4%	-4.2E-06
29	733	0.00012	3.0E-06	3%	-2.8E-06	0.00012	3.0E-06	3%	-3.0E-06	0.00011	5.0E-06	4%	-3.2E-06	0.00011	8.0E-06	7%	-4.2E-06
30	744	0.00009	1.3E-05	14%	-2.1E-06	0.00009	1.9E-05	21%	-2.2E-06	0.00010	5.0E-06	5%	-8.7E-07	0.00010	5.0E-06	5%	-4.3E-07
31	756	0.00009	1.0E-05	11%	-1.7E-07	0.00011	9.0E-06	8%	1.6E-06	0.00010	4.0E-06	4%	8.7E-08	0.00010	4.0E-06	4%	-8.7E-08
32	767	0.00007	7.0E-06	10%	-1.8E-06	0.00007	6.0E-06	8%	-3.4E-06	0.00008	3.0E-06	4%	-2.1E-06	0.00008	7.0E-06	9%	-2.4E-06
33	779	0.00010	3.7E-05	39%	2.0E-06	0.00009	3.4E-05	40%	1.3E-06	0.00010	4.0E-06	4%	1.8E-06	0.00010	7.0E-06	7%	1.7E-06
34	790	0.00012	1.2E-05	10%	1.7E-06	0.00011	1.3E-05	11%	2.4E-06	0.00010	5.0E-06	5%	-1.7E-07	0.00010	9.0E-06	9%	1.7E-07

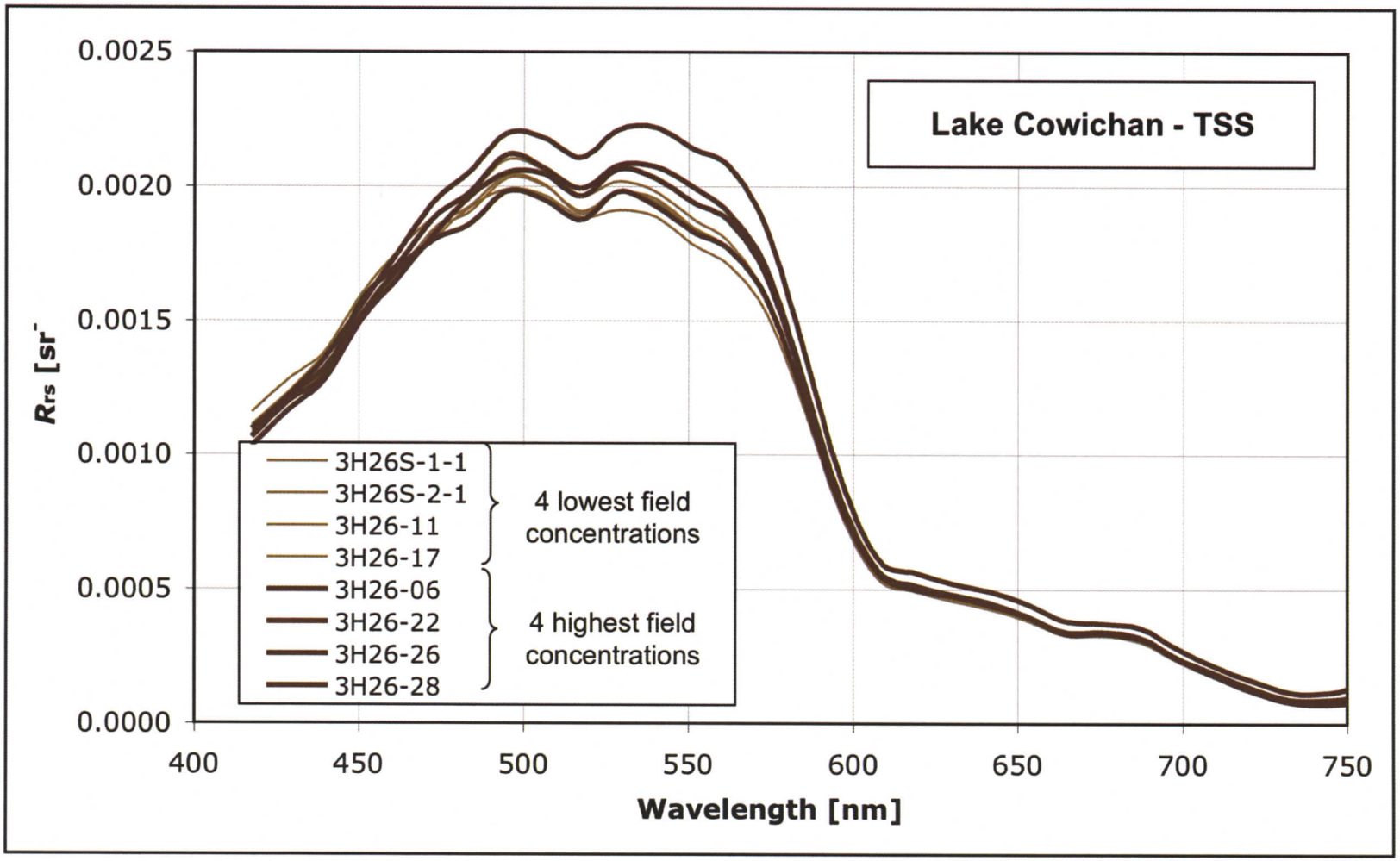

3H26-27
3H26-29
3H26-24
3H26-28
CV [%]
Mean
DyDx
Wavelength [nm]

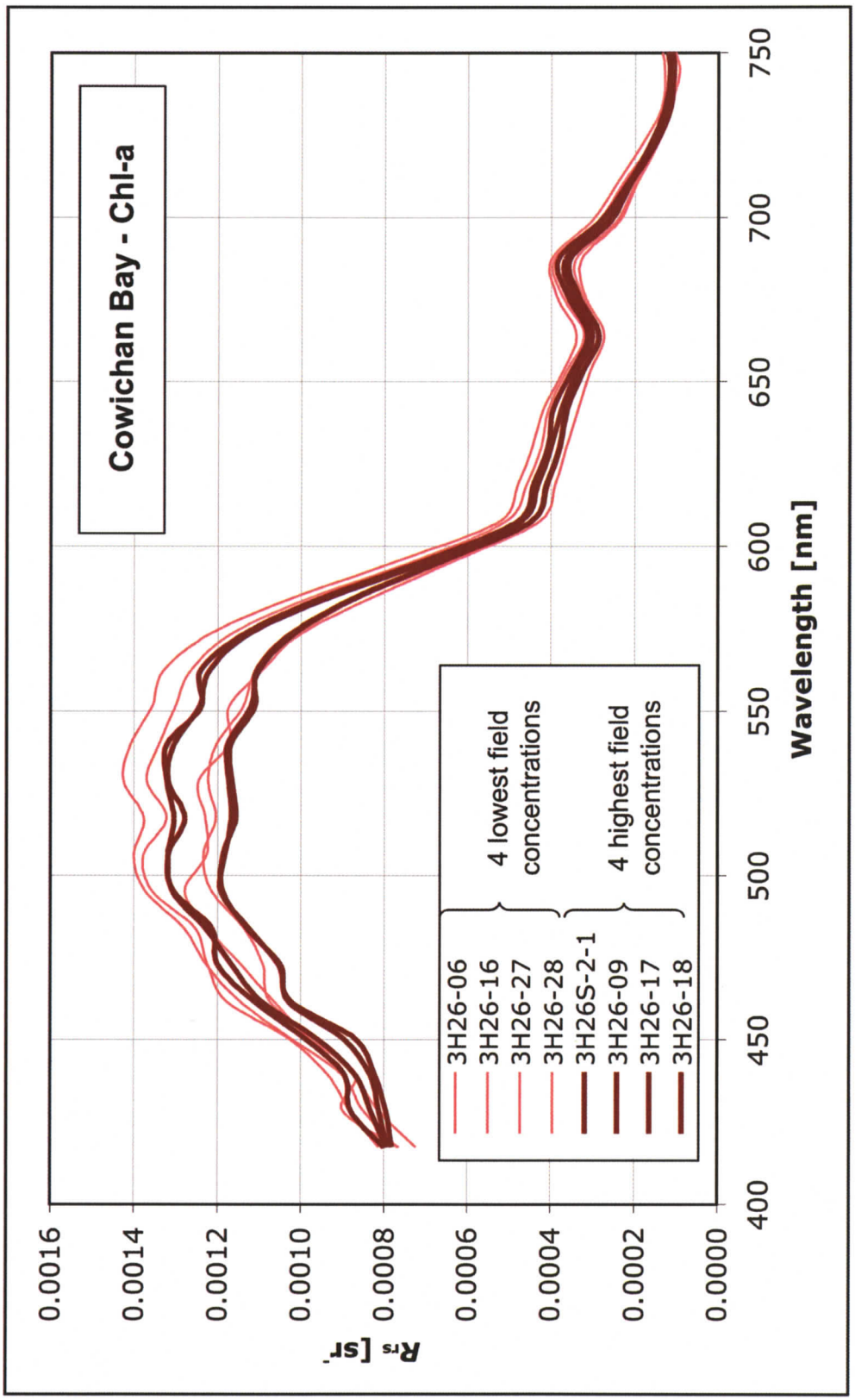
::: APPENDIX F :::

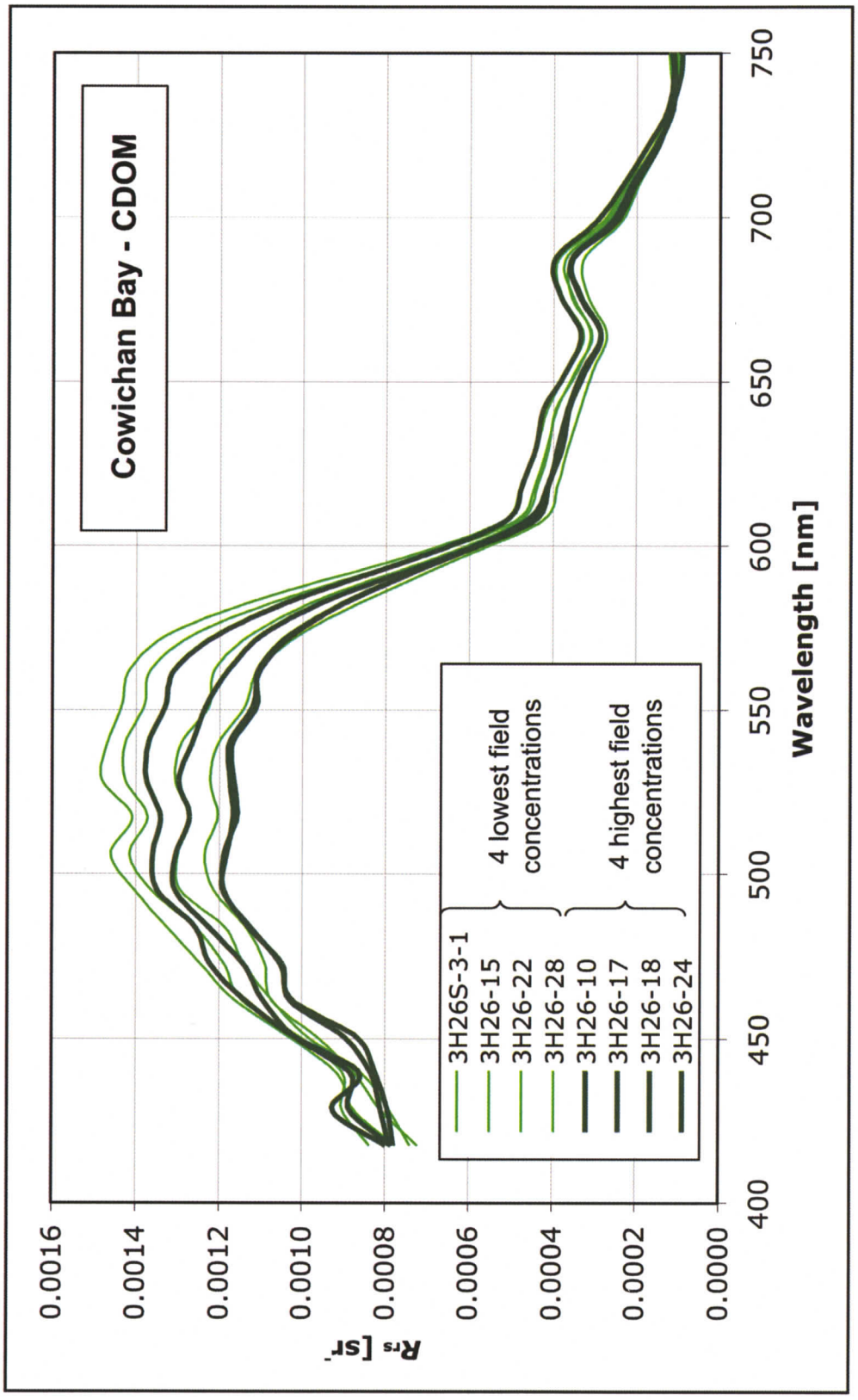
High/Low Parameters Vs. CASI R_{rs} Spectra Plots

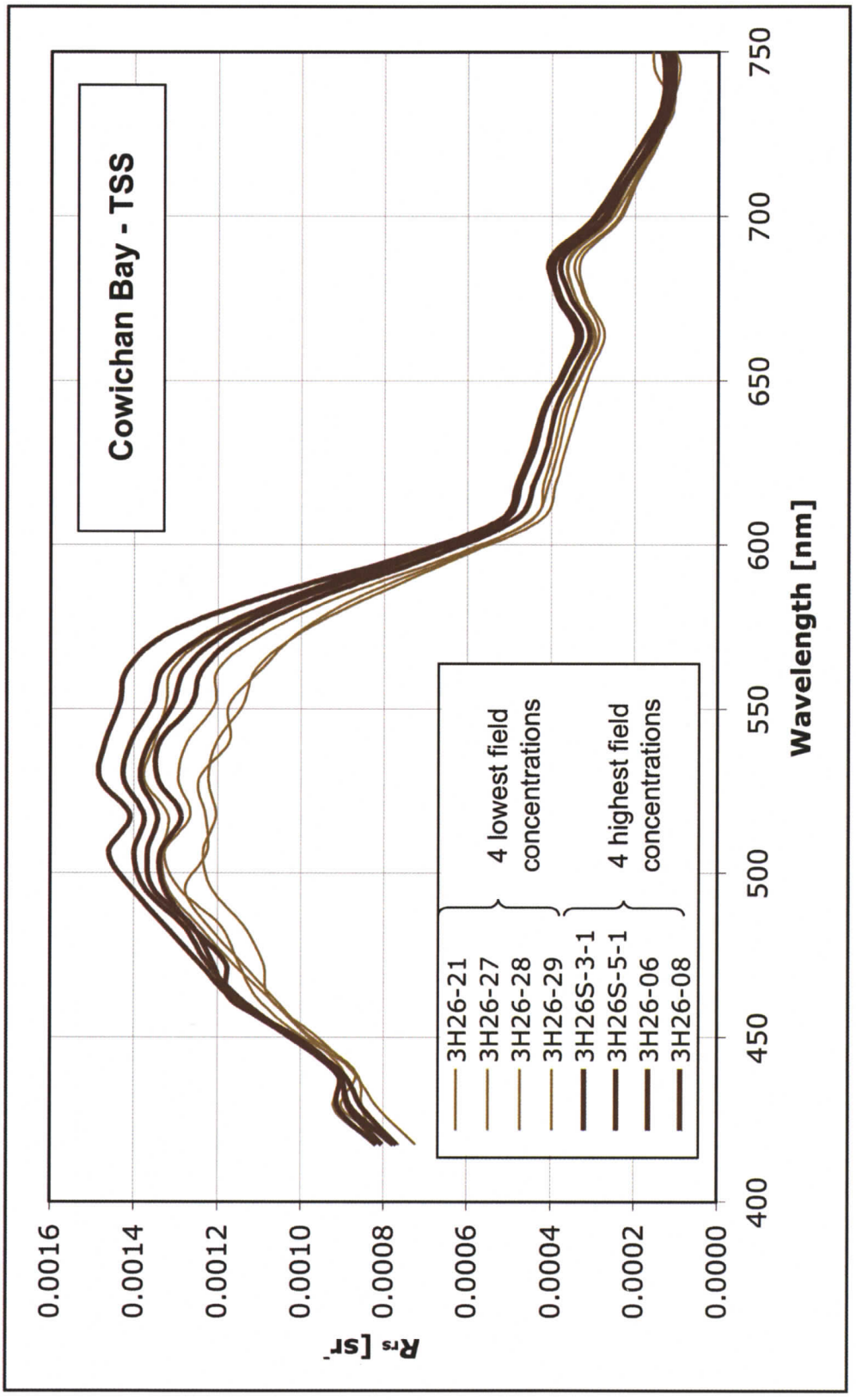

Lake Cowichan - Chl-a
Rrs [sr-1]
0.0025
0.0020
0.0015
0.0010
0.0005
0.0000
400
450
500
550
600
650
700
750
Wavelength [nm]
3H26-07
3H26-22
3H26-23
3H26-25
3H26-06
3H26-10
3H26-11
3H26-28
4 lowest field concentrations
4 highest field concentrations


LakeCowichan - CDOM
Rrs [sr-1]
0.0025
0.0020
0.0015
0.0010
0.0005
0.0000
400
450
500
550
600
650
700
750
Wavelength [nm]
3H26-06
3H26-15
3H26-27
3H26-28
3H26S-1-1
3H26-12
3H26-16
3H26-18
4 lowest field concentrations
4 highest field concentrations


Lake Cowichan - TSS
0.0025
0.0020
0.0015
0.0010
0.0005
0.0000
Rrs [sr-]
400
450
500
550
600
650
700
750
Wavelength [nm]
3H26S-1-1
3H26S-2-1
3H26-11
3H26-17
3H26-06
3H26-22
3H26-26
3H26-28
4 lowest field concentrations
4 highest field concentrations

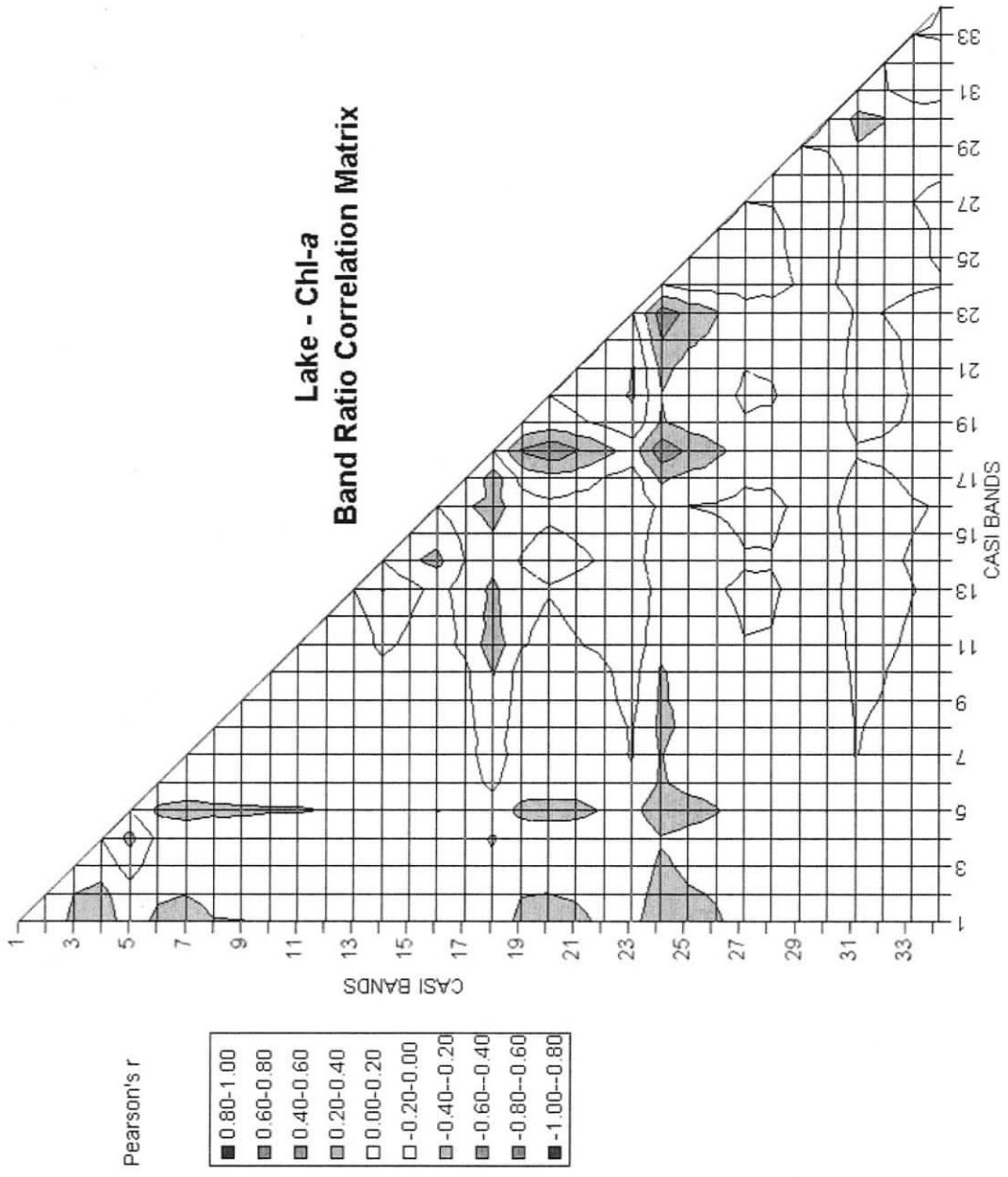

Cowichan Bay - Chl-a
Rrs [sr-1]
0.0016
0.0014
0.0012
0.0010
0.0008
0.0006
0.0004
0.0002
0.0000
400
450
500
550
600
650
700
750
Wavelength [nm]
3H26-06
3H26-16
3H26-27
3H26-28
3H26S-2-1
3H26-09
3H26-17
3H26-18
4 lowest field concentrations
4 highest field concentrations

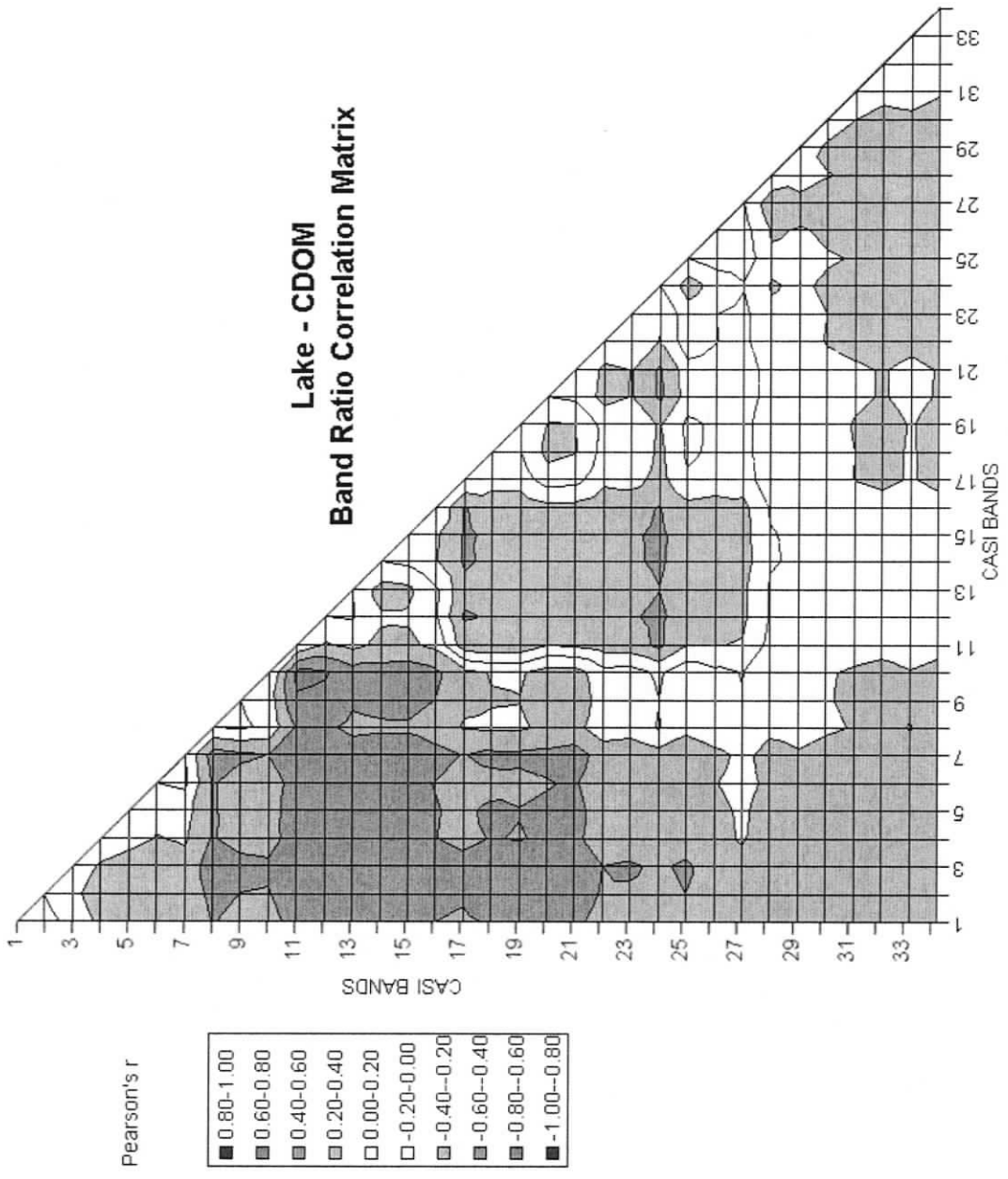

Cowichan Bay - CDOM
R_{rs} [sr^{-1}]
0.0016
0.0014
0.0012
0.0010
0.0008
0.0006
0.0004
0.0002
0.0000
400
450
500
550
600
650
700
750
Wavelength [nm]
3H26S-3-1
3H26-15
3H26-22
3H26-28
3H26-10
3H26-17
3H26-18
3H26-24
4 lowest field concentrations
4 highest field concentrations

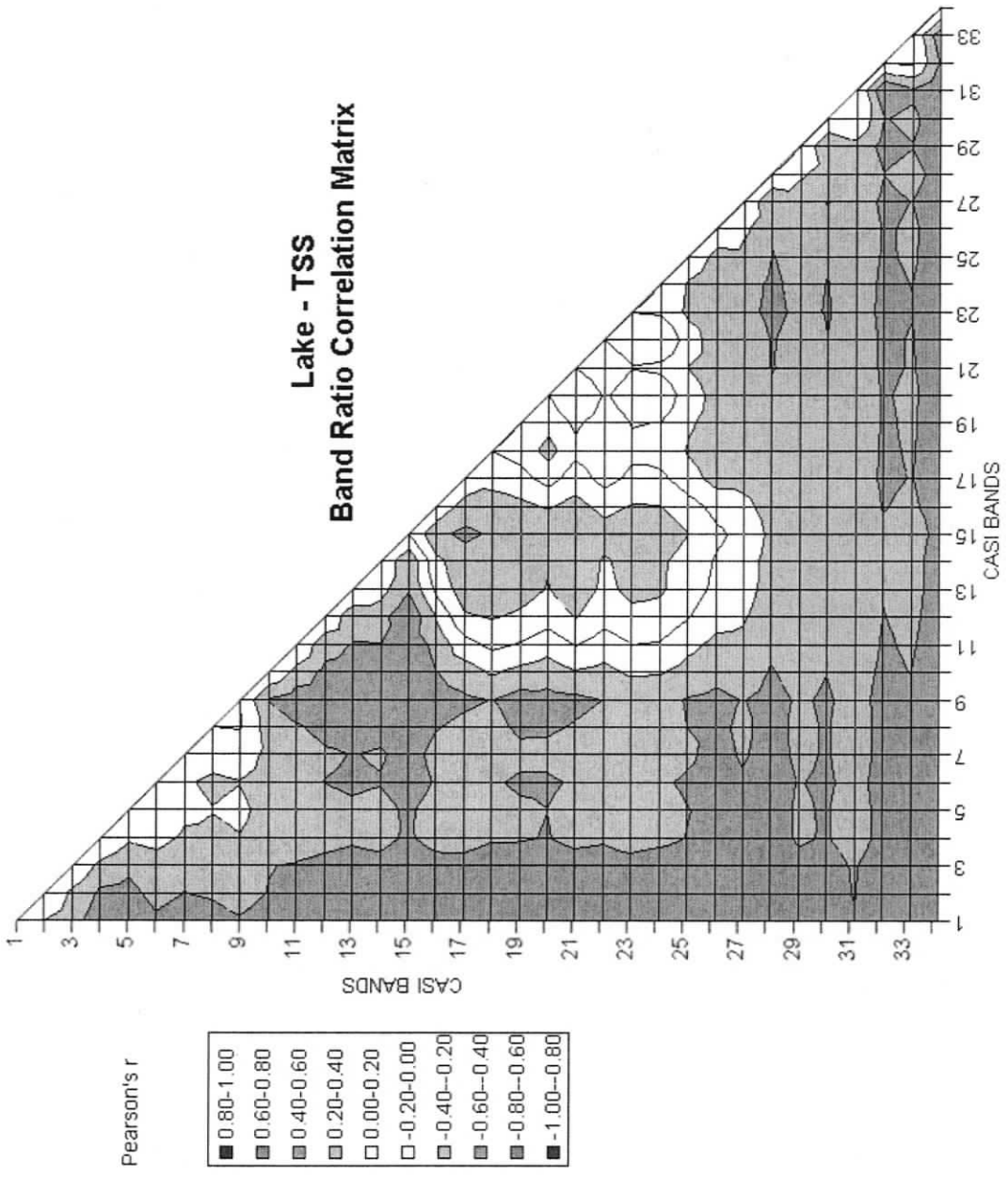

Cowichan Bay - TSS
R_{rs} [sr^{-1}]
0.0016
0.0014
0.0012
0.0010
0.0008
0.0006
0.0004
0.0002
0.0000
400
450
500
550
600
650
700
750
Wavelength [nm]
3H26-21
3H26-27
3H26-28
3H26-29
3H26S-3-1
3H26S-5-1
3H26-06
3H26-08
4 lowest field concentrations
4 highest field concentrations

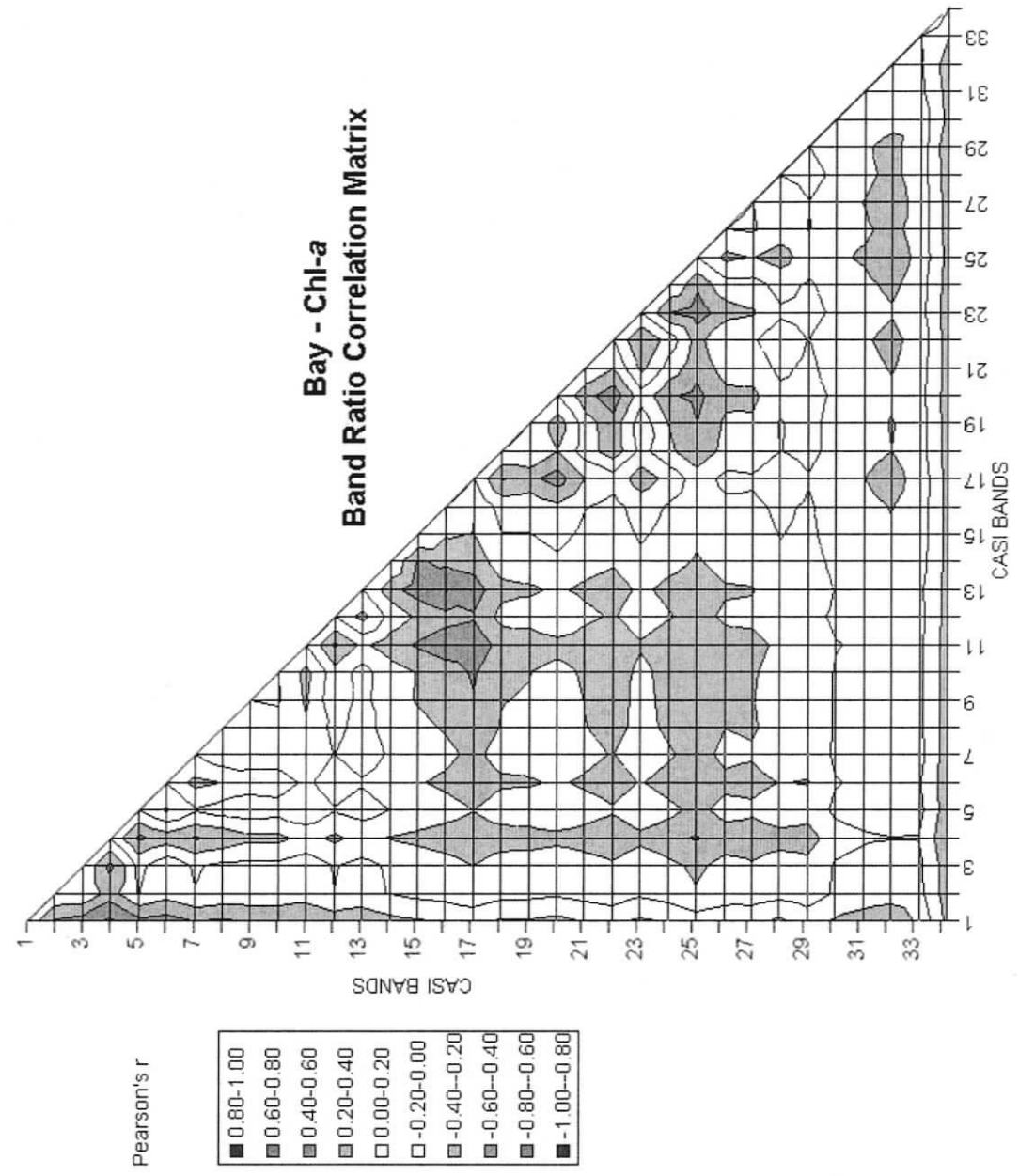
::: APPENDIX G :::

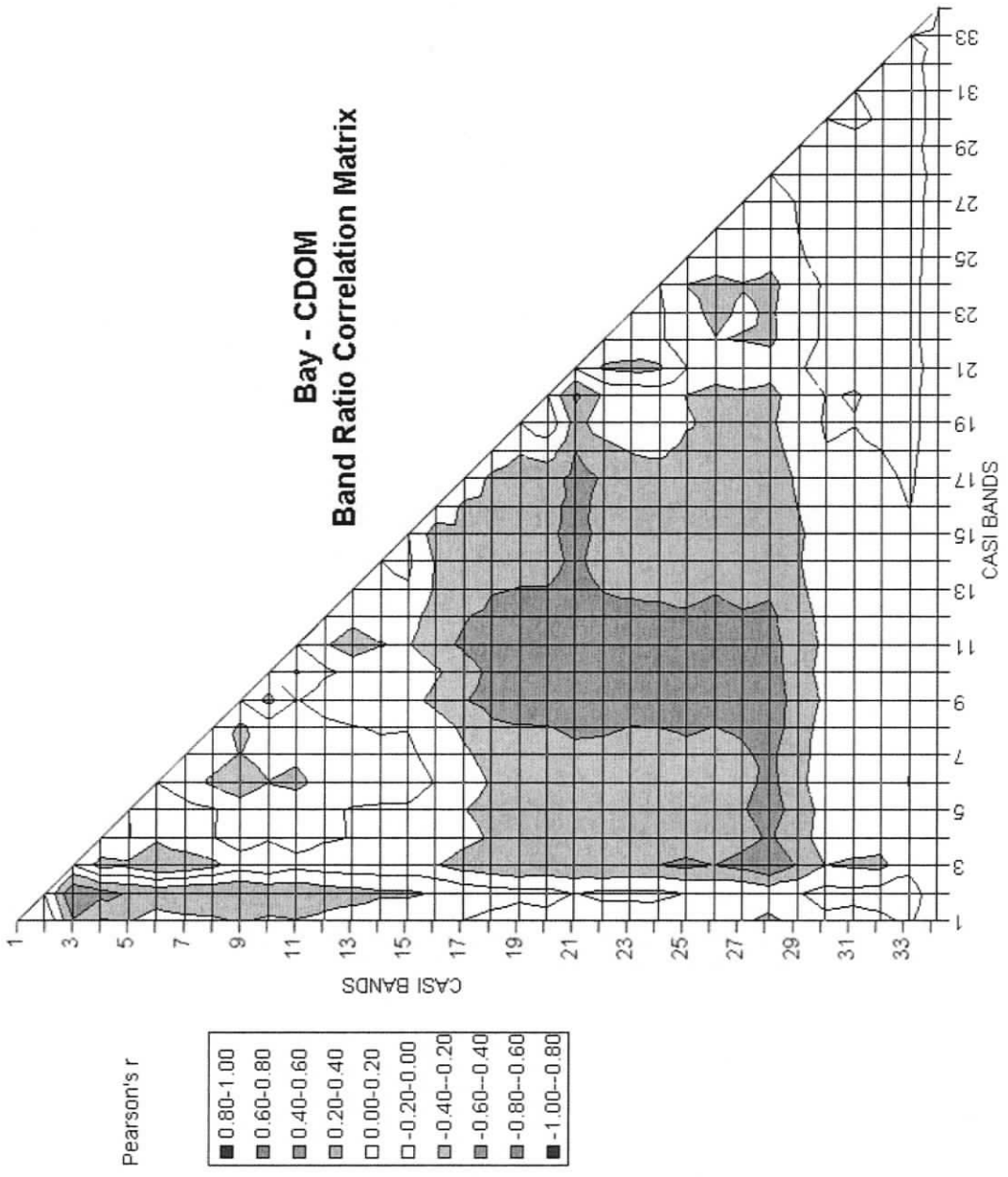
Band Ratio Correlation Matrices

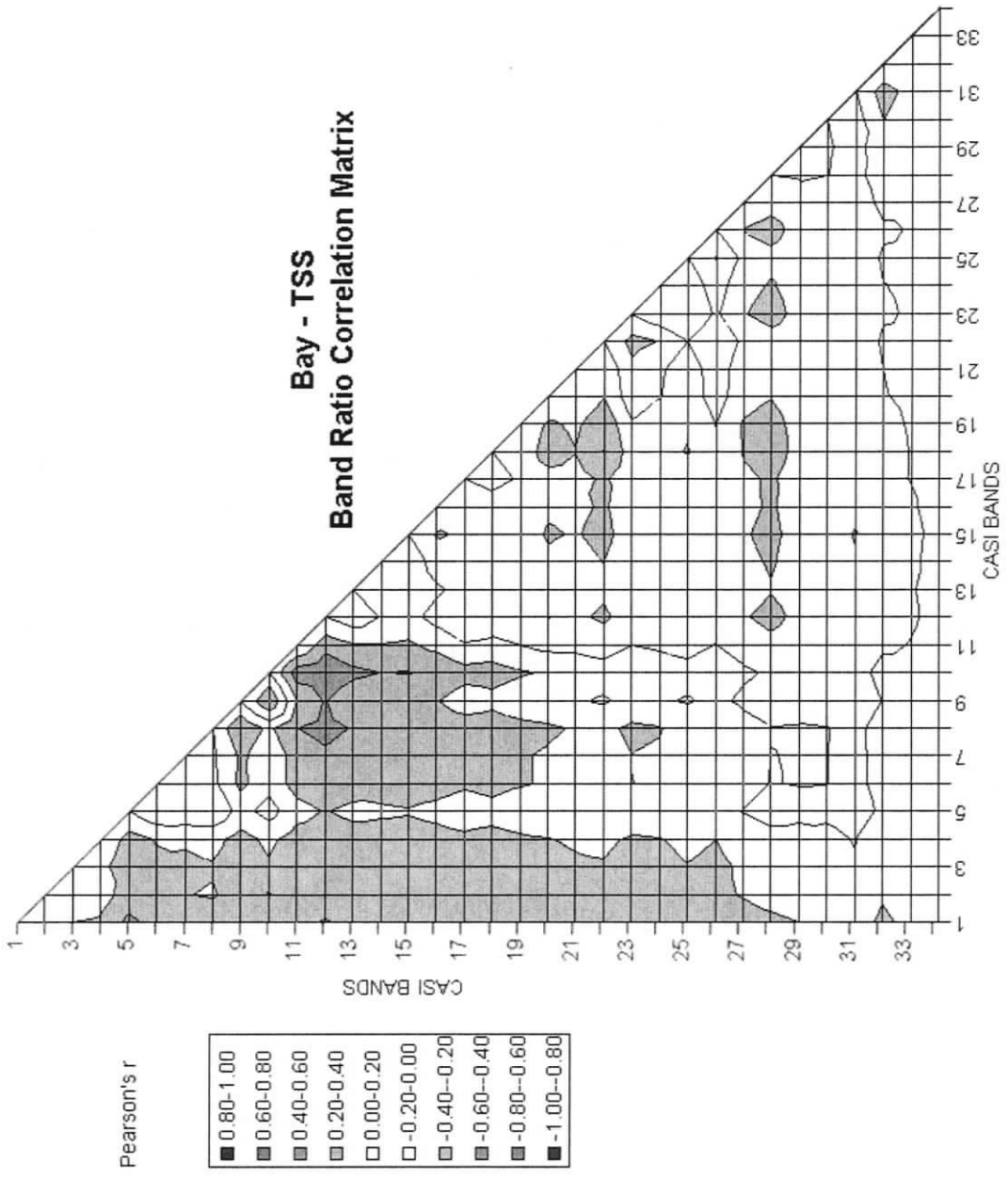

Lake - Chl-a
Band Ratio Correlation Matrix
CASI BANDS
CASI BANDS
Pearson's r
0.80-1.00
0.60-0.80
0.40-0.60
0.20-0.40
0.00-0.20
-0.20-0.00
-0.40--0.20
-0.60--0.40
-0.80--0.60
-1.00--0.80


Lake - CDOM
Band Ratio Correlation Matrix
CASI BANDS
CASI BANDS
Pearson's r
0.80-1.00
0.60-0.80
0.40-0.60
0.20-0.40
0.00-0.20
-0.20-0.00
-0.40--0.20
-0.60--0.40
-0.80--0.60
-1.00--0.80


Lake - TSS
Band Ratio Correlation Matrix
CASI BANDS
CASI BANDS
Pearson's r
0.80-1.00
0.60-0.80
0.40-0.60
0.20-0.40
0.00-0.20
-0.20-0.00
-0.40--0.20
-0.60--0.40
-0.80--0.60
-1.00--0.80


Bay - Chl-a
Band Ratio Correlation Matrix
CASI BANDS
CASI BANDS
Pearson's r
0.80-1.00
0.60-0.80
0.40-0.60
0.20-0.40
0.00-0.20
-0.20-0.00
-0.40--0.20
-0.60--0.40
-0.80--0.60
-1.00--0.80


Bay - CDOM
Band Ratio Correlation Matrix
CASI BANDS
CASI BANDS
Pearson's r
0.80-1.00
0.60-0.80
0.40-0.60
0.20-0.40
0.00-0.20
-0.20-0.00
-0.40--0.20
-0.60--0.40
-0.80--0.60
-1.00--0.80

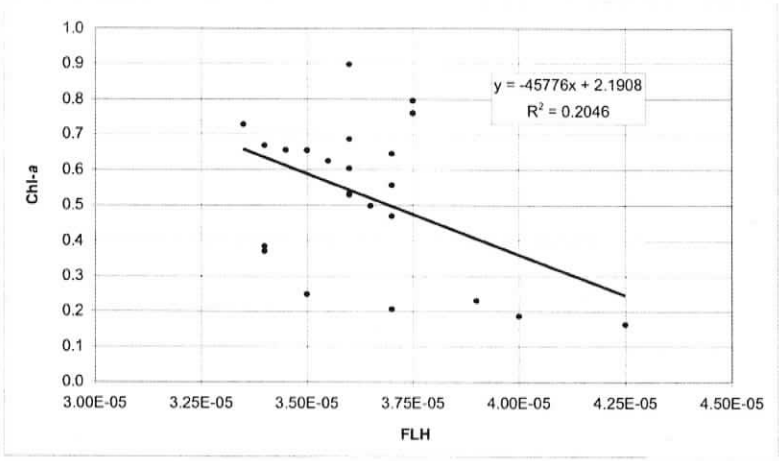

Bay - TSS
Band Ratio Correlation Matrix
CASI BANDS
CASI BANDS
Pearson's r
0.80-1.00
0.60-0.80
0.40-0.60
0.20-0.40
0.00-0.20
-0.20-0.00
-0.40--0.20
-0.60--0.40
-0.80--0.60
-1.00--0.80

::: APPENDIX H :::

Fluorescence Line Height Algorithm Results

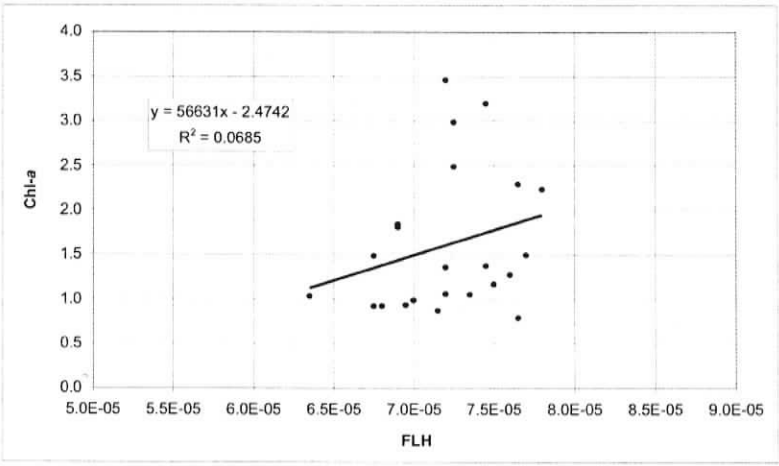
Lake Cowichan

SAMPLE	Chl-*a* [µg/L]	λ_1 664nm	λ_2 682nm	λ_3 699nm	FLH
3H26S-1-1	0.384	3.300E-04	3.150E-04	2.320E-04	3.400E-05
3H26S-2-1	0.370	3.380E-04	3.265E-04	2.470E-04	3.400E-05
3H26-06	0.761	3.340E-04	3.255E-04	2.420E-04	3.750E-05
3H26-07	0.186	3.320E-04	3.245E-04	2.370E-04	4.000E-05
3H26-08	0.499	3.230E-04	3.135E-04	2.310E-04	3.650E-05
3H26-10	0.897	3.410E-04	3.275E-04	2.420E-04	3.600E-05
3H26-11	0.795	3.380E-04	3.230E-04	2.330E-04	3.750E-05
3H26-12	0.469	3.290E-04	3.185E-04	2.340E-04	3.700E-05
3H26-13	0.604	3.310E-04	3.195E-04	2.360E-04	3.600E-05
3H26-14	0.687	3.270E-04	3.155E-04	2.320E-04	3.600E-05
3H26-15	0.656	3.510E-04	3.290E-04	2.380E-04	3.450E-05
3H26-16	0.533	3.390E-04	3.280E-04	2.450E-04	3.600E-05
3H26-17	0.529	3.390E-04	3.225E-04	2.340E-04	3.600E-05
3H26-18	0.655	3.350E-04	3.220E-04	2.390E-04	3.500E-05
3H26-19	0.248	3.420E-04	3.295E-04	2.470E-04	3.500E-05
3H26-20	0.669	3.390E-04	3.250E-04	2.430E-04	3.400E-05
3H26-21	0.625	3.440E-04	3.285E-04	2.420E-04	3.550E-05
3H26-22	0.231	3.390E-04	3.300E-04	2.430E-04	3.900E-05
3H26-23	0.163	3.460E-04	3.380E-04	2.450E-04	4.250E-05
3H26-25	0.207	3.430E-04	3.315E-04	2.460E-04	3.700E-05
3H26-26	0.557	3.420E-04	3.295E-04	2.430E-04	3.700E-05
3H26-27	0.645	3.570E-04	3.410E-04	2.510E-04	3.700E-05
3H26-28	0.728	3.810E-04	3.640E-04	2.800E-04	3.350E-05



Cowichan Bay

SAMPLE	Chl-*a* [µg/L]	λ_1 664nm	λ_2 682nm	λ_3 699nm	FLH
3H26S-1-1	1.032	2.790E-04	3.240E-04	2.420E-04	6.350E-05
3H26S-2-1	2.488	3.020E-04	3.575E-04	2.680E-04	7.250E-05
3H26S-3-1	2.233	3.290E-04	3.835E-04	2.820E-04	7.800E-05
3H26S-4-1	1.486	2.970E-04	3.520E-04	2.720E-04	6.750E-05
3H26S-5-1	1.272	3.330E-04	3.930E-04	3.010E-04	7.600E-05
3H26-06	0.865	3.400E-04	3.935E-04	3.040E-04	7.150E-05
3H26-07	1.357	3.070E-04	3.650E-04	2.790E-04	7.200E-05
3H26-08	1.373	3.080E-04	3.655E-04	2.740E-04	7.450E-05
3H26-09	2.984	3.140E-04	3.720E-04	2.850E-04	7.250E-05
3H26-10	1.050	3.350E-04	3.895E-04	2.970E-04	7.350E-05
3H26-11	1.805	3.070E-04	3.595E-04	2.740E-04	6.900E-05
3H26-12	1.169	3.020E-04	3.600E-04	2.680E-04	7.500E-05
3H26-13	1.492	3.670E-04	4.240E-04	3.270E-04	7.700E-05
3H26-15	0.932	3.110E-04	3.620E-04	2.740E-04	6.950E-05
3H26-16	0.787	3.220E-04	3.820E-04	2.890E-04	7.650E-05
3H26-17	3.196	2.860E-04	3.475E-04	2.600E-04	7.450E-05
3H26-18	3.458	2.870E-04	3.450E-04	2.590E-04	7.200E-05
3H26-21	0.984	2.990E-04	3.520E-04	2.650E-04	7.000E-05
3H26-22	1.840	3.080E-04	3.575E-04	2.690E-04	6.900E-05
3H26-24	2.293	2.860E-04	3.445E-04	2.500E-04	7.650E-05
3H26-27	0.916	2.850E-04	3.325E-04	2.440E-04	6.800E-05
3H26-28	0.916	2.730E-04	3.230E-04	2.380E-04	6.750E-05
3H26-29	1.058	2.950E-04	3.495E-04	2.600E-04	7.200E-05



::: APPENDIX I :::

Model Analysis

SUMMARY OUTPUT
Model: ***Lake, Chl-a***
Data-Set: ***model building***

Regression Statistics	
Multiple R	0.893524081
R Square	0.798385284
Adjusted R Sqı	0.63037302
Standard Error	0.129794422
Observations	12

ANOVA

	df	*SS*	*MS*	*F*	*Significance F*
Regression	5	0.400270518	0.080054104	4.751946473	0.0420899
Residual	6	0.101079552	0.016846592		
Total	11	0.50135007			

	Coefficients	*Standard Error*	*t Stat*	*P-value*	*Lower 95%*	*Upper 95%*	*Lower 95.0%*	*Upper 95.0%*
Intercept	-1.530031206	1.253968785	-1.220150952	0.2681843	-4.59838228	1.538319868	-4.59838228	1.538319868
Dev456	32079.37564	31319.14317	1.024273731	0.345215855	-44555.8068	108714.5581	-44555.8068	108714.5581
Dev591	42310.70195	18881.80918	2.240818215	0.066272463	-3891.420614	88512.82452	-3891.420614	88512.82452
Dev613	-530165.6186	166027.7153	-3.193235646	0.018759521	-936420.802	-123910.4352	-936420.802	-123910.4352
Dev625	-216584.8546	151687.2689	-1.427838052	0.203252931	-587750.2298	154580.5206	-587750.2298	154580.5206
Dev670	-276755.502	145826.1306	-1.897845748	0.106487416	-633579.1886	80068.18456	-633579.1886	80068.18456

RESIDUAL OUTPUT

Observation	*Predicted Chl-a*	*Residuals*	*Standard Residuals*
1	0.376414164	0.007205836	0.075170784
2	0.639377279	0.121222721	1.264587007
3	0.214401298	-0.028041298	-0.292524876
4	0.521334499	-0.022074499	-0.230279643
5	0.823892154	-0.029012154	-0.302652777
6	0.432092904	0.036607096	0.381882686
7	0.706707868	-0.102287868	-1.067059935
8	0.51547354	0.01342646	0.1400639
9	0.397738693	0.226981307	2.367853234
10	0.349520277	-0.118840277	-1.239733523
11	0.238419184	-0.075599184	-0.788645442
12	0.674768139	-0.029588139	-0.308661416

SUMMARY OUTPUT
Model: ***Lake, Chl-a***
Data-Set: ***validation***

Regression Statistics	
Multiple R	0.947637207
R Square	0.898016276
Adjusted R Sq	0.796032552
Standard Error	0.095469832
Observations	11

ANOVA

	df	*SS*	*MS*	*F*	*Significance F*
Regression	5	0.401287529	0.080257506	8.805486199	0.01611177
Residual	5	0.045572444	0.009114489		
Total	10	0.446859973			

	Coefficients	*Standard Error*	*t Stat*	*P-value*	*Lower 95%*	*Upper 95%*	*Lower 95.0%*	*Upper 95.0%*
Intercept	-1.491883577	0.594833992	-2.50806712	0.053955287	-3.020953032	0.037185877	-3.020953032	0.037185877
Dev456	59504.04142	22923.00318	2.595822238	0.048493908	578.5858514	118429.497	578.5858514	118429.497
Dev591	35747.77997	12826.29425	2.787070005	0.038578221	2776.740972	68718.81898	2776.740972	68718.81898
Dev613	-426577.3418	75538.21978	-5.647172293	0.002417075	-620754.5174	-232400.1662	-620754.5174	-232400.1662
Dev625	-161380.3027	79110.07805	-2.039946195	0.096875412	-364739.2323	41978.62686	-364739.2323	41978.62686
Dev670	-256119.5359	139507.4166	-1.835884731	0.12581172	-614734.7667	102495.6949	-614734.7667	102495.6949

RESIDUAL OUTPUT

Observation	*Predicted Chl-a*	*Residuals*	*Standard Residuals*
1	0.40270499	-0.03306499	-0.489798262
2	0.902026917	-0.004626917	-0.068539443
3	0.597309219	0.089270781	1.322385785
4	0.710460816	-0.054540816	-0.807923925
5	0.417078449	0.116081551	1.719539045
6	0.693901139	-0.039001139	-0.577731604
7	0.341538599	-0.093638599	-1.38708714
8	0.623169418	0.045710582	0.677119916
9	0.20521334	0.00176666	0.026169887
10	0.630953711	-0.074253711	-1.099934944
11	0.681423402	0.046296598	0.685800685

SUMMARY OUTPUT
Model: ***Lake, Chl-a***
Data-Set: ***complete***

Regression Statistics	
Multiple R	0.913159025
R Square	0.833859405
Adjusted R Sq	0.784994524
Standard Error	0.097817837
Observations	23

ANOVA

	df	*SS*	*MS*	*F*	*Significance F*
Regression	5	0.816398315	0.163279663	17.06459506	4.25377E-06
Residual	17	0.162661596	0.009568329		
Total	22	0.979059911			

	Coefficients	*Standard Error*	*t Stat*	*P-value*	*Lower 95%*	*Upper 95%*	*Lower 95.0%*	*Upper 95.0%*
Intercept	-1.409063052	0.47550226	-2.963315149	0.008709261	-2.412285119	-0.405840985	-2.412285119	-0.405840985
Dev456	48567.53532	14763.59568	3.289682024	0.004325363	17419.07145	79715.99918	17419.07145	79715.99918
Dev591	38232.68962	9211.344416	4.150609063	0.000669335	18798.45186	57666.92739	18798.45186	57666.92739
Dev613	-439768.8995	61396.39337	-7.162780668	1.589E-06	-569303.9655	-310233.8335	-569303.9655	-310233.8335
Dev625	-193951.0254	57514.62108	-3.372203829	0.003619006	-315296.2678	-72605.78304	-315296.2678	-72605.78304
Dev670	-250916.961	78718.27162	-3.187531381	0.005390212	-416997.9952	-84835.9268	-416997.9952	-84835.9268

RESIDUAL OUTPUT

Observation	*Predicted Chl-a*	*Residuals*	*Standard Residuals*
1	0.414709236	-0.031089236	-0.361558749
2	0.381188043	-0.011548043	-0.134300371
3	0.642060461	0.118539539	1.37858027
4	0.233397683	-0.047037683	-0.54703454
5	0.548506881	-0.049246881	-0.57272686
6	0.938691374	-0.041291374	-0.480206638
7	0.807547134	-0.012667134	-0.147315072
8	0.401979658	0.066720342	0.775938118
9	0.673923899	-0.069503899	-0.80831008
10	0.603444485	0.083135515	0.9668418
11	0.696838987	-0.040918987	-0.475875884
12	0.418635163	0.114524837	1.331890462
13	0.528603503	0.000296497	0.003448179
14	0.667831908	-0.012931908	-0.150394315
15	0.352880144	-0.104980144	-1.220888463
16	0.60008574	0.06879426	0.800057184
17	0.399261563	0.225458437	2.622015883
18	0.332831289	-0.102151289	-1.187989706
19	0.27746744	-0.11464744	-1.333316292
20	0.186828568	0.020151432	0.234355273
21	0.616369021	-0.059669021	-0.693933313
22	0.733819442	-0.088639442	-1.030850864
23	0.63901838	0.08870162	1.031573978

Lake Cowichan - Chl-*a*

Model Building Data-Set

Sample	Chl-a	Dev456	Dev591	Dev613	Dev625	Dev670	Chl-a'	e	e^2
3H25S-1-1	0.384	1.36E-05	-3.49E-05	-4.07E-06	-3.19E-06	-3.51E-07	0.376	0.007	0.000
3H25-06	0.761	1.53E-05	-3.55E-05	-5.22E-06	-2.12E-06	1.75E-07	0.639	0.121	0.015
3H25-07	0.186	1.22E-05	-3.35E-05	-4.25E-06	-2.74E-06	2.63E-07	0.214	-0.028	0.001
3H25-08	0.499	1.43E-05	-3.38E-05	-4.34E-06	-3.45E-06	8.77E-08	0.521	-0.022	0.000
3H25-11	0.795	1.46E-05	-3.47E-05	-4.87E-06	-3.01E-06	-4.39E-07	0.824	-0.029	0.001
3H25-12	0.469	1.16E-05	-3.40E-05	-4.69E-06	-2.83E-06	2.63E-07	0.432	0.037	0.001
3H25-13	0.604	1.30E-05	-3.43E-05	-4.78E-06	-2.74E-06	-5.26E-07	0.707	-0.102	0.010
3H25-17	0.529	1.37E-05	-3.58E-05	-4.42E-06	-3.01E-06	-4.39E-07	0.515	0.013	0.000
3H25-21	0.625	1.27E-05	-3.83E-05	-4.51E-06	-3.01E-06	-3.51E-07	0.398	0.227	0.052
3H25-22	0.231	1.23E-05	-3.92E-05	-4.87E-06	-2.83E-06	1.75E-07	0.350	-0.119	0.014
3H25-23	0.163	1.40E-05	-3.82E-05	-4.60E-06	-2.30E-06	0.00E+00	0.238	-0.076	0.006
3H25-27	0.645	1.78E-05	-4.12E-05	-4.96E-06	-2.57E-06	-7.02E-07	0.675	-0.030	0.001
									0.101

Validation Data-Set

("Validation Set" model)

Sample	Chl-a	Dev456	Dev591	Dev613	Dev625	Dev670	Chl-a'	e	e^2
3H25S-2-1	0.370	1.32E-05	-3.53E-05	-4.69E-06	-2.04E-06	-1.75E-07	0.403	-0.033	0.001
3H25-10	0.897	1.06E-05	-3.66E-05	-6.02E-06	-2.57E-06	-3.51E-07	0.902	-0.005	0.000
3H25-14	0.687	1.36E-05	-3.40E-05	-4.69E-06	-2.92E-06	-8.77E-08	0.597	0.089	0.008
3H25-15	0.656	1.60E-05	-3.67E-05	-4.07E-06	-3.72E-06	-8.77E-07	0.710	-0.055	0.003
3H25-16	0.533	1.30E-05	-3.57E-05	-4.42E-06	-2.83E-06	-2.63E-07	0.417	0.116	0.013
3H25-18	0.655	1.57E-05	-3.42E-05	-4.69E-06	-2.65E-06	-1.75E-07	0.694	-0.039	0.002
3H25-19	0.248	1.21E-05	-3.52E-05	-4.34E-06	-2.83E-06	-2.63E-07	0.342	-0.094	0.009
3H25-20	0.669	1.27E-05	-3.50E-05	-5.31E-06	-1.59E-06	-3.51E-07	0.623	0.046	0.002
3H25-25	0.207	1.31E-05	-4.08E-05	-4.69E-06	-2.48E-06	8.77E-08	0.205	0.002	0.000
3H25-26	0.557	1.40E-05	-3.84E-05	-5.31E-06	-2.48E-06	0.00E+00	0.631	-0.074	0.006
3H25-28	0.728	1.76E-05	-4.27E-05	-4.42E-06	-3.63E-06	-7.02E-07	0.681	0.046	0.002
									0.046

("Model Building Set" model)

Sample	Chl-a	Dev456	Dev591	Dev613	Dev625	Dev670	Chl-a'	e	e^2
3H25S-2-1	0.370	1.32E-05	-3.53E-05	-4.69E-06	-2.04E-06	-1.75E-07	0.374	-0.004	0.000
3H25-10	0.897	1.06E-05	-3.66E-05	-6.02E-06	-2.57E-06	-3.51E-07	1.104	-0.207	0.043
3H25-14	0.687	1.36E-05	-3.40E-05	-4.69E-06	-2.92E-06	-8.77E-08	0.612	0.075	0.006
3H25-15	0.656	1.60E-05	-3.67E-05	-4.07E-06	-3.72E-06	-8.77E-07	0.636	0.019	0.000
3H25-16	0.533	1.30E-05	-3.57E-05	-4.42E-06	-2.83E-06	-2.63E-07	0.409	0.124	0.015
3H25-18	0.655	1.57E-05	-3.42E-05	-4.69E-06	-2.65E-06	-1.75E-07	0.638	0.017	0.000
3H25-19	0.248	1.21E-05	-3.52E-05	-4.34E-06	-2.83E-06	-2.63E-07	0.352	-0.104	0.011
3H25-20	0.669	1.27E-05	-3.50E-05	-5.31E-06	-1.59E-06	-3.51E-07	0.652	0.017	0.000
3H25-25	0.207	1.31E-05	-4.08E-05	-4.69E-06	-2.48E-06	8.77E-08	0.162	0.045	0.002
3H25-26	0.557	1.40E-05	-3.84E-05	-5.31E-06	-2.48E-06	0.00E+00	0.645	-0.088	0.008
3H25-28	0.728	1.76E-05	-4.27E-05	-4.42E-06	-3.63E-06	-7.02E-07	0.555	0.173	0.030
									0.115

Statistic	Model Building Data-set	Validation Data-set	Complete Data-set
b_0	-1.53	-1.49	-1.41
$s\{b_0\}$	1.25	0.59	0.48
b_1	32079.38	59504.04	48568
$s\{b_1\}$	31319.14	22923.00	14764
b_2	42311	35748	38233
$s\{b_2\}$	18882	12826	9211
b_3	-530166	-426577	-439769
$s\{b_3\}$	166028	75538	61396
b_4	-216585	-161380	-193951
$s\{b_4\}$	151687	79110	57515
b_5	-276756	-256120	-250917
$s\{b_5\}$	145826	139507	78718
SSE	0.101	0.046	0.163
MSE	0.0168	0.0091	0.0096
MSPR	-	0.0105	-
R^2	0.798	0.898	0.834

SUMMARY OUTPUT
Model: ***Lake, CDOM***
Data-Set: ***model building***

Regression Statistics	
Multiple R	0.920737032
R Square	0.847756683
Adjusted R Sq	0.746261138
Standard Error	0.205459304
Observations	11

ANOVA

	df	*SS*	*MS*	*F*	*Significance F*
Regression	4	1.410379081	0.35259477	8.352649212	0.012503136
Residual	6	0.253281153	0.042213525		
Total	10	1.663660234			

	Coefficients	*Standard Error*	*t Stat*	*P-value*	*Lower 95%*	*Upper 95%*	*Lower 95.0%*	*Upper 95.0%*
Intercept	4.005675076	0.85896206	4.663389995	0.00345513	1.903870636	6.107479515	1.903870636	6.107479515
Dev501	30867.05447	82207.07586	0.37547929	0.720220217	-170286.4133	232020.5222	-170286.4133	232020.5222
Dev523	-214808.0531	54770.94994	-3.921934043	0.007784644	-348827.7394	-80788.36688	-348827.7394	-80788.36688
Dev545	182196.5644	67023.47391	2.718399298	0.034716496	18196.0321	346197.0967	18196.0321	346197.0967
Dev647	69027.53106	168654.9809	0.409282493	0.696541802	-343656.3397	481711.4018	-343656.3397	481711.4018

RESIDUAL OUTPUT

Observation	*Predicted CDOM*	*Residuals*	*Standard Residuals*
1	0.439680256	-0.094230256	-0.592091647
2	0.106037988	0.124262012	0.780794856
3	0.629751655	0.015088345	0.094806948
4	0.583386503	0.061453497	0.386140332
5	0.617280893	0.073619107	0.462582401
6	0.780497386	-0.296867386	-1.865353092
7	0.228505599	0.001794401	0.011275037
8	1.355526841	0.210513159	1.322750128
9	0.328904202	-0.006484202	-0.040743197
10	-0.044079192	0.159229192	1.000509584
11	0.432617868	-0.248377868	-1.56067135

SUMMARY OUTPUT
Model: ***Lake, CDOM***
Data-Set: ***validation***

Regression Statistics	
Multiple R	0.925455527
R Square	0.856467932
Adjusted R Sqı	0.760779886
Standard Error	0.162174629
Observations	11

ANOVA

	df	*SS*	*MS*	*F*	*Significance F*
Regression	4	0.941627728	0.235406932	8.95062624	0.010554618
Residual	6	0.157803661	0.02630061		
Total	10	1.099431389			

	Coefficients	*Standard Error*	*t Stat*	*P-value*	*Lower 95%*	*Upper 95%*	*Lower 95.0%*	*Upper 95.0%*
Intercept	3.856789497	1.018488526	3.786777563	0.009107703	1.364637859	6.348941136	1.364637859	6.348941136
Dev501	93460.17159	32289.13062	2.894477795	0.027532142	14451.51536	172468.8278	14451.51536	172468.8278
Dev523	-121855.8139	23907.0208	-5.097072317	0.002227801	-180354.1863	-63357.4415	-180354.1863	-63357.4415
Dev545	97985.96443	62156.40598	1.576441927	0.165996013	-54105.2817	250077.2106	-54105.2817	250077.2106
Dev647	326433.3419	151988.6303	2.147748428	0.075340073	-45469.43814	698336.122	-45469.43814	698336.122

RESIDUAL OUTPUT

Observation	*Predicted CDOM*	*Residuals*	*Standard Residuals*
1	1.237916218	0.143883782	1.145389789
2	0.433237587	-0.110817587	-0.882165669
3	0.793307226	-0.010287226	-0.081891674
4	0.481515022	-0.159095022	-1.266479173
5	0.645858662	0.160191338	1.275206424
6	0.708312356	-0.132562356	-1.055265343
7	0.302215626	0.020204374	0.160837333
8	0.486927839	-0.049357839	-0.392914086
9	0.367808367	0.069761633	0.555338903
10	0.044370756	0.185929244	1.480093548
11	0.601480341	-0.117850341	-0.938150052

SUMMARY OUTPUT
Model: ***Lake, CDOM***
Data-Set: ***complete***

Regression Statistics	
Multiple R	0.864675063
R Square	0.747662965
Adjusted R Sq	0.688289545
Standard Error	0.203209502
Observations	22

ANOVA

	df	*SS*	*MS*	*F*	*Significance F*
Regression	4	2.079992738	0.519998184	12.59255343	6.07336E-05
Residual	17	0.701999732	0.041294102		
Total	21	2.78199247			

	Coefficients	*Standard Error*	*t Stat*	*P-value*	*Lower 95%*	*Upper 95%*	*Lower 95.0%*	*Upper 95.0%*
Intercept	3.853439726	0.59734718	6.450921437	5.97813E-06	2.593147353	5.113732099	2.593147353	5.113732099
Dev501	75814.19995	32813.29544	2.310471988	0.033675138	6584.198707	145044.2012	6584.198707	145044.2012
Dev523	-145944.7502	23794.09715	-6.133653623	1.10326E-05	-196145.9066	-95743.59381	-196145.9066	-95743.59381
Dev545	116992.5604	43241.59331	2.70555619	0.01500001	25760.77408	208224.3468	25760.77408	208224.3468
Dev647	255688.2933	110872.5928	2.30614516	0.0339676	21767.57196	489609.0146	21767.57196	489609.0146

RESIDUAL OUTPUT

Observation	*Predicted CDOM*	*Residuals*	*Standard Residuals*
1	1.319627599	0.062172401	0.340046893
2	0.424362638	-0.078912638	-0.431606263
3	0.307053371	-0.076753371	-0.419796323
4	0.498589759	0.146250241	0.799903807
5	0.477979925	0.166860075	0.912627623
6	0.4905634	0.2003366	1.095724753
7	0.574577065	-0.252157065	-1.379152575
8	0.781442258	0.001577742	0.008629329
9	0.683769277	-0.200139277	-1.094645511
10	0.599683216	-0.277263216	-1.516468626
11	0.024855637	0.205444363	1.123661249
12	0.789088392	0.016961608	0.092770139
13	0.69813357	-0.12238357	-0.669366993
14	1.140860597	0.425179403	2.325484194
15	0.310863965	0.011556035	0.063204792
16	0.516883693	-0.079313693	-0.433799799
17	0.450076738	-0.012506738	-0.068404588
18	-0.029086029	0.259386029	1.418690806
19	0.347640298	-0.025220298	-0.137940372
20	0.537731729	-0.054101729	-0.295905008
21	0.115171118	-2.1118E-05	-0.000115503
22	0.501191784	-0.316951784	-1.733542026

Lake Cowichan - CDOM

Model Building Data-Set

Sample	CDOM	Dev501	Dev523	Dev545	Dev647	CDOM'	e	e^2
3H25S-2-1	0.345	-3.12E-06	6.96E-06	-9.20E-06	-4.30E-06	0.440	-0.094	0.009
3H25-06	0.230	-3.04E-06	9.37E-06	-8.41E-06	-3.77E-06	0.106	0.124	0.015
3H25-07	0.645	-3.66E-06	6.87E-06	-8.14E-06	-4.39E-06	0.630	0.015	0.000
3H25-08	0.645	-4.73E-06	7.50E-06	-7.61E-06	-4.04E-06	0.583	0.061	0.004
3H25-09	0.691	-4.11E-06	6.07E-06	-9.12E-06	-4.30E-06	0.617	0.074	0.005
3H25-13	0.484	-4.64E-06	5.18E-06	-9.38E-06	-3.77E-06	0.780	-0.297	0.088
3H25-15	0.230	-3.93E-06	6.52E-06	-1.04E-05	-5.35E-06	0.229	0.002	0.000
3H25-18	1.566	-3.12E-06	4.82E-06	-6.90E-06	-3.77E-06	1.356	0.211	0.044
3H25-25	0.322	-1.34E-06	8.57E-06	-8.05E-06	-4.74E-06	0.329	-0.006	0.000
3H25-27	0.115	-2.59E-06	8.21E-06	-1.04E-05	-4.39E-06	-0.044	0.159	0.025
3H25-28	0.184	-1.70E-06	9.11E-06	-6.99E-06	-4.21E-06	0.433	-0.248	0.062
								0.253

Validation Data-Set

("Validation Set" model)

Sample	CDOM	Dev501	Dev523	Dev545	Dev647	CDOM'	e	e^2
3H25S-1-1	1.382	-2.14E-06	2.32E-06	-8.94E-06	-3.86E-06	1.238	0.144	0.021
3H25-11	0.322	-3.93E-06	4.64E-06	-8.76E-06	-5.00E-06	0.433	-0.111	0.012
3H25-12	0.783	-9.82E-07	4.73E-06	-1.07E-05	-4.12E-06	0.793	-0.010	0.000
3H25-14	0.322	-5.98E-06	5.00E-06	-8.50E-06	-4.21E-06	0.482	-0.159	0.025
3H25-16	0.806	-4.46E-06	4.02E-06	-8.32E-06	-4.56E-06	0.646	0.160	0.026
3H25-17	0.576	-2.50E-06	6.61E-06	-8.67E-06	-3.86E-06	0.708	-0.133	0.018
3H25-19	0.322	-4.91E-06	7.50E-06	-9.12E-06	-3.95E-06	0.302	0.020	0.000
3H25-21	0.438	-1.88E-06	7.50E-06	-7.79E-06	-4.65E-06	0.487	-0.049	0.002
3H25-22	0.438	-4.64E-06	7.68E-06	-6.73E-06	-4.47E-06	0.368	0.070	0.005
3H25-23	0.230	-2.41E-06	1.07E-05	-8.67E-06	-4.39E-06	0.044	0.186	0.035
3H25-26	0.484	-6.25E-07	8.93E-06	-7.79E-06	-4.12E-06	0.601	-0.118	0.014
								0.158

("Model Building Set" model)

Sample	CDOM	Dev501	Dev523	Dev545	Dev647	CDOM'	e	e^2
3H25S-1-1	1.382	-2.14E-06	2.32E-06	-8.94E-06	-3.86E-06	1.546	-0.164	0.027
3H25-11	0.322	-3.93E-06	4.64E-06	-8.76E-06	-5.00E-06	0.946	-0.623	0.388
3H25-12	0.783	-9.82E-07	4.73E-06	-1.07E-05	-4.12E-06	0.723	0.060	0.004
3H25-14	0.322	-5.98E-06	5.00E-06	-8.50E-06	-4.21E-06	0.908	-0.586	0.343
3H25-16	0.806	-4.46E-06	4.02E-06	-8.32E-06	-4.56E-06	1.174	-0.368	0.136
3H25-17	0.576	-2.50E-06	6.61E-06	-8.67E-06	-3.86E-06	0.663	-0.087	0.008
3H25-19	0.322	-4.91E-06	7.50E-06	-9.12E-06	-3.95E-06	0.310	0.013	0.000
3H25-21	0.438	-1.88E-06	7.50E-06	-7.79E-06	-4.65E-06	0.597	-0.159	0.025
3H25-22	0.438	-4.64E-06	7.68E-06	-6.73E-06	-4.47E-06	0.679	-0.241	0.058
3H25-23	0.230	-2.41E-06	1.07E-05	-8.67E-06	-4.39E-06	-0.253	0.483	0.234
3H25-26	0.484	-6.25E-07	8.93E-06	-7.79E-06	-4.12E-06	0.365	0.119	0.014
								1.237

Statistic	Model Building Data-set	Validation Data-set	Complete Data-set
b_0	4.01	3.86	3.85
$s\{b_0\}$	0.86	1.02	0.60
b_1	30867.05	93460.17	75814
$s\{b_1\}$	82207.08	32289.13	32813
b_2	-214808	-121856	-145945
$s\{b_2\}$	54771	23907	23794
b_3	182197	97986	116993
$s\{b_3\}$	67023	62156	43242
b_4	69028	326433	255688
$s\{b_4\}$	168655	151989	110873
SSE	0.253	0.158	0.702
MSE	0.0422	0.0263	0.0413
MSPR	-	0.1125	-
R^2	0.848	0.856	0.748

SUMMARY OUTPUT
Model: ***Lake, TSS***
Data-Set: ***model building***

Regression Statistics	
Multiple R	0.584825611
R Square	0.342020995
Adjusted R Sqı	0.276223094
Standard Error	0.279055219
Observations	12

ANOVA

	df	*SS*	*MS*	*F*	*Significance F*
Regression	1	0.404781847	0.404781847	5.198053313	0.045791632
Residual	10	0.778718153	0.077871815		
Total	11	1.1835			

	Coefficients	*Standard Error*	*t Stat*	*P-value*	*Lower 95%*	*Upper 95%*	*Lower 95.0%*	*Upper 95.0%*
Intercept	8.41033747	3.483103692	2.414610133	0.036395431	0.649498842	16.1711761	0.649498842	16.1711761
Ratio 09:15	-6.293886772	2.760568709	-2.279923971	0.045791632	-12.44481714	-0.142956405	-12.44481714	-0.142956405

RESIDUAL OUTPUT

Observation	*Predicted TSS*	*Residuals*	*Standard Residuals*
1	0.28812818	-0.17187818	-0.645991702
2	0.642565821	0.193684179	0.727947971
3	0.267399217	-0.081149217	-0.30499346
4	0.227887074	-0.211637074	-0.795422629
5	0.393543146	0.412706854	1.551128847
6	0.376611934	-0.350361934	-1.316809978
7	0.397735464	-0.091485464	-0.343841497
8	0.374212292	0.422037708	1.586198188
9	0.520703344	0.165546656	0.622195127
10	0.714089402	0.122160598	0.459131768
11	0.6259919	-0.0397419	-0.149367056
12	0.826132225	-0.369882225	-1.39017558

SUMMARY OUTPUT
Model: ***Lake, TSS***
Data-Set: ***validation***

Regression Statistics	
Multiple R	0.613293316
R Square	0.376128691
Adjusted R Sqı	0.313741561
Standard Error	0.227303634
Observations	12

ANOVA

	df	*SS*	*MS*	*F*	*Significance F*
Regression	1	0.311497245	0.311497245	6.028946776	0.033943154
Residual	10	0.516669422	0.051666942		
Total	11	0.828166667			

	Coefficients	*Standard Error*	*t Stat*	*P-value*	*Lower 95%*	*Upper 95%*	*Lower 95.0%*	*Upper 95.0%*
Intercept	7.039138986	2.670260877	2.636124076	0.024899063	1.089427006	12.98885097	1.089427006	12.98885097
Ratio 09:15	-5.207140649	2.120696812	-2.455391369	0.033943154	-9.932347589	-0.481933709	-9.932347589	-0.481933709

RESIDUAL OUTPUT

Observation	*Predicted TSS*	*Residuals*	*Standard Residuals*
1	0.369878436	-0.343628436	-1.585546772
2	0.428631251	0.027618749	0.12743654
3	0.426036483	-0.199786483	-0.921841095
4	0.368862775	0.147387225	0.68006403
5	0.292991539	0.043258461	0.199600227
6	0.457845565	0.138404435	0.638616256
7	0.38594317	-0.09969317	-0.45999739
8	0.339263556	0.366986444	1.693323694
9	0.608445456	-0.242195456	-1.117521671
10	0.638375643	-0.202125643	-0.932634284
11	0.625045206	0.231204794	1.066809309
12	0.873680921	0.132569079	0.611691156

SUMMARY OUTPUT
Model: ***Lake, TSS***
Data-Set: ***complete***

Regression Statistics	
Multiple R	0.59432446
R Square	0.353221564
Adjusted R Sqı	0.323822544
Standard Error	0.243253751
Observations	24

ANOVA

	df	*SS*	*MS*	*F*	*Significance F*
Regression	1	0.710940816	0.710940816	12.01473948	0.002194769
Residual	22	1.301792517	0.059172387		
Total	23	2.012733333			

	Coefficients	*Standard Error*	*t Stat*	*P-value*	*Lower 95%*	*Upper 95%*	*Lower 95.0%*	*Upper 95.0%*
Intercept	7.682384611	2.079067683	3.695110397	0.001264949	3.370662157	11.99410707	3.370662157	11.99410707
Ratio 09:15	-5.717469706	1.649478629	-3.466228423	0.002194769	-9.138278994	-2.296660418	-9.138278994	-2.296660418

RESIDUAL OUTPUT

Observation	*Predicted TSS*	*Residuals*	*Standard Residuals*
1	0.30403682	-0.18778682	-0.789329148
2	0.359499034	-0.333249034	-1.400754194
3	0.626013772	0.210236228	0.883691321
4	0.424009955	0.032240045	0.135515407
5	0.421160886	-0.194910886	-0.819273915
6	0.358383833	0.157866167	0.663562902
7	0.285206291	-0.098956291	-0.415945511
8	0.249312814	-0.233062814	-0.979638892
9	0.275076789	0.061173211	0.257130925
10	0.456087436	0.140162564	0.589148891
11	0.377138202	-0.090888202	-0.382032706
12	0.325883723	0.380366277	1.598803306
13	0.3997975	0.4064525	1.708452199
14	0.38441691	-0.35816691	-1.505492141
15	0.40360587	-0.09735587	-0.409218421
16	0.382237035	0.414012965	1.740231292
17	0.515311904	0.170938096	0.718508475
18	0.621446963	-0.255196963	-1.072675929
19	0.690986962	0.145263038	0.610587844
20	0.610957751	-0.024707751	-0.103854721
21	0.654310476	-0.218060476	-0.916579182
22	0.639673583	0.216576417	0.910341199
23	0.792768496	-0.336518496	-1.414496809
24	0.912676995	0.093573005	0.393317807

Lake Cowichan - TSS

Model Building Data-Set

Sample	TSS	Ratio 09:15	TSS'	e	e^2
3H25S-1-1	0.116	1.290	0.288	-0.172	0.030
3H25-06	0.836	1.234	0.643	0.194	0.038
3H25-10	0.186	1.294	0.267	-0.081	0.007
3H25-11	0.016	1.300	0.228	-0.212	0.045
3H25-16	0.806	1.274	0.394	0.413	0.170
3H25-17	0.026	1.276	0.377	-0.350	0.123
3H25-18	0.306	1.273	0.398	-0.091	0.008
3H25-19	0.796	1.277	0.374	0.422	0.178
3H25-20	0.686	1.254	0.521	0.166	0.027
3H25-22	0.836	1.223	0.714	0.122	0.015
3H25-23	0.586	1.237	0.626	-0.040	0.002
3H25-27	0.456	1.205	0.826	-0.370	0.137
					0.779

Validation Data-Set

("Validation Set" model)

Sample	TSS	Ratio 09:15	TSS'	e	e^2
3H25S-2-1	0.026	1.281	0.370	-0.344	0.118
3H25-07	0.456	1.270	0.429	0.028	0.001
3H25-08	0.226	1.270	0.426	-0.200	0.040
3H25-09	0.516	1.281	0.369	0.147	0.022
3H25-12	0.336	1.296	0.293	0.043	0.002
3H25-13	0.596	1.264	0.458	0.138	0.019
3H25-14	0.286	1.278	0.386	-0.100	0.010
3H25-15	0.706	1.287	0.339	0.367	0.135
3H25-21	0.366	1.235	0.608	-0.242	0.059
3H25-25	0.436	1.229	0.638	-0.202	0.041
3H25-26	0.856	1.232	0.625	0.231	0.053
3H25-28	1.006	1.184	0.874	0.133	0.018
					0.517

("Model Building Set" model)

Sample	TSS	Ratio 09:15	TSS'	e	e^2
3H25S-2-1	0.026	1.281	0.349	-0.323	0.104
3H25-07	0.456	1.270	0.420	0.036	0.001
3H25-08	0.226	1.270	0.417	-0.191	0.036
3H25-09	0.516	1.281	0.348	0.168	0.028
3H25-12	0.336	1.296	0.256	0.080	0.006
3H25-13	0.596	1.264	0.456	0.141	0.020
3H25-14	0.286	1.278	0.369	-0.082	0.007
3H25-15	0.706	1.287	0.312	0.394	0.155
3H25-21	0.366	1.235	0.638	-0.271	0.074
3H25-25	0.436	1.229	0.674	-0.237	0.056
3H25-26	0.856	1.232	0.658	0.199	0.039
3H25-28	1.006	1.184	0.958	0.048	0.002
					0.530

Statistic	Model Building Data-set	Validation Data-set	Complete Data-set
b_0	8.41	7.04	7.68
$s\{b_0\}$	3.48	2.67	2.08
b_1	-6.29	-5.21	-5.72
$s\{b_1\}$	2.76	2.12	1.65
SSE	0.779	0.517	1.302
MSE	0.0779	0.0517	0.0592
MSPR	-	0.0442	-
R^2	0.342	0.376	0.353

SUMMARY OUTPUT
Model: ***Bay, Chl-a***
Data-Set: ***model building***

Regression Statistics	
Multiple R	0.785802791
R Square	0.617486026
Adjusted R Sqı	0.474043285
Standard Error	0.602701433
Observations	12

ANOVA

	df	*SS*	*MS*	*F*	*Significance F*
Regression	3	4.691095378	1.563698459	4.304756198	0.043847337
Residual	8	2.90599214	0.363249017		
Total	11	7.597087517			

	Coefficients	*Standard Error*	*t Stat*	*P-value*	*Lower 95%*	*Upper 95%*	*Lower 95.0%*	*Upper 95.0%*
Intercept	17.46566729	5.279451326	3.308235309	0.010726376	5.291230707	29.64010387	5.291230707	29.64010387
Band04	-23790.03232	6622.292546	-3.592416396	0.00705965	-39061.0663	-8518.998337	-39061.0663	-8518.998337
Band16	6840.258467	4159.264669	1.644583601	0.138676528	-2751.023051	16431.53998	-2751.023051	16431.53998
Band31	11335.17709	22797.78011	0.4972053	0.632419425	-41236.59807	63906.95224	-41236.59807	63906.95224

RESIDUAL OUTPUT

Observation	*Predicted Chl-a*	*Residuals*	*Standard Residuals*
1	1.50376826	-0.63891826	-1.243066679
2	3.240699861	-0.044219861	-0.086033284
3	1.595185264	0.893054736	1.73750956
4	1.28482128	-0.36874128	-0.717415713
5	1.198844272	-0.283244272	-0.551074432
6	1.1846975	0.3015225	0.586636188
7	1.018273258	0.355126742	0.690927538
8	2.212057825	0.771742175	1.50148625
9	1.872329238	-0.032349238	-0.062938035
10	2.185887564	-0.380827564	-0.740930546
11	0.920878727	0.137181273	0.266897162
12	1.64212695	-0.71032695	-1.381998009

SUMMARY OUTPUT
Model: ***Bay, Chl-a***
Data-Set: ***validation***

Regression Statistics	
Multiple R	0.91575394
R Square	0.838605279
Adjusted R Sqı	0.769436113
Standard Error	0.382352978
Observations	11

ANOVA

	df	*SS*	*MS*	*F*	*Significance F*
Regression	3	5.317350169	1.772450056	12.12397554	0.003676631
Residual	7	1.023356601	0.1461938		
Total	10	6.34070677			

	Coefficients	*Standard Error*	*t Stat*	*P-value*	*Lower 95%*	*Upper 95%*	*Lower 95.0%*	*Upper 95.0%*
Intercept	18.01668082	2.892394238	6.228985171	0.000432881	11.17725526	24.85610637	11.17725526	24.85610637
Band04	-17451.21634	3317.661611	-5.260095328	0.001173221	-25296.23944	-9606.193237	-25296.23944	-9606.193237
Band16	5644.996715	1901.94364	2.968014717	0.020866416	1147.614659	10142.37877	1147.614659	10142.37877
Band31	-38448.82459	9613.436133	-3.999488223	0.005193296	-61180.98881	-15716.66038	-61180.98881	-15716.66038

RESIDUAL OUTPUT

Observation	*Predicted Chl-a*	*Residuals*	*Standard Residuals*
1	1.784997507	0.447682493	1.399447509
2	1.874093945	0.418946055	1.309617915
3	1.88856011	-0.39666011	-1.239952447
4	3.349747595	0.108052405	0.337769897
5	0.754499396	0.032660604	0.102096466
6	0.689901072	0.294518928	0.920660929
7	1.308573027	-0.258273027	-0.807356887
8	1.744550343	-0.387350343	-1.210850284
9	1.05423394	0.21766606	0.680420232
10	1.349636056	-0.317976056	-0.993987496
11	1.328067008	-0.159267008	-0.497865834

SUMMARY OUTPUT
Model: ***Bay, Chl-a***
Data-Set: ***complete***

Regression Statistics	
Multiple R	0.774752654
R Square	0.600241674
Adjusted R Sq	0.537121938
Standard Error	0.542594791
Observations	23

ANOVA

	df	*SS*	*MS*	*F*	*Significance F*
Regression	3	8.399113863	2.799704621	9.509572051	0.000475687
Residual	19	5.593773044	0.294409108		
Total	22	13.99288691			

	Coefficients	*Standard Error*	*t Stat*	*P-value*	*Lower 95%*	*Upper 95%*	*Lower 95.0%*	*Upper 95.0%*
Intercept	16.4741797	2.98784991	5.51372398	2.55728E-05	10.22053798	22.72782142	10.22053798	22.72782142
Band04	-18365.8166	3620.428471	-5.07282957	6.7584E-05	-25943.46046	-10788.17274	-25943.46046	-10788.17274
Band16	6369.098289	2121.526391	3.002130125	0.007327083	1928.692531	10809.50405	1928.692531	10809.50405
Band31	-23228.38247	10929.95907	-2.125203061	0.046907833	-46105.04967	-351.7152722	-46105.04967	-351.7152722

RESIDUAL OUTPUT

Observation	*Predicted Chl-a*	*Residuals*	*Standard Residuals*
1	1.278874058	-0.247214058	-0.490266346
2	1.259275541	1.228964459	2.437239695
3	1.763610776	0.469069224	0.930241818
4	1.346810116	0.139409884	0.276472847
5	1.162403675	0.109496325	0.217149315
6	0.897470542	-0.032620542	-0.064691927
7	1.639570346	-0.282370346	-0.559987078
8	1.124570816	0.248829184	0.493469409
9	2.200621334	0.783178666	1.553172772
10	1.348605668	-0.298305668	-0.591589456
11	2.495440967	-0.690380967	-1.369139591
12	1.147306385	0.021493615	0.042625391
13	2.075362013	-0.583462013	-1.157101631
14	1.629455094	-0.697655094	-1.383565388
15	0.840108303	-0.052948303	-0.105005238
16	2.844783883	0.351696117	0.697471543
17	3.35490566	0.10289434	0.204056486
18	1.192628627	-0.208208627	-0.412912128
19	1.641678493	0.198301507	0.393264672
20	1.461381566	0.831658434	1.649316166
21	1.321552704	-0.405952704	-0.805071324
22	1.581303878	-0.665223878	-1.319248925
23	1.378709557	-0.320649557	-0.635901081

Cowichan Bay - Chl-*a*

Model Building Data-Set

Sample	Chl-a	Band04	Band16	Band31	Chl-a'	e	e^2
3H26-06	0.865	1.03E-03	1.01E-03	1.36E-04	1.504	-0.639	0.408
3H26-17	3.196	8.98E-04	8.58E-04	1.12E-04	3.241	-0.044	0.002
3H26S-2-1	2.488	9.91E-04	9.21E-04	1.24E-04	1.595	0.893	0.798
3H26-28	0.916	9.65E-04	8.20E-04	1.03E-04	1.285	-0.369	0.136
3H26-27	0.916	9.80E-04	8.48E-04	1.10E-04	1.199	-0.283	0.080
3H26S-4-1	1.486	1.01E-03	9.40E-04	1.12E-04	1.185	0.302	0.091
3H26-08	1.373	1.02E-03	9.42E-04	1.15E-04	1.018	0.355	0.126
3H26-09	2.984	9.63E-04	9.37E-04	1.10E-04	2.212	0.772	0.596
3H26-22	1.840	1.01E-03	1.02E-03	1.22E-04	1.872	-0.032	0.001
3H26-11	1.805	9.67E-04	9.62E-04	1.01E-04	2.186	-0.381	0.145
3H26-29	1.058	1.00E-03	8.92E-04	1.03E-04	0.921	0.137	0.019
3H26-15	0.932	9.88E-04	9.34E-04	1.14E-04	1.642	-0.710	0.505
							2.906

Validation Data-Set

("Validation Set" model)

Sample	Chl-a	Band04	Band16	Band31	Chl-a'	e	e^2
3H26S-3-1	2.233	1.03E-03	1.07E-03	1.11E-04	1.785	0.448	0.200
3H26-24	2.293	1.02E-03	9.11E-04	9.20E-05	1.874	0.419	0.176
3H26-13	1.492	1.03E-03	1.14E-03	1.21E-04	1.889	-0.397	0.157
3H26-18	3.458	8.70E-04	8.61E-04	1.13E-04	3.350	0.108	0.012
3H26-16	0.787	1.03E-03	9.64E-04	1.23E-04	0.754	0.033	0.001
3H26-21	0.984	9.86E-04	9.80E-04	1.47E-04	0.690	0.295	0.087
3H26-10	1.050	1.02E-03	9.91E-04	1.18E-04	1.309	-0.258	0.067
3H26-07	1.357	9.88E-04	9.21E-04	1.10E-04	1.745	-0.387	0.150
3H26S-5-1	1.272	1.02E-03	9.80E-04	1.23E-04	1.054	0.218	0.047
3H26S-1-1	1.032	9.76E-04	8.48E-04	1.15E-04	1.350	-0.318	0.101
3H26-12	1.169	1.03E-03	9.56E-04	1.06E-04	1.328	-0.159	0.025
							1.023

("Model Building Set" model)

Sample	Chl-a	Band04	Band16	Band31	Chl-a'	e	e^2
3H26S-3-1	2.233	1.03E-03	1.07E-03	1.11E-04	1.498	0.734	0.539
3H26-24	2.293	1.02E-03	9.11E-04	9.20E-05	0.546	1.748	3.054
3H26-13	1.492	1.03E-03	1.14E-03	1.21E-04	2.216	-0.725	0.525
3H26-18	3.458	8.70E-04	8.61E-04	1.13E-04	3.939	-0.481	0.231
3H26-16	0.787	1.03E-03	9.64E-04	1.23E-04	0.950	-0.163	0.027
3H26-21	0.984	9.86E-04	9.80E-04	1.47E-04	2.378	-1.394	1.943
3H26-10	1.050	1.02E-03	9.91E-04	1.18E-04	1.364	-0.313	0.098
3H26-07	1.357	9.88E-04	9.21E-04	1.10E-04	1.508	-0.151	0.023
3H26S-5-1	1.272	1.02E-03	9.80E-04	1.23E-04	1.345	-0.073	0.005
3H26S-1-1	1.032	9.76E-04	8.48E-04	1.15E-04	1.351	-0.319	0.102
3H26-12	1.169	1.03E-03	9.56E-04	1.06E-04	0.655	0.514	0.264
							6.811

Statistic	Model Building Data-set	Validation Data-set	Complete Data-set
b_0	17.47	18.02	16.47
$s\{b_0\}$	5.28	2.89	2.99
b_1	-23790.03	-17451.22	-18366
$s\{b_1\}$	6622.29	3317.66	3620
b_2	6840	5645	6369
$s\{b_2\}$	4159	1902	2122
b_3	11335	-38449	-23228
$s\{b_3\}$	22798	9613	10930
SSE	2.906	1.023	5.594
MSE	0.3632	0.1462	0.2944
MSPR	-	0.6192	-
R^2	0.617	0.839	0.600

SUMMARY OUTPUT
Model: ***Bay, CDOM***
Data-Set: ***model building***

Regression Statistics	
Multiple R	0.761748381
R Square	0.580260596
Adjusted R Sqı	0.460335052
Standard Error	0.387609426
Observations	10

ANOVA

	df	*SS*	*MS*	*F*	*Significance F*
Regression	2	1.45388494	0.72694247	4.838507105	0.047910323
Residual	7	1.051687469	0.150241067		
Total	9	2.50557241			

	Coefficients	*Standard Error*	*t Stat*	*P-value*	*Lower 95%*	*Upper 95%*	*Lower 95.0%*	*Upper 95.0%*
Intercept	1.931734884	0.878600082	2.198650926	0.063858054	-0.145824177	4.009293945	-0.145824177	4.009293945
Dev434	-79789.22089	32443.96001	-2.459293529	0.043510356	-156506.9955	-3071.44626	-156506.9955	-3071.44626
Dev636	754218.3346	472023.3596	1.597841122	0.154110224	-361939.5486	1870376.218	-361939.5486	1870376.218

RESIDUAL OUTPUT

Observation	*Predicted CDOM*	*Residuals*	*Standard Residuals*
1	-0.087386275	0.386776275	1.13145616
2	-0.002593198	0.071683198	0.209698477
3	0.395689878	-0.165389878	-0.483823358
4	1.267069291	0.621390709	1.817785608
5	0.155687083	0.304912917	0.891977147
6	0.391572223	-0.276422223	-0.808631881
7	0.516424045	-0.055824045	-0.163304898
8	0.431630968	-0.293450968	-0.85844693
9	0.890350869	-0.452780869	-1.324542732
10	0.486345116	-0.140895116	-0.412167593

SUMMARY OUTPUT
Model: ***Bay, CDOM***
Data-Set: ***validation***

Regression Statistics	
Multiple R	0.847932819
R Square	0.718990066
Adjusted R Sqı	0.638701514
Standard Error	0.116514482
Observations	10

ANOVA

	df	*SS*	*MS*	*F*	*Significance F*
Regression	2	0.24314149	0.121570745	8.955075709	0.01176321
Residual	7	0.095029371	0.013575624		
Total	9	0.338170862			

	Coefficients	*Standard Error*	*t Stat*	*P-value*	*Lower 95%*	*Upper 95%*	*Lower 95.0%*	*Upper 95.0%*
Intercept	1.139849605	0.190646763	5.978856329	0.000553828	0.689041646	1.590657564	0.689041646	1.590657564
Dev434	-34217.16601	13818.45181	-2.476193895	0.04244608	-66892.61228	-1541.719751	-66892.61228	-1541.719751
Dev636	312383.1873	96618.51063	3.233160864	0.014388625	83916.714	540849.6607	83916.714	540849.6607

RESIDUAL OUTPUT

Observation	*Predicted CDOM*	*Residuals*	*Standard Residuals*
1	0.408559342	-0.063109342	-0.614166293
2	0.301692219	0.112847781	1.098209885
3	0.484258575	-0.069718575	-0.678485898
4	0.311289817	-0.150079817	-1.460543904
5	0.214012191	0.177497809	1.727369802
6	0.480151105	-0.019551105	-0.190267067
7	0.657918661	0.102071339	0.993335914
8	0.612020862	0.032819138	0.319388666
9	0.543170113	-0.059540113	-0.579431334
10	0.178387117	-0.063237117	-0.615409769

SUMMARY OUTPUT
Model: ***Bay, CDOM***
Data-Set: ***complete***

Regression Statistics	
Multiple R	0.694546954
R Square	0.482395471
Adjusted R Sqı	0.42150082
Standard Error	0.294418199
Observations	20

ANOVA

	df	*SS*	*MS*	*F*	*Significance F*
Regression	2	1.373356787	0.686678394	7.921803757	0.003706667
Residual	17	1.473595289	0.086682076		
Total	19	2.846952076			

	Coefficients	*Standard Error*	*t Stat*	*P-value*	*Lower 95%*	*Upper 95%*	*Lower 95.0%*	*Upper 95.0%*
Intercept	1.395494395	0.381720242	3.65580402	0.001956891	0.59013509	2.200853701	0.59013509	2.200853701
Dev434	-57539.20107	18795.86402	-3.061269277	0.007066859	-97195.00742	-17883.39472	-97195.00742	-17883.39472
Dev636	439357.2886	201604.0548	2.179307798	0.043663611	14009.91723	864704.66	14009.91723	864704.66

RESIDUAL OUTPUT

Observation	*Predicted CDOM*	*Residuals*	*Standard Residuals*
1	0.159508974	0.139881026	0.502280707
2	0.354235892	-0.008785892	-0.031548126
3	0.229826809	-0.160736809	-0.577169045
4	0.197145859	0.217394141	0.78061254
5	0.498704372	-0.268404372	-0.963778589
6	0.451375515	-0.036835515	-0.132267892
7	1.07207003	0.81638997	2.931469291
8	0.15297436	0.00823564	0.029572295
9	0.298118291	0.162481709	0.583434582
10	0.019548755	0.371961245	1.335627587
11	0.431543896	-0.316393896	-1.136097971
12	0.421851923	0.038748077	0.139135464
13	0.698167328	0.061822672	0.221991046
14	0.628524944	0.016315056	0.058583626
15	0.594940766	-0.134340766	-0.482386904
16	0.524622931	-0.386442931	-1.387628004
17	0.557979332	-0.074349332	-0.266971413
18	0.818743602	-0.381173602	-1.368707051
19	-0.010202613	0.125352613	0.450112508
20	0.536569034	-0.191119034	-0.686264652

Cowichan Bay - CDOM

Model Building Data-Set

Sample	CDOM	Dev434	Dev636	CDOM'	e	e^2
3H26S-1-1	0.299	5.41E-06	-2.11E-06	-0.087	0.387	0.150
3H26S-3-1	0.069	3.51E-06	-2.19E-06	-0.003	0.072	0.005
3H26S-5-1	0.230	1.80E-07	-2.02E-06	0.396	-0.165	0.027
3H26-10	1.888	-5.77E-06	-1.49E-06	1.267	0.621	0.386
3H26-12	0.461	5.68E-06	-1.75E-06	0.156	0.305	0.093
3H26-15	0.115	6.04E-06	-1.40E-06	0.392	-0.276	0.076
3H26-21	0.461	-2.16E-06	-2.11E-06	0.516	-0.056	0.003
3H26-22	0.138	-2.70E-07	-2.02E-06	0.432	-0.293	0.086
3H26-27	0.438	-2.70E-06	-1.67E-06	0.890	-0.453	0.205
3H26-29	0.345	1.53E-06	-1.75E-06	0.486	-0.141	0.020
						1.052

Validation Data-Set

("Validation Set" model)

Sample	CDOM	Dev434	Dev636	CDOM'	e	e^2
3H26S-2-1	0.345	1.35E-06	-2.19E-06	0.409	-0.063	0.004
3H26S-4-1	0.415	2.07E-06	-2.46E-06	0.302	0.113	0.013
3H26-08	0.415	2.34E-06	-1.84E-06	0.484	-0.070	0.005
3H26-11	0.161	8.20E-06	-1.75E-06	0.311	-0.150	0.023
3H26-13	0.392	7.84E-06	-2.11E-06	0.214	0.177	0.032
3H26-16	0.461	4.86E-06	-1.58E-06	0.480	-0.020	0.000
3H26-17	0.760	2.07E-06	-1.32E-06	0.658	0.102	0.010
3H26-18	0.645	2.61E-06	-1.40E-06	0.612	0.033	0.001
3H26-24	0.484	-1.80E-07	-1.93E-06	0.543	-0.060	0.004
3H26-28	0.115	5.68E-06	-2.46E-06	0.178	-0.063	0.004
						0.095

("Model Building Set" model)

Sample	CDOM	Dev434	Dev636	CDOM'	e	e^2
3H26S-2-1	0.345	1.35E-06	-2.19E-06	0.170	0.176	0.031
3H26S-4-1	0.415	2.07E-06	-2.46E-06	-0.086	0.501	0.251
3H26-08	0.415	2.34E-06	-1.84E-06	0.355	0.059	0.003
3H26-11	0.161	8.20E-06	-1.75E-06	-0.046	0.207	0.043
3H26-13	0.392	7.84E-06	-2.11E-06	-0.281	0.673	0.453
3H26-16	0.461	4.86E-06	-1.58E-06	0.353	0.108	0.012
3H26-17	0.760	2.07E-06	-1.32E-06	0.774	-0.014	0.000
3H26-18	0.645	2.61E-06	-1.40E-06	0.665	-0.020	0.000
3H26-24	0.484	-1.80E-07	-1.93E-06	0.491	-0.007	0.000
3H26-28	0.115	5.68E-06	-2.46E-06	-0.374	0.489	0.239
						1.032

Statistic	Model Building Data-set	Validation Data-set	Complete Data-set
b_0	1.93	1.14	1.40
$s\{b_0\}$	0.88	0.19	0.38
b_1	-79789.22	-34217.17	-57539
$s\{b_1\}$	32443.96	13818.45	18796
b_2	754218	312383	439357
$s\{b_2\}$	472023	96619	201604
SSE	1.052	0.095	1.474
MSE	0.1502	0.0136	0.0867
MSPR	-	0.0938	-
R^2	0.580	0.719	0.482

SUMMARY OUTPUT
Model: ***Bay, TSS***
Data-Set: ***model building***

Regression Statistics	
Multiple R	0.767470312
R Square	0.58901068
Adjusted R Sqı	0.5433452
Standard Error	0.25167211
Observations	11

ANOVA

	df	*SS*	*MS*	*F*	*Significance F*
Regression	1	0.816968522	0.816968522	12.89837925	0.005825742
Residual	9	0.570049659	0.063338851		
Total	10	1.387018182			

	Coefficients	*Standard Error*	*t Stat*	*P-value*	*Lower 95%*	*Upper 95%*	*Lower 95.0%*	*Upper 95.0%*
Intercept	-3.230944091	2.312279825	-1.39729805	0.195812913	-8.461684449	1.999796266	-8.461684449	1.999796266
Band05	7473.122289	2080.820021	3.591431366	0.005825742	2765.980384	12180.26419	2765.980384	12180.26419

RESIDUAL OUTPUT

Observation	*Predicted TSS*	*Residuals*	*Standard Residuals*
1	4.690565535	0.425684465	1.782918355
2	5.079167894	0.127082106	0.532265182
3	5.460297131	-0.004047131	-0.016950827
4	5.333254052	0.352995948	1.478472923
5	5.019382916	-0.133132916	-0.557608131
6	4.952124815	-0.185874815	-0.778510016
7	5.273469074	0.052780926	0.221065344
8	5.49018962	-0.26393962	-1.105473259
9	4.795189247	-0.148939247	-0.623810684
10	4.952124815	0.084125185	0.352346277
11	4.712984902	-0.306734902	-1.284715162

SUMMARY OUTPUT
Model: ***Bay, TSS***
Data-Set: ***validation***

Regression Statistics	
Multiple R	0.743336161
R Square	0.552548648
Adjusted R Sqı	0.502831831
Standard Error	0.43038086
Observations	11

ANOVA

	df	*SS*	*MS*	*F*	*Significance F*
Regression	1	2.058605381	2.058605381	11.11391843	0.008746661
Residual	9	1.667049164	0.185227685		
Total	10	3.725654545			

	Coefficients	*Standard Error*	*t Stat*	*P-value*	*Lower 95%*	*Upper 95%*	*Lower 95.0%*	*Upper 95.0%*
Intercept	-4.516339315	2.903220997	-1.555630563	0.154219227	-11.08388147	2.051202846	-11.08388147	2.051202846
Band05	8744.428386	2622.997175	3.333754405	0.008746661	2810.79655	14678.06022	2810.79655	14678.06022

RESIDUAL OUTPUT

Observation	*Predicted TSS*	*Residuals*	*Standard Residuals*
1	5.128765195	-0.292515195	-0.716430765
2	5.679664184	-0.143414184	-0.351251268
3	5.705897469	0.980352531	2.401087962
4	5.251187193	0.165062807	0.404273266
5	5.627197613	-0.340947613	-0.835051866
6	4.866432344	-0.100182344	-0.245367469
7	4.490421923	0.285828077	0.700052617
8	4.429210924	0.277039076	0.678526518
9	5.496031188	-0.129781188	-0.317861215
10	4.875176772	-0.238926772	-0.585181532
11	5.128765195	-0.462515195	-1.132796247

SUMMARY OUTPUT
Model: ***Bay, TSS***
Data-Set: ***complete***

Regression Statistics	
Multiple R	0.739102564
R Square	0.5462726
Adjusted R Sqı	0.52358623
Standard Error	0.341849077
Observations	22

ANOVA

	df	*SS*	*MS*	*F*	*Significance F*
Regression	1	2.81392962	2.81392962	24.07933044	8.51258E-05
Residual	20	2.337215835	0.116860792		
Total	21	5.151145455			

	Coefficients	*Standard Error*	*t Stat*	*P-value*	*Lower 95%*	*Upper 95%*	*Lower 95.0%*	*Upper 95.0%*
Intercept	-3.994346708	1.856946066	-2.151030006	0.043878152	-7.867868313	-0.120825102	-7.867868313	-0.120825102
Band 05	8216.289072	1674.377993	4.907069435	8.51258E-05	4723.597792	11708.98035	4723.597792	11708.98035

RESIDUAL OUTPUT

Observation	*Predicted TSS*	*Residuals*	*Standard Residuals*
1	4.714919708	0.401330292	1.202990445
2	5.14216674	0.06408326	0.192090034
3	5.561197483	-0.104947483	-0.314580837
4	5.068220138	-0.231970138	-0.695332164
5	5.58584635	-0.04959635	-0.148665417
6	5.421520569	0.264729431	0.793528381
7	5.076436428	-0.190186428	-0.570085189
8	5.610495217	1.075754783	3.224582725
9	5.002489826	-0.236239826	-0.708130583
10	5.355790256	-0.029540256	-0.08854713
11	5.594062639	-0.367812639	-1.10252104
12	5.183248185	0.233001815	0.698424621
13	5.536548616	-0.250298616	-0.750271906
14	4.821731466	-0.055481466	-0.166306096
15	4.468431036	0.307818964	0.922689565
16	4.410917013	0.295332987	0.885262761
17	4.829947755	-0.183697755	-0.550635347
18	5.413304279	-0.047054279	-0.141045542
19	5.002489826	0.033760174	0.101196366
20	4.739568576	-0.333318576	-0.999124836
21	4.829947755	-0.193697755	-0.58061042
22	5.068220138	-0.401970138	-1.204908391

Cowichan Bay - TSS

Model Building Data-Set

Sample	TSS	Band05	TSS'	e	e^2
3H26S-1-1	5.116	1.06E-03	4.691	0.426	0.181
3H26S-2-1	5.206	1.11E-03	5.079	0.127	0.016
3H26S-3-1	5.456	1.16E-03	5.460	-0.004	0.000
3H26-06	5.686	1.15E-03	5.333	0.353	0.125
3H26-07	4.886	1.10E-03	5.019	-0.133	0.018
3H26-09	4.766	1.10E-03	4.952	-0.186	0.035
3H26-10	5.326	1.14E-03	5.273	0.053	0.003
3H26-11	5.226	1.17E-03	5.490	-0.264	0.070
3H26-21	4.646	1.07E-03	4.795	-0.149	0.022
3H26-24	5.036	1.10E-03	4.952	0.084	0.007
3H26-27	4.406	1.06E-03	4.713	-0.307	0.094
					0.570

Validation Data-Set

("Validation Set" model)

Sample	TSS	Band05	TSS'	e	e^2
3H26S-4-1	4.836	1.10E-03	5.129	-0.293	0.086
3H26S-5-1	5.536	1.17E-03	5.680	-0.143	0.021
3H26-08	6.686	1.17E-03	5.706	0.980	0.961
3H26-12	5.416	1.12E-03	5.251	0.165	0.027
3H26-13	5.286	1.16E-03	5.627	-0.341	0.116
3H26-15	4.766	1.07E-03	4.866	-0.100	0.010
3H26-17	4.776	1.03E-03	4.490	0.286	0.082
3H26-18	4.706	1.02E-03	4.429	0.277	0.077
3H26-22	5.366	1.15E-03	5.496	-0.130	0.017
3H26-28	4.636	1.07E-03	4.875	-0.239	0.057
3H26-29	4.666	1.10E-03	5.129	-0.463	0.214
					1.667

("Model Building Set" model)

Sample	TSS	Band05	TSS'	e	e^2
3H26S-4-1	4.836	1.10E-03	5.012	-0.176	0.031
3H26S-5-1	5.536	1.17E-03	5.483	0.054	0.003
3H26-08	6.686	1.17E-03	5.505	1.181	1.395
3H26-12	5.416	1.12E-03	5.117	0.300	0.090
3H26-13	5.286	1.16E-03	5.438	-0.152	0.023
3H26-15	4.766	1.07E-03	4.788	-0.021	0.000
3H26-17	4.776	1.03E-03	4.466	0.310	0.096
3H26-18	4.706	1.02E-03	4.414	0.292	0.085
3H26-22	5.366	1.15E-03	5.326	0.040	0.002
3H26-28	4.636	1.07E-03	4.795	-0.159	0.025
3H26-29	4.666	1.10E-03	5.012	-0.346	0.119
					1.870

Statistic	Model Building Data-set	Validation Data-set	Complete Data-set
b_0	-3.23	-4.52	-3.99
$s\{b_0\}$	2.31	2.90	1.86
b_1	7473.12	8744.43	8216
$s\{b_1\}$	2080.82	2623.00	1674
SSE	0.570	1.667	2.337
MSE	0.0633	0.1852	0.1169
MSPR	-	0.1700	-
R^2	0.589	0.553	0.546